

DISCLAIMER

This book was prepared as an account of work sponsored by an agency of the United States Government. Neither the United States Government nor any agency thereof, nor any of their employees, makes any warranty, express or implied, or assumes any legal liability or responsibility for the accuracy, completeness, or usefulness of any information, disclosure, embodied in this report, or for the results of its use; and it is understood that any views or opinions stated herein do not necessarily represent those of the United States Government or any agency thereof.

**Distribution Categories:
Magnetic Fusion Energy (UC-20)
Fusion Systems (UC-20d)**

ANL/FPP/TM-150

ANL/FPP/TM--150

DE82 013712

**ARGONNE NATIONAL LABORATORY
9700 South Cass Avenue
Argonne, Illinois 60439**

WILDCAT: A CATALYZED D-D TOKAMAK REACTOR

by

**K. Evans, Jr., C. C. Baker, J. N. Brooks, R. G. Clemmer, D. A. Ehst,
H. Herman, J. Jung, R. F. Mattas, B. Misra, D. L. Smith,
H. C. Stevens, L. R. Turner, and R. B. Wehrle**

**Fusion Power Program
Argonne National Laboratory**

K. M. Barry

**The Ralph M. Parsons Company
Pasadena, California 91124**

A. E. Bolon

**University of Missouri
Rolla, Missouri 65401**

R. T. McGrath

**Pennsylvania State University
University Park, Pennsylvania 16802**

L. M. Waganer

**McDonnell Douglas Astronautics Company
St. Louis, Missouri 63166**

November 1981

DISTRIBUTION OF THIS DOCUMENT IS UNLIMITED

TABLE OF CONTENTS

	<u>Page</u>
LIST OF FIGURES	viii
LIST OF TABLES	xi
ACKNOWLEDGMENTS	xiv
ABSTRACT	xvi
1. INTRODUCTION	1-1
1.1 Scope and Guidelines	1-1
1.2 Overview	1-2
1.3 Conclusions	1-12
References	1-14
2. PLASMA ENGINEERING	2-1
2.1 Reference Design	2-1
2.2 MHD Considerations	2-6
2.3 Design Sensitivity	2-9
2.4 Burn Cycle	2-14
2.4.1 Plasma Initiation	2-17
2.4.2 Startup	2-17
2.4.3 Burn Phase	2-23
2.4.4 Shutdown	2-23
2.5 Limiter Impurity Control	2-24
2.5.1 Limiter Design	2-24
2.5.2 Limiter Lifetime	2-27
2.6 Steady-State Current Drive	2-31
2.7 ECRH Preionization	2-40
References	2-41

	<u>Page</u>
3. FIRST-WALL/BLANKET/SHIELD	3-1
3.1 First Wall	3-1
3.2 Blanket/Shield Nuclear Analysis	3-7
3.2.1 Nuclear Response	3-8
3.2.2 Inboard Radiation Shielding	3-15
3.2.3 Outboard Radiation Shielding	3-19
3.2.4 Neutron Energy Multiplication	3-22
3.2.5 Reactor Activation	3-25
3.3 Thermal Hydraulic Analysis	3-33
3.4 Reactor Maintenance and Repair	3-42
References	3-45
4. MAGNETS	4-1
4.1 Toroidal Field Coils	4-1
4.1.1 Choice of TF Coil Parameters	4-1
4.1.2 Conductor Design and Plane Force Support	4-2
4.1.3 Support Against Out-of-Plane Forces	4-3
4.1.4 Ripple	4-5
4.2 Ohmic Heating Coils	4-6
4.3 Equilibrium Field Coils	4-7
4.4 Correction Field Coils	4-11
References	4-15
5. TRITIUM/FUEL/VACUUM	5-1
5.1 Fuel Cycle	5-1
5.2 Vacuum Systems	5-3
5.3 Design of the Isotopic Separation System and Tritium Inventory	5-4
5.3.1 Distillation Cascade	5-5
5.3.2 Tritium Inventory	5-6
5.4 Tritium Inventories and Source Terms	5-9
References	5-11

	<u>Page</u>
6. COST ANALYSIS	6-1
6.1 Economic Guidelines and Assumptions	6-3
6.2 Capital Costs	6-5
6.2.1 Land and Land Rights	6-5
6.2.2 Structures and Site Facilities	6-11
6.2.2.1 Site Improvements and Facilities	6-11
6.2.2.2 Reactor Building	6-12
6.2.2.3 Turbine Building	6-12
6.2.2.4 Cooling System Structures	6-12
6.2.2.5 Electrical Equipment and Rf Power Supply Building	6-13
6.2.2.6 Plant Auxiliary Systems Building	6-13
6.2.2.7 Hot Cell Building	6-13
6.2.2.8 Reactor Service Building	6-14
6.2.2.9 Service Water Building (Pump Houses)	6-14
6.2.2.10 Fuel Handling and Storage Building	6-14
6.2.2.11 Control Room Building	6-15
6.2.2.12 On-site ac Power Supply Building	6-15
6.2.2.13 Administration Building	6-15
6.2.2.14 Site Service Building	6-15
6.2.2.15 Cryogenics Building	6-15
6.2.2.16 Security Building	6-16
6.2.2.17 Ventilation Stack	6-16
6.2.3 Reactor Plant Equipment	6-16
6.2.3.1 Blanket and First Wall	6-16
6.2.3.2 Shielding	6-17
6.2.3.3 Magnets	6-18
6.2.3.4 Rf Heating and Current Drive	6-21
6.2.3.5 Primary Structure and Support System	6-21
6.2.3.6 Reactor Vacuum System	6-23
6.2.3.7 Power Supply, Switching, and Electrical Energy Storage	6-24
6.2.3.8 Impurity Control	6-25
6.2.3.9 ECRH Plasma Breakdown	6-25

	<u>Page</u>
6.2.3.10 Main Heat Transfer and Transport	6-26
6.2.3.11 Cryogenic Cooling Systems	6-27
6.2.3.12 Radioactive Waste Treatment and Disposal ...	6-28
6.2.3.13 Fuel Handling and Storage System	6-28
6.2.3.14 Other Reactor Plant Equipment	6-29
6.2.3.15 Instrumentation and Control	6-30
6.2.3.16 Reactor Spare Parts Allowance	6-30
6.2.4 Turbine Plant Equipment	6-32
6.2.4.1 Turbine Generator	6-32
6.2.4.2 Main Steam System	6-32
6.2.4.3 Heat Rejection System	6-33
6.2.4.4 Condensing System	6-34
6.2.4.5 Feedwater Heating System	6-34
6.2.4.6 Other Turbine Plant Equipment	6-34
6.2.4.7 Instrumentation and Control	6-34
6.2.5 Electrical Plant Equipment	6-35
6.2.6 Miscellaneous Plant Equipment	6-35
6.2.7 Special Materials	6-36
6.2.8 Construction Facilities, Equipment, and Services	6-36
6.2.9 Engineering and Construction Management Service	6-37
6.2.10 Other Costs	6-37
6.2.11 Interest During Construction	6-37
6.2.12 Escalation During Construction	6-38
6.3 Busbar Energy Costs	6-38
6.3.1 Annual Levelized Capital Cost	6-38
6.3.2 Annual Operations and Maintenance Cost	6-39
6.3.3 Annual Scheduled Component Replacement Cost	6-39
6.3.4 Annual Fuel Cost	6-40
6.3.5 Plant Availability	6-40
6.3.6 Plant Capacity	6-41
6.3.7 Busbar Cost of Electricity	6-41
References	6-43

	<u>Page</u>
7. SAFETY ASSESSMENT	7-1
7.1 Issues of Concern	7-2
7.2 Methodology of the Safety Assessment	7-7
7.3 Accident-Related Dose Rates Due to Corrosion Products	7-8
7.4 Tritium Dose Rates	7-11
7.5 Engineered Safety Features	7-14
7.5.1 Inerting the Reactor Building Atmosphere	7-14
7.5.2 Reactor Building Overpressurization Following a LOCA	7-16
7.5.3 Ventilation Stack	7-17
7.6 Conclusions	7-17
References	7-20
Appendix A. THERMAL STORAGE SYSTEM (PULSED VERSION)	A-1
A.1 Thermal Storage System	A-1
A.2 Design Features	A-3
A.3 System Operation	A-5
Appendix B. PLASMA DISRUPTION EFFECTS	B-1
B.1 Disruption Characteristics	B-1
B.2 First-Wall Response Models	B-2
B.3 First-Wall Response Analysis	B-8
B.4 Conclusions	B-15
References	B-17

LIST OF FIGURES

<u>No.</u>	<u>Title</u>	<u>Page</u>
1-1	A schematic comparison of WILDCAT and STARFIRE.	1-4
1-2	WILDCAT.	1-6
1-3	Power flow diagrams.	1-11
2-1	WILDCAT flux function, pressure, current, and safety factor profiles.	2-11
2-2	Poloidal field lines and current density.	2-12
2-3	Plasma current drive model.	2-15
2-4	Plasma densities during startup.	2-18
2-5	Radiation power, transport power, and fusion product heating power to the plasma during startup.	2-18
2-6	Plasma ion and electron temperature, deuterium density, and toroidal beta during startup.	2-19
2-7	Plasma current and plasma kinetic energy during startup.	2-19
2-8	D-T, D-D, D- ³ He, and total fusion power during startup.	2-20
2-9	OH and EF current and voltage during startup.	2-20
2-10	Rf and EF power during startup.	2-20
2-11	Cross section of the WILDCAT limiter design.	2-25
2-12	Schematic drawing of the leading edge model.	2-28
2-13	Side view of antenna and Faraday shield.	2-38
2-14	Isometric view of antenna assembly.	2-38
2-15	Circuit schematic including transmission line inside reactor building.	2-39
3-1	Schematic cross section of first wall.	3-2
3-2	WILDCAT first-wall temperature distribution.	3-4
3-3	WILDCAT PCA swelling.	3-5
3-4	WILDCAT first-wall stress distribution.	3-5
3-5	WILDCAT crack growth.	3-6
3-6	Vertical cross section of first wall.	3-8
3-7	Two geometrical models used for one-dimensional nuclear analyses.	3-9
3-8	Spatial variation of neutron fluxes.	3-11
3-9	Neutron spectrum in outboard first-wall blanket.	3-12

<u>No.</u>	<u>Title</u>	<u>Page</u>
3-10	Spatial variation of nuclear heating.	3-12
3-11	Impact of B_4C content upon inboard radiation shielding.	3-17
3-12	Neutron spectrum at inboard shield.	3-17
3-13	Photon spectrum at inboard shield.	3-18
3-14	Radioactivity concentration in the outboard bulk shield.	3-21
3-15	Maximum biological dose in reactor room at 24 h after shutdown.	3-21
3-16	Radioactivity inventory for the WILDCAT design.	3-26
3-17	Isotopic contribution to the PCA blanket radioactivity of the WILDCAT design.	3-30
3-18	First-wall coolant panel and blanket coolant channel layout (outboard wall).	3-34
3-19	Blanket block manifold layout.	3-35
3-20	First-wall/blanket computer model with node representation. ...	3-37
3-21	Steady-state temperature distribution (x-direction) in first-wall/blanket segment (inboard).	3-40
3-22	Steady-state temperature distribution (y-direction) in first-wall/blanket segment (inboard).	3-40
3-23	Steady-state temperature distribution (x-direction) in first-wall/blanket segment (outboard).	3-41
3-24	Steady-state temperature distribution (y-direction) in first-wall/blanket segment (outboard).	3-41
3-25	Mechanical configuration of the limiter and the adjacent first wall, blanket, and shield.	3-44
3-26	Disassembly concepts for the major reactor components.	3-44
4-1	Cutaway view of one coil showing support bars in high load region.	4-5
4-2	Field contours for the WILDCAT steady-state OH systems.	4-9
4-3	Field contours for the WILDCAT pulsed OH system.	4-10
4-4	Field contours for the WILDCAT steady-state EF systems.	4-13
5-1	Schematic of fuel reprocessing loop.	5-1
5-2	Tritium facility scenario for D-T reactor.	5-2
5-3	Schematic of the isotopic separation system for a D-D fusion reactor.	5-7
7-1	External dose rates due to an accidental release of corrosion products.	7-12

<u>No.</u>	<u>Title</u>	<u>Page</u>
A-1	Conceptual design of the thermal storage system necessary for the pulsed version of WILDCAT.	A-2
A-2	Reactor thermal power between pulses.	A-3
B-1	Stainless steel melting zone thickness with no vapor shield as a function of energy density.	B-9
B-2	Evaporation thickness of stainless steel for 1000 disruptions for different energy deposited.	B-9
B-3	Stainless steel melting zone thickness with vapor shield as a function of energy density (Hassanein model).	B-10
B-4	Beryllium maximum melt layer thickness for plasma disruptions of 5, 20, and 60 ms duration (Merrill model).	B-10
B-5	Molybdenum melting zone thickness with no vapor shield as a function of energy density (Hassanein model).	B-11
B-6	Tungsten melt layer thickness for plasma disruptions of 5, 20, and 60 ms duration (Merrill model).	B-11
B-7	Beryllium vaporization depth for plasma disruptions of 5, 20, and 60 ms duration (Merrill model).	B-12
B-8	Evaporation thickness of molybdenum for 1000 disruptions as a function of energy density (Hassanein model).	B-12
B-9	Tungsten vaporization depth for plasma disruptions of 5, 20, and 60 ms duration (Merrill model).	B-13
B-10	Evaporation thickness of carbon for 1000 disruptions as a function of energy density (Hassanein model).	B-13

LIST OF TABLES

<u>No.</u>	<u>Title</u>	<u>Page</u>
1-1	Power Densities for Different Reactor Types	1-3
1-2	A Summary of the WILDCAT Reference Parameters	1-7
1-3	Economic Comparison of STARFIRE and WILDCAT (1980 Dollars)	1-7
2-1	Parameters from Previous Work	2-2
2-2	A Sequence of Possible Design Choices	2-4
2-3	WILDCAT Reference Parameters	2-5
2-4	Power Breakdown in MW for WILDCAT	2-7
2-5	MHD Parameters	2-10
2-6	Sensitivity of WILDCAT to Major Parameter Changes	2-13
2-7	WILDCAT Burn Cycle Parameters	2-15
2-8	WILDCAT Impurity Control System Parameters	2-26
2-9	Limiter Operating Conditions	2-28
2-10	Maximum Calculated Stresses of Leading Edge	2-29
2-11	Wave Frequency and Current Drive Power Versus Parallel Mode Number	2-36
3-1	First-Wall Parameters for Lifetime Calculations	3-3
3-2	Nuclear Response Rates at First Wall	3-11
3-3	X-Ray Attenuation Coefficients of the Photoelectric Reaction for Beryllium and Iron	3-14
3-4	Dimensions and Material Compositions of the Inboard System Used for the Shielding Optimization Analysis	3-16
3-5	Nuclear Response Rates in Toroidal Field Magnets	3-18
3-6	Contact Biological Dose	3-22
3-7	Breakdown of Nuclear Energy Deposition	3-24
3-8	Breakdown of Energy Multiplication by Fusion Neutrons	3-24
3-9	Impact of Inboard Blanket Thickness and Energy Mutiplication on WILDCAT Performance	3-25
3-10	Specific Radioactivity of Reactor Components: MCI/m^3	3-27
3-11	Post-Shutdown Dose of Reactor Components: rem/h	3-28
3-12	Classification of Radioactive Reactor Components	3-29
3-13	Time Required for Biological Dose to Decrease Below 2.5 mrem/h	3-30
3-14	System Decay Heat	3-31

<u>No.</u>	<u>Title</u>	<u>Page</u>
3-15	Zone Average Decay Heating Rate (MW/m ³).....	3-32
3-16	Reactor Room Atmospheric Activation (MCl/m ³)	3-32
3-17	Summary of Thermal Hydraulics Calculations for the Outboard Blanket	3-36
3-18	Summary of Temperature Distribution in First-Wall/Blanket Segment (Inboard)	3-38
3-19	Summary of Temperature Distribution in First-Wall/Blanket Segment (Outboard)	3-39
4-1	Parameters for WILDCAT TF Magnets	4-2
4-2	Comparison of Candidate Materials for Coil-to-Coil Support	4-6
4-3	OH System Parameters	4-8
4-4	Steady-State OH System Coil Locations and Currents	4-8
4-5	EF System Parameters	4-12
4-6	Steady-State EF System Coil Locations and Currents	4-12
4-7	CF System Parameters	4-14
5-1	Mass Flow Rates for WILDCAT (Cat-D) Versus STARFIRE (D-T)	5-3
5-2	WILDCAT Vacuum Pumping Parameters	5-5
5-3	Product Compositions for Three-Column Cascade (30-Plate Column)	5-8
5-4	Product Compositions for Three-Column Cascade (50-Plate Column)	5-8
5-5	Product Composition for Redistillation of Heavy Fraction from Column 1	5-8
5-6	Distillation Column Data	5-9
5-7	Tritium Inventories (g)	5-10
5-8	Tritium Source Terms	5-11
6-1	Summary of Capital Costs	6-2
6-2	Capital Costs	6-6
6-3	First-Wall/Blanket Costs	6-17
6-4	Shielding Costs	6-18
6-5	Cost of the Magnets (Steady State)	6-19
6-6	Cost of the Magnets (Pulsed)	6-20
6-7	Cost of the CAW Heating/Current-Drive System	6-22
6-8	Primary Structure and Support Systems Cost	6-22

<u>No.</u>	<u>Title</u>	<u>Page</u>
6-9	Primary Structure Cost Trade Studies	6-23
6-10	Reactor Vacuum System Costs	6-24
6-11	Power Supply, Switching, and Electrical Storage	6-25
6-12	Comparison of STARFIRE and WILDCAT Thermal and Electrical Powers	6-27
6-13	Main Heat Transfer and Transport System Costs	6-27
6-14	Comparison of Coil Dewar Volumes	6-28
6-15	Cryogenic System Costs	6-28
6-16	Fuel Handling and Storage System Costs	6-29
6-17	Other Reactor Plant Equipment Costs	6-30
6-18	Cost of the Reactor Plant Equipment Spare Parts	6-31
6-19	Thermal Storage System Costs	6-33
6-20	Costs of the Electrical Plant Equipment	6-35
6-21	Costs of the Miscellaneous Plant Equipment	6-36
6-22	Operations and Maintenance Costs	6-39
6-23	Scheduled Component Replacement Costs	6-40
6-24	Economic Comparison of STARFIRE and WILDCAT	6-43
7-1	System Decay Heat in WILDCAT Versus STARFIRE	7-3
7-2	WILDCAT Zone Average Heating Rate (MW/m ³)	7-3
7-3	Inductive Energy Stored in WILDCAT and STARFIRE Magnet Systems	7-7
7-4	Structural Material Composition: PCA Versus Type 316 Stainless Steel	7-9
7-5	Design Goals for Tritium Handling	7-13
7-6	WILDCAT Reactor Building Atmospheric Activation (MCi/m ³)	7-16
B-1	WILDCAT Disruption Times	B-3
B-2	Required Energy Densities for Several Phenomena	B-14
B-3	Vaporization Thickness for a 60-ms Disruption with Vapor Shielding	B-15

ACKNOWLEDGMENTS

Contributions to this report were made by P. A. Finn in the area of tritium handling and by Y. Gohar in the area of neutronics. E. Singleton provided coordination of the drafting services and significant input to the engineering design. Cyrilla Hytry was responsible for the typing and final assembly of the report.

ABSTRACT

WILDCAT is a conceptual design of a catalyzed D-D, tokamak, commercial, fusion reactor. WILDCAT utilizes the beneficial features of no tritium breeding, while not extrapolating unnecessarily from existing D-T designs. The reactor is larger and has higher magnetic fields and plasma pressures than typical D-T devices. It is more costly, but eliminates problems associated with tritium breeding and has tritium inventories and throughputs approximately two orders of magnitude less than typical D-T reactors. There are both a steady-state version with Alfvén-wave current drive and a pulsed version. Extensive comparison with D-T devices has been made, and cost and safety analyses have been included. All of the major reactor systems have been worked out to a level of detail appropriate to a complete, conceptual design.

1. INTRODUCTION

WILDCAT is a conceptual design of a deuterium-fueled, commercial, tokamak reactor. The primary purpose of the study has been to assess the consequences of the deuterium fuel cycle when all of the tradeoffs, constraints, and optimizations of an integrated design are considered. This report presents a detailed analysis of the WILDCAT device including both a steady-state and a pulsed version and a comparison with similar D-T devices, in particular STARFIRE.¹ A previous report² treated the studies which led to the choice of the important WILDCAT parameters. The pulsed version is described mainly in that report. The steady-state version is developed in this report and is the reference version.

This introduction presents the scope and guidelines of the study, an overview of the principle features of WILDCAT, and a summary of conclusions regarding WILDCAT in particular and D-D tokamak reactors in general. Section 2 includes a description of the reference parameters, including those associated with the MHD equilibrium, and the sensitivity of the design to these parameters as well as a description of the burn cycle, the limiter impurity control concept, the Alfvén-wave current driver, and the ECRH preionization system. The analysis of the first-wall lifetime and the nuclear analysis of the blanket and shield are presented in Sec. 3 along with thermal hydraulic considerations and a description of maintenance and repair procedures. Section 4 describes the four magnetic systems: toroidal coils, ohmic heating coils, equilibrium field coils, and correction field coils. The fuel processing and tritium handling systems are discussed in Sec. 5. An extensive cost analysis, which is directly comparable to the STARFIRE costing, is presented in Sec. 7. A description of the thermal storage system required for pulsed operation and an analysis of the problems associated with disruptions are treated in the two appendices.

1.1. Scope and Guidelines

WILDCAT has been a two-year study with the goal of developing an attractive and well-defined conceptual design for an alternate-fueled reactor. It is the first in-depth study of a deuterium-fueled tokamak reactor. The deuterium-based fuel cycle has been chosen because it is substantially closer

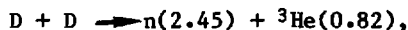
to practical realization than other alternate fuel cycles. In a similar manner, the tokamak configuration has been chosen because it has been more extensively studied and is probably closer to reactor viability than any other concept. In particular, the choice has been to make WILDCAT a commercial, tokamak reactor that is similar in purpose to STARFIRE¹ in order to have a convenient means of comparison between D-D and D-T systems.

The primary guideline has been to make as much use as possible of the beneficial features of the D-D fuel cycle, that is, of not breeding tritium, while at the same time not extrapolating unnecessarily from existing D-T tokamak designs, in particular STARFIRE. In this way, a fair comparison of the advantages and penalties of a D-D reactor relative to a D-T reactor can be made.

WILDCAT is not a modification of STARFIRE. It is a complete reactor study in itself and has been optimized from the initial design stages for D-D operation. On the other hand, many of the systems do not have to be essentially different from the corresponding systems in STARFIRE. It is thus possible to use much of the STARFIRE analysis, so that WILDCAT is a reasonably well-defined system even though the effort that has gone into the study is less than the STARFIRE effort.

1.2. Overview

A D-D reactor for the purposes of this study is one for which the only source of fuel is deuterium and which does not breed tritium. The important reactions in a D-D reactor are:



where the energies of the reaction products are shown in MeV. The tritium and ³He which are produced by fusion reactions in the plasma and which diffuse out instead of reacting with the deuterium may be reinjected. If all of the tritium and ³He is replaced, the reactor is termed a Semi-Cat-D reactor. WILDCAT is fully catalyzed (Cat-D), since reinjection of the tritium and ³He provides the best reactor performance.

The major disadvantage of a D-D reactor is that the reaction rates are substantially lower than for D-T. The reactivities, $\langle\sigma v\rangle$, of the last three reactions are significantly lower than those for D-T. The D-T reaction rate is also low because there is not much tritium in the absence of tritium fueling. This effect can be seen quantitatively in Table 1-1, which shows the power densities in WILDCAT if it were operated as a D-T, D-³He, or D-D reactor. Some of this disadvantage can be made up by a more efficient blanket/shield since there are no constraints regarding tritium breeding, but the power density is still substantially more than an order of magnitude less than for a D-T reactor.

Table 1-1. Power Densities for Different Reactor Types

All of the cases have the WILDCAT plasma parameters except there is no iodine impurity. Neutron energy multiplication in the blanket/shield has not been included.

Reactor Type	\bar{T}_e (keV)	Power Density (MW/m ³)
D-T	10	83
	30	13
D- ³ He	30	1
Cat-D	30	1

As a consequence, in order to have a reasonable power output for WILDCAT, it is necessary to increase the size, the toroidal field, and/or the plasma beta relative to values for, say, STARFIRE. These are the three parameters which most influence the power apart from the plasma temperatures and the reactivities. The choice for WILDCAT has been to extend each of these parameters somewhat from the STARFIRE values and to also produce less thermal power. In this case no individual parameter is unreasonably extrapolated beyond a value considered viable for STARFIRE. A schematic comparison of WILDCAT and STARFIRE is shown in Fig. 1-1. The increase in size is readily apparent. The thicker coils are an indication of the higher field. It can also be seen that the space between the plasma and the peak field position of the toroidal coils has been reduced in order to make more effective use of the

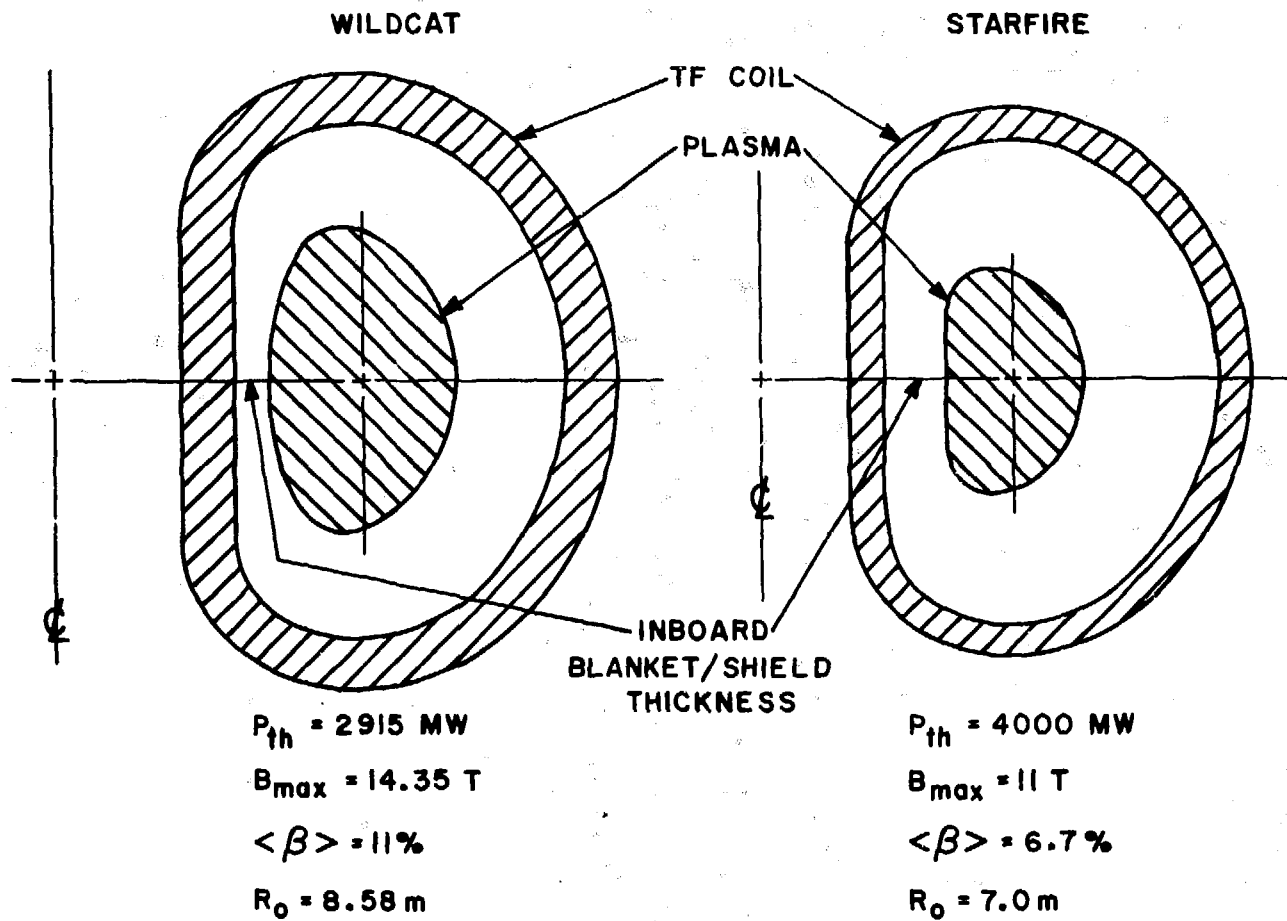


Fig. 1-1. A schematic comparison of WILDCAT and STARFIRE.

toroidal field. This is possible since the inboard blanket/shield can be made thinner when there is no tritium breeding. In addition, the plasma has been made less D-shaped, which reduces the requirements on the equilibrium field coil system.

In all fairness, both WILDCAT and STARFIRE would probably operate at the same value of beta (the highest practical), but at the present time that value is not known. Consequently, the choice has been made to extend all of the parameters in order not to extend any one of them excessively. In all likelihood, a higher beta in STARFIRE would not result in a higher power density and smaller reactor. The wall loading in STARFIRE was primarily determined by first-wall/blanket design and materials considerations. Thus, a higher beta in STARFIRE would likely result in a correspondingly lower toroidal magnetic field, with the other features remaining unchanged.

WILDCAT is shown in cross section and plan view in Fig. 1-2 and the important reference parameters are listed in Table 1-2. Additional parameters are given in Tables 2-1 and 2-3 as well as throughout the report. Two versions have been considered: a steady-state version and a pulsed version. The steady-state version, which is more desirable from many points of view, relies on an efficient rf current drive using compressional Alfvén waves. This driver requires 120 antennas inside the chamber leading to maintenance and reliability problems but also to increased coupling efficiency. The pulsed version, while less speculative for current drive, is more expensive because of the power supplies and the large thermal storage system required.

Two versions have been developed because it is not clear that steady-state operation is as practical for a D-D reactor as it appears to be for a D-T reactor.¹ For a D-D reactor with its typically larger plasma current and/or lower fusion power, the current driver requires a larger fraction of the gross electric power than for a similar D-T system, so much so that unless a very efficient current driver, such as the Alfvén waves, is possible, steady-state operation is not feasible. The lower hybrid wave current drive used for STARFIRE, for example, would not be practical for WILDCAT.

It is necessary to operate WILDCAT at a higher temperature, $\bar{T}_e = 30$ keV, than STARFIRE: Typically, an ignited plasma cannot be achieved for $\bar{T}_e \lesssim 25$ keV, depending on the plasma density and temperature profiles. This higher temperature operation is a further disadvantage. (Table 1-1 shows the decrease in power density for a D-T reactor if it were operated at 30 keV.)

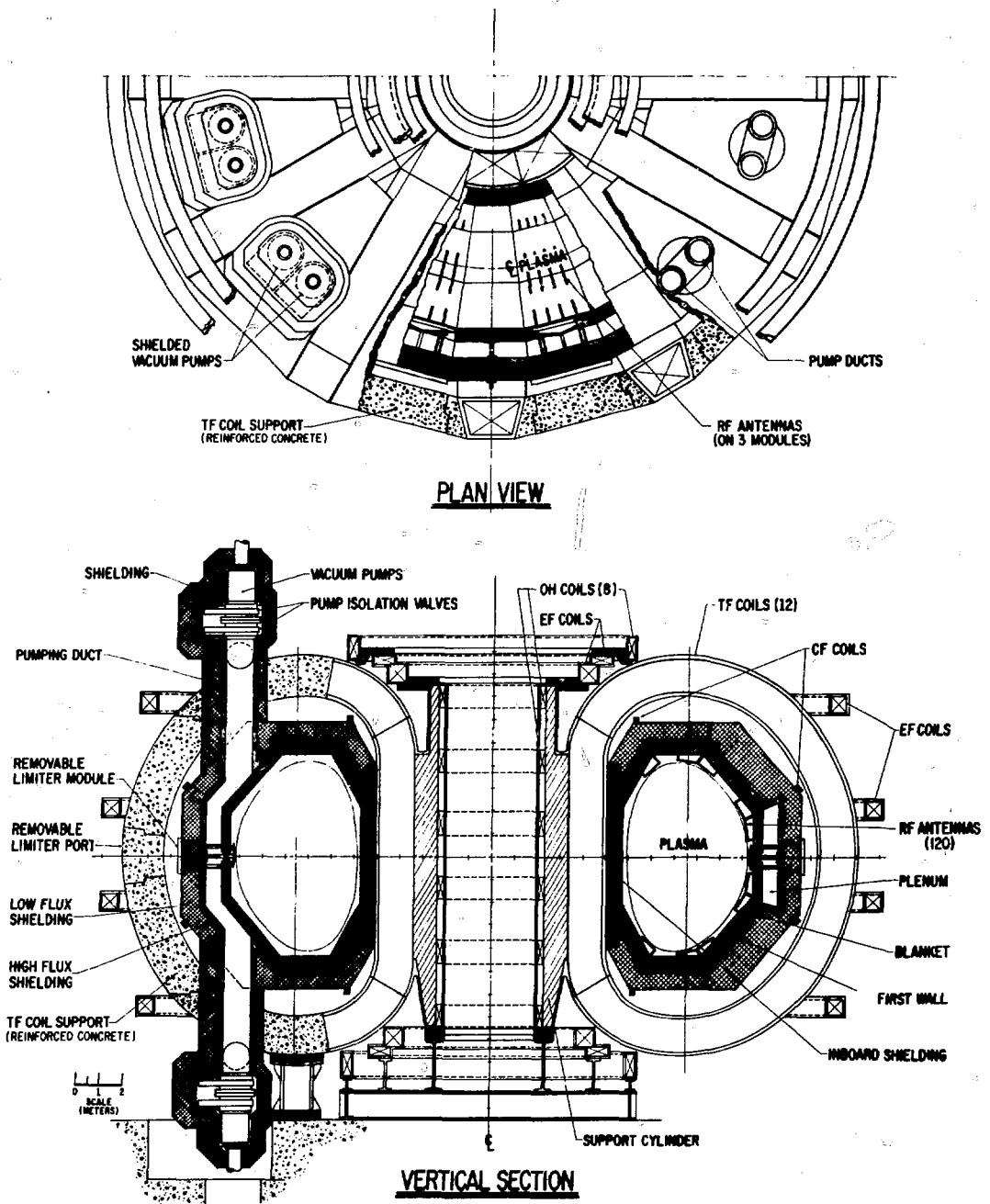


Fig. 1-2. WILDCAT.

Table 1-2. A Summary of the WILDCAT Reference Parameters

Parameter	Steady-State	Pulsed
Major radius, m	8.58	8.58
Aspect ratio, A	3.25	3.25
Peak toroidal field, T	14.35	14.0
Plasma beta	0.11	0.11
Average electron temperature, keV	30	30
Plasma current, MA	29.9	29.2
Plasma elongation	1.6	1.6
Safety factor		
Edge	3.0	3.0
Axis	1.0	1.0
Neutron wall load, MW/m ²		
14.06 MeV	0.50	0.46
2.45 MeV	0.10	0.09
Net heat load, MW/m ²	1.00	0.83
Thermal power, Gwt	2.9	2.6
Net electric power, MWe	810	850

Table 1-3. Economic Comparison of STARFIRE and WILDCAT (1980 Dollars)

Parameter	STARFIRE	WILDCAT	
		Steady-State	Pulsed
Plant capacity, MW	1200	812	849
Cost of reactor plant equipment, M\$	969	1497	1885
Total capital cost, constant, M\$	2400	3077	3844
Cost of capacity, constant, \$/kWe	2000	3788	4528
Cost of energy, constant, mills/kWh	35.1	62.8	73.8

Since WILDCAT does not have to breed tritium, the blanket/shield can be optimized to have a thinner inboard extent (82 cm vs. 120 cm for STARFIRE) leading to more efficient use of the toroidal field and to increased neutron energy multiplication (2.02 vs. 1.14). These benefits help to overcome the reduced reaction rates and lead to a 60% more efficient blanket in terms of

power generation. In addition to enjoying increased blanket energy multiplication, the blanket/shield has been designed for personnel access after 24 h and uses as much as possible materials which are not resource limited and which have lower activation. Ninety percent of the material in WILDCAT can be recycled after 40 y.

About one-half of the neutrons produced in WILDCAT are 14-MeV, D-T neutrons. Their blanket neutron energy multiplication is 1.54 and they contribute about 33% of the thermal power. Even though WILDCAT is termed a D-D reactor, the largest single source of power (38%) is, in fact, the neutrons and heating from the D-T reaction. The 2.5-MeV, D-D neutrons have a higher energy multiplication of 4.43, but only contribute 19% of the thermal power. The remainder of the thermal power comes from fusion heating (45%) and rf heating (<4%). A further breakdown of the power production is given in Table 2-4. The numbers given are for the steady-state case, but the pulsed case is not essentially different apart from having no rf heating.

The first wall is PCA stainless steel consisting of a corrugated plate bonded to a backing plate. There is a 3-mm beryllium cladding bonded to the corrugated part, which faces the plasma. Light-water coolant flows in the closed part of the corrugations. The configuration is shown in Fig. 3-1. The lifetime is estimated to be 20 y, or half of the expected plant life, and is limited primarily by sputtering loss of the beryllium cladding. The longer lifetime (compared to STARFIRE with a 6-y replacement schedule for first-wall/blanket sections) is due to the lower neutron flux of the D-D fuel cycle for a fixed heat load on the wall. The heat load is 1 MW/m² for both STARFIRE and the steady-state version of WILDCAT. The pulsed version is limited to less than this value because of increased materials damage resulting from the pulsed loading.

The WILDCAT steady-state burn cycle is characterized by long start-up and shut-down times to minimize power supply requirements and extra tritium and ³He injection to provide heating during startup. The burn cycle starts with a 19-s "ohmic heating" period during which enough current (1 MA) is induced for the rf current drive to take over. This is followed by a 20-min "current inducement" period with low deuterium density and rf heating from the Alfvén waves at 107 MW. After a "fusion power ramp" period of 19 min with extra tritium and ³He, the plasma is brought to full operating conditions, and

iodine is added for burn control. The burn then continues for typically up to 6 mo. Shutdown is similar to startup. The small amount of extra tritium and ^3He for startup is recovered and stored during the rest of the cycle.

The pulsed version burn cycle is described in Ref. 2. The startup and shutdown are necessarily faster, and all of the current is generated by the poloidal coils. The power supply requirements for the ohmic heating and equilibrium field system are substantially larger. In addition, thermal storage is required to keep the power to the turbine constant during the dwell period between cycles. The D-D reactor requires a substantially higher value of $n\tau$, but the confinement is still compatible with empirical scaling laws.³ Impurity control is via a pumped limiter. The heat loads on the limiter are somewhat higher than for STARFIRE, but a limiter similar to that for STARFIRE is expected to be adequate.

Disruptions present a potential problem for WILDCAT. Because of the large amount of energy stored in the plasma (8.3 GJ vs 1.1 GJ for STARFIRE and 240 MJ for INTOR⁴), disruption scenarios which are marginal for other devices become deleterious for WILDCAT, involving more melting and vaporization of the wall. No solutions to this problem have been identified for WILDCAT except to operate the plasma in a mode where disruptions do not occur, except perhaps as very low probability accidents. It is not unreasonable to expect our understanding of plasma behavior to be sufficiently advanced for this to be possible by the time that one would consider building WILDCAT, and quite likely similar requirements would be necessary for other than near-term devices in any event. A small number of disruptions should not be catastrophic.

The high toroidal fields (14.35 T for the steady-state version and 14.0 T for the pulsed version) present problems primarily related to the stresses, which increase as the square of the field. The conductor design itself is similar to that for STARFIRE, utilizing various amounts of Nb_3Sn in the regions with different field strengths. Substantially more material, however, is required. The out-of-plane loads are supported by filling essentially all of the space between the outer legs of the toroidal field coils with reinforced concrete, as shown in Fig. 1-2. There are three blocks (upper, middle, and lower) between each coil. The middle block has a plug for access to the limiter, which can be removed as a drawer-like unit, and the rest of the interior of the machine, especially the current-drive antennas. This support

concept is relatively inexpensive and appears to adequately handle the large forces. A detailed structural analysis has not been performed, however.

A small ohmic heating system has been supplied for the steady-state case, and a larger, conventional ohmic heating system with a solenoid, for the pulsed case. The pulsed reactor design is substantially constricted by the need to supply a large number of volt-seconds (695). The plasma has been made less D-shaped to reduce the requirements on the equilibrium field system. For the pulsed version these two systems represent a large, additional cost item.

The real advantages of WILDCAT lie in not having to breed tritium and in reduced tritium inventories and throughputs. Both factors should lead to increased safety. It should be noted, however, that the higher magnetic fields in WILDCAT would probably result in increased magnet safety issues compared to STARFIRE. This study has not made an in-depth safety comparison of DT-fueled and alternate-fueled fusion reactors, nor could this be done at this time. The benefits of not breeding tritium, including not having to deal with liquid lithium or not having to extract tritium from solid breeders, are also difficult to quantify at this time. It is, however, most likely that the ease with which tritium can be bred will determine the desirability of D-D reactors.

The reduced tritium inventories and throughputs in WILDCAT (approximately two orders of magnitude less than for STARFIRE) are, however, a significant and quantifiable advantage. The vulnerable inventory is 15 g vs. 397 g for STARFIRE, and the nonvulnerable inventory is 20 g (33 g for the pulsed version) vs. 11,000 g for STARFIRE. The tritium throughput is 10 g/day vs. 760 g/day for STARFIRE. Normal releases of tritium are reduced from 13 Ci/day to 0.31 Ci/day, and accidental releases are reduced from 10 g to 0.56 g. In addition, no significant inventory of the more toxic HTO or T₂O has been identified. Additional savings lie in longer-lived vacuum pump valves (plant life vs. 2 y for STARFIRE) and lack of necessity for a ventilation stack. Even with the reduced inventories, there is still enough tritium present that no major tritium handling systems could be eliminated, and in view of the higher gas loads, the tritium/vacuum/fuel system is roughly the same size as for STARFIRE.

The power flow diagrams for WILDCAT are shown in Fig. 1-3. It has been determined that the turbine could have a high efficiency (35.7%, same as for STARFIRE), helped in part by using the lower-grade heat from the limiter as

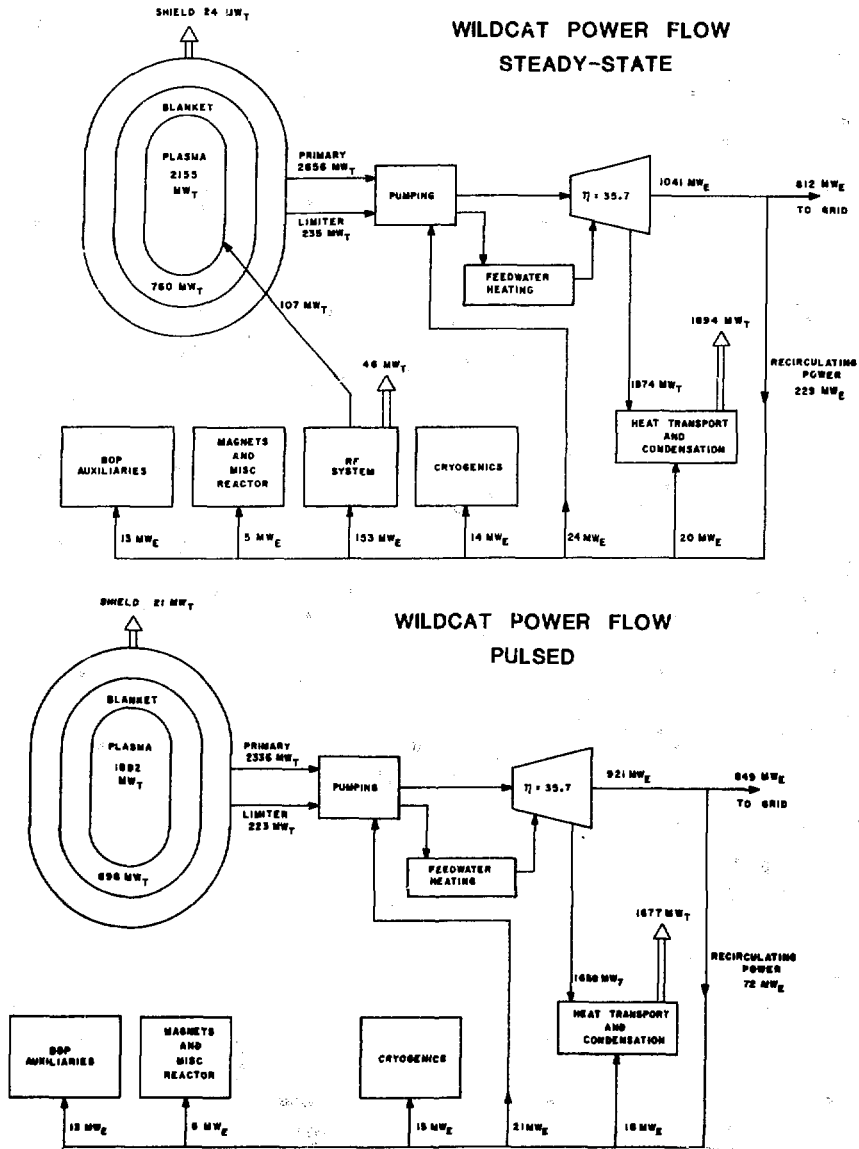


Fig. 1-3. Power flow diagrams.

feedwater heating. The main difference in the two flow diagrams is the lack of the rf system as a net power loss in the pulsed case.

WILDCAT has been costed in a manner exactly analogous to that for STARFIRE. A summary of the cost analysis is shown in Table 1-3. Both the steady-state (\$3077 M) and the pulsed (\$3843 M) WILDCAT power plants are considerably more costly than the comparable STARFIRE design (\$2400 M). These cost increases are principally due to the more massive reactor. The toroidal field coils are also larger and have four times the stored energy. The pulsed WILDCAT power supplies are an order of magnitude larger than those for the steady-state system. The reactor power output is reduced from STARFIRE, which lowers the balance of plant costs. The structures costs remain essentially the same as for STARFIRE. The net result is a significant increase in capital costs. When this capital cost is coupled with the reduced net power output, the WILDCAT cost of electricity is increased over the STARFIRE design by 180% for the steady-state design and by 210% for the pulsed design. Both designs, of course, have many assumptions which could substantially impact the cost.

1.3. Conclusions

A D-D reactor such as WILDCAT is quite similar to a D-T device in that approximately one-half of the neutrons produced are 14-MeV neutrons from the D-T reaction, and most of the energy comes from these D-T neutrons. It is, in fact, largely a D-T reactor operated without tritium fueling.

The principal advantages of the D-D reactor arise from the lack of necessity to breed tritium. This feature makes the use of lithium and lithium compounds unnecessary. In addition, the blanket/shield can be optimized for reactor power performance rather than for tritium breeding. In particular, the inboard section can be made thinner, leading to better utilization of the toroidal magnetic field, and increased neutron energy multiplication can be achieved, leading to a greater power output. The tritium levels in a D-D reactor appear to be as much as two orders of magnitude less than in a comparable D-T reactor. This can lead to increased safety, and perhaps reduced requirements on components such as piping. However, there is still sufficient tritium that it is not possible to eliminate any major components of a D-T tritium-handling system if worker and public safety is to be assured.

The principal disadvantage of a D-D reactor is that the plasma power density is less than 2% of that of a tritium-fueled reactor. As a consequence, a D-D reactor must necessarily be substantially larger and/or operate at substantially higher fields or higher plasma betas than a D-T reactor of comparable thermal power. The design of larger devices and higher-field magnets is, of course, more difficult. Moreover, since the auxiliary systems, such as plasma heating, current drive, magnet power supplies, and vacuum pumping are then typically larger, the parasitic power losses represent a larger fraction of the thermal power, resulting in lower efficiency and even further reduced net electric power. The larger energy stored in the plasma is a more serious problem in the event of a plasma disruption.

A second disadvantage is that a D-D reactor must likely operate at higher temperatures (25-30 keV compared to 8-10 keV for a typical D-T system). Cyclotron and bremsstrahlung radiation losses both increase with temperature. It is not known if diffusion losses increase or decrease with temperature in these temperature ranges, but there are models such as ripple diffusion and trapped particle modes which show losses increasing strongly with temperature. These factors affect the achievement of ignition. Using the assumptions made in the present study, ignition in a D-D reactor appears to require an order-of-magnitude larger confinement parameter, $n\tau$, and an order-of-magnitude fewer impurities compared to a D-T reactor.

A third feature of a D-D reactor is that a larger fraction of the power coming out of the plasma is in the form of heat (charged particles or radiation) rather than neutrons. If neutron damage of the first-wall/blanket/shield system were the limiting factor, this would be an advantage. For the type of design considered in this report, this becomes a disadvantage for a D-D reactor. STARFIRE, for example, supports a total wall load of 4.8 MW/m² with a heat load of 1.0 MW/m², while the WILDCAT steady-state version supports a total wall load of only 1.7 MW/m² for the same heat load. The reduced neutron flux does lead to longer life for the first-wall/blanket, however.

It is especially difficult to overcome the disadvantage of lower power production, and it would seem that D-D reactors would not be built for power production if it were possible to utilize D-T reactors. If, however, D-T reactors (because of problems associated with tritium fueling and/or breeding or lifetime limitations due to neutron damage effects) are not feasible, then D-D

reactors could likely be built in their place with reasonable extrapolations of parameters considered adequate for D-T reactors.

REFERENCES

1. C. C. Baker, et al., "STARFIRE - A Commercial Tokamak Fusion Power Plant Study," Argonne National Laboratory, ANL/FPP-80-1 (1980).
2. K. Evans, Jr., et al., "D-D Tokamak Reactor Studies," Argonne National Laboratory, ANL/FPP/TM-138 (1980).
3. D. R. Cohn, R. R. Parker, and D. L. Jassby, Nucl. Fusion 16, 31 (1976); and D. L. Jassby, D. R. Cohn, and R. R. Parker, Nucl. Fusion 16, 1045 (1976).
4. W. M. Stacey, et al., "U. S. INTOR," United States INTOR Group, USA INTOR/81-1 (1981).

2. PLASMA ENGINEERING

This section presents plasma engineering analyses for the major aspects of WILDCAT. Section 2.1 contains a description of the reference design and the rationale for the parameter choices with discussions of the MHD equilibrium in Sec. 2.2 and the sensitivity to the important parameter choices in Sec. 2.3. The burn cycle is described in Sec. 2.4 along with impurity control in Sec. 2.5. The current-drive concept appears in Sec. 2.6, and the ECRH startup is described in Sec. 2.7. These analyses are typically similar to those done for D-T systems, but the range of parameters is often different.

2.1 Reference Design

In Ref. 1 a number of studies leading to the choice of parameters for the pulsed version of WILDCAT were described. In many cases the same choices are also applicable to the steady-state, reference version. In particular, the blanket/shield thickness, scrapeoff thickness, beryllium concentration, plasma temperatures, density and temperature profiles, cyclotron reflection coefficient, confinement time ratios, particle reflection coefficients, as well as most MHD equilibrium parameters, have been chosen the same as in Ref. 1. The values of these parameters are listed in Table 2-1. As for the pulsed version, the steady-state version is assumed to be fully catalyzed; that is, all of the tritium and ^3He that diffuses out is replaced into the plasma.

It is useful to review the reasons for selecting some of the more important parameters. The impurity concentration, which is represented as the concentration of a single species, beryllium, was chosen to be a little more than half the maximum fractional concentration of beryllium that would still allow ignition. This allows some margin for operation. It was shown in Ref. 1 that for a given species the maximum concentration that would allow ignition is an order of magnitude less for a D-D reactor than it would be for a D-T reactor, as well as that the allowed concentration decreases approximately exponentially with atomic charge. It has not been demonstrated, of course, that a reacting plasma can be kept as clean as the 3% beryllium concentration would indicate. In addition to beryllium another impurity, taken to be iodine in the WILDCAT design, is added to increase the radiation and hence reduce the heat load on the limiter as well as to provide burn control. This is possible

Table 2-1. Parameters from Previous Work

Plasma elongation, ^a κ	1.6
Plasma D-shapedness, ^a d	0.2
Safety factor at limiter, $q(a)$	3.0
Safety factor at axis, $q(0)$	1.0
Average electron temperature, \bar{T}_e (keV)	30
Cyclotron reflection coefficient, Γ_c	0.9
Ratio of particle to electron energy confinement times, τ_p/τ_E	0.25
Ratio of ion energy to electron energy confinement time, τ_I/τ_E	4.0
Pressure profile exponent, ^b α_p	1.4
Density profile exponent, ^b α_n	0.7
Temperature profile exponent, ^b α_T	0.7
Beryllium concentration, \bar{n}_{Be}/\bar{n}_D	0.03
Proton recycling coefficient, R_p	0.90
⁴ He recycling coefficient, R_{He}	0.75
Scrapeoff width, Δ_v (m)	0.2
Inner blanket/shield thickness, Δ_{BS}^i (m)	0.82

^aThe plasma boundary is specified by:

$$R = R_0 + a \cos(\theta + d \sin \theta) \text{ and } Z = \kappa a \cos \theta$$

where R_0 and a are the major and minor radii.

^bThe profiles are proportional to $\hat{\psi}_\alpha$, where $\hat{\psi} = (\psi_\ell - \psi)/(\psi_\ell - \psi_m)$.

ψ is the MHD flux function, and ψ_ℓ and ψ_m are its values at the limiter and axis, respectively.

since the confinement required for ignition in WILDCAT does not have to be as good as the empirical scaling laws² indicate it would be. Iodine is added until the required confinement time for power balance is equal to that predicted by empirical scaling.

The average electron temperature, \bar{T}_e , is chosen to be slightly higher than the lowest temperature that allows ignition, because the performance is better for lower temperatures. The reason the performance is better at lower temperatures is related to the fact that the peak temperature in the plasma (the temperature at which most of the power is produced) is beyond the maximum in $\langle \sigma v \rangle / T^2$ for all of the D-D reactions whenever it is high enough (~50 keV)

to allow ignition. For the density and temperature profiles chosen (somewhat arbitrarily, since the plasma transport is not known for a high-temperature, reacting plasma) the lowest average temperature is 25-30 keV. The peak temperature is 45-50 keV, relatively independent of the profiles.

The most important parameters are the maximum toroidal field, B_{TFC} , the major radius, R_0 , and the total average plasma beta, β_t , since the power is proportional to $B_{TFC}^4 R_0^3 \beta_t^2$ for a beta limited device. The major disadvantage of a D-D reactor is that it has less than 5% of the reactivity of a D-T reactor even after improvements such as blanket/shield optimization have been made. For WILDCAT it has been chosen to compensate for this disadvantage by making the toroidal field, the major radius, and the plasma beta a little larger and the power a little less than values for a typical commercial reactor such as STARFIRE.³ It could be argued that the plasma beta would probably be the same (the highest possible value) for both WILDCAT and STARFIRE. The situation with regard to beta limits is, however, uncertain. Beta values as high as those specified for either STARFIRE or WILDCAT have not yet been obtained, and the theory is also not definitive. Current experimental and theoretical programs are expected to resolve these uncertainties in the next several years. Similarly, no large, toroidal, superconducting magnets with the fields required by either STARFIRE or WILDCAT have been built; however, there is substantial confidence that such technology could be developed. In view of the nature of both of these design studies, it was deemed most appropriate to extend each of the important parameters so that none of them would be an unreasonable extrapolation from STARFIRE.

The aspect ratio, A, is the last of the important parameters to be discussed here. In Ref. 1 a sequence of reactors differing in aspect ratio, but having the same values of wall load, ohmic-heating magnetic field swing, and MHD credibility was presented. A choice was made among these based on the considerations of the last paragraph. For the RF-driven, steady-state case the ohmic-heating field swing is not a restriction, allowing some extra freedom in choosing design parameters.

A similar sequence of steady-state reactors with Alfvén wave current drive is shown in Table 2-2. These devices all have a net first-wall heat load of 1 MW/m² a maximum toroidal field of 14 T, and sufficient iodine to make the required confinement equal to that predicted by empirical² scaling,

Table 2-2. A Sequence of Possible Design Choices

All have the same net first-wall heat load, $P_{w,heat,net} = 1.0$ MW/m², and the same toroidal field, $B_{TFC} = 14$ T. The plasma beta is assumed to scale as 0.36/A. Iodine has been added to make $\alpha_{EMP} = 1$. The average temperature is $\bar{T}_e = 30$ keV.

A	R ₀ (m)	B _t	I _p (MA)	$\bar{n}_D \tau_E$ (10 ²⁰ s/m ²)	P _T (GW)	P _{RF} (MW)	\bar{n}_I/\bar{n}_D (10 ⁻⁵)
2.4	8.8	0.15	48	38	3.8	150	4.4
3.0	8.8	0.12	34	30	3.2	116	4.0
3.25	9.1	0.11	31	28	3.1	115	3.8
3.5	9.5	0.10	29	27	3.2	118	3.7
4.0	10.5	0.09	26	26	3.4	128	3.4

that is, $\alpha_{EMP} = 1$. (α_{EMP} is the ratio of the required confinement to that predicted by empirical scaling.²) The net heat load consists of the heat load from the radiation power and from one-half the charged particle diffusion power from the core of the plasma. The other half of the charged particles are assumed to hit the limiter. The value of 1 MW/m² for the net heat load was determined in Ref. 3 to be the maximum permissible from failure considerations for a steel structure. The value of 14 T for the field strength is also considered to be near the practical design limit. The plasma beta has been assumed to scale as 0.36/A. This gives fairly optimistic values for β_t , but the scaling (for equal MHD credibility) is consistent with Ref. 4. (STARFIRE falls on a similar sequence scaling as 0.24/A.)

Simple cost estimates indicate that both the capital costs and the cost of electricity for the choices in Table 2-2 are the same within the limits of errors in the costing. In view of this insensitivity to cost a reactor similar to that chosen in Ref. 1 for the pulsed version was taken as the reference case in order to make use of much of the analysis already done for the pulsed version. The magnetic field was raised slightly to raise the net heat load up to 1 MW/m². The steady-state reference parameters along with those for the pulsed version are given in Table 2-3.

The steady-state version, rather than the pulsed, has been chosen as the reference case because steady-state operation solves many design problems.

Table 2-3. WILDCAT Reference Parameters
(The numbers in parenthesis are for the pulsed version.)

Major radius, R_0 (m)	8.58
Aspect ratio, A	3.25
Peak toroidal field, B_{TFC} (T)	14.35 (14.0)
No. of TF coils, N_{TFC}	12
Total average plasma beta, β_t	0.11
Plasma current, I_p (MA)	29.9 (29.2)
Temperature (keV)	
Average electron, \bar{T}_e	30
Peak electron, T_{e0}	52
Average ion, \bar{T}_e	32
Average densities (m^{-3})	
Proton, \bar{n}_p	$1.2 (1.1) \times 10^{19}$
Deuterium, \bar{n}_D	$1.7 (1.7) \times 10^{20}$
Tritium, \bar{n}_T	$8.2 (7.8) \times 10^{17}$
Helium 3, \bar{n}_3	$1.9 (1.8) \times 10^{19}$
Helium 4, \bar{n}_4	$5.0 (4.3) \times 10^{18}$
Electron, \bar{n}_e	$2.6 (2.4) \times 10^{20}$
Impurities	
Beryllium, \bar{n}_{Be}/\bar{n}_D	0.03
Iodine, \bar{n}_I/\bar{n}_D	$3.8 (2.2) \times 10^{-5}$
Energy confinement parameter, $\bar{n}_D \tau_E$ (s/ m^3)	$2.7 (2.4) \times 10^{21}$
14.06-MeV neutron multiplication, $\epsilon_{14.06}$	1.54
2.45-MeV neutron multiplication, $\epsilon_{2.45}$	4.43
Wall loading: total, P_w (MW/ m^2)	1.7 (1.5)
14.06-MeV neutron, P_w (14.06)	0.50 (0.46)
2.45-MeV neutron, P_w (2.45)	0.10 (0.09)
Charged particle, $P_{w,diff}$	0.13 (0.13)
Radiation, $P_{w,rad}$	0.87 (0.70)
Net heat, $P_{w,heat,net}$	1.00 (0.83)
Rf heating power, P_{rf} (MW)	107 (0)
Thermal power, P_T (GWt)	2.9 (2.6)
Net electric power, P_e (MWe)	810 (850)

If, however, the rf current drive were lower-hybrid waves, as for STARFIRE, the auxiliary power required to drive the rf system would be too large a fraction of the thermal power to be practical. There are two effects that cause this to be so. First, the plasma current is higher, requiring more rf power, and second, the thermal power is less because of the lower reactivities. The Alfvén-wave current drive has one of the highest current-to-required-power ratios of candidate current drivers, and it is only because of this low power requirement that the steady-state version of WILDCAT is viable. It should be recognized that STARFIRE could also be made more efficient if Alfvén wave current drive could be used. A further description of current drive is given in Sec. 2.6.

The power breakdown for the steady-state reference version is shown in Table 2-4. It can be seen that most of the energy comes from the D-T reaction. The major source of plasma heat, however, is from the D-³He reaction, and nearly all of this energy is necessary for the ignited operation. For this reason it is difficult to divert any of the ³He to run separate D-³He reactors, for example.

2.2 MHD Considerations

The only important feature of the MHD equilibrium that is different for D-D reactors from D-T reactors is that it is even more important to have a high beta. Many of the MHD parameters for STARFIRE were chosen to represent the most likely values for obtaining a high beta equilibrium, and the same considerations apply to WILDCAT. For this reason most of the MHD parameters have been taken to have the same values as for STARFIRE. The three exceptions are discussed below.

The specified plasma profiles are assumed to vary as $\hat{\psi}^\alpha$, where $\hat{\psi} = (\psi_\ell - \psi) / (\psi_\ell - \psi_m)$, and ψ_ℓ and ψ_m are the values of the flux function, ψ , at the limiter and magnetic axis respectively. The flux function is constant on the magnetic surfaces, so this choice assumes the pressure, density, and temperatures are also. (It is necessary that the pressure be constant on a flux surface for MHD equilibrium, but it is not necessary that the density and temperature separately be constant.) The pressure profile exponent, α_p , has been taken to be 1.4 for both STARFIRE and WILDCAT for the reason that such broader profiles seem to support higher beta.⁴ In STARFIRE, however, the den-

Table 2-4. Power Breakdown in MW for WILDCAT

D + D → n + ⁴He			
Ions	90		
Electrons	<u>54</u>		
Total plasma heating		144	
14.06 MeV neutrons	620		
Blanket enhancement	<u>336</u>		
Total Neutrons		<u>956</u>	
Total			<u>1109</u>
D + ³He → p + ⁴He			
Ions	221		
Electrons	<u>703</u>		
Total plasma heating		<u>924</u>	
Total			<u>924</u>
D + D → p + T			
Ions	105		
Electrons	<u>84</u>		
Total plasma heating		<u>189</u>	
Total			<u>189</u>
D + D → n + ³He			
Ions	38		
Electrons	<u>8</u>		
Total plasma heating		<u>46</u>	
2.45 MeV neutrons	124		
Blanket enhancement	<u>425</u>		
Total neutrons		<u>549</u>	
Total			<u>595</u>
Rf heating			
Ions	11		
Electrons	<u>96</u>		
Total plasma heating		<u>107</u>	
Total			<u>107</u>
Thermal power	2915	2915	2915

sity was assumed to be peaked with $\alpha_n = 1.1$, and the temperature, broad with $\alpha_T = 0.3$. This choice optimized the lower-hybrid current drive and also optimizes the power. Both present experiments and expected refueling and/or recycling at the wall would indicate, however, a broad density and a peaked temperature. For WILDCAT a compromise of $\alpha_n = \alpha_T = 0.7$ has been taken. This choice should be considered more conservative than that for STARFIRE. Neither the experimental nor theoretical plasma physics basis is sufficient to accurately characterize the profiles at this time.

For STARFIRE the plasma was taken to be more D-shaped having a value $d = 0.5$ in the expressions for the plasma edge:

$$R = R_0 + a \cos(\theta + d \sin \theta)$$

$$Z = \kappa a \sin \theta ,$$

with R_0 being the major radius; a , the minor radius; and κ , the elongation. The MHD stability appears to increase with d ,⁴ but it has been found difficult to design equilibrium field coils outside the toroidal field coils when $d \geq 0.25$, especially when no inboard EF coils are practical.^{5,6} For WILDCAT with its larger size and higher plasma current, it has been felt necessary to keep $d = 0.2$ in order to keep the EF system reasonably sized. The indicated increase in beta with d in this range of d is not particularly large in any event.⁴

The third exception is that WILDCAT has a higher beta than STARFIRE, as discussed in the previous section. A stability analysis has not been performed for the WILDCAT equilibrium. It would clearly be unstable to the existing theoretical stability codes. The most optimized, theoretically stable, equilibria⁷ have a maximum beta scaling approximately as $\beta_t \sim 0.5 A^{-2/3}$ or about 8% for WILDCAT. The PEST⁴ results for low N mode stability for more conventional equilibria (like the WILDCAT reference equilibrium) scale approximately as $\beta_t \sim 0.7/qA$ or about 7% for WILDCAT. On the other hand, it is not clear that these calculations include all of the physical effects that might give rise to stable, higher beta equilibria. For example, the sawtooth oscillations that regularly appear in experimental tokamaks seem to have a safety factor near the center that is less than unity and hence unstable. Instead of being catastrophic, however, the instability causes the current profile to reshape itself, and the plasma continues to operate with an equilibrium somewhat different than the one that would have been analyzed in a

stability code. Since in general the large existing stability codes only examine the stability of a particular equilibrium and do not indicate how the unstable equilibrium would evolve, it is not clear that the equilibria found to be unstable in the codes would not evolve to similar, stable equilibria or to nondestructive oscillations such as the sawteeth. Such a scenario is made more plausible by the fact that the stability codes are sensitive to the parameters of the equilibria they investigate, small changes in parameters sometimes giving rise to large differences in stability.

Further support for higher than commonly calculated values of beta is the appearance of the second stability region.⁸ If a plausible means can be found for the stable evolution of low beta equilibria into the second stability region, betas as high or higher than that assumed for WILDCAT may be feasible. Indeed, it is possible that the unstable equilibria may as a consequence of their instability naturally evolve through the unstable region into the second stability region. It is in any event premature to assume the beta limits for a reacting plasma are well known.

The parameters for the WILDCAT equilibrium are presented in Table 2-5, some of the profiles are shown in Fig. 2-1, and the magnetic fields and current density contours are shown in Fig. 2-2.

2.3 Design Sensitivity

The choice of the major design parameters, B_{TFC} , β_t , and R_0 , has been made on the basis of minimum extrapolation from D-T devices tempered by some consideration of technology limitations. This choice is by no means unique, so that it is interesting to examine how WILDCAT would be changed if other design choices were made. It is also interesting to note what the device would look like if some or all of the STARFIRE values for these parameters were used. Such a study is presented in Table 2-6, which shows how some of the major characteristics of WILDCAT would change over a broad range of values of B_{TFC} , β_t , and R_0 .

Clearly, higher values of these three parameters give more power and require more rf power and plasma current. For lower values of the three parameters the required confinement, even though it is less in magnitude, needs to be better than would be predicted by empirical scaling;² that is, α_{EMP} (the ratio of the required confinement time to that predicted by the

Table 2-5. MHD Parameters

Major radius, R_0 (m)	8.58
Elongation, κ	1.6
D-shapedness, d	0.2
Aspect ratio, A	3.25
Safety factor at limiter, $q(\psi_l)$	3.0
Safety factor at axis, $q(\psi_m)$	1.0
Toroidal beta, $\beta_t = 2\mu\bar{p}/B_{t0}^2$	0.11
Poloidal beta, β_p	
$\beta_p = 2\mu\bar{p}/[\int B_p^2 dx / \int dx]$	2.2
β_p (Callen and Dory) ^a	2.9
β_p (Shafranov) ^b	2.6
β_p (Zakharov and Shafranov) ^c	2.7
Diamagnetic function, $F^2 = R^2 B_t^2 = F_0^2(1 - \delta\hat{\psi}\beta)$	
At wall, F_0 (T-m)	70.6
Profile exponent, β	1.7
Well depth, δ	0.20
Pressure profile exponent, α_p	1.4
Magnetic axis, R_a (m)	9.5
Peak pressure, p_0 (MPa)	8.0
Average pressure, \bar{p} (MPa)	3.0
Inductive volt seconds, $\Delta\phi_{ind}$ (V-s)	509
External field at axis, B_{z0} (T)	1.3
Plasma current, I_p (MA)	30

^aSee Ref. 9.

^bSee Ref. 10.

^cSee Ref. 11.

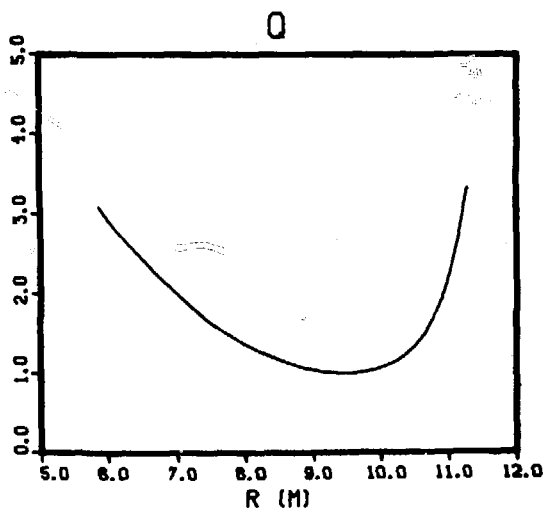
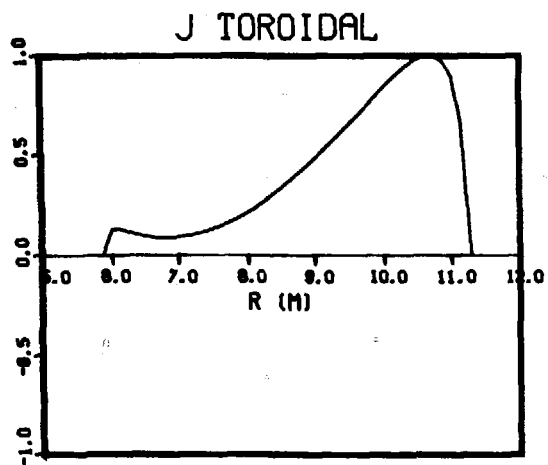
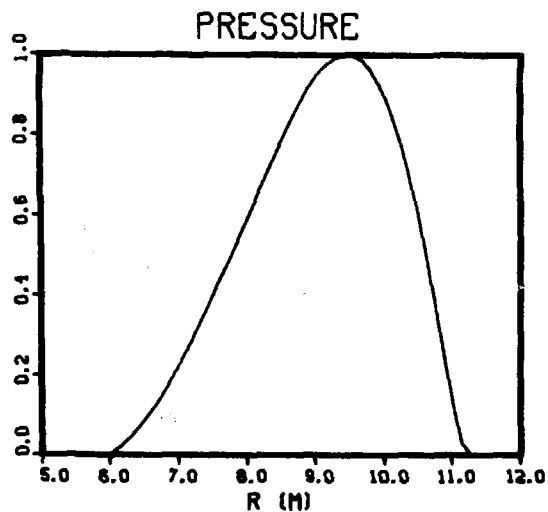
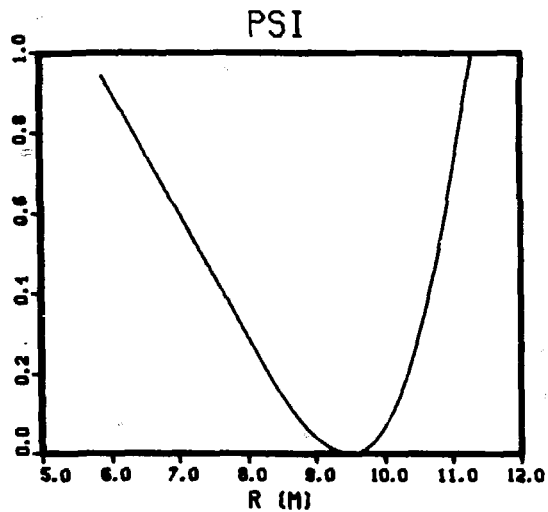


Fig. 2-1. WILDCAT flux function, pressure, current, and safety factor profiles.

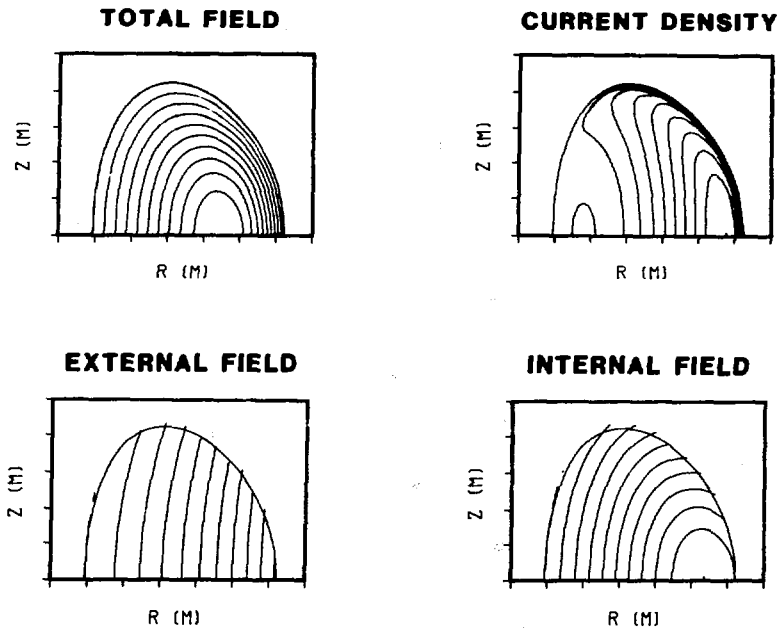


Fig. 2-2. Poloidal field lines and current density.

scaling) is greater than unity. If this confinement scaling does in fact continue to hold for the conditions typical of ignited D-D reactors, then these cases would not be viable. (A reduction in the beryllium impurity level, however, would reduce α_{EMP} , in some cases to as low as unity.)

It should be noted that the heat load on the first wall exceeds the accepted limiting value of 1 MW/m^2 for a PCA wall³ for the higher values of the three parameters and is less than optimum for the lower values. If the device were designed with different parameters, some consideration of the first-wall load and the aspect ratio with regard to the combination of parameters would likely be made, as it has been for the reference design.

The last line in Table 2-6 shows what the device would be like if all of the STARFIRE parameters were used. The power would be reduced to 7% of the design value and the first-wall heat load to 10%. Confinement would have to be nearly six times better than predicted by empirical scaling. The plasma current would be 17 MA. (The lower STARFIRE value of 10 MA for these parameters was achieved by further optimization of the MHD equilibrium.) The required rf power to the plasma would only be 20 MW compared to 90 MW for

Table 2-6. Sensitivity of WILDCAT to Major Parameter Changes

If $\alpha_{EMP} < 1$ with no iodine, then iodine has been added to make $\alpha_{EMP} = 1$. In all cases, $\bar{T}_e = 30$ keV, $A = 3.25$, $\kappa = 1.6$, $d = 0.2$, and a 3% beryllium impurity is present.

	B_{TFC} (T)	β_t	R_0 (m)	α_{EMP}	\bar{n}_I/\bar{n}_D (10^{-5})	$\bar{n}_D \tau_E$ (10^{20} s/m ³)	P_T (GW)	P_{rf} (MW)	I_p (MA)	$P_{w,heat,net}$ (MW/m ²)
(S)	8.0	0.111	8.58	4.3	0.	11.	0.3	18.	17.	0.09
	10.0			1.8	0.	12.	0.7	36.	21.	0.22
	11.1			1.2	0.	13.	1.1	49.	23.	0.23
	12.0			1.0	0.9	14.	1.5	62.	25.	0.47
(W)	14.0			1.0	3.6	24.	2.6	99.	29.	0.91
	14.4			1.0	3.8	27.	2.9	107.	30.	1.00
	16.0			1.0	4.0	40.	4.0	149.	33.	1.49
(S)	14.4	0.06	8.58	1.6	0.	12.	0.9	42.	27.	0.31
		0.067		1.2	0.	1	1.2	75.	28.	0.37
		0.08		1.0	1.0	1	1.6	84.	28.	0.52
		0.10		1.0	3.3	22.	2.4	100.	29.	0.82
(W)		0.111		1.0	3.8	27.	2.9	107.	30.	1.00
		0.12		1.0	3.9	31.	3.2	113.	30.	1.14
(S)	14.4	0.111	6.0	1.2	0.	12.	0.7	39.	19.	0.45
			7.0	1.0	1.7	15.	1.3	61.	23.	0.65
			8.0	1.0	3.4	22.	2.2	89.	28.	0.88
			8.58	1.0	3.8	27.	2.9	107.	30.	1.00
(W)			10.0	1.0	4.0	40.	4.6	160.	36.	1.27
(S)	11.1	0.067	7.0	5.8	0.	11.	0.2	20.	17.	0.10

(S) STARFIRE parameter(s).

(W) WILDCAT reference case.

STARFIRE, even though the current is larger. This represents the increased efficiency of the Alfvén wave current drive compared to the lower hybrid waves used in STARFIRE.

2.4 Burn Cycle

A burn cycle has been developed for WILDCAT and is summarized in Table 2-7. Most of the burn cycle has been analyzed using the profile-averaged, time dependent, advanced fuel computer code described in Ref. 1 with modifications to model the Alfvén wave rf current drive. The code solves particle balance equations for the fuel and fusion product species, i.e., protium, deuterium, tritium, ^3He , and ^4He , as well as for beryllium, oxygen, and iodine. The beryllium comes from sputtering of the first wall and limiter coatings. Oxygen comes from various leak sources, and iodine is intentionally added to the plasma to establish a power balance through increased radiation. The electron density is determined by requiring charge neutrality. The code solves energy balance equations for the ions, taken as one species for this purpose, and the electrons. Plasma heating by ohmic heating, fusion product slowing down, and external rf heating are included, and losses are due to transport and radiation.

The rf current drive has been modeled in a similar manner to the STARFIRE study,³ using the equivalent circuit shown in Fig 2-3. This circuit models the coupled dynamics of the plasma, poloidal coils, rf system, and the power supplies. Both the ohmic heating (OH) and equilibrium field (EF) coils are represented as single equivalent inductances, and the plasma is represented as a series combination of inductance and resistance. The Alfvén wave current drive is represented as a controlled current source in the plasma loop. The coupled system of Fig. 2-1 is described by the following set of equations:

$$L_{\text{OH}} \frac{dI_{\text{OH}}}{dt} - M_{\text{OH,p}} \frac{dI_{\text{p}}}{dt} = V_{\text{OH}} \quad (2-1)$$

$$V_{\text{p}} = - \frac{d}{dt} (L_{\text{p}} I_{\text{p}}) + M_{\text{OH,p}} \frac{dI_{\text{OH}}}{dt} + M_{\text{EF,p}} \frac{dI_{\text{EF}}}{dt} \quad (2-2)$$

$$I_{\text{p}} = \frac{V_{\text{p}}}{R_{\text{p}}} + I_{\text{RF}} \quad (2-3)$$

Table 2-7. WILDCAT Burn Cycle Parameters

Type of burn cycle	Steady state
Plasma initiation method	ECRH
Initiation power, MW	5
Startup	
Ohmic heating period, s	19
Rf current induction period, min	20
Fusion power ramp period, min	19
Total start-up time, min	39
Required rf power, MW	107
Required OH power, MW	40
Required EF power, MVA	83
Burn time	Continuous
Burn control method	Enhanced radiation
High-Z control material	Iodine
Shutdown time, min	30

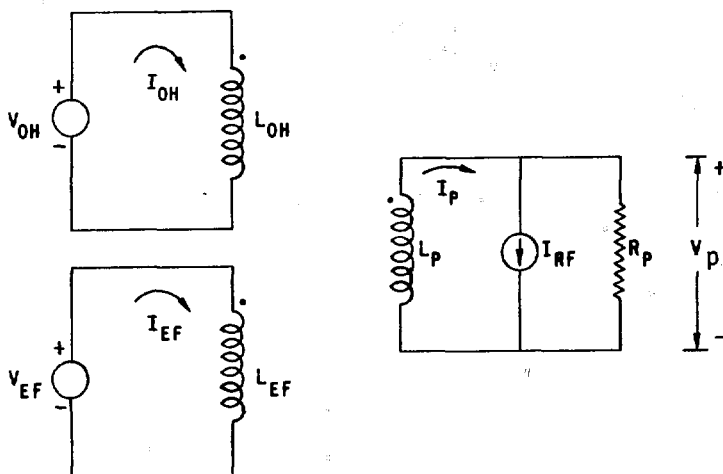


Fig. 2-3. Plasma current drive model.

$$I_{EF} = f(I_p, \beta_t) . \quad (2-4)$$

The M terms represent mutual inductances. The required current, I_{EF} , needed to maintain MHD equilibrium is a function of I_p and β_t and is determined by these quantities as the plasma evolves through a sequence of equilibria during the burn cycle. The plasma resistance, R_p , is computed at each time step using the neoclassical Spitzer resistivity. The rf current, I_{rf} , is given as a function of rf power, P_{rf} , according to the following algorithm (whose derivation is discussed in Sec. 2.6):

$$I_{rf} = \frac{P_{rf} [1 + 8\sqrt{\beta_t}]}{39.5 \times 10^{-20} \bar{n}_e} , \quad (2-5)$$

where \bar{n}_e is the average value of electron density, and β_t is the plasma toroidal beta. All units are MKS. This algorithm applies for $\bar{n}_e > 0.1 \times 10^{20} \text{ m}^{-3}$, $\bar{T}_e > 1 \text{ keV}$, and $I_p < 1 \text{ MA}$, these conditions being assumed necessary for proper absorption of the collisional Alfvén wave.

In evaluating the burn cycle for WILDCAT, use has been made of the many studies of the burn cycle for D-T reactors, particularly STARFIRE,³ which is also steady state and the previous study of the pulsed D-D reactor.¹ The latter study showed several problems related to the startup period. These are: (1) large power supplies (>1 GW) are needed to change the current in the poloidal coils for any reasonable startup time; and (2) thermal energy storage is needed to compensate for the necessarily long plasma down time. Such thermal storage is needed to maintain a constant thermal input to the turbine generators. It is expected that steady-state operation would eliminate these problems, and this has been borne out in the study. Another potential problem with the pulsed D-D burn cycle is that extra tritium has to be used to heat the plasma to ignition. A tritium rich startup is needed to avoid a very excessive external heating requirement. The problem with this technique is not the extra tritium itself, but rather that very good control of the tritium density appears to be needed. Too little tritium causes the plasma to fizzle out while too much causes a too rapid temperature rise and an excessive EF voltage requirement. While the computer simulations indicate that adequate control could probably be achieved, this is of course uncertain due to

uncertainties in the particle diffusion coefficients and other parameters. For steady-state operation it has been found that a tritium-rich startup is still needed. However, the control problem appears to be considerably easier. This is due to the much longer start-up time that can be used for the steady state case. The longer start-up time also reduces the EF and OH power requirements and the need for thermal storage, two very expensive items.

2.4.1 Plasma Initiation

The purpose of the plasma initiation (breakdown) system is to create a low density, ionized plasma from the initial fill gas. The initiation requirements for WILDCAT are examined in Sec. 2.7. As concluded in the STARFIRE study, an electron cyclotron resonance heating (ECRH) initiation system is one of the most attractive from an engineering standpoint. Such a system eliminates the complexities of high voltage initiation coils and their power supplies. Accordingly, ECRH has been adopted as the reference initiation system for WILDCAT. The ECRH system for WILDCAT is similar to that of STARFIRE, i.e., ~5 MW delivered to the plasma through a series of waveguides built into the first wall. Steady-state operation helps the initiation process because there is as much time as needed between burn pulses to thoroughly pump impurities from the torus.

2.4.2 Startup

Various features of the WILDCAT startup phase are shown in Figs. 2-4 through 2-10. Startup is the most important part of the burn cycle in setting the plasma driving system requirements. As with a D-T device, a number of control algorithms need to be used to control density, rf power, etc. The startup developed for WILDCAT and described here is not unique; however, it is typical of the strategies to be employed for a future fusion reactor.

The start-up phase begins just after plasma initiation. At this point the torus is filled with a fresh charge of ionized deuterium at low density and temperature. Although WILDCAT uses rf current drive, a small OH coil is included to induce some of the initial plasma current. This coil is reverse biased prior to startup. It is then ramped down in 19 s through the use of a constant voltage power supply. During this "ohmic heating" period the plasma is heated by ohmic heating and by external rf power. The rf power is varied

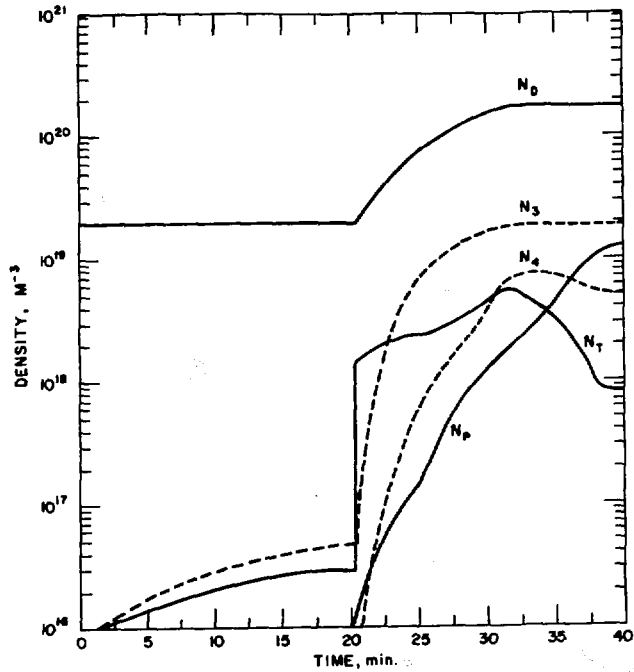


Fig. 2-4. Plasma densities during startup.

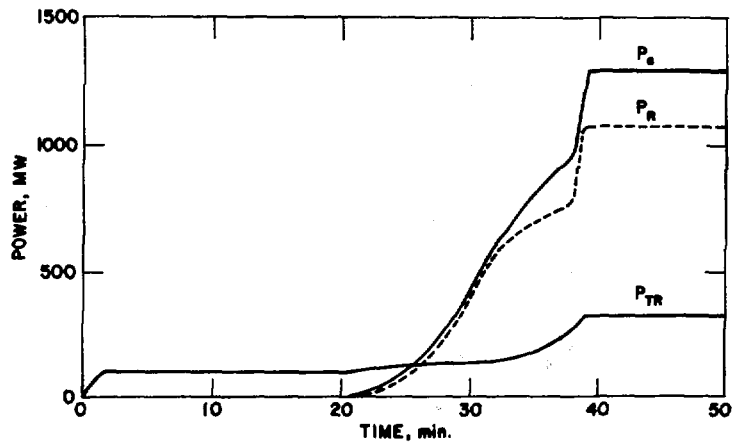


Fig. 2-5. Radiation power, transport power and fusion product heating power to the plasma during startup.

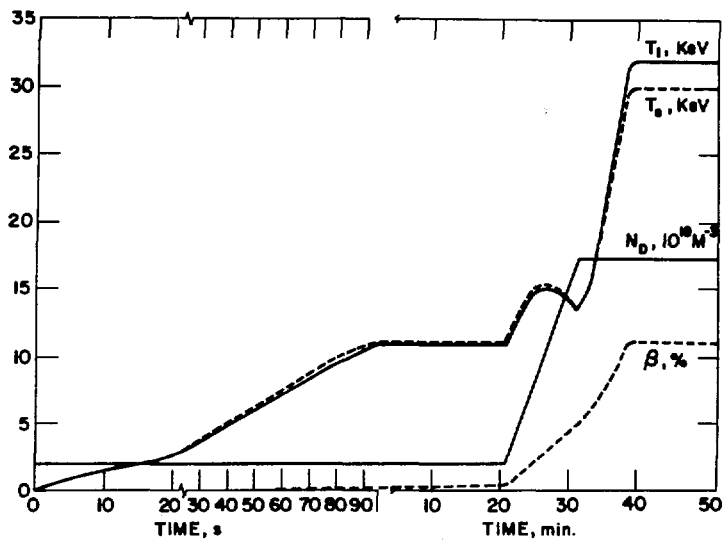


Fig. 2-6. Plasma ion and electron temperature, deuterium density, and toroidal beta during startup.

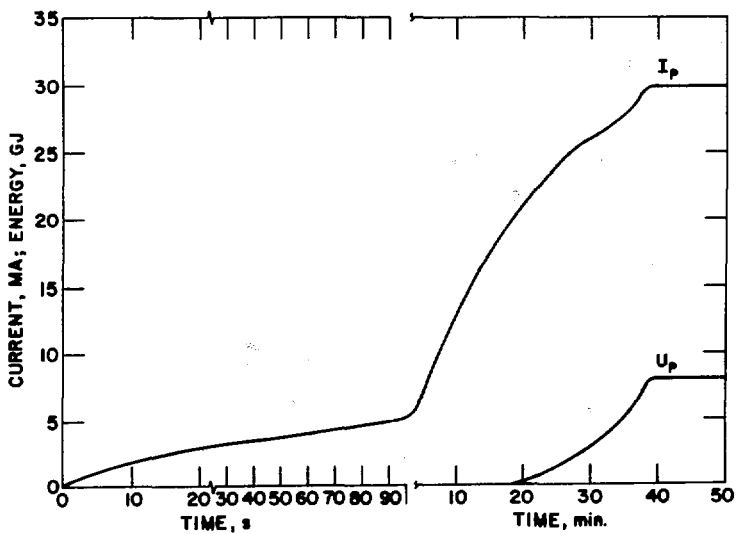


Fig. 2-7. Plasma current and plasma kinetic energy during startup.

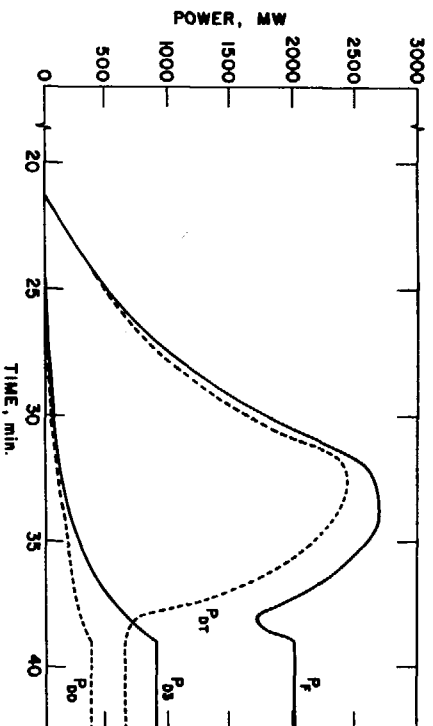


Fig. 2-8. D-T, D-D, D-³He, and total fusion power during startup.

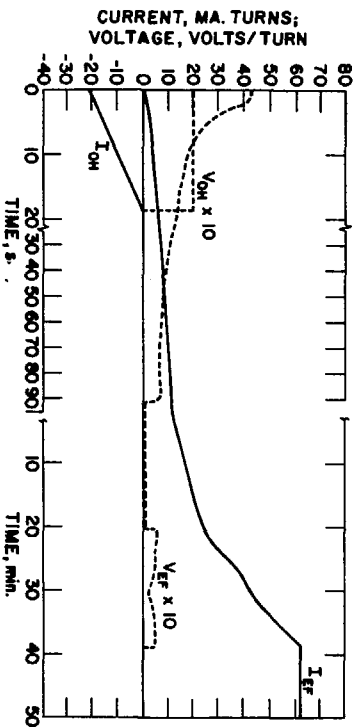


Fig. 2-9. OH and EF current and voltage during startup.

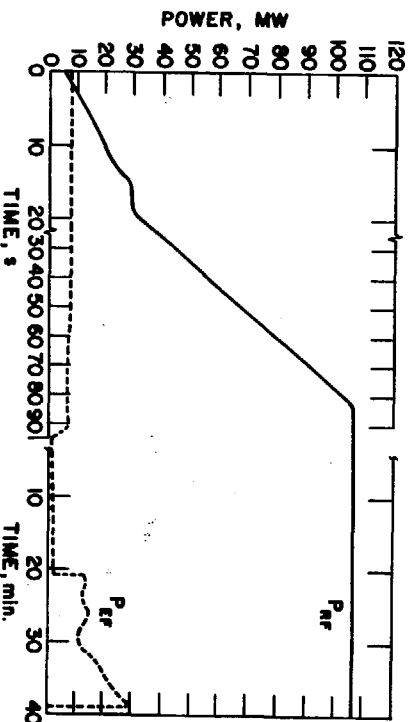


Fig. 2-10. RF and EF power during startup.

so as to apply a net heating power of 3 MW to the plasma. This is done to gradually heat the plasma so as to minimize resistive losses. The rf power also serves to induce plasma current once the current reaches 1 MA. Once the OH coil is fully discharged, it is disconnected and serves no further function. The OH power supply requirement is set during this period, and is a very modest 40 MW. This is much less than the 2160 MW needed to operate the OH coil for the pulsed D-D cycle.¹

The next period in the startup is the "current inducement" period, which begins after the 19-s ohmic heating period and lasts for about 20 min. The purpose of this phase is to allow the rf system to induce in the plasma its share of the full plasma current of 30 MA. Of this current, about 55% needs to be supplied by the rf drive, the rest coming from the coupling to the OH and EF systems. At the start of this period the rf power is ramped up to its full value of 107 MW. It is held constant thereafter. The plasma deuterium density is kept at a low value of about 10% of the full operating density. The low density serves two purposes. First it makes for a more efficient use of the rf power to induce current [see Eq. (2-5)], although this is not a critical consideration. Second it allows for an easier approach to ignition in the subsequent phase of the startup.

The third and final phase of the startup is the "fusion power ramp" phase during which the plasma is brought to full operating conditions. For a steady-state reactor starting off cold the fusion power must be ramped up gradually. This is to minimize thermal stress in the first wall, blanket, and heat transport system. A second requirement is to minimize the amount of external heating power needed to reach ignition. The ideal case for WILDCAT is to use no more than the 107 MW needed anyway for rf current drive. This is the approach used.

As mentioned previously, extra tritium must be added to heat WILDCAT to ignition. The reason for this is that the D-D reaction is negligible for temperatures below ~15 keV. In contrast, the D-T reaction is significant at ~6 keV. Therefore, the D-D reaction is not of much use in heating the plasma during most of the startup. The D-³He reaction lies somewhere between D-T and D-D in terms of effectiveness, it has a lower cross section than D-T but a higher percentage (100% vs. 20%) of the fusion energy goes into heating of the plasma.

The tritium and ^3He densities are controlled in the following way. (See Fig. 2-4.) Prior to the fusion ramp phase T and ^3He are merely allowed to build up in the plasma due to the very small amount of D-D fusion. At the start of the fusion ramp phase a pulse of tritium equivalent to about 1.5% of the full deuterium density is injected. At the same time a ramp of both the deuterium and ^3He densities is begun. All of these densities are controlled by varying the respective refueling currents. After the initial pulse of tritium is injected, the T density is modulated so as to maintain a net heating power of 5 MW. The fusion powers corresponding to the D-T, D-D, and D- ^3He reactions over this period are as shown in Fig. 2-10. Also shown is the total fusion power. (This is not equal to the thermal power, which is greater due to neutron multiplication in the blanket.) As shown, the D-T fusion power is much higher during this period than its equilibrium value during the burn. The peak value of total fusion power is, however, only about 25% greater than the burn value. This over-power condition and the different mix of neutron and surface heating during this period do not appear to be detrimental to the reactor.

During the last minute of startup iodine (not shown) is added to the plasma to begin to stabilize the final operating point. This operating point is reached after a total of 39 min. At this time the plasma has reached full density, temperature, and current, and the startup is completed.

During the startup period the EF current is increased to keep the plasma in MHD equilibrium. The EF current is a function of plasma current and plasma beta. The required EF voltage and the instantaneous EF power ($V_{\text{EF}} \times I_{\text{EF}}$) are shown in Figs. 2-4 and 2-5. The EF reactive power requirement is given by the product of the individual maximum values of current and voltage:

$$P_{\text{EF}}^{\text{R}} = V_{\text{EF}}^{\text{MAX}} \times I_{\text{EF}}^{\text{MAX}} .$$

Since the voltage is high at the beginning and the current high later, dividing the EF system into two separate power supplies with switchover at approximately 90 μ s gives a lower requirement for each supply. The largest reactive power requirement is then $P_{\text{EF}}^{\text{R}} = 83 \text{ MVA}$. As with the OH system, this is much less than the 1000 MVA needed for pulsed operation.¹

2.4.3 Burn Phase

The normal burn phase of WILDCAT lasts on the order of up to six months. Most of the features of the burn phase area are covered in the discussions of the WILDCAT operating parameters in Secs. 2.1, 2.2, and 2.6. To summarize briefly, the plasma current is driven in steady state by the Alfvén wave rf system. Impurities in the plasma, specifically ^4He and P from fusion and Be from sputtering, are held to steady state values by the impurity control system. The D, T, and ^3He densities are maintained by the refueling system, which recycles all of these ions that are pumped out plus adding D ions to make up for those lost by fusion. A small iodine concentration is also maintained in the plasma to stabilize the operating point.

2.4.4 Shutdown

The general types of shutdown envisioned for a steady-state fusion reactor are a "normal" shutdown used once or twice a year to routinely shut the plant down and an "emergency" shutdown used in accident or other non-routine situations. These types of shutdowns have not been examined in detail but have been compared to the equivalent scenarios for STARFIRE. Like STARFIRE, the normal shutdown period for WILDCAT would be essentially the reverse of the startup period. Since there are no particular time limitations, the shutdown parameters can be made to have the same or reduced power supply requirements as for startup. Normal shutdown is accomplished by gradually reducing the fusion power, e.g., by reducing the rate of tritium and ^3He reinjection.

The emergency shutdown for a WILDCAT-type reactor might be a problem. The STARFIRE analysis subdivided emergency shutdowns into two generic types labeled "abrupt" emergency shutdown and "rapid" emergency shutdown. In the abrupt shutdown the plasma fusion power was terminated almost instantaneously (in less than 100 ms) by causing a plasma disruption to occur. A disruption could be caused by a number of means, such as by injecting excess high-Z material into the plasma. The abrupt shutdown would be used for critical system failures such as loss of cooling to minimize damage to the reactor. The trouble with this technique for WILDCAT is that a disruption appears to result in catastrophic damage to the first wall. (See Appen. B.) Therefore, an intentional disruption might be counterproductive. The rapid emergency shutdown, however, could be an acceptable option for WILDCAT. As employed for STARFIRE,

this method also used a disruption to terminate the plasma but with a preceding interval of 2.5 s in which most of the plasma energy was radiated and convected away.

The rapid shutdown is initiated by terminating the refueling current and the rf current drive power. The plasma thermal energy for STARFIRE was reduced to 20% of its full value, and the plasma magnetic energy to 60% of its full value prior to the disruption. The disadvantage of this technique for STARFIRE is that it requires a special power supply to ramp down the EF current prior to the disruption. This may be a small consideration for WILDCAT however, in light of the severe full-power, disruption problem.

2.5 Limiter Impurity Control

WILDCAT uses a limiter/vacuum system to control impurities. The system is modeled after the STARFIRE system and consists of a toroidal "belt" limiter located at the outboard midplane. A series of vacuum ducts connect the back of the limiter with the vacuum cryopumps. Both the limiter and first wall are coated with beryllium to prevent sputtering of the highly radiative structural material.

The basic principles of a limiter vacuum system are discussed in Ref. 1. In general, the impurity control requirements for D-D are fairly similar to those for D-T. The ash products to be removed for the D-D reaction are protons and alpha particles, compared to only alphas for D-T. The amounts of the ash products are similar. Because sputtering increases with the mass of the incident particle, the WILDCAT plasma with an average mass of 2.08 amu sputters somewhat less than a D-T plasma with an average mass of ~2.5 amu, all other things being equal. Another difference with D-D is that the gas processing system must separate all three isotopes of hydrogen and both helium isotopes, but this is only a minor change. More substantial differences are due to the increased size and plasma density of the D-D reactor over a D-T device. Specifically, the heat load to the limiter is increased because of the higher thermal transport power from the plasma.

2.5.1 Limiter Design

Major parameters of the WILDCAT impurity control system are summarized in Table 2-8. The limiter design, shown in Fig. 2-11, is similar to that of

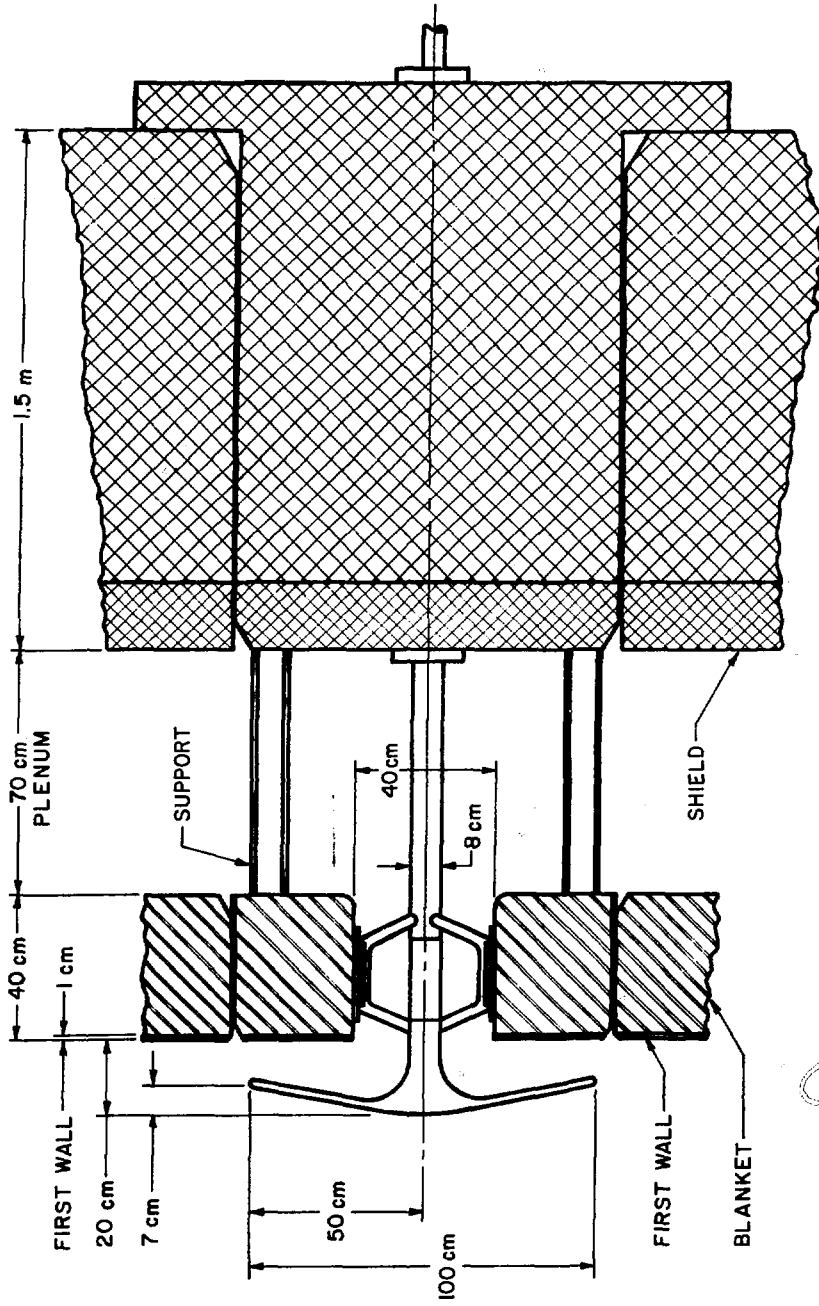


Fig. 2-11. Cross section of the WILDCAT limiter design.

Table 2-8. WILDCAT Impurity Control System Parameters

Parameter	Value
Impurity control system	Belt-type limiter/vacuum system on outboard midplane
Vacuum pumps	Cryopumps
Limiter major radius, m	11.2
Limiter height, m	1.0
Transport power to limiter, MW	166
Plasma edge temperature, keV	1.2
Particle e-folding distance, cm	10.
Energy e-folding distance, cm	5.0
Displacement of leading edge, cm	7.0
Heat load on leading edge, MW/m ²	6.0
Particle confinement time, s	3.9
Helium removal efficiency, %	25
Hydrogen removal efficiency, %	10
Fractional concentration of P, %	10
Fractional concentration of ⁴ He	2.9

STARFIRE and consists of a two-bladed structure located at the outer midplane of the first wall. The blades extend ~10 cm into the scrape-off region. The leading edges of the blades are recessed towards the first wall to reduce the heat flux. A thin beryllium coating is bonded to the limiter surface to prevent high-Z impurities from getting into the plasma. The limiter is the same height as that for STARFIRE but lies at a larger major radius. The limiter and the first-wall/blanket/shield behind it are removable as a drawer-like structure in alternate first-wall/blanket/shield modules. (See Sec. 3.4.) The transport power to the limiter is 166 MW compared to 90 MW in STARFIRE. This would be substantially higher without the enhancement of plasma radiation resulting from adding iodine to the plasma. (See Secs. 2.1 and 2.4.) Based on a plasma edge temperature of 1.2 keV, on the geometry and safety factor of WILDCAT, and on the assumption of Bohm diffusion, the particle and energy e-folding distances in the scrapeoff zone have been estimated as shown in Table 2-8.. For a leading edge displacement of 7 cm the heat load on the

leading edge is 6 MW/m^2 , a value 50% greater than STARFIRE but probably achievable.

Pumping efficiency calculations for WILDCAT have assumed a significant helium enrichment effect in the limiter slot region whereby hydrogen is preferentially released to the plasma while helium tends to be pumped more. This helps minimize the deuterium gas load to the pump at the expense of increasing the protium concentration in the plasma. It remains to be seen whether any helium enrichment is actually obtainable in practice. Based on their generation rates and removal efficiencies, the proton and alpha concentrations are held to about 7% and 3%, respectively. These are reasonably low values, particularly since protium is a "mild" form of ash, contributing only one excess electron to the plasma.

2.5.2 Limiter Lifetime

Since the limiter in WILDCAT is geometrically similar to the pumped limiter in STARFIRE, the lifetime analysis is similar. The major concerns for the limiter lifetime are high thermal stresses due to the high surface heat loads, neutron irradiation damage of the structural material, and the buildup of beryllium from the first wall on the limiter surface.

The thermal stresses at the leading edge, where the highest heat load occurs, have been calculated. The basic configuration of the leading edge is shown in Fig. 2-12. The leading edge has been modeled as a cylinder in which the top skin is constrained from thermal expansion by the cooler internal rib structure shown at the bottom of Fig. 2-11.³ The stresses at the leading edge are due to the thermal gradient through the outer skin, the difference in temperature between the rib structure and the average skin temperature, and the pressure of the water coolant. The limiter structural materials examined for the stress analysis are a tantalum alloy (Ta-5W) and a copper alloy (AMAX-MZC). Both materials have been selected for their excellent thermal properties and adequate mechanical properties for the limiter operating conditions. Additional information on the properties of these materials can be found in Ref. 3.

The operating parameters used for the stress calculations are shown in Table 2-9, and the results of the calculations are shown in Table 2-10. The thermal stresses dominate the total stresses, and they are quite high in both

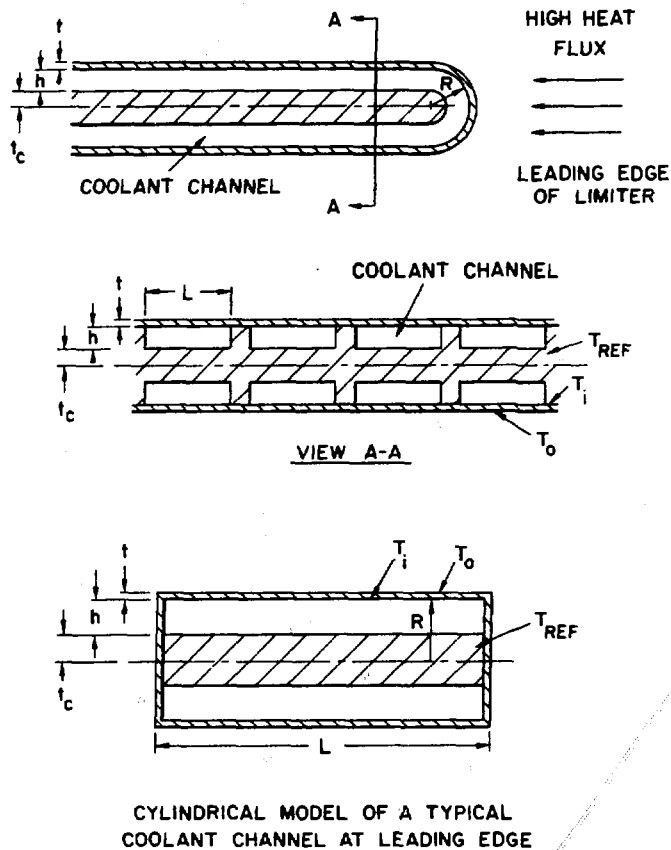


Fig. 2-12. Schematic drawing of the leading edge model.

Table 2-9. Limiter Operating Conditions

Leading edge radi, mm	8.5
Outer wall thickness, mm	1.5
Coolant channel width, mm	8.0
Surface heat flux, MW/m^2	6.0
Coolant temperature, $^{\circ}C$	130
Heat transfer coefficient, $W/m^2/K$	57,000
Coolant pressure, MPA	4.2

Table 2-10. Maximum Calculated Stresses of Leading Edge

Material:	Tantalum-Ta-5W	Copper AMAX-MZC
Inner wall temperature, °C	235	216
Outer wall temperature, °C	388	240
Pressure stress, MPa		
Hoop	-12	-12
Axial	-38	-38
Temperature gradient stress, MPa		
Hoop	-172	-47
Axial	-136	-37
Temperature stress, MPa		
Hoop	-308	-170
Axial	-403	-278
Combined stress, MPa		
Hoop	-328	-190
Axial	-467	-341
Effective Stress, ^a MPa	415	296
Percent of 0.2% yield strength	128 ^b 60 ^c	70

^aThe effective stress is

$$\sigma_{\text{eff}} = (\sigma_A^2 + \sigma_H^2 - \sigma_A \sigma_H + 3 \tau^2)^{1/2},$$

where σ_H and σ_A are the combined hoop and axial stresses, respectively, and τ is the shear stress, which is zero in this analysis.

^bAnnealed.

^c40% cold worked.

cases but, both cold-worked Ta-5W and AMAX-MZC are acceptable for use in the limiter, since the total stresses are substantially below the yield stress.

Neutron irradiation is known to induce swelling, accelerate creep, alter the strength, and decrease the ductility. All of these changes can potentially affect the heat carrying capacity and the lifetime of the limiter materials. The amount of information available on irradiation effects on the reference alloys is sparse, and thus a rigorous evaluation of the operating lifetime is not possible. Rather, the available data has been used to indicate general trends and, where possible, to determine areas of major concerns.

Swelling in metals is caused by the segregation of radiation produced vacancies into voids during irradiation at temperatures from 0.3 to 0.5 of the absolute melting temperature, T_m . Several factors, including temperature, neutron flux rate, total neutron fluence, helium generation rate, cold-worked properties, grain size, and precipitate structure can influence the amount of swelling. Pure copper exhibits a peak swelling at $\sim 325^\circ\text{C}$ ($0.44 T_m$).¹² Alloying the copper can reduce the observed swelling,¹³ but it is not known what, if any, reduction in swelling will be observed in AMAX-MZC. Therefore, in order to reduce the amount of swelling, the temperature of AMAX-MZC should be kept significantly below 325°C . Pure tantalum exhibits a swelling peak at $\sim 650^\circ\text{C}$ ($0.28 T_m$). This temperature is far higher than the expected limiter operating temperatures of $200\text{--}300^\circ\text{C}$, and thus void swelling in tantalum alloys should be low. The swelling rates of the refractory metals like tantalum exhibit a less than linear dependence with neutron fluence, and the swelling rates are considerably below that of pure copper. Alloying can significantly reduce the swelling in the refractory metals. Limited data on the tantalum alloy, T-111, indicated densification rather than swelling after irradiation to a fluence of 1.9×10^{22} n/cm² (>0.1 MeV at 414°C and 643°C).⁵ No explanation for the densification was given.

Neutron irradiation is known to reduce the ductility of metals at low temperatures. Since the limiter is designed to operate in the elastic range, residual ductility is only necessary to prevent catastrophic failure during an off-normal event. The amount of ductility required depends upon the severity of the event, and cannot be realistically estimated at this time. However, the greater the amount of residual ductility, the more likely the limiter is to successfully withstand off-normal conditions. Unfortunately, there is no available information on copper and copper alloys near the range of interest, and only limited data are available on the refractory alloys. Tantalum and T-111 appear to become highly embrittled by neutron fluences of $1\text{--}3 \times 10^{22}$ n/cm² at energies above 1 MeV.⁵ Although the values for the total elongation of irradiated tantalum and T-111 are 8-15%, the values for the uniform elongation are as low as 0.2% at room temperature. The reduced ductility at low temperatures in tantalum alloys represents a potential problem area for these materials, and further experimental work is needed to more carefully evaluate the influence of radiation on ductility.

Radiation is expected to accelerate creep in all of the reference alloys at the limiter operating temperatures. This is similar to the effect of radiation on creep in stainless steels. Again, there is insufficient data to evaluate the magnitude of this effect. During operation, radiation creep would reduce the thermal stresses to low values. After stress relaxation, the highest stresses would then occur when the temperature gradient is removed and not during normal operation. The stresses produced when the temperature gradient is removed would be equal in magnitude but opposite in sign to the original thermal stresses. Since the primary stresses in the limiter are expected to be low, the dimensional changes due to radiation creep are expected to be low.

The redeposition of beryllium from the first wall is likely to lead to a net buildup of beryllium on the limiter surface. If the beryllium layer becomes sufficiently thick, it would result in high temperatures and stresses. At high temperatures the thermal vaporization rate of beryllium could become equal to the deposition rate leading to a buildup of beryllium in the plasma. For STARFIRE the beryllium thickness required to reach these temperatures is ~ 10 mm.³ The net deposition was estimated to be considerably below this value for the desired limiter lifetime of 6.5 y. For WILDCAT the calculation of the redeposition rate is a difficult problem, which has not been done. If the buildup rate is similar to the STARFIRE predictions, then limiter operation should be possible for several years before replacement or surface grinding is required.

In summary, the structural materials, Ta-5W and AMAX-MZC, both meet the stress requirements of the limiter in WILDCAT. The response of these materials to radiation is not well known, and it is not possible to estimate their lifetime at this time. The buildup of beryllium on the limiter would result in unacceptable temperatures and stresses, but again it is not possible to estimate the resultant lifetime. For design purposes it is assumed that the limiter could successfully operate for several years before replacement.

2.6 Steady-State Current Drive

Numerous studies have pointed out the advantages and possibilities for operating tokamaks in a steady state.^{3,16-19} There are two main difficulties with steady state operation of WILDCAT. First, the toroidal current is very

large, about three times that in STARFIRE, so proportionally larger driver power is needed. Second, the gross electric power produced by the D-D reactor is much less than that of the D-T fueled STARFIRE, so a greater fraction of the power would have to be recycled to maintain steady operation in WILDCAT compared to STARFIRE if the same current drive technique were used. In this case the net electric production of the D-D reactor would be significantly reduced compared to STARFIRE. Therefore, in order to retain the benefits of steady state operation, a search has been conducted to identify current drivers for WILDCAT which promise much greater efficiencies than the lower hybrid waves used in STARFIRE. As outlined in the preliminary D-D reactor study,¹ waves with toroidal phase speeds less than the electron thermal speed offer this potential; the theory²⁰ of these waves predicts efficiencies as much as three times greater than that for lower hybrid waves. A general discussion of alternative wave drivers appears in Ref. 21.

For alternate fuel reactors the compressional Alfvén wave (CAW) appears ideally suited²⁰ since the electron temperature is generally very high, and higher temperature implies more efficient power generation for these waves. The power-to-current-density ratio is $p/j \approx 1.7 \times 10^{-18} n_e / [n_i T_e^{3/2}]$, where units are MKS, and T_e is in keV. The quantity, $n_i \equiv ck_i / \omega$, is the index of refraction parallel to the field lines.²¹ Additionally, the plasma beta in a D-D reactor must be very high to allow economical operation. For such high beta the cavity modes of the CAW can be shown to fit into a device the size of WILDCAT.²⁰ This is an attractive feature since cavity modes couple well to antennas and may deliver negligible power to the plasma first wall structure. However, the necessity of a loop antenna inside the plasma chamber rather than a waveguide launcher may be less desirable from an engineering viewpoint.

This development of the CAW current drive problem relies heavily on Ref. 20, to which the inquisitive reader is referred. It is desirable to excite the lowest order radial eigenmode of the torus, and the radial wave number is approximated as $k_r = \pi / (Sa)$, where a is the minor radius, and S is the usual shape factor (ratio of the poloidal circumference to $2\pi a$). An integral number, n , of wavelengths around the torus is required, and the toroidal wave-number is denoted as $k_z = n/R$, where R is the major radius. Assuming no poloidal wave structure, the approximate dispersion relation²⁰ is $\alpha = \{4[1 + (\pi A/Sn)^2] \beta_e^{-1}\}^{1/2}$, where $\alpha = \omega / k_z \bar{v}_D$ is the ratio of CAW toroidal

phase speed to the average ion thermal speed, $\bar{v}_D \equiv \sqrt{T_D/m_D}$. For these studies it is assumed β_t is related to the aspect ratio, A, by $\beta_t = 0.36 A^{-1}$. Using this and the value $S = 1.32$:

$$\alpha = 3.33\sqrt{A} [1 + 5.66A^2/n^2]^{1/2} . \quad (2-6)$$

The aspect ratio and antenna structure determine α , and the angular frequency is thus:

$$\omega = \alpha k_z \bar{v}_D = 1.24 \times 10^6 \alpha n/R , \quad (2-7)$$

where MKS units are understood, and $\bar{T}_D = 31.8$ keV for WILDCAT. To avoid ion cyclotron damping, it is required that $\omega \ll \Omega_D$, where Ω_D is the deuterium cyclotron frequency. This constraint is easily satisfied in practice. To avoid strong ion Landau damping, it is required that $\alpha \geq 6$ (which occurs automatically for $A \geq 3.25$). When these two constraints are satisfied, most of the wave power is dissipated by electron transit time magnetic pumping, which is necessary for efficient current generation. In order to reach the most efficient current generation regime, an antenna design is chosen which has a large n and a consequently slow phase speed, ω/k_z . The quantity w is defined as $w \equiv \omega/(k_z v_e) \ll 1$, where v_e is the electron thermal speed ($v_e \equiv \sqrt{T_e/m_e}$) which is taken to be local in minor radius. Our theory neglects the differences between electron motion toroidally and parallel to magnetic field lines, and it is assumed the wave spectrum is quite narrow. Thus,

$$w = \alpha \bar{v}_D / v_e = \frac{0.0931\alpha}{(1 + \alpha_T)^{1/2} \bar{T}_e^{1/2}} [1 - (r/\tilde{a})^2]^{-\alpha_T/2} , \quad (2-8)$$

where the temperature profile is modeled as

$$T_e(r) = (1 + a_T)[1 - (r/\tilde{a})^2]^{-\alpha_T} ,$$

where $\tilde{a} = aS$ is the effective minor radius of the noncircular plasma.

Fokker-Planck calculations have determined the ratio of current density, j, and absorbed power density, p, for the CAW.²⁰ These quantities can be normalized as $\hat{j} = j/(en_e v_e)$ and $\hat{p} = (n_e m_e v_e^2 v_0)$, where n_e is the electron density, and the collision frequency is $v_0 \equiv \omega_p^4 \ln \Lambda / (2\pi n_e v_e^3)$; $\ln \Lambda$ is the Coulomb logarithm, taken to be 22, and ω_p is the electron plasma frequency. Thus,

$$p/j = \frac{e^3 \mu n \Lambda}{2\pi \epsilon_0^2} \frac{n_e}{n_e v_e^2} \hat{p}/\hat{j} = 1.1 \times 10^{-18} (n_e/T_e) \hat{p}/\hat{j} .$$

We let $n_e = (1 + \alpha_n) \bar{n}_e [1 - (r/\tilde{a})^2]^{\alpha_n}$. For WILDCAT $\alpha_n = \alpha_T$ (see Sec. 2.1), so:

$$p/j = 1.1 \times 10^{-18} (\bar{n}_e/\bar{T}_e) \hat{p}/\hat{j} ; \quad (2-9)$$

the only radial dependence of this expression is in \hat{p}/\hat{j} which depends on the local value of w . For values of $w \ll 1$ a good approximation is

$$\hat{j}/\hat{p} = 5 + 13 w^{-1} . \quad (2-10)$$

Transit time damping power is given as a function of w by:²²

$$P = p_1 n_e T_e w \left(\frac{b_{\parallel}}{B_t} \right)^2 w e^{-w^2/2} ,$$

where b_{\parallel}/B_t is the ratio of the parallel magnetic field of the CAW to the static toroidal field, and p_1 is a constant. It is assumed that the power dissipated to the first wall is negligible (high Q cavity mode), so all wave power is deposited with the electrons. For simplicity let b_{\parallel}/B be spatially uniform; then the model density and temperature profiles give:

$$p = p_0 [1 - (r/\tilde{a})^2]^{\alpha_n + \alpha_T} , \quad (2-11)$$

where we set $e^{-w^2/2} = 1$. The quantity p_0 is a constant determined by setting the volume integral of the power density equal to the CAW power launched by the transmitter:

$$\begin{aligned} P_{rf} &= \int_0^1 dx \chi^2 2\pi \tilde{a}^2 2\pi R_p(\chi) \\ &= 2\pi^2 R \tilde{a}^2 p_0 / (1 + \alpha_n + \alpha_T) , \end{aligned} \quad (2-12)$$

where we define $\chi \equiv r/\tilde{a}$.

Now the total current may be found in the cylindrical approximation by use of Eqs. (2-8)-(2-11) as:

$$\begin{aligned}
I &= \int_0^1 dx \chi^2 2\pi \tilde{a}^2 j(\chi) \\
&= 2\pi \tilde{a}^2 p_0 \frac{2.73 \times 10^{19}}{\bar{n}_e} (1.22 + 2.71 w_0), \quad (2-13)
\end{aligned}$$

where $\alpha_n = \alpha_T = 0.7$. The quantity w_0 is the minimum value of w , which occurs at the peak temperature. Evaluating Eq. (2-8) at $r = 0$ and taking $\alpha_T = 0.7$ and

$\bar{T}_e = 30$ keV, the result for WILDCAT is:

$$w_0 = 1.3 \times 10^{-2} \alpha. \quad (2-14)$$

Eliminating p_0 from Eqs. (2-12) and (2-13), the result specialized to $\alpha_n = \alpha_T = 0.7$ is:

$$P_{rf} = 4.6 \times 10^{-20} R \bar{n}_e (1 + 171 \alpha^{-1})^{-1}. \quad (2-15)$$

This relationship has been used in the reactor parameter surveys such as those presented in Tables 2-2 and 2-6. In Table 2-2, which has beta varying as $\beta_t = 0.36/A$, the maximum field and neutron wall load are held constant, and \bar{T}_e is fixed at 30 keV as A is varied. At low A (<3.0) the equilibrium current increases quickly as A is reduced, and this drives P_{rf} towards larger values. At the other extreme, R increases substantially as A is increased above ~ 3.5 , and this trend forces P_{rf} to increase. Indeed, $A = 3.25$ appears to minimize P_{rf} (although the fusion power is also a minimum here). Of course, for a fixed β_t , P_{rf} could be decreased further according to Eq. (2-15) via reductions in \bar{n}_e and operation at higher plasma temperatures; however, the ensuing reductions in fusion power density have been deemed unacceptable. For the Table 2-2 parameters, n varies from 9 to 24 depending on A . Higher values of n complicate the antenna design and lead to negligible reduction in P_{rf} . Typically, α is in the range 6.1-7.2.

Equation (2-15) has also been used to compute the rf driven current during the start-up phase. For these computations $A = 3.25$, $R = 8.58$ m, and an antenna design with $n = 24$ has been assumed. Hence, the circuit equations are:

$$I_{rf} = P_{rf} (1 + 81/\beta_t) / (3.95 \times 10^{-20} \bar{n}_e)$$

$$I = V/R + I_{rf}$$

$$v = - \frac{d}{dt} (LI) + M \frac{dI^{EF}}{dt} .$$

The value of α has been eliminated from these equations by the use of the general form²⁰ of Eq. (2-6), $\alpha = 2\beta_t^{-1/2} [1 + (\pi A/Sn)^2]^{1/2}$, and β_t has been computed consistently with the P_{rf} supplying the energy increase required for ignition.

The detailed design of the WILDCAT antenna has examined the required rf current drive power as a function of the toroidal mode number. Table 2-11 shows large decreases in α as n is doubled, until $n \sim 12-24$. Larger n requires more antenna elements and yields only small decreases in P_{rf} ; $n = 24$ has been selected as the reference design. The low (\sim MHz) frequencies needed prevent the use of waveguide launchers (which would require dimensions ~ 10 m across), so short loop antennas have been selected. These loops carry rf current in the poloidal direction and consequently couple well to the CAW.

Table 2-11. Wave Frequency and Current Drive Power Versus Parallel Mode Number

For this table, $A = 3.25$, $I = 29.9$ MA, $R = 8.58$ m, $\bar{n} = 2.55 \times 10^{20} \text{ m}^{-3}$, and $\beta_t = 0.111$.

n	α	f (MHz)	P_{rf} (MW)
3	16.6	1.1	266
6	9.79	1.4	163
9	7.91	1.6	133
12	7.14	2.0	121
24	6.30	3.5	107

Figure 1-2 shows the antennas, which are located in sets consisting of ten poloidal locations. These sets are located at twelve toroidal locations, a group of four on each of three blanket modules. Each four-set group spans $1/24$ of the torus with the sets being separated by 3 deg toroidally. By phasing the elements by $0, \pi/2, \pi,$ and $3\pi/2$, a toroidally traveling wave with $n = 24$ can be excited. The loops are mounted on the first-wall/blanket sectors and can be removed with the blanket segments, but maintenance access has been provided without first-wall/blanket removal. (See Sec. 3.4.)

In order to launch an $m = 0$ (poloidally uniform) cavity mode all antennas in a toroidal plane are driven in phase. Theory predicts good coupling if the loops are close to the plasma.²² The antennas are placed within 8 cm of the plasma edge, but they are located in corners of the first wall so the return currents are an average of over 20 cm from the loops. Figures 2-13 and 2-14 show the details of a single antenna loop. The antenna and Faraday shield are actively cooled; being 8 cm into the limiter shadow they are easier to cool than the limiter. One end of the loop is directly attached to the first wall while the other is anchored by a dielectric window in the coaxial lead at a good distance (~ 75 cm) from the first wall. Although longer antennas would increase the loading resistance, a longer span might be difficult to support. Similar all metal antennas have worked well on TFR²³ and PLT²⁴ although at somewhat higher frequencies. The necessity of the Faraday screens and their geometry for large tokamaks is still open to debate. Rather than using a cage which completely encloses the antenna loop, an open screen approach as proposed for TCA, the Swiss Alfvén wave heated tokamak,²⁵ has been adopted. The screen is a staggered bank of tubes which inhibits electron motion along the toroidal field in order to prevent plasma shorting of the antenna. In addition, the screen provides some protection from the thermal load associated with a plasma disruption. The structural members of the antenna are the same steel used in the reactor blanket; all exposed surfaces are plated to several millimeters with beryllium, a good conductor.

The requisite 107 MW of current drive power is divided roughly equally among the 120 antennas. Each antenna lead is 3-1/8 in., 50 Ω coax which carries less than a megawatt, well within breakdown limits. The coax is pressurized beyond the BeO window, and additional windows at the reactor building serve as multiple barriers to tritium escape (see Fig. 2-15). Operating at 3.5 MHz, this coax suffers a very low loss (~ 0.021 db/100 ft). Assuming a typical run of 22 m, the power transmission efficiency through each coax is $\eta_{TL} = 0.9986$.

Both triodes and tetrodes are suitable high power amplifiers (HPA) at this frequency. The tubes on PLT (EIMAC X2159) operate above 50% efficiency for short pulses.²⁶ CW operation at 75% efficiency was projected in the Argonne EPR study (EIMAC X2176).²⁷ The WILDCAT efficiency is based on predictions²⁸ that a development program can deliver an amplifier combination in the

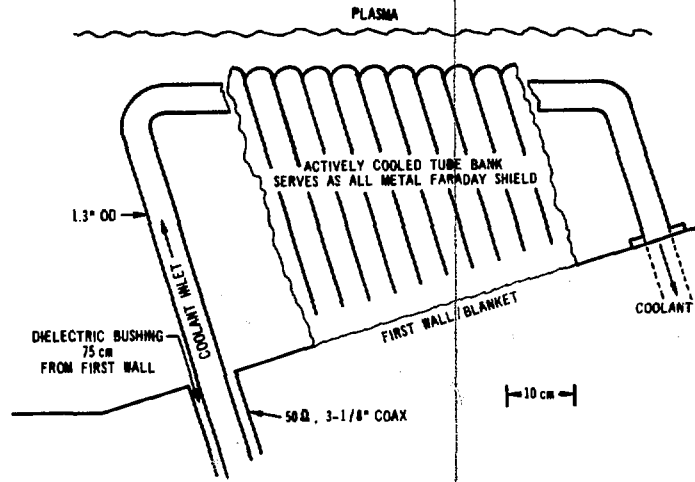


Fig. 2-13. Side view of antenna and Faraday shield.

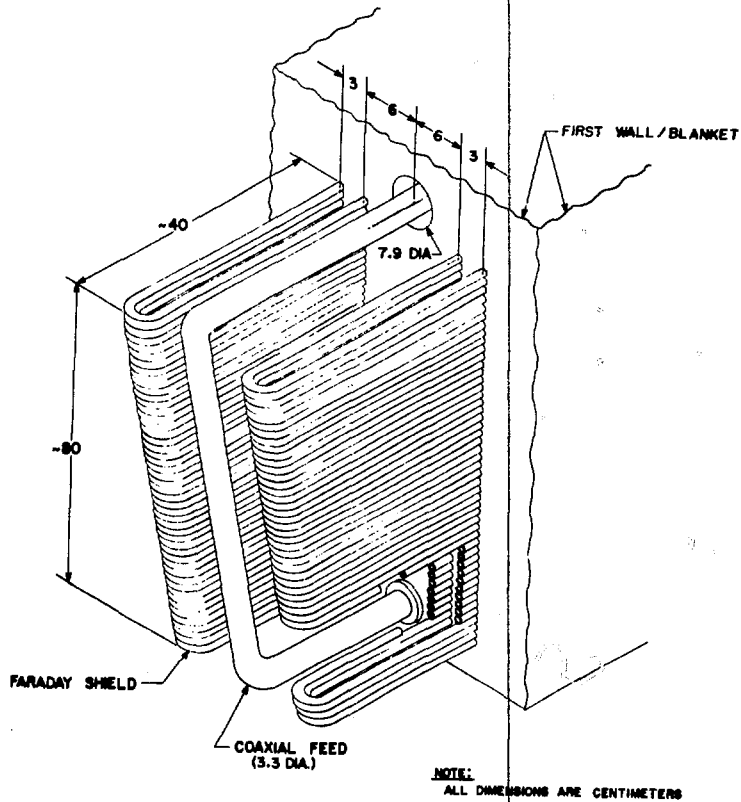


Fig. 2-14. Isometric view of antenna assembly. Dimensions are approximate.

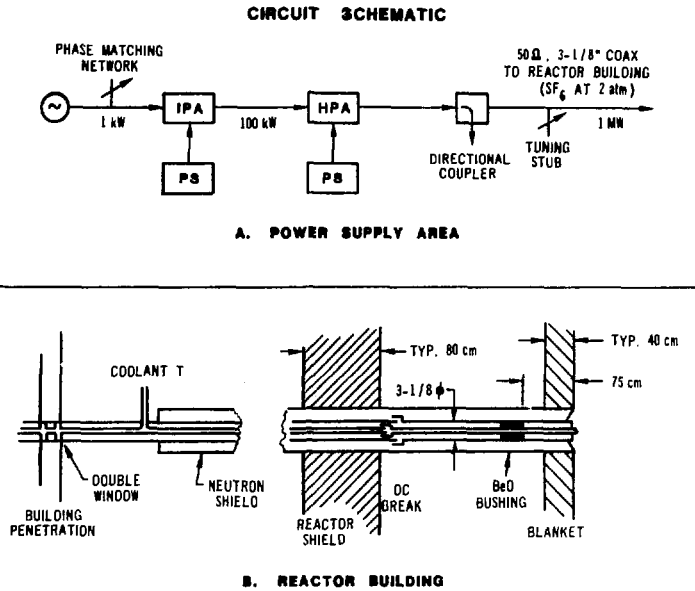


Fig. 2-15. Circuit schematic including transmission line inside reactor building.

WILDCAT time frame with an efficiency $\eta_T = 0.85$. The HPA can use a low regulation power supply with $\eta_{PS} = 0.95$. Additional losses at the windows, directional couplers, and tuners are accounted for with $\eta_E = 0.96$. If the antennas are not perfectly matched to the load, some power is reflected into the coaxial feeds. Based on ICRF experiments,^{23,29} the loop radiation efficiency will be at least $\eta_L = 0.90$. Thus, the overall electric-to-current-drive power efficiency is $\eta = \eta_{TL} \eta_T \eta_{PS} \eta_E \eta_L = 0.70$. In consequence, the electrical power required to maintain steady state operation with $I = 29.9$ MA is $P_{rf}^{(e)} = P_{rf} / \eta = 153$ MW.

The electric power required to maintain the toroidal current is identical to that of STARFIRE, even though the toroidal current is three times larger. The reason for this is principally that the CAW is several times more efficient than lower hybrid waves for driving current in a large aspect ratio torus.

There is a potential problem with trapped electrons for WILDCAT with $A = 3.25$. In particular, waves such as the CAW, which have parallel phase speeds much less than the electron thermal speed ($w \ll 1$), transfer their momentum to

magnetically trapped electrons. In neoclassical theory these electrons should drift in minor radius rather than being accelerated around the torus in analogy to the Ware drift. This momentum source could establish a bootstrap current. However, in light of present experiments,³⁰ it is clear that electrons do not behave neoclassically, so there is less confidence compared to the lower hybrid system proposed for STARFIRE that the CAW would drive currents as calculated here.

Loop antennas appear workable at these low frequencies. Circular ducts with diameters less than 10 cm are almost invisible to neutrons diffusing through the blanket and shield.³¹ Neutronics calculations show a three decade decrease in the neutron flux 50 cm from the first wall at the top or bottom of the reactor. Thus, ceramic windows placed 75 cm from the first wall may be expected to last several years before requiring replacement.

2.7 ECRH Preionization

The electron cyclotron resonance heating (ECRH) system required to preionize the WILDCAT plasma is based on known experimental results on the Tokapole³² and ISX-B tokamak.³³ Power is initially absorbed at the radial location of the electron cyclotron resonance and is absorbed over an undetermined narrow radial width δ . The power density required to reduce the loop voltage during startup is in the range of $1 \times 10^2 \text{ W/cm}^{-3}/\delta$ with δ in meters. The WILDCAT design calls for breakdown at the minor axis where $B_0 = 8.23 \text{ T}$, so a frequency of 230 GHz is required. The resonance area at $R_0 = 8.58 \text{ m}$ has a height of $2\kappa R_0/A = 8.45 \text{ m}$ and a width δ , giving a required absorbed power of $P_{\text{ECR}} \sim 5 \text{ MW}$. The waves are launched from the inboard side with mixed polarization for $\sim 50 \text{ ms}$ into an initial pressure of 10^{-4} torr, resulting in fully ionized plasma of density $\sim 5 \times 10^{12} \text{ cm}^{-3}$ and electron temperature $\sim 10\text{-}20 \text{ eV}$ in the resonance and nearby upper hybrid layers. The power is delivered through 2-1/2 in. waveguides, which have demonstrated very high intensity transmission ($>20 \text{ kW/cm}^2$) on current experiments. As few as three waveguide systems may be adequate to deliver the power.

Gyrotron oscillators generally must produce less power as the frequency is increased. According to Ref. 34, the USSR has a 150-GHz source which generates 22 kW CW (22% efficiency), and MIT is designing a 100-kW tube at 150 GHz. However, the only source at 240 GHz is a 3 kW oscillator under construc-

tion at NRL. It appears likely that new concepts must be developed if a megawatt source is desired at these very high frequencies. The quasioptical klystrogyrotron is one such promising approach; a 1 MW tube at 150 GHz (<26% efficiency) is being developed at NRL.³⁵ It should be noted that frequencies in excess of 200 GHz cannot utilize commercial magnets in the tube. The high frequency requirement is a result of the high toroidal field in WILDCAT. An optimistic estimate of the tube efficiency is $\eta_T \sim 0.25$ at 230 GHz and a few megawatts output. This efficiency may require energy recovery in the tube. The high voltage (~ 80 kV), highly regulated power supplies for these tubes are also likely to be relatively inefficient, with $\eta_{PS} \sim 0.70$.³⁴ The waveguide transmission lines are over 10 m in length and result in power transmission efficiencies $\eta_{TL} \sim 0.80$, so the overall power efficiency is ~ 0.14 . Thus, about 15 MW of primary electric power is required for ECRH preionization.

The tube power supply occupies about 50 m² floor space in a room adjacent to the reactor hall. Electrical equipment in the transmission system includes such items as: launcher assembly in the vacuum vessel, launcher cooling system, two to three windows per waveguide, window cooling system, directional couplers with a d.c. break, SF₆ (at 3 atm) pressurization, high-power waveguide switches, power dumps, (possibly) mode filters or converters, and arc detectors and switchgear. System costs are expected to be in the range of \$6/W, based on our limited present-day experience with (lower frequency) gyrotrons.³⁴

REFERENCES

1. K. Evans, Jr. et al., "D-D Tokamak Reactor Studies," Argonne National Laboratory Report, ANL/FPP/TM-138 (1980).
2. D. R. Cohn, R. R. Parker, and D. L. Jassby, Nucl. Fusion 16, 31 (1976); and D. L. Jassby, D. R. Cohn, and R. R. Parker, Nucl. Fusion 16, 1045 (1976).
3. C. C. Baker, et al., "STARFIRE - A Commercial Tokamak Fusion Power Plant Study," Argonne National Laboratory, ANL/FPP-80-1 (1980)
4. A. M. Todd, et al., Nucl. Fusion 19, 743 (1979).
5. J. Brooks, K. Evans, Jr., H. Stevens, and L. Turner, "The Equilibrium Field Coil Design for the Argonne EPR Design," Proc. 7th Symp. Engineering Problems of Fusion Research, IEEE Pub. 77CH1267-4-NPS (1977), p. 1678.

6. K. Evans, Jr., D. A. Ehst and P. Messerschmidt, "Equilibrium Field Coil Considerations for Tokamak Reactors," in Proc. 3rd Topical Mtg. on the Technology of Controlled Nuclear Fusion, ANS Publication No. CONF-780508, Vol. 2, (1978), p. 1084.
7. L. C. Bernard and R. W. Moore, "Systematic Optimization of Tokamaks to All Ideal MHD Modes," General Atomic Company, GA-A15694 (1980).
8. B. Coppi, A. Ferreira, J. W. K. Mark, and J. J. Ramos, "A Second Stability Region of Finite- β Plasmas," in Comments on Plasma Physics and Controlled Fusion, 5, 1 (1979).
9. J. D. Callen and R. A. Dory, Phys. Fluids 15, 1523 (1972).
10. V. S. Mukhovatov and V. D. Shafranov, Nucl. Fusion 11, 605 (1971).
11. L. E. Zakharov, V. D. Shafranov, Sov. Phys. Tech. Phys. 18, 151 (1973).
12. M. Gomolinski and G. Bube, J. Nucl. Mater. 43, 59 (1972).
13. D. E. Mazey and F. Menzinger, J. Nucl. Mater. 48, 15 (1973).
14. J. F. Bates and A. L. Pitner, Nucl. Technol. 16, 406 (1972).
15. F. W. Wiffen, Nucl. Metall. 18, 176 (1973).
16. T. Ohkawa, Nucl. Fusion 10, 185 (1970).
17. N. J. Fisch, Phys. Rev. Lett. 41, 873 (1978).
18. D. A. Ehst, Nucl. Fusion 19, 1369 (1979).
19. D. A. Ehst, "Lower Hybrid Heating and Current Drive System for a Tokamak Reactor," J. Fusion Energy (to be published).
20. N. J. Fisch and C. F. F. Karney, Phys. Fluids 24, 27 (1981).
21. D. A. Ehst, "Wave-Driver Options for Low Aspect Ratio Steady-State Tokamak Reactors," J. Fusion Energy (to be published); see also "ANL/FPP/TM-141 (1981).
22. E. Ott, J. M. Wersinger, and P. T. Bonoli, Phys. Fluids 21, 2306 (1978).
23. J. Jacquinet, et al., Proc. 11th Symp. on Fusion Technology, Oxford, (1980).
24. P. Colestock, private communication.
25. A. D. Cheetham, et al., "The TCA Tokamak Project Report 1979," Ecole Polytechnique Federale de Lausanne, LRP 162/80 (1980).
26. J. Q. Lawson, et al., Proc. 7th Symp. Engineering Problems of Fusion Research, IEEE Pub. No. 77CH1267-4-NPS, (1977) p. 1125.

27. W. M. Stacey, Jr., "Tokamak Experimental Power Reactor Studies," Argonne National Laboratory, ANL/CTR-75-2 (1975).
28. TRW presentation to U.S. Department of Energy, Frederick, MD, February 24, 1981.
29. J. Adam, et al., Proc. 5th Conf. on Plasma Physics and Controlled Nuclear Fusion, Tokyo, 1974, (IAEA, Vienna, 1975), Vol. ii, p. 65.
30. J. T. Hogan, Nucl. Fusion 21, 365 (1981).
31. J. Jung and M. A. Abdou, Nucl. Technol. 41, 71 (1978).
32. D. J. Holly, et al., "Tokamak Startup with Electron Cyclotron Heating," University of Wisconsin, COO-2387-120 (1980).
33. R. M. Gilgenbach, et al., Nucl. Fusion 21, 319 (1981).
34. A. Bondeson, et al., Bull. Am. Phys. Soc. 26, 1034 (1981).
35. "A Design Analysis of Supplemental Heating Systems," TRW Final Report for USDOE Contract DE-AC03-80EK 52058 (1981).

Section 3

FIRST-WALL/BLANKET/SHIELD



3. FIRST-WALL/BLANKET/SHIELD

The limiting factor on fusion reactor first-wall power loading appears to be the heat load.¹ Since the D-D fuel cycle has a higher ratio of charged particles to neutrons, this means the neutron wall load is consequently reduced. The resulting lower power density (most of the D-D power still comes from neutrons) is a disadvantage, but some advantage is obtained in longer component lifetimes. These considerations are treated in Sec. 3.1. Since no tritium breeding occurs in a D-D reactor, there is an opportunity to design the blanket/shield for increased power generation performance. A substantial amount of effort in this direction has been made for WILDCAT and is discussed in Sec. 3.2. Section 3.3 treats the thermal hydraulics for WILDCAT, and the disassembly and maintenance concepts, which are somewhat different from those for STARFIRE, are described in Sec. 3.4.

3.1. First Wall

A schematic of the first wall, which utilizes a coolant panel concept is shown in Fig. 3-1. The panels are made of PCA stainless steel and consist of a 1.5-mm thick corrugated sheet attached to a backplate which is 3 mm thick. The light-water coolant flows in the closed parts of the corrugation. The center-to-center distance between the coolant channels is 19 mm and the cross-sectional area of the coolant channels is 35% of the volume of the first wall. The corrugated part of the coolant panels has a low-Z coating consisting of 3 mm of beryllium. The coolant panels are attached to monolithic blanket blocks. The coolant fraction for the blanket region is 10% on the average, the balance being PCA stainless steel. The neutronic calculations in Sec. 3.2 are based on these coolant volume fractions.

The lifetime of the first wall in WILDCAT has been estimated with a one-dimensional computer code. The code predicts the interactions of physical sputtering rates, induced stresses, and mechanical properties with time for a given set of reactor operating conditions. The details of the code will be given elsewhere.² The reactor conditions used for the calculations are given in Table 3-1. The first wall configuration represents the outer part of the corrugations and is assumed to be a plate that receives uniform surface heat and neutron fluxes. The outer 3 mm of the plate facing the plasma is

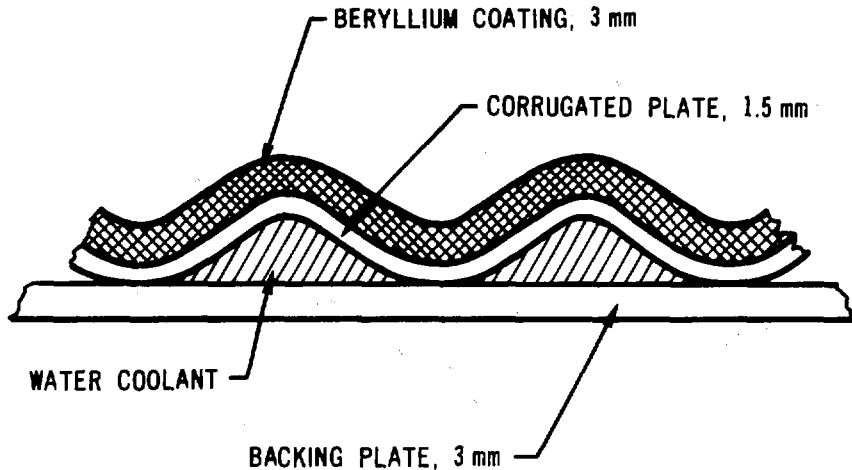


Fig. 3-1. Schematic cross section of first wall.

beryllium, and the remaining 1.5 mm is PCA, an austenitic stainless steel that is very similar to Type 316 stainless steel. The primary differences between the two steels are the lower swelling and creep rates predicted for PCA. The STARFIRE first-wall structural material is also PCA and additional property data are given in that report.¹ The sputtering loss rate of the first wall has been determined assuming the sputtering characteristics of beryllium. The bulk stresses and property changes have been determined assuming the physical characteristics of PCA alone, since the code cannot at this time determine the characteristics of duplex structures.

The sputtering rate of the first wall has been determined using the particle flux parameters shown in Table 3-1. All ionized particles coming out of the plasma are expected to strike the limiter so that only charge exchange neutrals strike the first wall. Since the helium and beryllium particles are predicted to remain in the ionized state, they do not strike the first wall. The particle energy distribution is assumed to be a Maxwellian that is peaked at 1200 eV. This energy is considerably above the peak sputtering energy of ~400 eV for beryllium, and therefore the sputtering loss rate is quite low. The model used to determine the sputtering rate is that developed by Smith.^{3,4} The physical sputtering coefficient is calculated to be 0.0105 and results in a calculated sputtering loss rate of 1.45×10^{-4} m/y at a 100% duty factor.

The temperature distribution through the first wall at several times during the reactor lifetime is shown in Fig 3-2. The surface of the plate

Table 3-1. First-Wall Parameters for Lifetime Calculations

<u>Operating Parameters</u>	
Surface heat flux, MW/m ²	1.13
Neutron wall load, MW/m ²	0.6
Surface particle flux, (n/m ²)/s	3.72 × 10 ¹⁹
Particle flux composition, %	
Hydrogen	6.6
Deuterium	93
Tritium	0.4
Average particle energy, eV	1200
Burn time	
Pulsed case, h	2.5
Steady state case, mo	6
<u>Design Parameters</u>	
Effective plate thickness, mm	
PCA	1.5
Beryllium	3
Coolant inlet temperature, °K	553
Heat transfer coefficient, (W/m ²)/K	20,000
Plate constraint	Free to expand, but not bend
Initial crack length, mm	0.45
<u>Material Parameters</u>	
Material	
For bulk property calculations	PCA
For sputtering calculations	Beryllium
DPA rate, DPA/(MW-y/m ²)	17.7
Helium generation rate, appm/(MW-y/m ²)	125

exposed to the plasma for this and all other relevant figures in this section is at the zero point of the abscissa. Early in the plant life the temperature of this outer surface reaches 835°K during the burn cycle. As the first wall is sputtered, the surface temperature decreases until it reaches 710 K at the end of 20 y, when the wall thickness has been reduced to 1.8 mm. The changes in the temperatures of the first wall have an impact upon many other property changes. In particular, radiation induced swelling, which is strongly

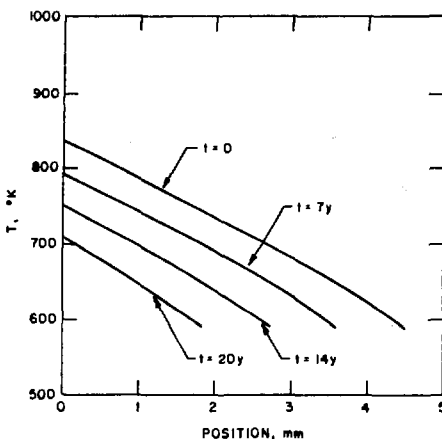


Fig. 3-2. WILDCAT first-wall temperature distribution.

temperature dependent, changes with time on the outer surface, as shown in Fig. 3-3. After approximately 10 y the swelling rate starts declining, since the material with the highest swelling sputters, continuously exposing material with a lower total swelling. The swelling near the back surface of the stainless steel, adjacent to the coolant, remains quite low during the 20-y period.

The thermal and swelling gradient through the first wall affect the stress levels during the burn cycle. At the beginning of reactor operation there is a large thermal stress gradient as shown in Fig. 3-4 for $t = 0$. The stress gradient is approximately linear with position. There are compression stresses at the top surface and tensile stresses at the back surface. The maximum stresses are below the yield strength of PCA in the 20% cold-worked condition. During operation, radiation creep causes the stresses to relax during the burn cycle until the stress gradient approaches zero after about 1.6 y. When the swelling rate becomes large near the outer surface, the stresses again change. In order to compensate for the volume change that accompanies swelling, the stresses near the top surface become compressive, and the stresses towards the back surface become tensile at about 8 y. The resulting stress distribution is the one that produces a uniform strain rate (from swelling and creep) through the entire plate. The magnitude of the stresses is proportional to the ratio of the swelling rate to the creep rate.

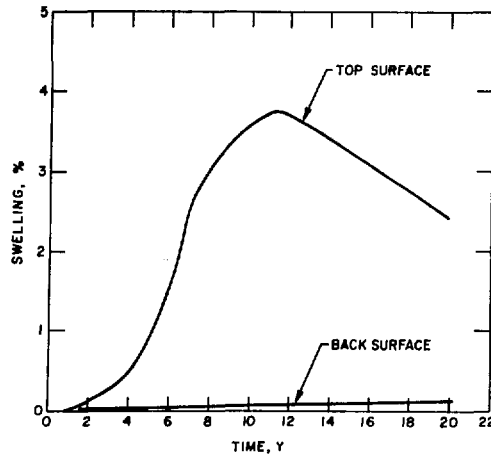


Fig. 3-3. WILDCAT PCA swelling.

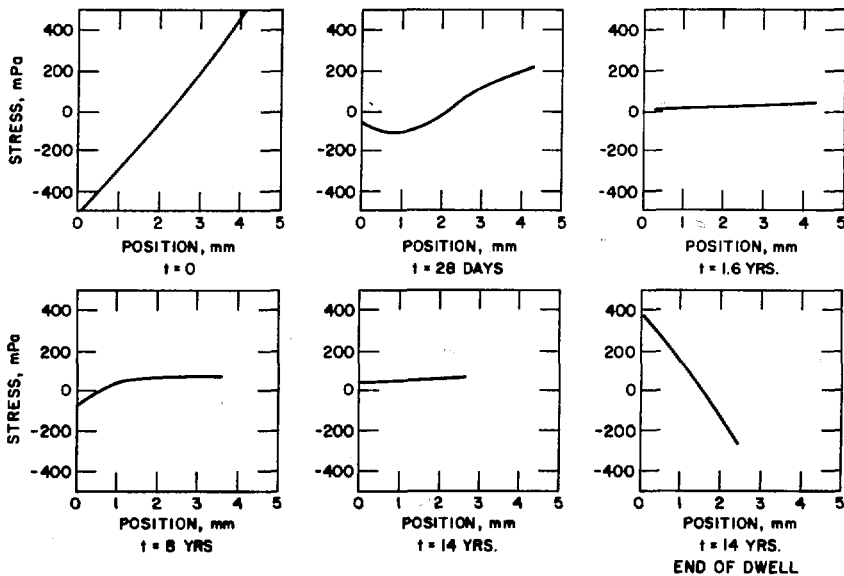


Fig. 3-4. WILDCAT first-wall stress distribution.

As the swelling rate is reduced near the outer surface, the stress gradient returns to approximately zero at about 14 y. The total strain increase due to swelling and creep is <2.5% during the twenty-year period. It should be noted that the stress gradient during the dwell part of the burn cycle is large when the stresses are close to zero. This occurs at the end of the dwell period in the fourteenth year. The stresses at the outer surface are tensile, and the stresses at the back surface are compressive during the dwell period.

The crack growth rate within the first wall depends on the temperature and stress distributions as well as on the initial flaw size and the burn cycle frequency. Two cases have been examined for WILDCAT: steady-state operation (6-mo burn period) and pulsed operation (2.5 h burn period). For initial crack lengths of 0.45 mm at the top and back surfaces, there is no significant crack growth predicted for steady-state operation. The much higher number of cycles for the 2.5 h burn time results in significant crack growth, as shown in Fig. 3-5. At the outer surface crack growth is initially slow when the stress cycle is from zero to compressive, but it increases rapidly after stress relaxation, when the stress cycle becomes tensile to zero. The crack growth continues to the middle of the plate, where it stops. The length of the crack then decreases due to the sputtering loss of material from the top surface. Crack growth at the back surface is initially rapid when the stress cycle is from zero to tensile, but the growth slows to close to zero after stress relaxation occurs. Although the crack growth rate is slow from the back surface, it is continuous with time so that at the end of 20 y, it is larger than the crack from the top surface. Neither crack is predicted to cause a failure in the first wall, however.

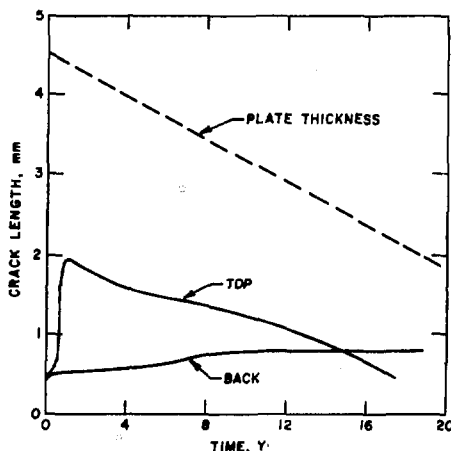


Fig. 3-5. WILDCAT crack growth.

Radiation embrittlement is also a concern for the first wall lifetime. At the end of 4 y, the uniform elongation is reduced to ~2%; at the end of 8 y it is reduced to ~1%; and at the end of 20 y it is reduced to ~0.5%. For

normal operation, the ductility loss is not predicted to cause failure of the first wall, but off-normal events may lead to brittle failure of the wall.

In conclusion, for normal operation the WILDCAT first wall design should achieve a lifetime of ~20 y. The primary limit on the lifetime is the sputtering loss of the beryllium cladding. It may not be advisable to substantially increase the cladding thickness, however, because of the additional thermal stresses that would result. The total creep and swelling strains are expected to be modest, and little crack growth is predicted for steady-state operation. Radiation embrittlement could be a concern, but additional analysis of off-normal events is needed.

Based on the more extensive analyses of the heat stresses on the first-wall structure which was done for STARFIRE,¹ it can be assumed that if the WILDCAT heat load were much larger than 1 MW/m^2 , then the heat load would become the limiting factor for the WILDCAT first-wall life. This fact has limited the power density in WILDCAT. In order to increase the power density (e.g. by the use of more heat-resistant wall materials), however, one would also need to increase the thermal power. This could not be done in any substantial manner without increasing either the size, toroidal field, or the plasma beta further. Thus, the use of more heat-resistant materials does not seem necessary.

3.2 Blanket/Shield Nuclear Analysis

The nuclear analysis presented in this section is categorized into the following five major design areas: (1) the nuclear response of the first-wall/blanket; (2) the inboard radiation shielding; (3) the outboard radiation shielding; (4) the system neutron energy multiplication; and (5) the reactor activation and its environmental impact. Effort has been devoted to make comparisons with the D-T fueled STARFIRE design¹ in order to identify the advantages as well as the disadvantages of D-D fuel cycles for commercial-grade reactors. Many of the nuclear design aspects for WILDCAT are driven by the same design criteria as those employed for STARFIRE, such as the radiation protection of the superconducting magnets, reactor accessibility shortly after shutdown, and minimization of the radioactive inventories. The primary objective of the nuclear analysis for the WILDCAT design is to reveal how the reactor performance is impacted by the two major conceptual differences associated

with the D-D reactor, that is, the elimination of tritium breeding and the lower neutron wall loading.

Figure 3-6 shows the first-wall surface configuration of WILDCAT. The actual wall area as shown in Fig. 3-6 is 1304 m². (An area of 1250 m², which is the area of a surface 0.2 m from the plasma edge, has been used to calculate wall loads throughout the report, however.) Two, one-dimensional, cylindrical models have been used to represent the first-wall/blanket/shield configuration. Sections A and E in Fig. 3-6 have been modeled by cylindrical shells with axis along the reactor major axis. Sections B, C, and D have been modeled by cylindrical shells with axis corresponding to the reactor minor axis. A detailed layout of the first-wall/blanket/shield models used for the analysis is shown in Fig. 3-7.

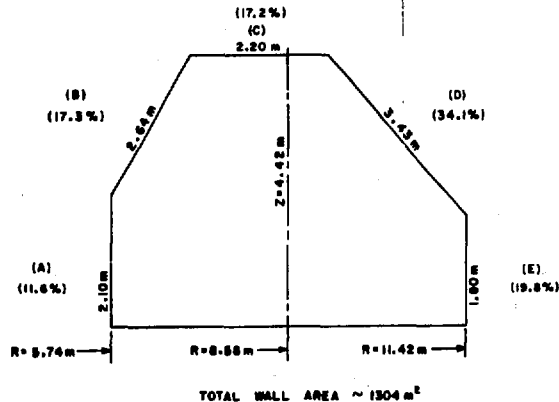


Fig. 3-6. Vertical cross section of first wall.

The neutron and gamma transport problems have been solved by ANISN⁵ with the S_8 - P_3 approximation. The cross-section libraries for the particle transport⁶ and the nuclear response function⁷ used for the analysis consist of 46 neutron groups and 21 gamma groups. The reactor activation analysis presented in Sec. 3.2.5 has been performed by RACC⁸ based upon the Gear stiff matrix method.⁹

3.2.1 Nuclear Response

The WILDCAT first wall has a 3-mm beryllium coating on a PCA structure for protection against erosion. The coolant is light water. The first wall configuration is shown in detail in Fig. 3-1. An effective total wall thickness

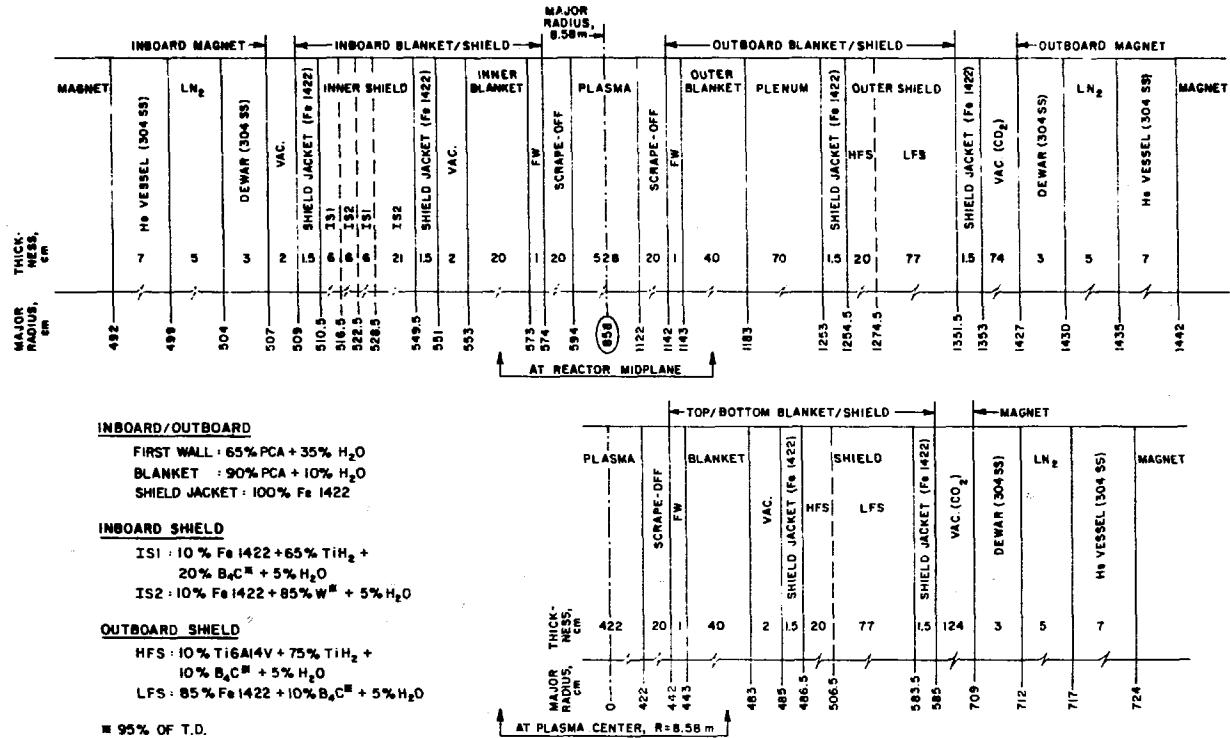


Fig. 3-7. Two geometrical models used for one-dimensional nuclear analyses.

of 7.0 mm consisting of 35% water has been used for the neutronic analysis. The inboard first wall (section A in Fig. 3-6), which occupies ~12% of the total wall area, is followed by a 20 cm-thick inner blanket. The outboard wall (section E) with ~20% of the total area and the top and bottom walls (sections B, C, and D) with ~68% of the area are followed by a 40 cm-thick outer blanket. The material composition of all the blanket segments is represented neutronically by a homogeneous mixture of 90% PCA plus 10% H₂O. The difference in the blanket thickness between the inner and outer regions is due to the inboard radiation shielding considerations discussed below.

Table 3-2 summarizes several nuclear response rates at the first wall. The total neutron wall load is 0.6 MW/m² (0.5 MW/m² of 14 MeV neutrons and 0.1 MW/m² of 2.45 MeV neutrons). The plant availability is assumed to be 75%. Except for the instantaneous response of the particle fluxes, all of the accumulated response rates account for this plant availability. It is found that there exists a substantial variation of the response rates along the poloidal direction due to the toroidal curvature.¹⁰ The maximum variation amounts to slightly less than 40% in the gas production rates and the atomic displacement and to ~10% in the particle fluxes. Note that the analysis presented here does not account for the shifting of the neutron source toward the outboard direction for the high beta MHD plasma equilibrium. It is also noticed that all of the response rates presented in Table 3-2 are high in comparison with those of D-T systems. For instance, the INTOR first-wall design,¹¹ based on a neutron wall load of 1.3 MW/m², shows total neutron fluxes of 5.0×10^{18} n/m²-s and 5.3×10^{18} n/m²-s at the inboard and outboard regions, respectively. The significantly high neutron flux on the WILDCAT first wall reflects the relatively large population of soft neutrons resulting from the 2.45-MeV source neutrons. In fact, the energy breakdown of the neutron flux presented in Fig. 3-8 indicates that almost half of the total neutron flux is contributed by neutrons with energies below 0.1 MeV over the entire first-wall/blanket region. The neutron spectra displayed in Fig. 3-9, which are plotted at the respective midpoints of the first wall and blanket, show large increases at ~2.45 MeV particularly in the first-wall region (which is closer to the source region) and exhibit a nearly 1/v spectrum variation with energy below an energy of 0.1 MeV. This 1/v variation results largely from the presence of the light-water coolant in the system.

Table 3-2. Nuclear Response Rates^a at First Wall

	Gas Production (appm/y)		Atomic Displacement (dpa/y)	Particle Flux (10 ⁻¹⁸ n/m ² -s)	
	Hydrogen	Helium		Neutron	Photon
Inboard					
Be	28	1553	---	4.84	1.91
PCA	207	55	5.7	4.55	1.87
Top/Bottom					
Be	28	1590	---	4.79	1.90
PCA	219	58	6.0	4.58	1.87
Outboard					
Be	38	2090	---	5.46	2.11
PCA	284	76	7.5	5.15	2.08

^a Neutron wall load:

14.06 MeV neutron: 0.498 MW/m²
 2.45 MeV neutron: 0.0998 MW/m²
 Total: 0.5978 MW/m²

Plant availability: 75%

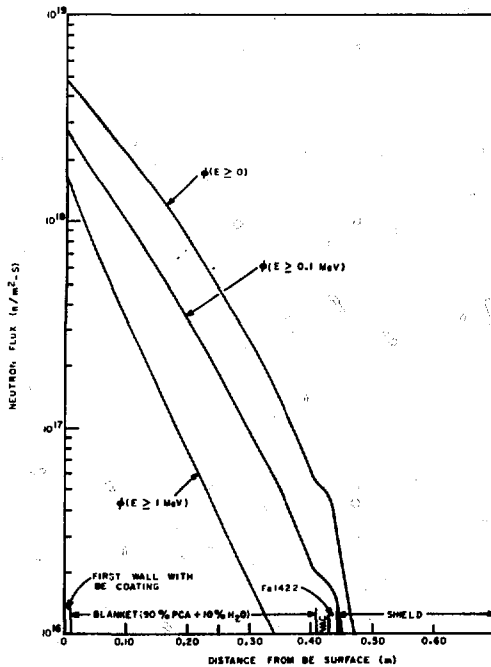


Fig. 3-8. Spatial variation of neutron fluxes.

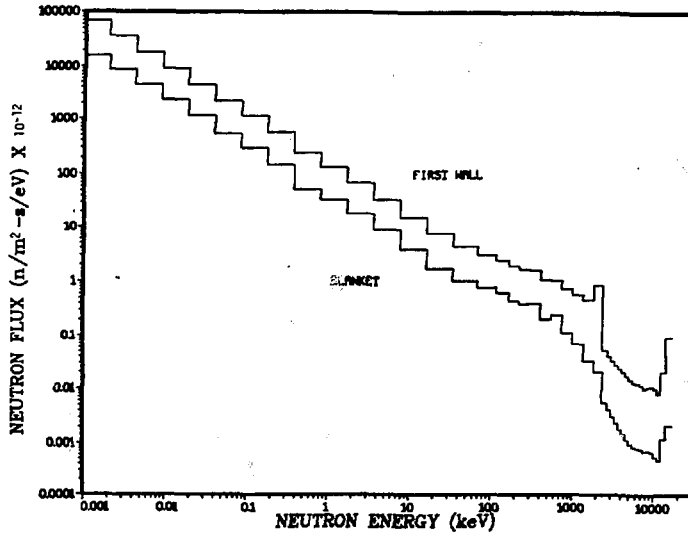


Fig. 3-9. Neutron spectrum in outboard first-wall blanket.

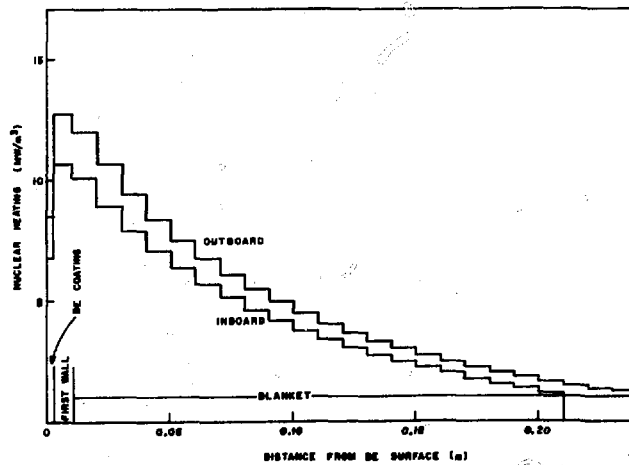


Fig. 3-10. Spatial variation of nuclear heating.

A large geometrical effect owing to the toroidal curvature can be also seen in the nuclear heating rates presented in Fig. 3-10. The regional maximum nuclear heating in the inboard section is $\sim 6.8 \text{ MW/m}^3$, $\sim 10.7 \text{ MW/m}^3$, and $\sim 10.1 \text{ MW/m}^3$ in the beryllium coating, first wall, and blanket respectively, whereas the corresponding outboard values are $\sim 8.5 \text{ MW/m}^3$, $\sim 12.7 \text{ MW/m}^3$, and $\sim 11.9 \text{ MW/m}^3$, indicating an approximately 20% poloidal variation from the inner-most region to the outer-most region. The nuclear heating rate at the top and bottom regions is in between these two extremes. Again it is noted that these heating rates are substantially higher than what one expects for D-T systems operating at the same neutron wall load of 0.6 MW/m^2 . The STARFIRE¹ first-wall design, for example, has a maximum PCA wall heating rate of $\sim 35 \text{ MW/m}^3$ at the 3.6 MW/m^2 neutron wall load, which can be scaled to a maximum heating rate of $\sim 5.8 \text{ MW/m}^3$ for a 0.6 MW/m^2 wall load.

Another important design consideration regarding the first-wall heat load is the energy deposition of bremsstrahlung radiation. The most dominant X-ray interaction with the first-wall material in the energy range of interest is the absorption reaction due to the photoelectric effect. Table 3-3 lists the experimental results for the photoelectric cross section^{12,13} along with the associated linear absorption coefficient, μ , and the e-fold distance defined as $1/\mu$. Data on the two relevant first-wall materials, beryllium and iron, are given as a function of X-ray energy ranging from 10 keV to 100 keV.

It is found that at $\sim 10 \text{ keV}$ X-ray energy, for instance, most of the bremsstrahlung radiation power is likely to be dissipated in a wall depth on the order of microns or less for a first-wall design using an iron-base material. This result justifies the assumption that the radiation power in a D-T system can be treated as a surface heat load at the first-wall. In the case of the higher temperature in alternate fuel systems, however, the e-fold distance in the energy range of interest can be two to three orders of magnitude higher than in D-T cases. The peak electron temperature of the WILDCAT design, for example, is $\sim 55 \text{ keV}$. From Table 3-3 the distance required for an order of magnitude energy attenuation is as large as $\sim 2.4 \text{ mm}$ for the 55-keV X-ray energy. Not all of the bremsstrahlung power of 951 MW is delivered to the first-wall by monochromatic X-rays of 55 keV, however.¹⁴ Further investigation is required to determine to what extent the radiation power penetrates through the first-wall and is dissipated as volumetric heat. This issue should be

Table 3-3. X-Ray Attenuation Coefficients of the Photoelectric Reaction for Beryllium and Iron

X-Ray Energy (keV)	Beryllium ^d			Iron ^b		
	Experiment ^c (barn/atom)	Linear Coefficient, μ (cm ² /g)	e-Fold Distance (cm)	Experiment ^c (barn/atom)	Linear Coefficient, μ (cm ² /g)	e-Fold Distance (cm)
10	5.23	6.46(-1) ^c	1.55(0)	16600	1.41(3)	7.10(-4)
15	1.34	1.66(-1)	6.04 (0)	5335	4.52(2)	2.21(-3)
20	0.51	6.30(-2)	1.59(1)	2300	1.95(2)	5.13(-3)
30	0.13	1.61(-2)	6.22(1)	718	6.98(2)	1.43(-3)
40	0.05	6.18(-3)	1.62(2)	306	2.59(1)	3.85(-2)
50	0.02	2.47(-3)	4.05(2)	152	1.29(1)	7.76(-2)
60	0.01	1.24(-3)	8.09(2)	89.1	7.56(0)	1.32(-1)
80	—	—	—	37.5	3.18(0)	3.14(-1)
100	—	—	—	18.9	1.60(0)	6.24(-1)

^a1.236 × 10²³ atom/cc.

^b8.480 × 10²² atom/cc.

^cSee Refs. 12 and 13.

^dReads as 6.46 × 10⁻¹.

further emphasized for beryllium-coated, first-wall designs, as the X-ray attenuation coefficient for beryllium is several orders of magnitude lower than that of iron. As shown in Table 3-3 the e-fold distance of beryllium is, even at ~10 keV, on the order of centimeters, substantially greater than the physical thickness of the beryllium coating in the WILDCAT design.

3.2.2 Inboard Radiation Shielding

The inboard radiation shielding is one of the most important nuclear design areas because the reactor power performance is strongly dependent upon the distance, Δ_{BS}^i , between the first wall and the peak field position of the toroidal field coil. Note that the toroidal field falls as 1/R over this distance. The relatively short distance of 1.2 m (including a total gap spacing of 4 cm) for Δ_{BS}^i in the STARFIRE design was achieved with the combined use of tungsten and boron carbide shield layers. Although there are some concerns about the use of tungsten, such as the resource limitation and the high material cost, the possible reduction in Δ_{BS}^i with tungsten may compensate for the associated penalty. The inboard shield optimization for the WILDCAT design has been further extended by including a high-hydrogen-content material (TiH₂) in the inboard shield. Based on the STARFIRE results, the shield layer dimensions and material composition described in Table 3-4 have been chosen for the WILDCAT shield optimization. Figure 3-11 presents the variation of absorbed nuclear dose in an epoxy insulator and the variation of anticipated plant lifetime for the three shield layer cases. The dose limit criterion used for the analysis is 10⁸ Gy,¹⁶ and the plant availability is assumed to be 75%. Figure 3-11 clearly indicates the importance of the use of the hydrogenous material in the radiation field environment, particularly in its co-use with boron-carbide. By employing 10-20 vol-% B₄C along with TiH₂ in the inboard shield, the reactor lifetime can be prolonged by 20-30 y for a given dose limit relative to shield designs without TiH₂. As shown in Fig. 3-12, the primary impact of the use of TiH₂ is substantial neutron spectrum softening, resulting in a drastic decrease of the neutron population in the energy interval of 1 MeV to 0.1 keV. Most of the nuclear dose in the epoxy insulator is contributed by the neutrons in this energy interval. The decrease in the neutron distribution at the energies under question also reduces the secondary gamma generation as shown in Fig. 3-13 and thereby further reduces the heat load in the epoxy.

Table 3-4. Dimensions and Material Compositions of the Inboard System Used for the Shielding Optimization Analysis

Region	Thickness (m)	Composition
First wall	0.01	50% PCA + 5% H ₂ O
Blanket	0.20	90% PCA + 10% H ₂ O
Shield 1	0.20	10% Fe-1422 ^a + 10% H ₂ O + 80% W ^b
Shield 2	0.05	10% Fe-1422 ^a + 10% H ₂ O + 80% X
Shield 3	0.09	10% Fe-1422 ^a + 10% H ₂ O + 80% W ^b
Shield 4	0.08	10% Fe-1422 ^a + 10% H ₂ O + 80% X

Material Composition of X (vol-%)			
Material	Case-1	Case-2	Case-3
Fe 1422 ^a	0	X ₁ ^c	X ₁
TiH ₂	X ₁	0	50
B ₄ C ^b	80-X ₁	80-X ₁	30-X ₁

^aFe14Mn2Cr2Ni: Ref. 15.

^bB₄C, W: 95% of theoretical density.

^cX₁ is varied.

Based on the optimization study presented in this section, the WILDCAT inboard system has been designed to consist of: (1) a 21-cm first-wall/blanket including a 3-mm thick beryllium wall coating; (2) a 42-cm thick shield in which tungsten-base layers and B₄C/TiH₂-base layers are alternately placed; (3) a total space gap of 4 cm; (4) a 3-cm thick magnet dewar; (5) a 7-cm thick liquid nitrogen region; and (6) a 5-cm thick liquid-helium vessel, resulting in $\Delta_{BS}^i = 82$ cm. See Fig. 3-7. The difference of ~40 cm in Δ_{BS}^i between STARFIRE and WILDCAT has primarily been brought about by the nonbreeding blanket and the low integral wall loading in the WILDCAT design (18 MW-y/m² over the 40-yr plant life).

Table 3-5 summarizes major nuclear response rates in the toroidal field (TF) magnets for the inboard design with $\Delta_{BS}^i = 82$ cm and the outboard design with $\Delta_{BS}^i = 1.41$ m, which will be discussed later. It is clear that the

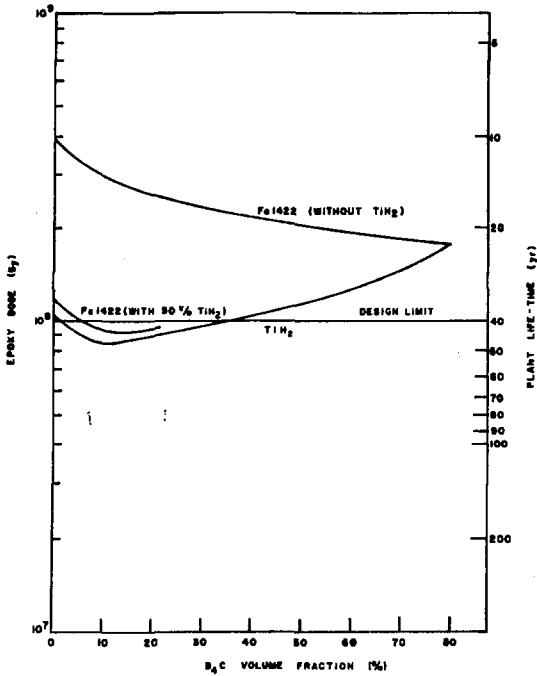


Fig. 3-11. Impact of B₄C content upon inboard radiation shielding.

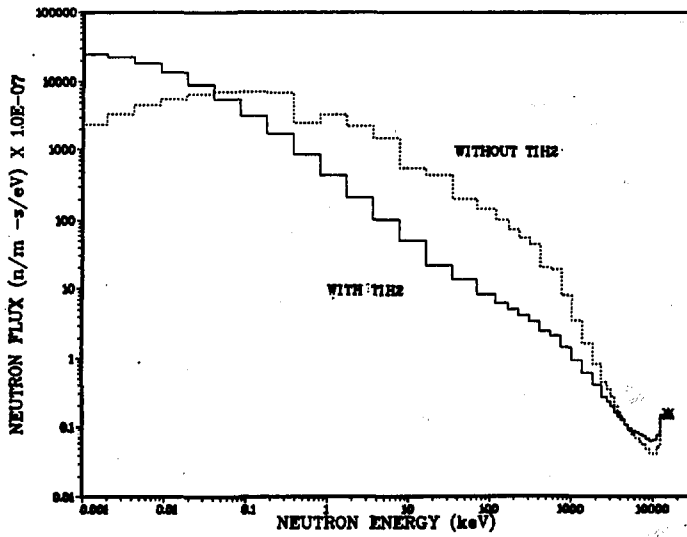


Fig. 3-12. Neutron spectrum at inboard shield.

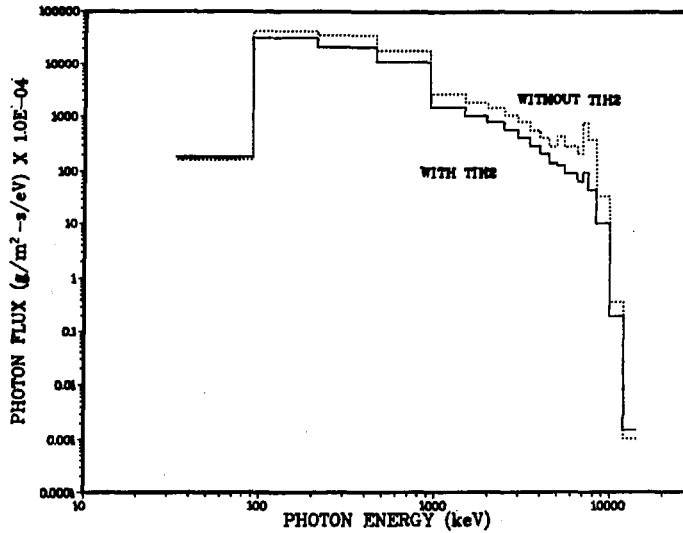


Fig. 3-13. Photon spectrum at inboard shield.

Table 3-5. Nuclear Response Rates^a in Toroidal Field Magnets

	Inboard	Top/Bottom	Outboard
1. Insulator dose (Gy)			
Thermal ins. in LN ₂	8.4×10^7	1.8×10^4	1.8×10^4
Electric ins. in magnet	3.8×10^7	8.1×10^3	7.5×10^3
2. Copper-stabilizer response			
Atomic displacement (dpa)			
(a) at 10 y	3.7×10^{-4}	7.0×10^{-8}	6.5×10^{-8}
(b) at 40 y	1.5×10^{-3}	2.7×10^{-7}	2.5×10^{-7}
Resistivity increase ($\Omega\text{-m}$)			
(a) at 10 y	5.6×10^{-10}	1.2×10^{-13}	1.1×10^{-13}
(b) at 40 y	1.7×10^{-9}	5.7×10^{-13}	4.3×10^{-13}
3. Neutron fluence in Nb ₃ Sn (m^{-2})			
(a) $\phi(E > 1 \text{ MeV})$	3.7×10^{21}	1.7×10^{17}	1.6×10^{17}
(b) $\phi(E > 0.1 \text{ MeV})$	1.9×10^{22}	4.5×10^{18}	4.2×10^{18}
(c) $\phi(E > 0)$	3.7×10^{22}	1.4×10^{19}	1.3×10^{19}

^a Neutron wall load: 14.06 MeV neutron: 0.498 MW/m^2
2.45 MeV neutron: 0.0998 MW/m^2
Total: 0.5978 MW/m^2

Plant availability: 75%
Plant lifetime: 40 y

radiation damage to the TF magnets is of concern only in the inboard region. As far as the accumulated insulator dose is concerned, the plant lifetime can be in excess of 40 y. According to Ref. 17, the transition temperature of the Nb₃Sn superconductor is not affected to any appreciable degree by neutron irradiation up to $\sim 10^{22}$ m⁻² for energies greater than 1 MeV. Furthermore, Ref. 17 shows a critical current density increase, rather than a decrease, for Nb₃Sn in the vicinity of a neutron fluence of $\sim 5 \times 10^{21}$ m⁻² for a wide range of magnetic field strengths. In fact, based on the results of Ref. 17, the inboard Nb₃Sn superconductors of the WILD CAT design are anticipated to show a maximum critical current density increase of $\sim 2\%$ near the end of lifetime, assuming a maximum field strength of ~ 14 T in the Nb₃Sn.

The resistivity increase in the copper stabilizer has been estimated based on the atomic displacement rate of copper.¹⁸ The estimate of copper resistivity increase by this method tends to yield a slightly higher value than the experimental result of Brown et al.¹⁹ for an intrinsic (preirradiation) resistivity of 3.8×10^{-11} Ω-m. As shown in Table 3-5, the maximum resistivity increase near the end of plant life-time amounts to $\sim 1.7 \times 10^{-9}$ Ω-m, which is higher than the estimated magneto-resistivity increase of $\sim 6.0 \times 10^{-10}$ Ω-m at 14 T.^{20,21} The estimate is based on a commercial grade copper having a residual resistivity ratio of ~ 100 . If the TF magnets are scheduled for annealing once every 10 y, for example, the maximum resistivity increase in the copper stabilizers can be suppressed to below 6×10^{-10} Ω-m. As Ref. 18 indicates, an increase in the stabilizer resistivity can be accommodated without violating cryostability by adding more stabilizer and modifying the conductor design.²² Although this results in an increase in the magnet cost, the penalty can possibly be compensated for by the economic gain achievable with smaller Δ_{BS}^1 . Such a trade-off study has not been performed for WILD CAT.

3.2.3 Outboard Radiation Shielding

In addition to the superconducting magnet protection, the outboard blanket/shield system must fulfill some other design criteria²³ because of the essential difference in its function and configuration from the inboard design. Among these, the most stringent criterion is the realization of reactor accessibility within 24 h after reactor shutdown. The reactor accessi-

bility shortly after shutdown provides a degree of confidence in improving the plant availability factor by allowing some maintenance tasks to be carried out in contact or semi-remote mode. The facts that the access to the outboard section is not as restrictive as that to the inboard section and that approximately 90% of the reactor material volume is present in the outboard section, particularly in the outboard shield, lead to considerations with respect to the material selection for the outboard radiation shielding.^{23,24} For example, the use of a tungsten shield as for the inboard region may not be justified for the outboard region because of the high material cost involved. Less effective, but less expensive shielding materials may be sufficient to perform the required radiation shielding for the outboard region. In addition, it should be emphasized that in a mature fusion power economy, the continued use of materials without the ability to recycle them would result in a serious depletion of some resource-limited materials such as niobium and chromium. Selection of reactor materials that are less resource-limited (e.g., an Fe-1422¹⁵ shield instead of conventional stainless steel) complements the potential for material recycling and results in fusion power reactors which are less constrained by their environmental impacts. Figure 3-14 compares the radioactivity concentrations of two shielding systems: (1) an Fe-1422 base shield throughout the outboard shield region with a lead back-shield jacket; and (2) a combination of a titanium-base shield in the high-flux zone and an Fe-1422 base shield in the low-flux zone. It is assumed that below a concentration of 10^{-7} MCi/m³ radwastes have a high potential for reuse by material recycling.²⁵ One notices that Fig 3-14 clearly indicates a strong incentive to employ the second shield system in order to realize a high possibility for materials recycling within a reasonably short time period (e.g., within a human generation of 50 y) after reactor shutdown or decommissioning. The impact of the use of low-activation materials upon the outboard radiation shielding can be seen in Fig. 3-15, which displays the variation of contact biological dose as a function of outboard region thickness, Δ_{BS}^0 . The post-shutdown time is assumed to be 24 h. For a wide range of biological dose limit criteria the difference in the required shield thickness between the two shield systems is not more than 5 cm. These results have lead to the WILDCAT outboard design consisting of: (1) a 41-cm first-wall/blanket including a 3-mm beryllium coating; (2) a 20-cm high flux shield (HFS) represented by 10% Ti6Al4V + 75% TiH₂ + 10% B₄C + 5% H₂O; (3) a 77-cm low flux shield (LFS)

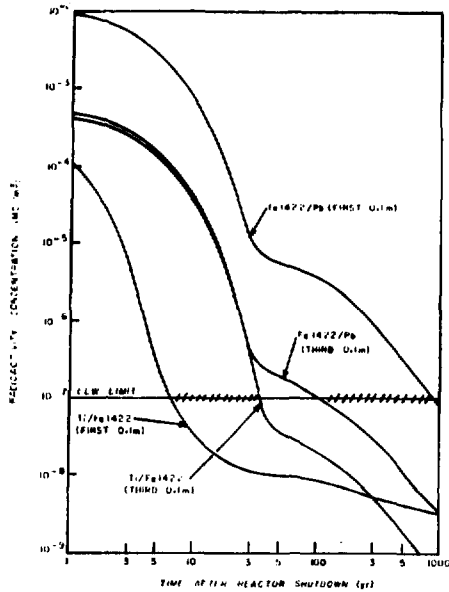


Fig. 3-14. Radioactivity concentration in the outboard bulk shield.

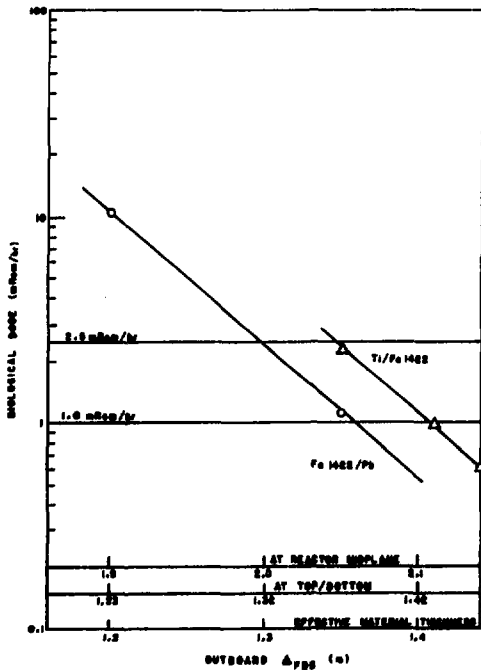


Fig. 3-15. Maximum biological dose in reactor room at 24 h after shutdown.

represented by 85% Fe-1422 + 10% B₄C + 5% H₂O; and (4) Fe-1422 front and back shield jackets of 1.5 cm each, resulting in a total outboard material region thickness of $\Delta_{BS}^0 = 1.41$ m, not including the dewar. (See Fig. 3-7.) This Δ_{BS}^0 is compared to $\Delta_{BS}^0 = 1.88$ m for the STARFIRE design, indicating a saving of 47 cm in WILDCAT on the outboard shield material thickness. Obviously, the difference reflects the fact that the breeding blanket (70 cm) of the STARFIRE design has been replaced by an efficient nonbreeding blanket (41 cm, 90% PCA + 10% H₂O) in the WILDCAT design. With the reference outboard design the contact biological dose in the reactor room varies with time as shown in Table 3-6. It can be seen that personnel access into the reactor building with all shielding in place is permissible within one day after shutdown based on the current NRC guidelines²⁶ of a dose limit of 2.5 mrem/h in a restricted area.

Table 3-6. Contact Biological Dose

	Dose (rem/h)	
	At End of Shield	At Magnet Dewar Surface
During operation	1.4×10^2	1.3×10^2
At shutdown	1.3×10^{-1}	7.7×10^{-2}
At 24 h after shutdown	1.0×10^{-3}	9.2×10^{-4}

3.2.4 Neutron Energy Multiplication

Because of the fact that the fusion power density of D-D reactors is intrinsically low compared to D-T reactors, the blanket energy multiplication in D-D reactor designs is a very important design consideration. On the other hand, the fact that tritium breeding, which is one of the primary blanket functions in D-T systems, can be eliminated in D-D fuel systems provides a great degree of flexibility in which the blanket can be optimized largely toward energy multiplication. In Ref. 27 a comprehensive scoping study was performed for the maximization of the system nuclear power. This study shows that among those candidate blanket materials investigated the PCA-base blanket design yields the maximum energy multiplication.

Based on the result of the scoping study, the WILDCAT blanket is designed to be a large block of PCA stainless steel (90 vol-% average) cooled by light

water (10%). The outboard blanket is chosen to be ~40 cm thick, while the inboard blanket is only 20 cm thick in order to maximize the effectiveness of the $W/TiH_2/B_4C$ shield for the inboard magnet protection.

Table 3-7 summarizes the breakdown of the system neutron energy multiplication for the WILDCAT design. It is found that the recoverable power (1482 MW) from the first-wall/blanket is more than 98% of the total nuclear power generation. The shield power of 24 MW, which must be discarded because of its low-grade heat, amounts to only ~1-2% of the total power. It should be noted that of this 24 MW approximately 13 MW (or 54%) is contributed by the inboard shield whose volume fraction is only ~10%. It appears that the energy deposition of 3 kW in the superconducting magnets is trivial from the standpoint of the refrigeration power requirement. Assuming an electric power requirement of 300 W per deposited watt for the refrigeration, the total power consumption for the nuclear heat retrieval results in only ~1 MWe, compared to the steady-state WILDCAT gross electric output of 1041 MWe. As shown in Table 3-8 and also addressed in Ref. 27, the large system neutron multiplication of ~2 stems largely from the substantial energy gain obtained by the 2.45-MeV source neutrons. In fact, the energy multiplication factor for those source neutrons amounts to ~4.43 compared with a factor of 1.54 for the 14.06-MeV source neutrons. The energy amplification in D-T reactors is generally lower than those in D-D reactors because of the presence of endothermic reactions associated with the tritium breeders and neutron multipliers (if any). For example, the STARFIRE design, which employs a ternary breeder of $LiAlO_2$ along with the Zr_5Pb_3 neutron multiplier, yields an energy multiplication factor of ~1.24.

One of the major advantages of the D-D fuel cycle is the ability to optimize the blanket/shield for energy multiplication and small inboard thickness. The impact of the optimization is shown in Table 3-9. There is a 60% increase in thermal power for WILDCAT using the optimized blanket/shield over using the STARFIRE blanket/shield. About 20% is due to the extra energy multiplication and about 40% is due to the reduced inboard thickness, which results in a higher magnetic field in the plasma. In addition, the reduced inboard blanket/shield results in more space in the center of the reactor. This allows better access and permits lower fields in the inboard poloidal coils. It is vitally important for a pulsed device.

Table 3-7. Breakdown of Nuclear Energy Deposition^a

	Inboard (MW)	Outboard (MW)	Total (MW)
Beryllium/First Wall	13	119	132
Blanket	110	1239	1350
Shield	13	11	24
Magnet	3 kW	11 W	3 kW
TOTAL:	136	1370	1506

^aFusion neutron power:

1.406 MeV neutron:	620 MW
2.45 MeV neutron:	124 MW
TOTAL:	744 MW

Table 3-8. Breakdown of Energy Multiplication by Fusion Neutrons^a

	14.06-MeV Neutron Only		2.45-MeV Neutron Only		Total ^b	
	ϵ	Power (MW)	ϵ	Power (MW)	ϵ	Power (MW)
Beryllium/first wall	0.143	88	0.354	44	0.178	132
Blanket	1.376	853	4.004	496	1.814	1350
Shield	0.024	15	0.075	9	0.032	24
Magnet	5×10^{-6}	3 kW	2×10^{-6}	0.2 kW	6×10^{-6}	3 kW
TOTAL:	1.542	956	4.433	550	2.024	1506

^a Fusion neutron power:

14.06 MeV neutron:	620 MW
2.45 MeV neutron:	124 MW
TOTAL:	744 MW

^bAverage source neutron energy: 7.86 MeV.

Table 3-9. Impact of Inboard Blanket Thickness and Energy Multiplication on WILDCAT Performance

P_T is the thermal power, B_{to} is the magnetic field on axis, and R_c is the radius of the center hole.

Inboard Blanket/Shield Thickness ^a	Energy Multiplication ^b	P_T (GW)	B_{to} (T)	R_c (m)
STARFIRE	STARFIRE	1.8	7.6	2.76
STARFIRE	WILDCAT	2.1	7.6	2.76
WILDCAT	STARFIRE	2.5	8.2	3.16
WILDCAT	WILDCAT	2.9	8.2	3.16

^aSTARFIRE: $\Delta_{BS}^i = 1.20$ m.

WILDCAT: $\Delta_{BS}^i = 0.82$ m.

^bSTARFIRE: $\epsilon_{14.06} = 1.24$, $\epsilon_{2.45} = 2.93$.

WILDCAT: $\epsilon_{14.06} = 1.54$, $\epsilon_{2.45} = 4.43$.

3.2.5 Reactor Activation

Long-term radwaste storage requirements for fusion reactors are an important design issue. Also important is an assessment of reactor materials recyclability, taking into account the availability of limited reactor materials resources. Both of these two issues, radwaste storage and material recycling, are a common consideration for the technical assessment of reactor decommissioning. The objective of this section is to provide the basic information on the long-term radioactive material inventories in the WILDCAT design for the future analysis of environmental impact and reactor decommissioning. An attempt is also made to assess the potential for recycling based on a biological dose criterion, and the result is compared with the STARFIRE design. Figure 3-16 shows the radioactivity inventories for major WILDCAT components as well as for the overall system as a function of post-shutdown time. It is assumed that the reactor has been operated up to an integral neutron wall load of 9 MW-y/m² (half of the plant lifetime of 40 y) before reactor shutdown. The total radioactivity inventory of STARFIRE is also shown for comparison.

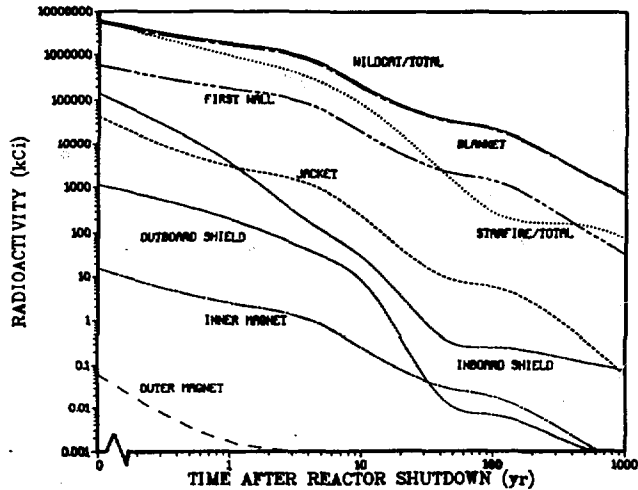


Fig. 3-16. Radioactivity inventory for the WILDCAT design.

It is noticed that the radioactivity in the first wall and blanket comprises ~97% of the total at shutdown, increasing further to more than 99% beyond one year after shutdown. Because of the much larger PCA volume in the WILDCAT blanket compared to STARFIRE, the fractional contribution of the WILDCAT blanket to the total radioactivity and also the absolute magnitude of the blanket inventory itself exceed those for the STARFIRE blanket. In fact, the total radioactivity of WILDCAT varies as 6.2 GCi, 1.7 GCi, 200 MCi, 23 MCi and 0.7 MCi at post-shutdown times of 0, 1, 10, 100, and 1000 y, respectively. The corresponding STARFIRE radioactivities are 6.1 GCi, 0.89 GCi, 78 MCi, 0.3 MCi, and 0.07 MCi. The reason for the larger difference beyond ~50 y stems from the larger ^{63}Ni production in WILDCAT due to the 2.45-MeV source neutrons.²⁸ (See Fig. 3-17.) Tables 3-10, 3-11, and 3-12 summarize the activation analyses for each reactor component in terms of the radioactivity concentration, the contact biological dose, and the recycling potential classification, respectively.¹ Most of the evaluation technique follows that established in the STARFIRE study. Although the WILDCAT radioactivity is relatively high compared to that of STARFIRE, the material recycling potential for both designs appears almost identical. Table 3-13 shows the maximum time required for the biological dose of major components to decrease below 2.5 $\mu\text{rem/h}$, which represents a measure for high recycling possibility. It should be emphasized that approximately 90% of the total reactor volume is present in the outboard shield and outboard magnet, both of which are likely to have a high potential for recycling.

Table 3-10. Specific Radioactivity of Reactor Components:^a MCl/m³

Component	Material	Time After Reactor Shutdown							
		0	1	5	10	50	100	500	1000
A. Inboard Design									
First Wall	Be	1.8(1) ^b	6.2(-6)	6.2(-6)	6.2(-6)	6.2(-6)	6.2(-6)	6.2(-6)	6.2(-6)
	PCA	7.6(1)	2.6(1)	9.0(0)	2.8(0)	3.4(-1)	2.3(-1)	1.8(-2)	5.2(-3)
	H ₂ O	1.4(0)							
Blanket	PCA	1.8(1)	5.1(0)	1.8(0)	6.0(-1)	1.1(-1)	7.7(-2)	6.6(-3)	2.3(-3)
	H ₂ O	2.4(-1)							
Front shield jacket	Fe-1422	7.3(0)	5.5(-1)	1.7(-1)	4.5(-2)	1.3(-3)	9.2(-4)	5.4(-5)	1.0(-5)
Shield 1	Fe-1422	3.9(-1)	6.9(-2)	2.0(-1)	5.3(-3)	2.7(-5)	1.8(-5)	1.4(-6)	4.9(-7)
	W	3.1(0)	6.8(-2)	1.9(-5)	4.5(-6)	3.3(-6)	3.2(-6)	2.3(-6)	1.6(-6)
Shield 2	Fe-1422	4.8(2)	2.7(-3)	8.0(-4)	2.1(-4)	2.4(-6)	1.6(-6)	9.7(-8)	1.9(-8)
	TiH ₂	7.5(-4)	2.8(-5)	4.4(-8)	2.1(-11)	5.3(-38)			
	B ₄ C	2.6(-4)	6.1(-10)	6.1(-10)	6.1(-10)	6.1(-10)	6.1(-10)	6.1(-10)	6.1(-10)
	H ₂ O	1.3(-4)							
Back shield jacket	Fe-1422	1.5(-3)	3.4(-4)	9.7(-5)	2.5(-5)	7.4(-8)	4.9(-8)	3.1(-9)	7.4(-10)
Magnet									
Dewar	SS-304	5.1(-4)	1.9(-4)	6.1(-5)	1.7(-5)	4.3(-7)	3.0(-7)	3.6(-8)	1.7(-8)
He vessel	SS-304	2.3(-4)	7.4(-5)	2.4(-5)	6.9(-6)	3.0(-7)	2.1(-7)	2.7(-8)	1.3(-8)
Structure	SS-304	5.0(-5)	1.4(-5)	4.5(-6)	1.4(-6)	1.5(-7)	1.0(-7)	1.1(-8)	4.8(-9)
Stabilizer	Cu	4.3(-4)	2.5(-6)	2.0(-6)	1.6(-6)	9.3(-7)	6.4(-7)	3.1(-8)	7.2(-10)
Superconductor	Nb ₃ Sn	1.7(-4)	1.2(-5)	6.6(-6)	4.0(-6)	5.0(-7)	1.0(-7)	6.7(-8)	6.6(-8)
Insulator	Epoxy	1.8(-7)	2.5(-13)	2.5(-13)	2.5(-13)	2.5(-13)	2.5(-13)	2.4(-13)	2.2(-13)
B. Outboard Design									
First wall	Be	1.9(1)	6.1(-6)	6.1(-6)	6.1(-6)	6.1(-6)	6.1(-6)	6.1(-6)	6.1(-6)
	PCA	7.8(1)	2.8(1)	9.4(0)	2.9(0)	3.3(-1)	2.3(-1)	1.7(-2)	5.2(-3)
	H ₂ O	1.5(0)							
Blanket	PCA	1.1(1)	3.3(0)	1.1(0)	3.8(-1)	6.6(-2)	4.6(-2)	4.0(-3)	1.4(-3)
	H ₂ O	1.6(-1)							
Front shield jacket	Fe-1422	9.1(-1)	5.0(-2)	1.6(-2)	4.3(-3)	1.9(-4)	1.3(-4)	7.5(-6)	1.3(-6)
HPS shield	Ti6Al4V	5.9(-3)	1.0(-4)	6.7(-7)	1.9(-7)	5.8(-8)	4.7(-8)	2.1(-8)	1.7(-8)
	TiH ₂	2.6(-3)	9.5(-5)	1.4(-7)	6.9(-10)	1.7(-37)			
	B ₄ C	9.0(-4)	2.3(-9)	2.3(-9)	2.3(-9)	2.3(-9)	2.3(-9)	2.2(-9)	2.2(-9)
	H ₂ O	4.3(-4)							
LFS shield	Fe-1422	3.4(-4)	1.1(-4)	3.0(-5)	7.7(-6)	8.2(-9)	5.1(-9)	4.5(-10)	2.0(-10)
	B ₄ C	1.4(-5)	3.8(-11)	3.8(-11)	3.8(-11)	3.8(-11)	3.8(-11)	3.8(-11)	3.8(-11)
	H ₂ O	6.4(-6)							
Back shield jacket	Fe-1422	4.0(-7)	8.8(-9)	2.5(-9)	6.8(-10)	1.5(-11)	1.1(-11)	7.1(-13)	2.0(-13)
Magnet									
Dewar	SS-304	6.1(-8)	6.2(-9)	2.2(-9)	7.5(-10)	1.6(-10)	1.1(-10)	1.7(-11)	9.3(-12)
He vessel	SS-304	4.5(-8)	4.3(-9)	1.6(-9)	5.7(-10)	1.5(-10)	1.1(-10)	1.2(-11)	5.6(-12)
Structure	SS-304	1.1(-8)	1.6(-9)	5.9(-10)	2.2(-10)	6.6(-11)	4.6(-11)	3.9(-12)	1.3(-12)
Stabilizer	Cu	1.7(-7)	5.7(-11)	4.6(-11)	3.8(-11)	2.3(-11)	1.6(-11)	7.8(-13)	1.8(-14)
Superconductor	Nb ₃ Sn	5.6(-8)	3.9(-9)	1.8(-9)	8.9(-10)	9.9(-11)	3.0(-11)	2.3(-11)	2.3(-11)
Insulator	Epoxy	3.5(-12)	1.2(-16)	1.2(-16)	1.2(-16)	1.2(-16)	1.2(-16)	1.1(-16)	1.1(-16)

^aIntegral neutron wall load before reactor shutdown: 9 MW-y/m².

^bReads as 1.8 × 10¹.

Table 3-11. Post-Shutdown Dose of Reactor Components:^a rem/h

Component	Material	Time After Reactor Shutdown							
		0	1	5	10	50	100	500	1000
A. Inboard Design									
First Wall	Be								
	PCA	9.6(6) ^b	7.2(5)	3.1(5)	1.5(5)	7.8(2)	4.5(0)	3.4(0)	3.3(0)
	H ₂ O	1.6(6)							
Blanket	PCA	2.6(5)	1.2(5)	5.2(4)	2.6(4)	1.3(2)	1.5(0)	1.3(0)	1.3(0)
	H ₂ O	2.7(5)							
Front shield jacket	Fe-1422	1.9(6)	1.1(4)	8.7(2)	2.8(2)	1.4(0)	1.8(-3)	1.9(-26)	
Shield 1	Fe-1422	8.6 (4)	1.8(3)	1.5(2)	4.6(1)	2.3(-1)	3.1(-4)	3.2(-27)	
	W	5.5(1)	1.7(0)	2.0(-1)	1.0(-1)	1.0(-3)	4.7(-4)	4.7(-4)	4.6(-4)
	H ₂ O	3.8(3)							
Shield 2	Fe-1422	1.3(4)	7.0(1)	5.5(0)	1.7(0)	8.5(-3)	1.1(-5)	1.2(-28)	
	TiH ₂	4.6(2)	5.4(0)	3.7(-5)	1.3(-11)				
	B ₄ C H ₂ O	1.4(2)							
Back shield jacket	Fe-1422	3.0(2)	9.8(0)	7.6(-1)	2.4(-1)	1.2(-3)	1.6(-6)	1.7(-29)	
Magnet									
Dewar	SS-304	6.4(1)	4.5(0)	1.5(0)	7.5(-1)	3.8(-3)	6.2(-6)	1.2(-6)	1.1(-6)
He vessel	SS-304	3.1(1)	1.7(0)	5.8(-1)	2.8(-1)	1.4(-3)	2.4(-6)	4.6(-7)	4.5(-7)
Structure	SS-304	7.2(0)	2.7(-1)	9.0(-2)	2.2(-4)	3.7(-7)	7.2(-8)	7.2(-8)	7.1(-8)
Stabilizer	Cu	5.6(-1)	4.9(-1)	2.9(-1)	1.5(-1)	7.5(-4)	1.0(-6)	1.0(-29)	
Superconductor	Nb ₃ Sn	1.2(0)	1.6(-2)	1.6(-2)	1.6(-2)	1.6(-2)	1.6(-2)	1.6(-2)	1.6(-2)
Insulator	Epoxy	2.0(-1)							
B. Outboard Design									
First wall	Be								
	PCA	9.8(6)	7.6(5)	3.2(5)	1.6(5)	8.2(2)	4.5(0)	3.4(0)	3.3(0)
	H ₂ O	1.7(6)							
Blanket	PCA	1.6(6)	8.2(4)	3.4(4)	1.7(4)	8.8(1)	9.4(-1)	8.1(-1)	8.0(-1)
	H ₂ O	1.7(5)							
Front shield jacket	Fe-1422	2.4(5)	8.0(2)	6.3(1)	2.0(1)	9.7(-2)	1.3(-4)	1.4(-27)	
HFS shield	Ti6Al4V	3.0(3)	2.0(1)	5.3(-2)	2.1(-2)	5.2(-4)	4.2(-4)	4.2(-4)	4.2(-4)
	TiH ₂	1.6(3)	2.0(1)	1.3(-4)	4.6(-11)				
	B ₄ C H ₂ O	4.8(2)							
LFS shield	Fe-1422	5.8(1)	3.4(0)	2.5(-1)	7.4(-2)	3.6(-4)	4.9(-7)	5.2(-30)	
	B ₄ C								
	H ₂ O	7.1(0)							
Back shield jacket	Fe-1422	1.1(-1)	2.4(-4)	1.7(-5)	4.7(-6)	2.3(-8)	3.1(-11)	3.3(-34)	
Magnet									
Dewar	SS-304	1.2(-2)	1.0(-4)	3.5(-5)	1.8(-5)	8.9(-8)	1.4(-10)	2.3(-11)	2.3(-11)
He vessel	SS-304	9.1(-3)	4.3(-5)	1.6(-5)	7.8(-6)	3.9(-8)	6.3(-11)	9.6(-11)	9.4(-12)
Structure	SS-304	2.0(-3)	7.1(-6)	2.7(-6)	1.4(-6)	6.8(-9)	1.1(-11)	1.5(-12)	1.5(-12)
Stabilizer	Cu	1.2(-5)	1.0(-5)	6.1(-6)	3.2(-6)	1.6(-8)	2.1(-11)	2.3(-34)	
Superconductor	Nb ₃ Sn	2.9(-5)	5.7(-6)	5.7(-6)	5.7(-6)	5.7(-6)	5.6(-6)	5.6(-6)	5.5(-6)
Insulator	Epoxy	3.9(-6)							

^aIntegral neutral wall load before reactor shutdown: 9 MW-y/m².

^bReads as 9.8 × 10⁶.

Table 3-12. Classification^a of Radioactive Reactor Components

Component	Material	Time After Shutdown							
		0	1	5	10	50	100	500	1000
A. Inboard Design									
First wall	Be	H/R	M/R						
	PCA	H/N	H/N	H/N	H/N	H/N	H/N	H/N	M/N
	H ₂ O	H/N	L/R						
Blanket	PCA	H/N	H/N	H/N	H/N	H/N	H/N	M/N	M/N
	H ₂ O	H/N	L/R						
Front shield jacket	Fe-1422	H/N	H/N	H/N	H/N	M/N	M/R	M/R	M/R
Shield 1	Fe-1422	H/N	H/N	H/N	M/N	M/N	M/R	M/R	M/R
	W	H/N	H/N	M/N	M/N	M/R	M/R	M/R	M/R
	H ₂ O	M/N	L/R						
Shield 2	Fe-1422	H/N	M/N	M/N	M/N	M/N	M/R	L/R	
	TiH ₂	M/N	M/N	L/R					
	B ₄ C	M/R	L/R						
	H ₂ O	M/N	L/R						
Back shield jacket	Fe-1422	M/N	M/N	M/N	M/N	L/R			
Magnet									
Dewar	SS-304	M/N	M/N	M/N	M/N	M/N	M/R	L/R	
He vessel	SS-304	M/N	M/N	M/N	M/N	M/R	M/R	L/R	
Structure	SS-304	M/N	M/N	M/N	M/R	M/R	M/R	L/R	
Stabilizer	Cu	M/N	M/N	M/N	M/N	M/R	M/R	L/R	
Superconductor	Nb ₃ Sn	M/N	M/N	M/N	M/N	M/N	M/N	L/N	L/N
Insulator	Epoxy	M/N	L/R						
B. Outboard Design									
First wall	Be	H/R	M/R						
	PCA	H/N	H/N	H/N	H/N	H/N	H/N	H/N	M/N
	H ₂ O	H/N	L/R						
Blanket	PCA	H/N	H/N	H/N	H/N	H/N	H/N	M/N	M/N
	H ₂ O	H/N	L/R						
Front shield jacket	Fe-1422	H/N	H/N	H/N	M/N	M/N	M/R	M/R	M/R
HFS shield	Ti6Al4V	M/N	M/N	M/N	M/N	L/R			
	TiH ₂	M/N	M/N	M/R	L/R				
	B ₄ C	M/R	L/R						
	H ₂ O	M/N	L/R						
LFS shield	Fe-1422	M/N	M/N	M/N	M/N	L/R			
	B ₄ C	M/R	L/R						
	H ₂ O	M/N	L/R						
Back shield jacket	Fe-1422	M/N	L/R						
Magnet									
Dewar	SS-304	L/N	L/R						
Helium vessel	SS-304	L/N	L/R						
Structure	SS-304	L/R							
Stabilizer	Cu	M/R	L/R						
Superconductor	Nb ₃ Sn	L/R							
Insulator	Epoxy	L/R							

^aClassification

H: $>10^{-2}$ MCi/m³

R: Dose ≤ 2.5 urem/h

M: 10^{-7} - 10^{-2} MCi/m³

N: Dose > 2.5 urem/h

L: $<10^{-7}$ MCi/m³

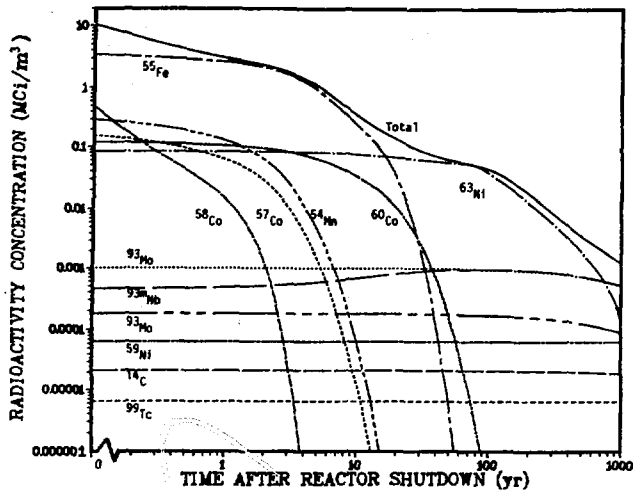


Fig. 3-17. Isotopic contribution to the PCA blanket radioactivity of the WILDCAT design.

Table 3-13. Time Required for Biological Dose to Decrease Below 2.5 mrem/h

Component	Required Time (y)
First wall	1000
Blanket	1000
Inboard shield	100
Outboard shield	50
Inboard magnet	50-100 ^a
Outboard magnet	0-1

^aExcept for Nb₃Sn > 1000 y.

Table 3-14 presents the short-term decay heat of the WILDCAT design. It is found that the total system decay heat of 39 MW at shutdown is approximately half of that of STARFIRE, the difference further increasing with post-shutdown time. The relatively large decay power (~2.2% of the total reactor thermal power) for STARFIRE stems in part from the activation decay of the Zr₅Pb₃ neutron multiplier used for tritium breeding enhancement. Much of the earlier work relevant to the decay-heat analysis for D-T fusion reactors has shown a maximum decay heat load of about 1% of the total operational reactor power. The result of Table 3-14 appears to show this relation to be also

Table 3-14. System Decay Heat^a

Post-Shutdown Time	Decay Heat (MW)	Fraction of Operating Nuclear Power ^b (%)	Fraction of Operating Total Reactor Power ^c (%)
0	39 (88) ^d	2.6	1.3
1 min	36 (70)	2.4	1.2
10 min	33 (65)	2.2	1.1
1 h	27 (61)	1.8	0.92
6 h	11 (52)	0.70	0.36
24 h	4.7 (39)	0.32	0.16
1 wk	4.2 (14)	0.28	0.14

^aIntegral neutron wall load before reactor shutdown: 9 MW-y/m².

^bTotal operating nuclear power: 1506 MW.

^cTotal operating reactor power: 2915 MW.

^dThe STARFIRE design with the Zr₅Pb₃ neutron multiplier.

valid with D-D reactors. However, it is noted that because of the substantially large size of D-D reactors in general, the volumetric decay heating rates in D-D systems become much less than those in D-T systems. For example, the maximum heating rates (just after shutdown) of 0.20 MW/m³ in the beryllium coating and 0.17 MW/m³ in the PCA first-wall of the WILDCAT design, which are presented in Table 3-15, are compared to the maximum heating rate of ~0.32 MW/m³ of the STARFIRE first-wall design. The reduced decay heating rate in D-D systems is expected to alleviate the design for emergency cooling systems in case of an accident.

As for the atmospheric activation, the radioactivity concentration is more or less comparable with the STARFIRE case. It is seen in Table 3-16 that carbon dioxide and air exhibit an activation saturation within several hundred seconds after reactor startup. Therefore, these two gas activation levels are considered to be independent of their residence times in the reactor building. After reactor shutdown the carbon dioxide gas activation decreases below the ¹⁴C MPC value of 10⁻¹³ MCi/m³ within 10 min because of the rapid decay of ¹⁶N radioactivity, whereas the air activation remains almost constant at ~10⁻¹³ MCi/m³ even beyond 1000 y. In addition, the ⁴¹Ar activation (which has been evaluated by extrapolating the STARFIRE result) shows the highest radioactivity concentration among those examined in the neighborhood of 0-6 h after

Table 3-15. Zone Average Decay Heating Rate (MW/m³)^a

Post-Shutdown Time	Beryllium Coating	First Wall	Blanket
0	2.0(-1) ^b	1.7(-1)	7.0(-2)
1 min	2.2(-2)	1.5(-1)	6.5(-2)
10 min	2.0(-2)	1.4(-1)	6.1(-2)
1 h	1.7(-2)	1.1(-1)	4.9(-2)
6 h	7.9(-3)	4.6(-2)	8.7(-3)
24 h	4.7(-3)	2.2(-2)	8.7(-3)
1 wk	4.3(-3)	1.9(-2)	7.6(-3)
During operation	6.9(0)	1.1(1)	1.6(0)

^aIntegral neutron wall load before reactor shutdown:
9 MW-y/m².

^bReads as 2.0×10^{-1} .

Table 3-16. Reactor Room Atmospheric Activation (MCI/m³)

	Co ₂	Air ^a	⁴¹ Ar	N ₂
Pre-shutdown time:				
0	0.0	0.0	0.0	0.0
10 ³ s	5.37(-13)	1.21(-13)	1.0(-12)	3.24(-19)
10 ⁵ s	5.37(-13)	1.21(-13)	1.0(-12)	3.24(-17)
1 mo	5.37(-13)	1.22(-13)	1.0(-12)	8.52(-16)
6 mo	5.37(-13)	1.25(-13)	1.0(-12)	5.11(-15)
1 y	5.37(-13)	1.29(-13)	1.0(-12)	1.02(-14)
5 y	5.37(-13)	1.64(-13)	1.0(-12)	5.10(-14)
15 y	5.37(-13)	2.49(-13)	1.0(-12)	1.53(-13)
Post-shutdown time:				
0	5.37(-13)	2.49(-13)	1.0(-12)	1.53(-13)
1 min	1.67(-15)	1.29(-13)	1.0(-12)	1.53(-13)
10 min	1.48(-19)	1.28(-13)	1.0(-12)	1.53(-13)
1 h	1.48(-19)	1.28(-13)	1.0(-12)	1.53(-13)
6 h	1.48(-19)	1.28(-13)	1.0(-12)	1.53(-13)
24 h	1.48(-19)	1.28(-13)	negligible	1.53(-13)
1 wk	1.48(-19)	1.28(-13)		1.53(-13)
1 mo	1.48(-19)	1.28(-13)		1.53(-13)
1 y	1.48(-19)	1.28(-13)		1.53(-13)
10 y	1.48(-19)	1.28(-13)		1.53(-13)
100 y	1.47(-19)	1.27(-13)		1.51(-13)
1000 y	1.32(-19)	1.14(-13)		1.36(-13)

MPC:

¹⁶ N	3.0(-14)
¹⁴ C	1.0(-13)
⁴¹ Ar	4.0(-14)

^aDoes not include ⁴¹Ar activation.

shutdown. Therefore, the use of air for inerting the WILDCAT reactor building atmosphere should be excluded from consideration. Although the nitrogen gas activation remains constant over the post-shutdown time span of interest, the activation level is very sensitive to the gas residence time in the reactor building. For a reasonable residence time (considering the ventilation of the reactor atmosphere) it is quite conceivable that the ^{14}C activation induced by ^{14}N remains far below the ^{14}C MPC limit. Therefore, both CO_2 and N_2 should be considered for the safety analysis relevant to the atmospheric activation.

3.3 Thermal Hydraulic Analysis

Since a breeding blanket is not required for D-D fusion reactors, the first-wall/blanket system design presents the opportunity for some unique design and cooling concepts. As a result, in the previous study²⁷ several blanket materials (such as silicon nitride, silicon carbide, and chromium nitride) and three coolants (water, helium, and sodium) were analyzed to evaluate their potential as first-wall/blanket material and coolant combinations. For the present analysis it has been decided to confine the studies to PCA stainless steel as the structural material and pressurized water as the coolant. These choices are based on the fact that (1) there is a large data base for stainless steel, both from the point of view of physical and mechanical properties and from fabrication techniques for complex components; and (2) there is substantial operating experience for water as the coolant in pressurized water reactors.

The cross-sectional areas of the coolant channels for the first wall and the blanket segment are based on assumption that the coolant velocities should be limited to 2-6 m/s (6 ft/s to 20 ft/s). These limits are used to reduce pressure losses for the first wall and to minimize maldistribution of coolant in the blanket segment where common inlet and outlet headers are used. Figure 3-18 shows the coolant channel arrangements for a typical first wall/blanket segment for the 0.4-m outboard wall. For the inboard blanket, which is 0.2 m thick, there are only three rows of coolant channels compared with five rows for the outboard wall. In these calculations the dimensions of the first wall coolant panels are assumed to be same both for the outboard blanket and the inboard blanket.

EQUIVALENT FLOW	
LETTER	AREA
A	18 mm ²
B, C, D	16 mm ²
E	12 mm ²

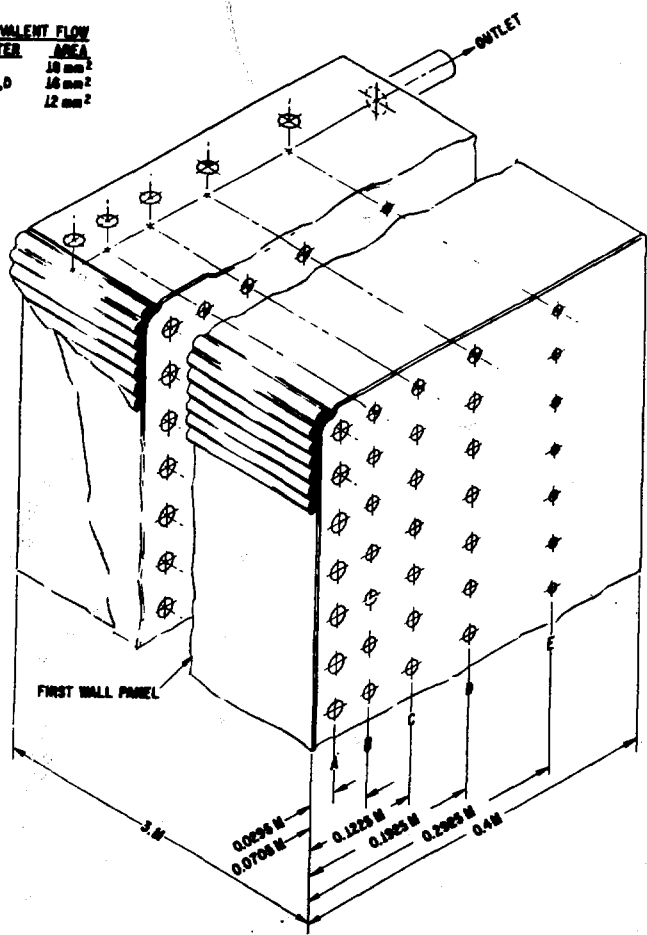


Fig. 3-18. First-wall coolant panel and blanket coolant channel layout (outboard wall).

Since the neutron heating rate in the blanket decays exponentially as the blanket regions are removed further and further away from the first wall, it is necessary to vary the coolant flow characteristics, keeping the same inlet and outlet temperature for each coolant channel. This can be done by varying the coolant velocity while keeping the cross sectional area of most of the channels approximately the same. An alternate method is to change the cross-sectional area while keeping the coolant velocity constant. This can be achieved either by using very small coolant channels or by using central inserts in uniform sized coolant channels to reduce the flow area. Figure 3-19 shows how filler elements may be used to reduce the effective area of the coolant channels. One drawback of this design is that when coolant channels

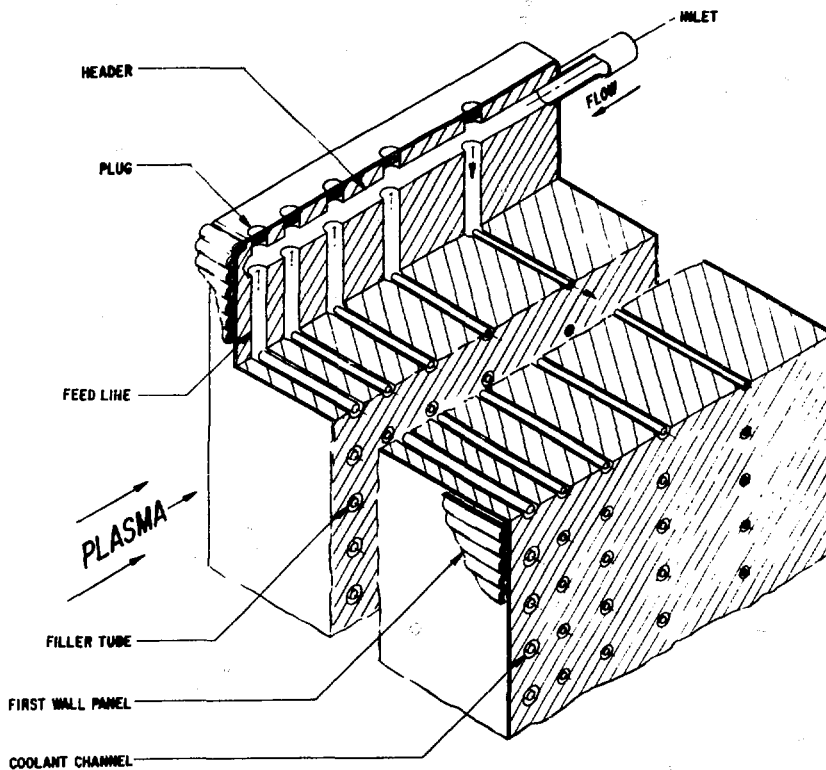


Fig. 3-19. Blanket block manifold layout.

are made very small, flow blockage by corrosion products is likely to occur leading to the creation of hot spots. The cross-sectional areas of the coolant channels are shown in Fig. 3-18.

The coolant operating conditions for the first-wall/blanket are assumed to be as follows:

- Coolant inlet temperature: 280°C
- Coolant outlet temperature: 320°C
- Coolant inlet pressure: 13.8 MPa (2000 psig)

With the above set of coolant operating conditions, arrangement of coolant channels has been carried out so that the temperature of neither the first wall nor the blanket exceeds 525°C. The coolant channel dimensions, the coolant velocity, and the maximum temperature of the structural material and beryllium coating are summarized in Table 3-17. The temperature distributions

Table 3-17. Summary of Thermal Hydraulics Calculations for the Outboard Blanket

Structural Material Fraction	First Wall 35%	Blanket, 10% (Average)				
		Region 1	Region 2	Region 3	Region 4	Region 5
Coolant velocity:						
ft/s	21.6	22.0	18.4	14.0	8.2	6.5
m/s	6.58	6.71	5.61	4.26	2.50	1.98
Maximum temperature of PCA alloy, °C	423	487	506	498	468	438
Maximum temperature of Be coating, °C	453					
Coolant channel dimensions, mm	12 x 6	4.5 x 4	4 x 4	4 x 4	4 x 4	4 x 3
Pressure drop:						
kPa	165	365				
psi	24	53				
Ratio of pumping power to thermal power, %	<1	<1	<1	<1	<1	<1

in the inboard and outboard blanket segments are shown in Tables 3-18 and 3-19. The representation of nodes for the outboard first-wall/blanket segment is shown in Fig. 3-20. There are 4 nodes in the x-direction, 20 nodes in the y-direction, and 2 nodes in the z-direction (see Fig. 3-20). Thus, the outermost PCA alloy and beryllium coating nodes corresponding to the second pass of coolant (i.e., $z = 2$) are 97, 117, 137, and 157, and 100, 120, 140, and 160, respectively. Similar nodal representations have been assumed for the inboard wall, except the total number of nodes used in the thermal hydraulic analysis is only 136 for the inboard wall compared to 160 nodes used for the outboard wall. Since the surface heat flux on the inboard wall and the outboard wall is the same, the maximum temperature of the first wall and beryllium coating is essentially the same as that shown in Tables 3-18 and 3-19 [nodes (100, 120, 140, and 160) and nodes (97, 117, 137, and 157); nodes (85, 102, 119, and 136) and nodes (82, 99, 116, and 138)].

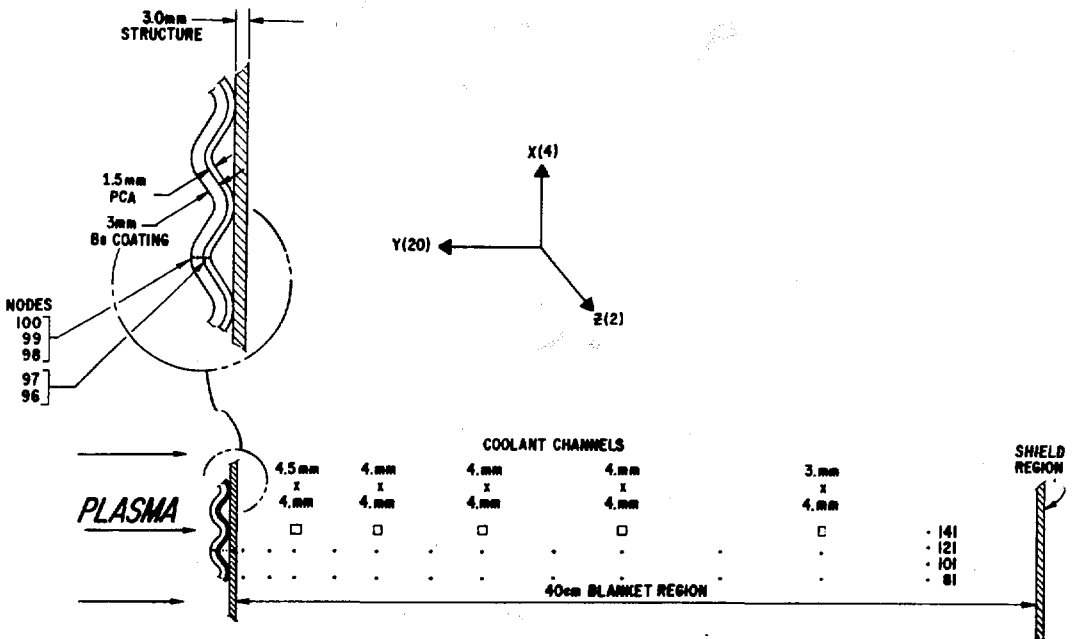


Fig. 3-20. First-wall/blanket computer model with node representation.

The steady-state temperature distribution for the inboard wall is shown in Figs. 3-21 and 3-22. The corresponding temperature distribution for the outboard wall is represented in Figs. 3-23 and 3-24. It can be seen from

Table 3-18. Summary of Temperature Distribution in First-Wall/Blanket Segment (Inboard)

1	472.1	2	365.5	3	472.8	4	376.7	5	484.9	6	386.8	7	471.9	8	331.5
9	315.5	10	299.9	11	299.9	12	299.9	13	345.8	14	385.6	15	410.0	16	420.1
17	430.0	18	471.8	19	320.9	20	472.1	21	323.8	22	483.5	23	326.4	24	471.1
25	350.4	26	339.7	27	330.9	28	329.7	29	336.8	30	387.1	31	403.2	32	415.1
33	423.1	34	432.2	35	471.7	36	300.0	37	471.9	38	300.1	39	483.2	40	300.0
41	470.8	42	355.3	43	347.7	44	346.2	45	368.8	46	357.5	47	390.6	48	400.3
49	411.3	50	421.7	51	431.6	52	471.7	53	299.9	54	471.8	55	300.0	56	483.0
57	300.0	58	470.7	59	357.6	60	351.1	61	351.3	62	354.1	63	359.9	64	391.0
65	400.0	66	410.4	67	421.1	68	431.3	69	489.3	70	383.6	71	490.6	72	395.1
73	502.9	74	405.2	75	489.9	76	350.3	77	334.5	78	319.1	79	319.0	80	319.1
81	369.7	82	404.0	83	428.2	84	438.3	85	468.2	86	489.0	87	339.7	88	489.9
89	342.8	90	501.5	91	345.4	92	489.1	93	369.9	94	358.4	95	349.7	96	348.5
97	355.6	98	405.4	99	421.4	100	433.3	101	441.3	102	450.4	103	483.9	104	319.0
105	489.7	106	319.3	107	501.2	108	319.3	109	488.9	110	373.8	111	366.3	112	364.8
113	367.4	114	376.0	115	408.9	116	418.6	117	429.6	118	440.0	119	449.8	120	488.9
121	318.9	122	489.6	123	319.2	124	501.0	125	319.2	126	488.8	127	376.0	128	369.7
129	369.9	130	372.5	131	378.3	132	409.3	133	418.3	134	428.6	135	439.4	136	449.5

Table 3-19. Summary of Temperature Distribution in First-Wall/Blanket Segment (Outboard)

1	397.8	2	339.2	3	423.7	4	345.0	5	451.3	6	364.5	7	480.5	8	382.5
9	489.3	10	393.1	11	469.3	12	335.0	13	317.0	14	299.8	15	299.8	16	345.2
17	395.4	18	410.1	19	420.2	20	430.2	21	397.8	22	316.6	23	423.6	24	316.2
25	451.0	26	320.4	27	479.6	28	325.0	29	487.5	30	328.4	31	468.1	32	354.7
33	342.9	34	330.1	35	337.1	36	387.5	37	403.7	38	415.6	39	423.5	40	432.6
41	397.8	42	300.3	43	423.6	44	300.2	45	450.9	46	299.7	47	479.3	48	300.2
49	487.1	50	300.2	51	467.8	52	359.7	53	350.9	54	347.5	55	352.3	56	391.3
57	400.9	58	411.9	59	422.3	60	412.2	61	397.7	62	300.2	63	423.6	64	300.2
65	450.8	66	299.7	67	479.2	68	300.2	69	456.9	70	300.1	71	467.7	72	352.0
73	354.3	74	353.0	75	360.7	76	391.6	77	400.7	78	411.0	79	421.7	80	431.8
81	413.5	82	357.4	83	441.6	84	363.8	85	469.3	86	352.6	87	498.4	88	401.2
89	507.6	90	411.8	91	487.5	92	353.6	93	335.9	94	318.7	95	318.7	96	363.9
97	403.6	98	428.1	99	438.2	100	443.1	101	413.4	102	335.4	103	441.4	104	335.4
105	469.0	106	335.9	107	497.5	108	344.3	109	505.8	110	347.7	111	486.3	112	373.1
113	361.4	114	348.8	115	355.7	116	405.6	117	421.7	118	433.6	119	441.5	120	450.6
121	413.4	122	319.3	123	441.4	124	319.6	125	468.9	126	318.3	127	497.3	128	319.8
129	505.3	130	319.8	131	485.9	132	378.0	133	369.3	134	365.8	135	376.5	136	409.4
137	419.0	138	429.9	139	440.3	140	450.2	141	413.4	142	319.3	143	441.4	144	319.6
145	463.9	146	318.3	147	497.2	148	319.7	149	505.2	150	319.7	151	485.8	152	380.2
153	372.7	154	371.3	155	378.9	156	409.7	157	418.7	158	429.0	159	439.7	160	449.9

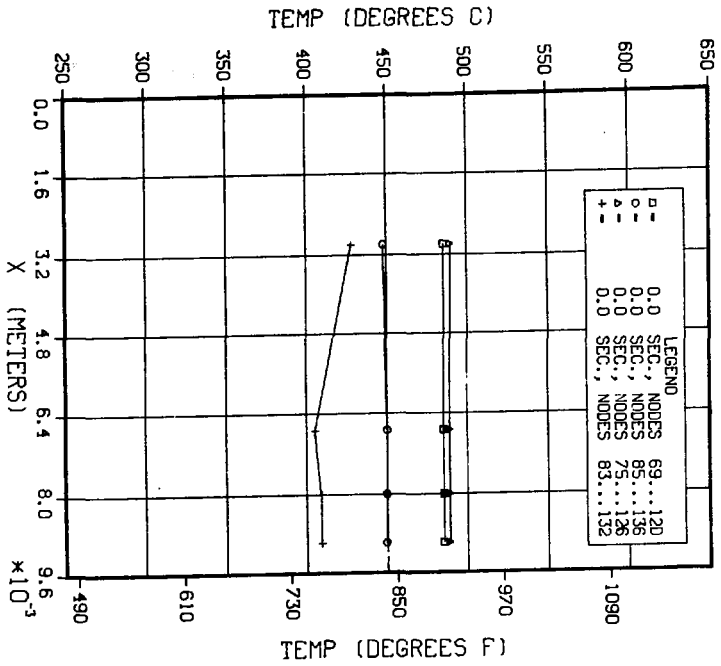


Fig. 3-21. Steady-state temperature distribution (x-direction) in first-wall/blanket segment (inboard).

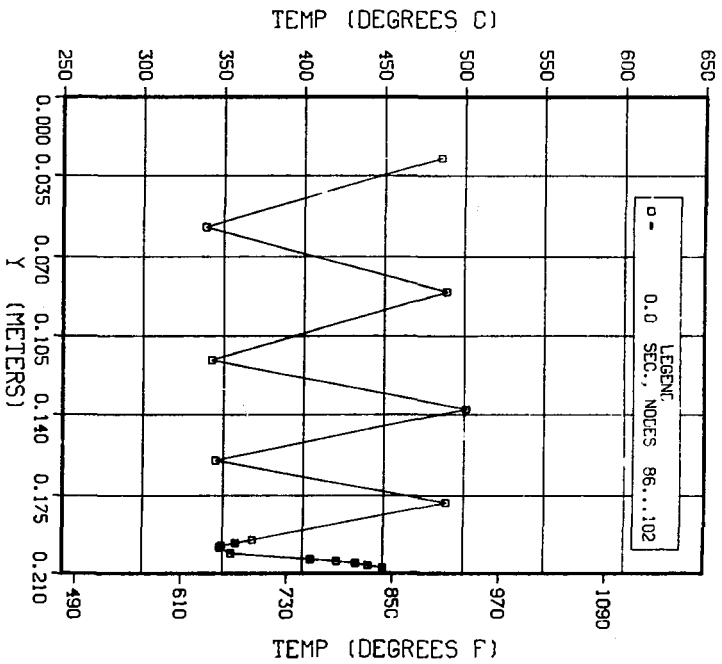


Fig. 3-22. Steady-state temperature distribution (y-direction) in first-wall/blanket segment (inboard).

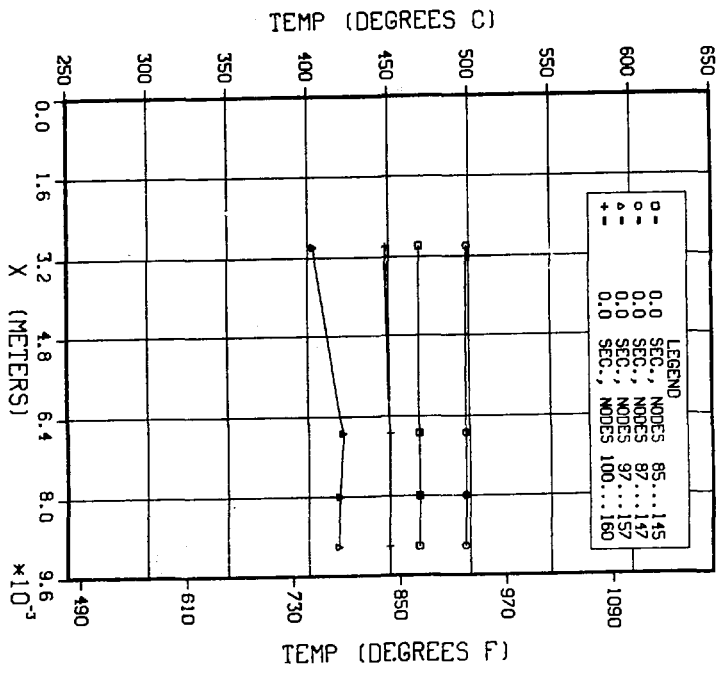


Fig. 3-23. Steady-state temperature distribution (x-direction) in first-wall/blanket segment (outboard).

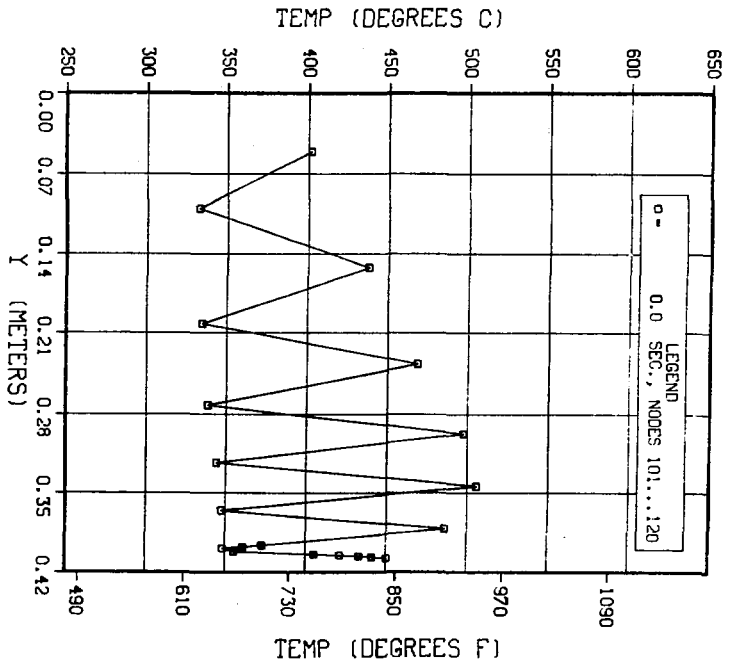


Fig. 3-24. Steady-state temperature distribution (y-direction) in first-wall/blanket segment (outboard).

these figures that the maximum temperature of the beryllium coating is only about 450°C. For the coolant channel arrangements as shown in Fig. 3-17 the maximum blanket temperature is only 510°C. The variation in the temperature within the blanket blocks could be minimized by rearrangement of the coolant channels. Since the maximum temperature of the blanket is only ~510°C, a limited number of trials of coolant channel rearrangement has been made to arrive at the coolant channel arrangement as shown in Figs. 3-18 and 3-19.

Since only a limited effort has been made during this study on inlet and outlet header arrangement and coolant channel layout, an exact pressure drop calculation has not been carried out. However, the pressure drop across the first-wall/blanket modules is modest, and it is not critical at this stage of reactor study to know the exact header sizes and the header layout. Approximate pressure drop calculations have been carried out based on the maximum coolant velocity. For low velocity coolant channels in systems with common inlet and outlet headers, additional pressure drop can be obtained by orificing the individual coolant channels or by use of filler rods so that the total pressure drop across each coolant channel is the same. To account for the pressure losses at the inlet and outlet bends, headers, fittings, etc, the total pressure drop between the first-wall/blanket modules has been assumed to be twice the pressure drop across the 3-m long straight sections. The pressure drop across the first wall and the blanket modules are estimated to be 165 kPa (24 psi) and 365 kPa (53 psi), respectively. Hence, the pumping power losses based on the maximum pressure drop are less than 1% of the thermal power.

3.4 Reactor Maintenance and Repair

The maintenance and repair procedures for WILDCAT have been based in large part on those utilized for STARFIRE.¹ Basic solutions to the major removal and disassembly problems have been developed, but these procedures have not been carried to the same level of detail as for STARFIRE. This section describes these solutions including some of the more important differences between the two machines.

The general approach to reactor disassembly and repair is the same as that used by STARFIRE in that the components are modular and are replaced as units in the event of failure or end-of-life rather than being repaired in

place. There are 24 first-wall/blanket/shield modules. The first-wall/blanket part of each module is removable as a single piece similarly to STARFIRE. The shield section is in two pieces. The inner section is semi-permanent, while the outer section is removable to accommodate replacement of the blanket sectors. Removal of components of the modules which are under the toroidal field (TF) coils requires removal of an adjacent unit for accessibility. Resealing of the vacuum boundary is similar to the method used for STARFIRE. The coolant lines, manifolds, and ancillaries are also similar to those used for STARFIRE.

The first-wall/blanket/shield modules have an expected life of twenty years or one-half of the plant life. They would all be replaced together at the end of twenty years rather than sequentially on a six-year cycle as for STARFIRE.

It is expected that the limiter would need repair or replacement on a more frequent basis than the rest of the modules. For the modules between the TF coils the limiter, first-wall, blanket, and shield behind it can be removed as a single, drawer-like unit. (See Figs. 2-11 and 3-25.) This removable unit also provides access to the plasma chamber and to the current drive antennas, which can also be expected to have a higher repair/replacement rate. The limiter sections on the modules under the TF coils are removed by detaching them from the module after removing the adjacent drawer-like unit to provide an access port. These limiters are in two sections, each section being removable to the adjacent side with a special fixture, and then out the access port in a conventional manner.

Figures 1-2 and 3-26 depict the shape of the reinforced concrete, anti-torque structure. Each section occupies the space between two TF coils and consists of more permanent upper and lower sections and a more easily removable middle section which allows access to the first-wall/blanket/shield modules. The lower and middle sections are moved horizontally away from the reactor using equipment similar to that used for STARFIRE. The upper sections are removed vertically by crane. Two equilibrium field coils must be raised or lowered to permit removal of the middle section. A port located at the midplane in the middle sections provides for removal and replacement of the limiter drawer without disassembly of any of the larger components.

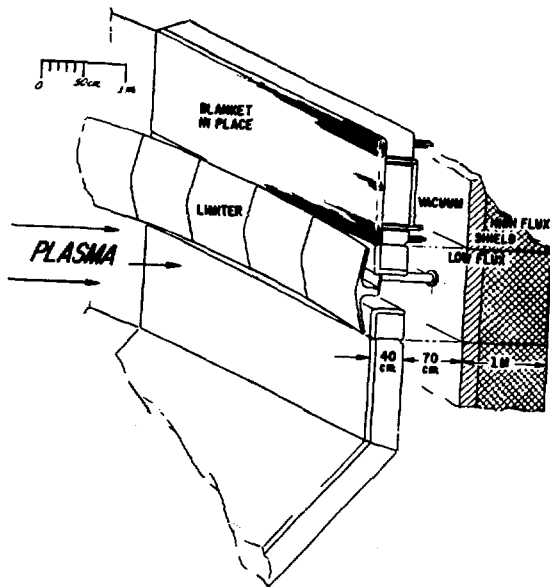


Fig. 3-25. Mechanical configuration of the limiter and the adjacent first wall, blanket, and shield.

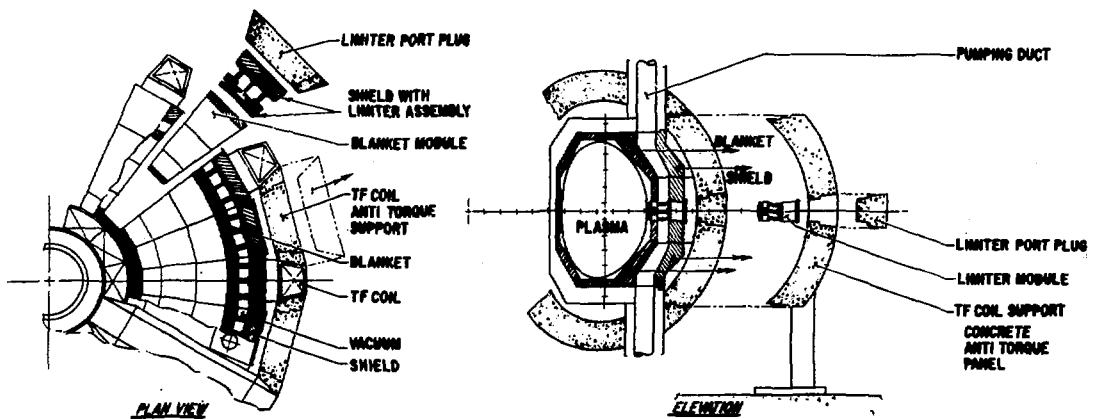


Fig. 3-26. Disassembly concepts for the major reactor components.

The current-drive antenna launchers represent the most difficult of all the maintenance problems. This situation arises from two sources: (1) some units are placed on the inner wall making horizontal access to lead lines and disconnects difficult; (2) the complexity of the antenna assembly with its coolant, electrical insulation and connections, and its ancillaries makes it virtually impossible to remove it radially outward from the plasma chamber without unduly segmenting the blanket modules. The proposed plan for antenna removal is initial removal of the electric, coolant, and structural ties through special ports in the anti-torque panels and reactor shield. The antenna removal follows, first moving into the plasma chamber using special remote operated fixtures placed through the limiter port. The antennas are then retrieved through the limiter port, and replacement units are positioned and hooked up in the reverse order.

The vacuum pumping components can be repaired independently of the major disassembly.

REFERENCES

1. C. C. Baker, et al., "STARFIRE - A Commercial Tokamak Fusion Power Plant Study," Argonne National Laboratory, ANL/FPP-80-2 (1980).
2. R. F. Mattas, Argonne National Laboratory, (to be published).
3. D. L. Smith, "Physical Sputtering Model for Fusion Reactor First-Wall Materials," J. Nucl. Mater. 75, 20 (1978).
4. D. L. Smith, "Analytical Expressions: Physical Sputtering," Proc. Workshop on Sputtering Caused by Plasma Surface Interactions, Argonne National Laboratory, CONF-790775 (1979).
5. "ANISN-ORNL: Multigroup One-Dimensional Discrete Ordinates Transport Code with Anisotropic Scattering," Oak Ridge National Laboratory, ORNL/RSIC-254 (1973).
6. R. W. Rossin, et al., "VITAMIN-C: The CTR Processed Multigroup Cross Section Library for Neutronics Studies," Oak Ridge National Laboratory, ORNL/RSIC-37 (ENDF-296) (1980).
7. Y. Gohar and M. Abdou, "MACKLIB-IV: A Library of Nuclear Response Functions Generated with the MACK-IV Computer Program from ENDF/B-IV," Argonne National Laboratory, ANL/FPP/TM-106 (1978).
8. J. Jung, "Theory and Use of the Radioactivity Code RACC," Argonne National Laboratory, ANL/FPP/TM-122 (1979).

9. C. W. Gear, Numerical Initial Value Problems in Ordinary Differential Equations (Prentice-Hall, New Jersey, 1971).
10. J. Jung, "A Computational Method for Neutron Transport Problems in Toroidal Geometry," Nucl. Sci. Eng. 65, 130 (1978).
11. D. L. Smith, ed., "First-Wall System," Chapt. VII, in INTOR - International Tokamak Reactor Phase-One Conceptual Design, (IAEA, Vienna, 1981), in press.
12. G. W. Grodstein, "X-Ray Attenuation Coefficients from 10 keV to 100 MeV," U. S. Department of Commerce, NBC Circular 583 (1957).
13. R. T. McGinnies, "X-Ray Attenuation Coefficients from 10 keV to 100 MeV," U. S. Department of Commerce, Supplement to NBC Circular 583 (1959).
14. D. J. Rose and M. Clark, Jr., Plasmas and Controlled Fusion (MIT Press, Cambridge, Mass., 1961).
15. "Kobe Steel's Nonmagnetic Steel Plate NONMAGNE-30," Kobe Steel Ltd., Kakogawa Works, Japan, No. A-282320 (1979).
16. R. R. Coltman, et al., "Effect of Radiation at 5°K on Organic Insulators for Superconducting Magnets," in Proc. 8th Symp. on Engineering Problems of Fusion Research (1979), Vol. III, p. 1694.
17. A. R. Sweedler, et al., "High-Energy Neutron Irradiation of Superconducting Compound," in Radiation Effects and Tritium Technology for Fusion Reactors, CONF-750979 (1975), Vol. II, p. II-422.
18. M. A. Abdou, "Radiation Considerations for Superconducting Fusion Magnets," Argonne National Laboratory, ANL/FPP/TM-92 (1977).
19. B. S. Brown, et al., "Low Temperature Fast-Neutron Radiation Damage Studies in Superconducting Materials," J. Nucl. Mater. 52, 215 (1974).
20. F. S. L. Hsu and J. E. Kunzler, "Magnetoresistance Probe for Measuring Magnetic Field Intensity in a Small Space," Rev. Sci. Instr. 34, 297 (1963).
21. E. S. Fisher, et al., "Effects of Cyclic Strains on Transport Properties of a Superconducting Composite: Phase 1, Degradation of Electrical Conductivity in Copper at 4.2 K," Argonne National Laboratory, ANL-77-50 (1977).
22. G. L. Kulcinski, et al., "Radiation Damage Limitations on the Design of the Wisconsin Tokamak Fusion Reactor," Nucl Technol. 22, 20 (1974).
23. J. Jung and M. Abdou, "Importance of Shield Design in Minimizing Radioactive Inventory in Tokamaks," in Proc. 4th Top. Mtg. on the Technology of Controlled Nuclear Fusion, CONF-801011 (1981), Vol. I, p. 458.

24. J. Jung and M. Abdou, "Radioactive Inventories and Material Recyclability in a Tokamak Reactor," Trans. Am. Nucl. Soc. 34, 645 (1980).
25. G. Kessler and G. L. Kulcinski, "Radioactive Inventories of Reactor Economics," in Fusion and Fast Breeder Reactors, W. Häfele, et al., International Institute for Applied Systems Analysis, Luxemburg, RR-77-8 (1976).
26. U. S. National Regulatory Commission, "Standards for Protection Against Radiation," in USNRC Rules and Regulations, Title 10, Chap. 1, pt. 20 (1975).
27. K. Evans, Jr., et al., "D-D Tokamak Reactor Studies," Argonne National Laboratory, ANL/FPP/TM-138 (1980).
28. C. C. Baker, et al., "The Impact of Alternate Fusion Fuels on Fusion Reactor Technology," Argonne National Laboratory, ANL/FPP/TM-128 (1979).

Section 4

MAGNETS



4. MAGNETS

Since WILDCAT is larger than STARFIRE and in addition has higher magnetic fields, the magnet design is considerably more difficult. For the most part the design procedures used for STARFIRE have also been used for WILDCAT. The space between the toroidal field (TF) coils is assumed to be filled with reinforced concrete to support the out-of-plane loads. This method is different from that used for STARFIRE. In addition, the plasma has been taken to be less D-shaped to reduce the requirements on the equilibrium field (EF) coils. A relatively slow startup and shutdown (even in the pulsed case) help to reduce the EF and ohmic heating (OH) coil requirements. The correction field (CF) coils, which are the least well-defined system, have been designed by scaling from those in STARFIRE. It should be noted that the EF and OH systems for the pulsed case are substantially larger and require more power than those for the steady-state case.

All of the magnet systems and their design bases are described in this chapter.

4.1 Toroidal Field Coils

The TF coil requirements for a D-D reactor were studied earlier, and a 15-T TF coil system described.¹ As the demands of the present design are only slightly relaxed from that design, the choice of conductor and in-plane support have not been reexamined. Instead, the study has focused on choice of coil parameters for pulsed and steady-state WILDCAT designs and on a conceptual design of a method of out-of-plane support which was not examined in Ref. 1.

4.1.1 Choice of TF Coil Parameters

The primary differences between the TF coils for a D-D tokamak reactor and those for a D-T tokamak reactor are the larger size and higher field typically required for the D-D reactor. These in turn make conductor design and support more difficult than for a D-T reactor. Parameters for the TF coils for the steady-state and pulsed reference designs appear in Table 4-1.

Since the reactor thermal power is proportional to the fourth power of the toroidal field, a high field is desirable. However, increasing the field

Table 4-1. Parameters for WILDCAT TF Magnets

	Steady-State	Pulsed
No. of coils	12	12
Total ampere turns, MA-turns	353	344
Total stored energy, GJ	192	179
Total inductance, H	375	350
Peak field, T	14.35	14.00
Current, kA	32	32
Average conductor current density, A/cm ²	3100	3100
Average overall current density, A/cm ²	900	900
Coil cooling	Liquid He bath, 4.2 K	Same
Conductor:		
Superconductor	Nb ₃ Sn, NbTi	Same
Stabilizer	Copper	Same
Configuration	Cable	Same
Structural material	Austenitic SS, G-10 epoxy-fiberglass insulator, reinforced concrete	Same

causes an increase in the cost and size of the TF coils, and especially an increase in the amount of support material required. In particular, the coil thickness increases rapidly with field, leading either to an unacceptable shrinking of the area within the OH solenoid or to an increase in the plasma major radius with a consequent increase in the overall size of the reactor.

The choice of operational peak field has been made on considerations of the advantages of high field vs. the accompanying disadvantage of large size and cost. The toroidal coils have been designed for a maximum field of 14.35 T for the steady-state design and 14.00 T for the pulsed design.

4.1.2 Conductor Design and Plane Force Support

A three level, unsoldered, uninsulated "Rutherford" cable has been chosen as the conductor. Four grades of conductor, two employing Nb₃Sn (11-15 T and 8-11 T regions) and two employing NbTi (5-8 T and 0-5 T regions) are envisioned. However, no attempt has been made to optimize the grading; a differ-

ent grading scheme, perhaps employing six grades, might result in savings of space and material.

In a cable conductor design the copper stabilizer contributes very little to supporting the hoop stress arising from the magnetic forces the TF coil system exerts upon itself. Moreover, in the region of the inner leg, the cable should not have to support the radial forces, lest the cable be compressed and the surface contact with helium coolant be reduced. Consequently, the conductor is surrounded by a support frame made of stainless steel strips, which carry almost all the hoop and radial forces generated in the coil. This support frame is designed for a combined stress of 500 MPa (80,000 psi).

In the curved portion of the coil each support frame generally carries the tension of its conductor, and radial loads are low. In the straight inner leg portion the radial force accumulates radially inward, away from the plasma region. Thus, the radial load is largest and the most stainless steel support material is needed in the turns where the toroidal field is lowest and where the least copper stabilizer and superconductor are needed.

4.1.3 Support Against Out-of-Plane Forces

The support of a TF coil system against out-of-plane forces from the poloidal field coils is one of the most serious problems encountered in a tokamak reactor design. It has caused great problems in the INTOR and FED design studies, particularly because of fatigue problems in those two reactors, which are designed for a lifetime of order one million pulses. The out-of-plane forces and overturning moments, 1.5 GNm per TF coil, also presented major support problems in the STARFIRE design study,² although as a steady-state reactor, STARFIRE did not have the added problem of fatigue lifetime. These problems become even greater for WILDCAT with its larger overturning moment. The out-of-plane forces on the outer leg of a WILDCAT TF coil exert an overturning moment of 3.9 GNm. The out-of-plane forces on the curved portion of the inner leg are in the opposite direction and exert an overturning moment of -1.2 GNm. Thus, the net overturning moment on each coil is 2.7 GNm. In addition to reducing the overall moment, the opposing moments act to twist the coil out of a plane shape.

Two basic approaches can be taken to the support of superconducting TF coils against out-of-plane forces. In the first, adopted in the FED and INTOR

studies, neighboring TF coils are joined together by cold (liquid helium temperature) structural members. In the second, adopted in the STARFIRE study, neighboring coils are joined by warm (room temperature) structural members, and warm-to-cold support structure is required inside each TF coil dewar. Cold support requires a dewar system enclosing the coil-to-coil supports as well as the TF coils. Even at the scale of FED and INTOR, such a dewar presents problems of accessibility, fabricability, and excessive cool-down time and cost. All of these problems become worse, and possibly prohibitive, for WILDCAT.

Warm support presents two design problems: the choice of the coil-to-coil support and the choice of the cold-to-warm support within each coil dewar. The cold-to-warm support elements must have a large cross-sectional area to transmit the massive forces at acceptable stress levels. Even for materials such as epoxy-fiberglass, which combine high mechanical strength with low thermal conductivity, these support elements introduce intolerable heat leaks into the magnet system unless the elements are long.

In STARFIRE these support elements were given a length roughly equal to the width of a TF coil by making the elements epoxy-fiberglass (G10) tie bars connected to the vacuum tank at one side of the coil and to the helium vessel at the opposite side as shown in Fig. 4-1. Pivoting end-hooks eliminated bending moments in the tie bars from differential thermal contraction. In STARFIRE 17,000 of these tie rods were required. This same concept has been adopted for WILDCAT. It is the one which allows the greatest length to the support members without unduly adding to the overall size of the TF coil system or itself degrading accessibility between coils. However, the concept can be criticized because the tie bars support only in tension and provide no support in an off-normal situation in which the out-of-plane force changes direction.

The coil-to-coil supports must also be addressed. In STARFIRE shear panels provided this support, but these did not appear scalable to the higher force levels of WILDCAT. For WILDCAT a support system has been adopted which essentially fills the space between TF coils with support material. Parts of the support system are removable with acceptable convenience to permit removal of a blanket sector. (See Sec. 3.4.)

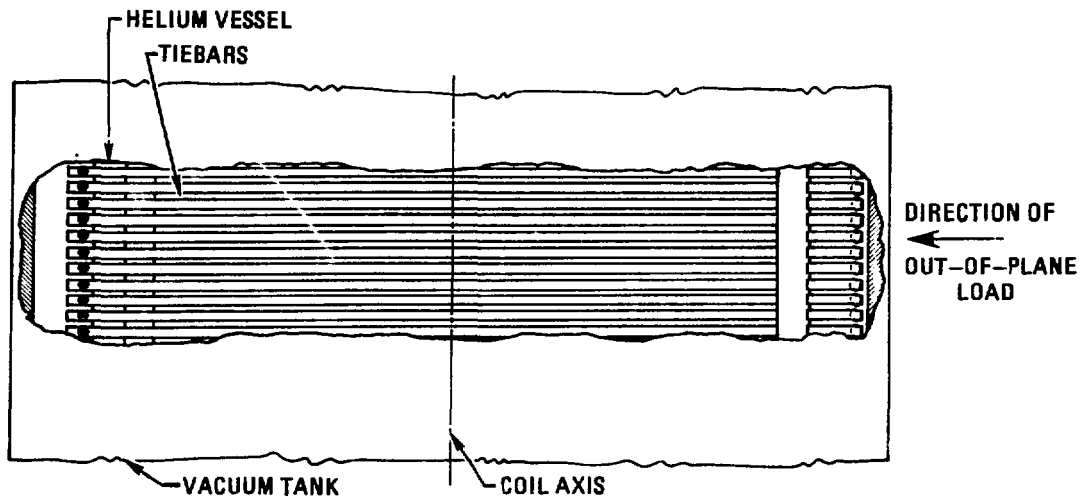


Fig. 4-1. Cutaway view of one coil showing support bars in high load region.

Several possible materials for the support are compared in Table 4-2. The table gives material costs per sector, but fabrication costs are expected to be roughly proportional to the material costs. Reinforced concrete is seen to be by far the least expensive, and also has desirable electromagnetic and fabrication properties. A concrete support may also serve as a biological shield against neutrons, but that effect has not been taken into account elsewhere in the shielding analysis of WILDCAT.

The reinforced concrete coil-to-coil support is shown in Figs. 1-2 and 3-25. Each sector consists of three blocks; only the central block needs to be removed to gain access to the blanket and shield region and only the plug needs to be removed to gain access to the limiter alone. Square keys 20 cm on a side and of full depth provide alignment and transfer the shear from the overturning moments. Because of concrete's weakness under shear, each block is entirely contained in a steel can with additional steel in regions of high shear stress such as around the shear keys.

4.1.4 Ripple

No great attempt has been made to minimize the field ripple for WILDCAT. The reason is that it is felt that the current theoretical analysis of ripple diffusion is not adequate to accurately assess the ripple requirement and

Table 4-2. Comparison of Candidate Materials for Coil-to-Coil Support

Material	Electromagnetic Considerations	Comparison for Similar Loading (tons/Section)	Material Cost per Sector (\$)	Shielding Quality
Concrete (reinforced)	Insulator	474	9,500	Good neutron
Aluminum	Requires insulation breaks	97.2	97,000	Fair gamma ray
Stainless steel, nonmagnetic	Requires insulation breaks	212	424,000	Good gamma ray
G-10 glass Epoxy	Insulator	96.6	250,000	Fair neutron
1020 steel	Magnetic and requires insulation breaks	232	186,000	Good gamma ray

that it is hence not reasonable to unduly penalize the device by matching such a requirement for low ripple. WILDCAT has a peak-to-average ripple of 0.2% at $R = R_0$, 0.9% at $R = R_0 + a/2$, and 3.9% at $R_0 = R_0 + a$. The corresponding STARFIRE values are 0.1%, 0.4%, and 1.5%. Adding 1.0 m to the outer leg of the WILDCAT TF coils would give essentially the same values as for STARFIRE. In fairness, it should be noted that if ripple diffusion were to exist, it would probably increase with plasma temperature. In that case the ripple for a D-D reactor, which typically operates at a higher temperature, would need to be less than for a D-T reactor.

4.2 Ohmic Heating Coils

For the pulsed version of WILDCAT the OH system induces and maintains the plasma current. This system, consisting of a solenoid plus trim coils, is described in Ref. 1. For the steady-state, reference version such an extensive system is not necessary, as it was not for STARFIRE,² because the current drive system maintains the plasma current once it has reached a minimal value, taken to be 1 MA for both STARFIRE and WILDCAT. The WILDCAT steady-state OH system provides 25 V-s, the same as for STARFIRE. It consists of six coils in the inboard region, also the same as for STARFIRE. The system was designed in both cases by choosing coil currents to make a least-squares fit to zero field

throughout the same plasma at the same time minimizing the OH system stored energy. The method used is similar to that described in Ref. 3 for EF coil design. The required absolute error in the least-squares fit has been taken to be the same value as the required error for the EF coil design. The latter error is sufficient to reproduce the desired equilibrium.

The OH system requirements are less for WILDCAT than for STARFIRE because the hole in the center is larger. A design with only four inboard coils would probably be adequate. The extra coils are useful, however, in that the toroidal coils are better protected from stray fields. The system could still provide the required volt-seconds with reasonable currents if some of the coils were not working. For this reason it might be appropriate to provide fewer spares.

The energy of the OH system could be further lowered if the outermost OH coil were further out (to about 30 deg relative to the major axis). It has been placed further inboard to be out of the way and to be smaller, since the OH stored energy is not large (relative to the EF stored energy). The cost is about 0.1 GJ out of 0.4 GJ.

The OH system parameters are shown in Table 4-3 for both versions of WILDCAT and for STARFIRE, and the coil locations and currents for the steady-state version are shown in Table 4-4. A plot of the OH field is shown for the steady-state version in Fig. 4-2 and for the pulsed version in Fig. 4-3. The steady-state OH system would be started cocked at full field and run to zero field, in contrast to the OH system for the pulsed case, which would be cocked at full negative field and run to full positive field.

4.3 Equilibrium Field Coils

The EF coil system for the steady-state version is quite similar to the EF system described in Ref. 1 for the pulsed version. The coil locations and sizes are in fact taken to be the same. The currents vary slightly. These coils are outside of the TF coils to ease the assembly, maintenance, and reliability of the coils, even though this means larger coil currents and stored energy.

Table 4-3. OH System Parameters

	WILDCAT		STARFIRE
	Steady-State	Pulsed	
Stored energy, U_{OH} (GJ)	0.4	20	1.1
Total ampere-turns, I_{OH} (MAT)	21	149	51
Approximate coil volume, V_{OH} (m ³)	28	266	34
Volt-seconds to plasma, $\Delta\phi_{OH,P}$ (V-s)	-25	-502 ^a	-25

^aThe pulsed version OH system is swung from full negative to full positive. The two steady-state versions are swung from full negative to zero.

Table 4-4. Steady-State OH System Coil Locations and Currents

The coils extend from $R = R_1$ to $R = R_2$ and from $Z = Z_1$ to $Z = Z_2$ with the center line along (R_0, Z_0) . The system is symmetric about the midplane, and the direction of the current is with respect to the plasma current. The locations and currents for the pulsed version are listed in Ref. 1.

N	R1 (m)	R0 (m)	R2 (m)	$\pm Z_1$ (m)	$\pm Z_0$ (m)	$\pm Z_2$ (m)	I (MAT)
1	2.10	2.22	2.35	0.90	1.40	1.90	-3.8
2	2.10	2.22	2.35	3.70	4.20	4.70	-2.8
3	2.10	2.22	2.35	6.50	7.00	7.50	-1.5
4	6.02	6.22	6.42	8.71	9.21	9.71	-2.2

The required EF field is determined from the MHD equilibrium, which is chosen to optimize the achievement of high beta. The currents in the coils are then determined so as to make a least squares fit to the required field, at the same time minimizing the stored energy and possibly decoupling the EF system from the OH system. This procedure is described in detail in Ref. 3.

For the pulsed version it is considered necessary to decouple the EF and OH systems in order to prevent changes in one system from producing unwanted voltages in the other. For the steady-state version it is also necessary to decouple the two systems, but only for the short time during which the OH

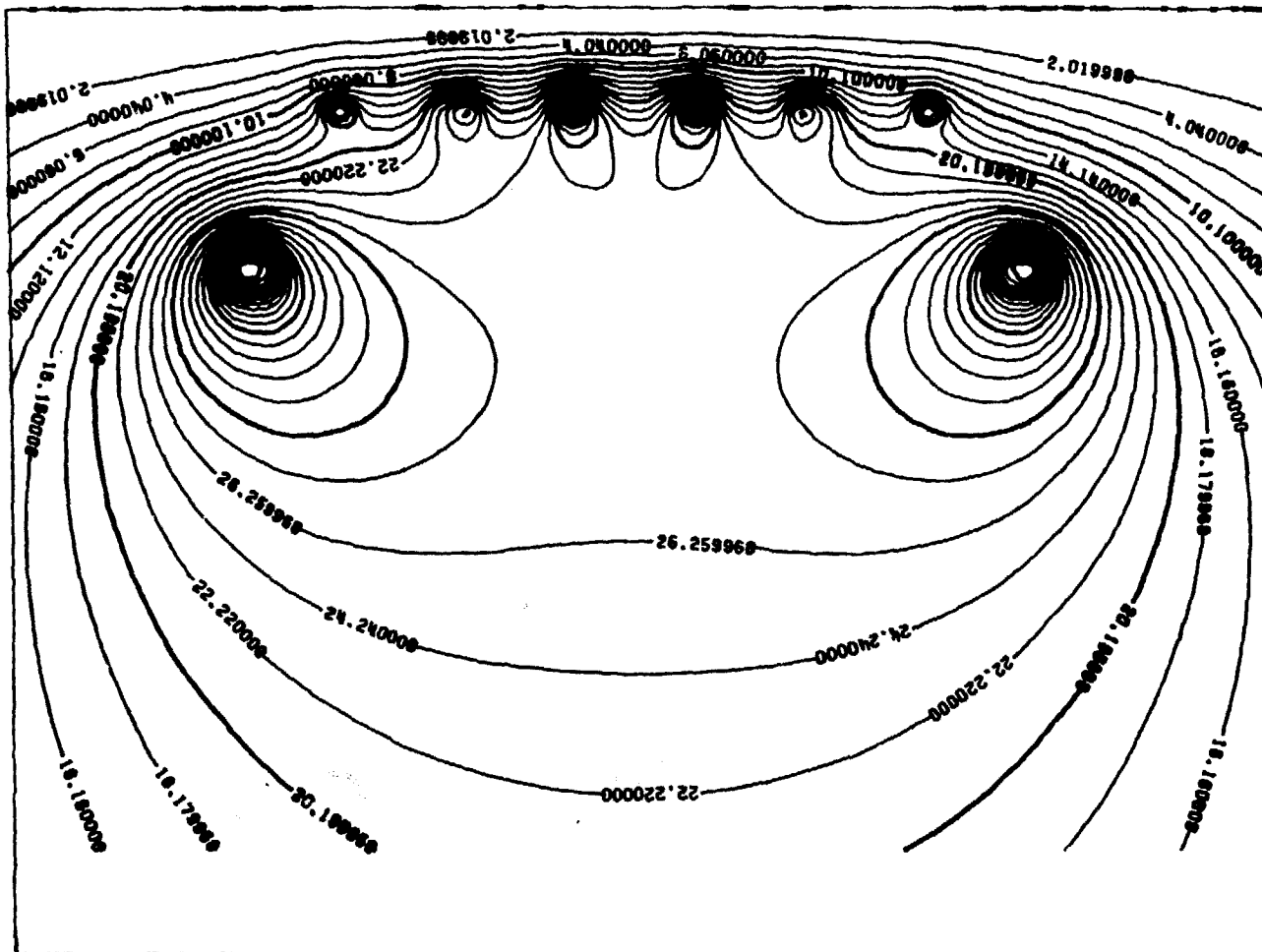
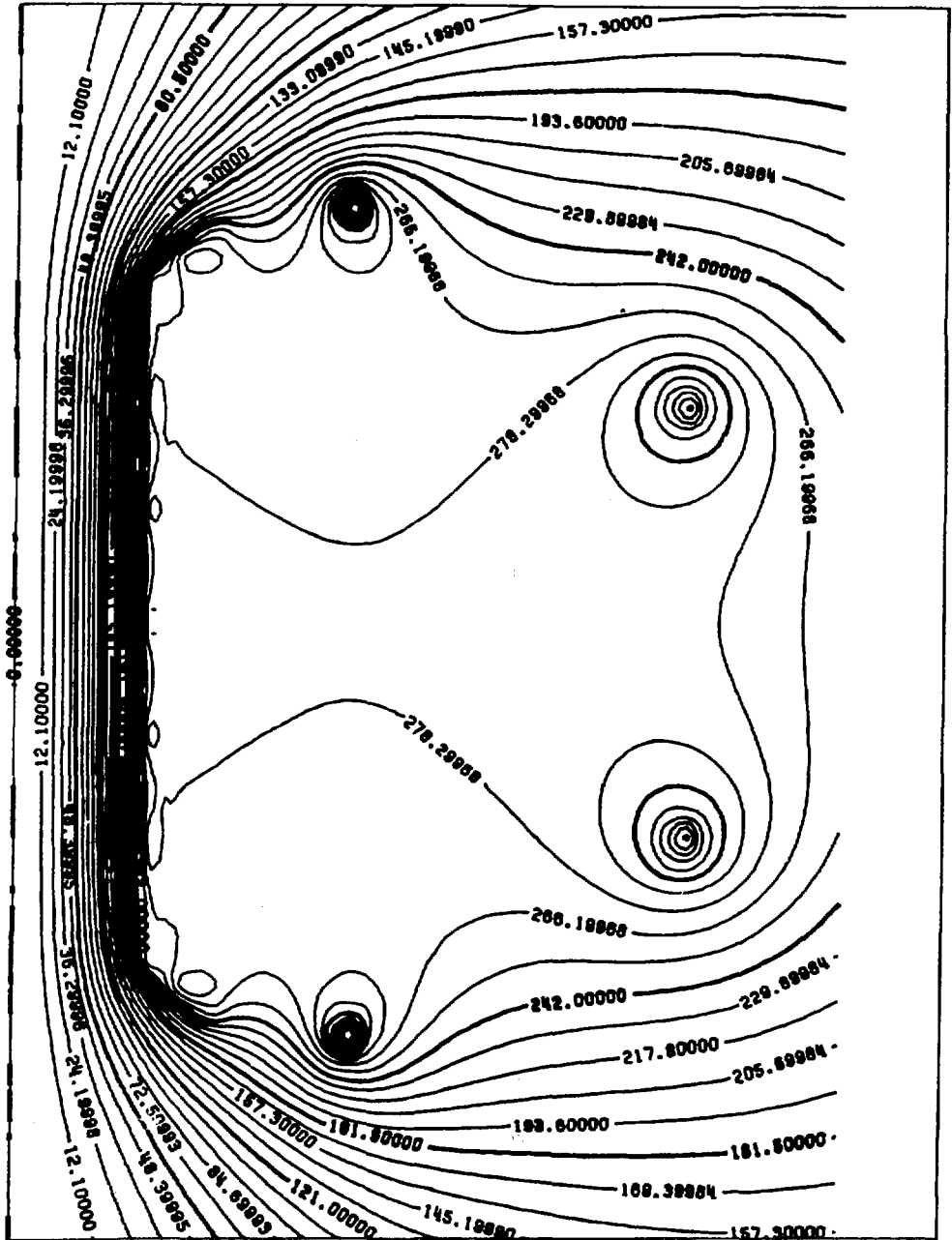


Fig. 4-2. Field contours for the WILDCAT steady-state OH systems. The lines are labeled by the flux in webers.



system is in operation. (The OH system can be disconnected after it is run to zero current.) If the EF system is decoupled, the currents and energies are higher because of the additional constraint on the system. Since the cost of the EF system depends primarily on the peak energy, and since the systems do not have to be decoupled at the time the peak energy is stored, it would seem reasonable to design the system to be decoupled during the OH current ramp and change to a non-decoupled system thereafter. This was not done for STARFIRE: the two systems were assumed always decoupled. This has also not explicitly been implemented in the WILDCAT design, but it is assumed to have been done so that the EF coil peak parameters are based on a less restrictive, nondecoupled design.

The parameters for both the non-decoupled and decoupled designs are given in Table 4-5, along with those for the pulsed version and for STARFIRE. The coil currents for both the non-decoupled and decoupled steady-state cases and the coil locations (common to all the WILDCAT EF systems) is given in Table 4-6. During the short OH ramp for the steady-state system the EF currents would be proportional to those in the decoupled column of Table 4-6, but before the final values were reached, the currents would become proportional to those in the non-decoupled column and would reach those final values at the end of the startup.

One small difference between the steady-state and pulsed versions is that the two top EF coils were constrained to have the same current in the steady-state version. This requires negligible additional energy. Also EF coil 3 has been moved slightly higher than the location listed in Ref. 1 to facilitate blanket/shield removal. For reference and costing purposes the non-decoupled design is assumed to be the reference case. A plot of the EF field contours is shown in Fig. 4-4. The contours are not essentially different for the decoupled and pulsed cases.

4.4 Correction Field Coils

Since the EF coil system has large currents and is located a relatively large distance from the plasma, it is unlikely that it could provide fine-scale control of the plasma on short time scales. For this reason a CF system consisting of normal conducting coils just outside the shield is provided. The WILDCAT CF system has been scaled from that for STARFIRE. In view

Table 4-5. EF System Parameters

	WILDCAT			STARFIRE
	Steady-State		Pulsed	
	Non-decoupled	Decoupled		
Stored energy, U_{EF} (GJ)	21	22	22	10
Total ampere turns, I_{EF} (MAT)	55	62	67	86
Approximate coil volume, V_{EF} (m ³)	238	238	238	164
Volt-seconds to plasma, $\Delta\phi_{EF,P}$ (V-s)	-215	-206	-195	-83

Table 4-6. Steady-State EF System Coil Locations and Currents

The coils extend from $R = R_1$ to $R = R_2$ and from $Z = Z_1$ to $Z = Z_2$ with the center line along (R_0, Z_0) . The system is symmetric about the mid-plane, and the direction of the current is with respect to the plasma current. Both the nondecoupled, decoupled, and pulsed version currents are shown. The coil locations are the same for the pulsed version.

N	R_1 (m)	R_0 (m)	R_2 (m)	$\pm Z_1$ (m)	$+Z_0$ (m)	$\pm Z_2$ (m)	Steady-State		
							Non-decoupled	Decoupled	Pulsed
							I (MAT)	I (MAT)	I (MAT)
1	3.81	4.20	4.59	7.61	8.00	8.39	5.7	7.4	10.8
2	4.35	4.80	5.25	8.40	8.60	8.60	5.7	7.4	6.4
3	14.76	15.09	15.42	5.96	6.29	6.62	-6.4	-7.2	-7.5
4	16.31	16.66	17.01	1.69	2.04	2.39	-9.8	-9.2	-8.7

of the relatively small impact on the overall reactor design and the uncertain nature of this system, it has not been considered necessary to define separate requirements for the pulsed and steady-state versions.

A CF coil system which had sufficient maximum current capability to restore several typical perturbations to the STARFIRE equilibrium was defined in Sec. 9.4 of Ref. 2. The STARFIRE CF power supply requirements were defined in Sec. 5.3 of Ref. 2 based on a stored energy of 9.84 MJ, not including

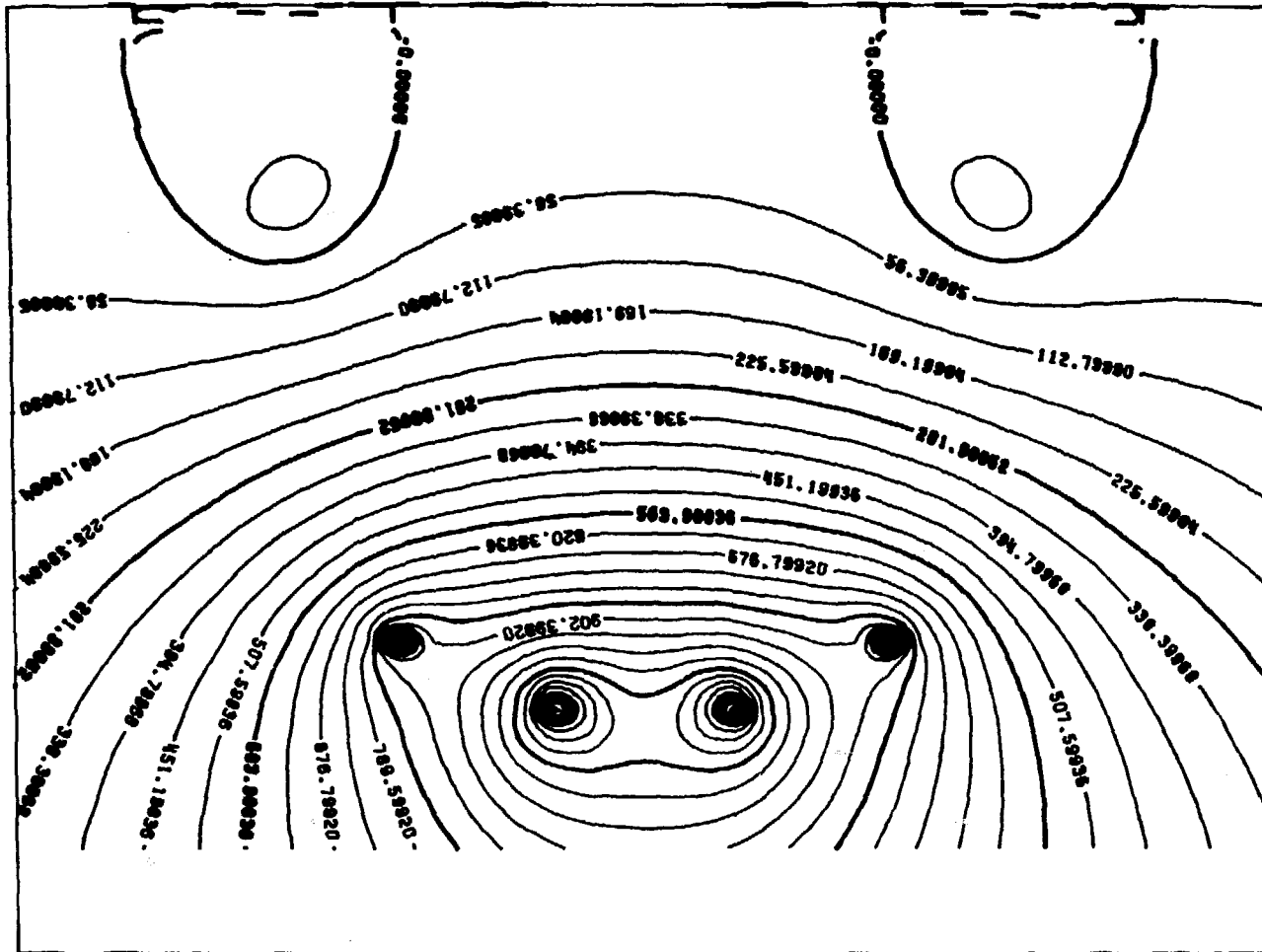


Fig. 4-4. Field contours for the WILDCAT steady-state EF systems. The contours for the pulsed version are similar. The lines are labeled by the flux in webers.

Table 4-7. CF System Parameters

	Inside Coil	Outside Coil
Current (MA)	-0.13	-0.23
Cross section (m)		
Length	0.2	0.3 ^a
Width	0.2	0.2 ^a
Centerline (m)		
Major radius	6.25	13.40
Height, m	±5.90	±3.05
Stored energy (MJ)	6.5	
Total ampere turns (MAT)	0.72	
Approximate coil volume (m ³)	13.2	
First-wall time constant (s)	350.	
Power required (MW)	18.	

^aThe outside coil has a rectangular cross section which is tilted with respect to the midplane. See Fig. 1-2.

mutual inductance terms. Based on the calculations in Sec. 9.4 of Ref. 2, this stored energy would correspond to currents in the coils of -0.20 MAT and -0.36 MAT for the inner and outer coils respectively.

The WILDCAT CF system has been designed by locating the coils on the outside of the shield in positions which are both convenient and likely to be effective for plasma control, then determining the maximum currents in the coils from the STARFIRE by scaling as the ratio of the respective total EF currents for the two devices. This scaling is appropriate since the CF and EF coils perform the same function (i.e. control the MHD equilibrium). The cross-sectional area has been determined by using approximately the same current density ($\sim 3\text{-}4 \text{ MA/m}^2$) as for STARFIRE. The parameters of the resulting WILDCAT CF system are shown in Table 4-7. It can be seen that the system is smaller than that for STARFIRE even though the device is larger. The reason is that the less D-shaped equilibrium is easier to control.

In order to determine the power requirements for the CF system, it is necessary to know how fast the system must respond. For STARFIRE it was assumed that the first wall, being a conducting structure, would hold the plasma in equilibrium for times shorter than the stated first-wall L/R time of

300 ms. The power supply was then sized at 33 MW by requiring it to respond in 300 ms. The WILDCAT system has been designed according to the same philosophy in order to make it comparable to that of STARFIRE. Assuming a first wall of 2.64 m minor radius consisting of 3 mm of beryllium and an average thickness of 4.8 mm of stainless steel (see Sec. 3), the WILDCAT first-wall time constant is 350 ms, giving a power supply requirement of 18 MW.

REFERENCES

1. K. Evans, Jr., et al., "D-D Tokamak Reactor Studies," Argonne National Laboratory, ANL/FPP/TM-138 (1980).
2. C. G. Baker, et al., "STARFIRE - A Commercial Tokamak Fusion Power Plant Study," Argonne National Laboratory, ANL/FPP-80-1 (1980).
3. K. Evans, Jr., D. A. Ehst, and P. Messerschmidt, "Equilibrium Field Coil Considerations for Tokamak Reactors," Proc. 3rd Top. Mtg. on the Technology of Controlled Nuclear Fusion, CONF-780508 (American Nuclear Society, 1978), Vol. 12, p. 1084.

Section 5

TRITIUM/FUEL/VACUUM



5. TRITIUM/FUEL/VACUUM

Fuel processing and tritium handling systems for a catalyzed D-D reactor are in general similar to those for D-T reactors, with the major advantage being that the amounts of tritium are reduced by about two orders of magnitude. A comprehensive analysis of tritium systems for STARFIRE, a commercial D-T reactor design, has been previously presented.¹ Presented below is a comparative analysis of fuel processing and vacuum pumping systems for WILDCAT and a comparison with STARFIRE. In addition, the implications of steady-state and pulsed burn cycles are examined.

5.1 Fuel Cycle

A schematic of the fuel reprocessing cycle for the WILDCAT is shown in Fig. 5-1. The exhaust from the plasma is removed with compound cryopumps, which are part of the limiter/vacuum system. Upon regeneration of the vacuum pumps the fuel is processed for chemical purification, isotopic enrichment, storage, and refueling. The chemical purification subsystem is designed to remove all condensible impurities (CD_x , D_2O , N_2 , etc.). The helium is separated from the D_2 fuel by a falling film condenser, after which the helium is isotopically enriched by means of cryogenic distillation.¹⁻³ Separation factors for helium are reportedly higher than those for the cryogenic distillation of hydrogen isotopes.⁴ The hydrogen isotopes are separated by means of cryogenic distillation at ~ 20 K. The protium waste stream is primarily HD; the fuel stream can consist of D_2/DT or separate D_2 , T_2 streams depending on fueling requirements. The components of the fuel reprocessing cycle are quite similar to those in a D-T fuel processing cycle (Fig. 5-2) with the additional feature of isotopic enrichment of helium.

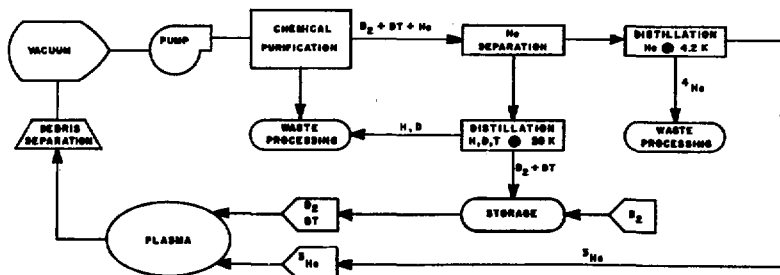


Fig. 5-1. Schematic of fuel reprocessing loop.

The mass flow rates for WILDCAT and STARFIRE are shown in Table 5-1. It can be seen that although the amount of tritium exhausted from the plasma is much less for WILDCAT, it is still a significant amount (10 g/day).

Table 5-1. Mass Flow Rates for WILDCAT (Cat-D)
Versus STARFIRE (D-T)

	WILDCAT Cat-D	STARFIRE D-T
Thermal power, MW	2700	4000
Net electric power, MW	810	1200
Burn cycle	Steady-State	Steady-State
Ion density, 10^{20} ions/m ³	1.66	0.8
Plasma volume, m ³	1850	780
Surface area, m ²	1250	750
Particle confinement time, s	4	4
Tritium reflection coefficient	0.9	0.9
Fractional burnup		
D	0.17	0.42
T	0.90	0.42
³ He	0.12	----
Deuterium burned, g/day	480	360
Deuterium exhaust, g/day	2400	506
Tritium burned, g/day	100	536
Tritium exhaust, g/day	10	760
³ He burned, g/day	125	----
³ He exhaust, g/day	1000	----
Protium exhaust, g/day	80	10
⁴ He exhaust, g/day	320	712
Tritium breeding, g/day	----	560

5.2 Vacuum Systems

Vacuum pumping and impurity control for WILDCAT are quite similar to D-T systems, e.g., STARFIRE.¹ Large quantities of hydrogen isotopes and helium isotopes must be removed simultaneously, and high pumping speeds are required. As discussed elsewhere,² the vacuum pumping requirements are best satisfied

by compound cryosorption pumps. WILDCAT has somewhat higher gas loads but has reduced tritium levels. These differences and their impact upon design, compared to STARFIRE, are discussed below.

The total gas load, $44 \text{ Pa}\cdot\text{m}^3/\text{s}$, is more than twice that for STARFIRE. The result of this is that a higher effective pumping speed is required for WILDCAT. The trade-offs between pump speed, conductance losses in a rather complicated network of vacuum pathways as a function of geometry, and radiation steaming are discussed in considerable detail in the STARFIRE report, and are not reiterated here. Rather, the results of the trade-off study⁶ for WILDCAT are discussed. The vacuum pumping parameters are shown in Table 5-2. The key point is that the duct conductance is the major limitation to pumping speed. In order to achieve greater overall speeds necessitated by the higher gas loads in WILDCAT, the duct conductance has been increased by increasing the duct diameter to 1.2 m and by reducing the length to 2 m. The width of the plenum has been reduced to 50 cm, resulting in a 50% decrease in plenum conductance.

The tradeoff between vacuum pump regeneration frequency, tritium inventory, and valve lifetime is of considerable interest for D-D systems. For STARFIRE it was estimated that the large valves would have a lifetime of 8000 to 10,000 cycles. Because the STARFIRE plasma exhaust is about one-third tritium, considerations of tritium inventories provided strong motivation to minimize the cycle time to two hours. This resulted in a maximum amount of 2.6 g tritium in each pump with a total tritium inventory of 63 g in all the pumps. However, owing to the limited valve lifetime, it was estimated that vacuum valves would require replacement every two years. In WILDCAT the tritium accumulation rate is much less, a total of 10 g/day. Accordingly, assuming a 10,000 cycle valve lifetime, the valves would last 40 y if the pumps were regenerated every 32 h. This scenario has been adopted for WILDCAT. The resultant tritium inventory is a maximum of 0.56 g per pump with a total of 13.4 g.

5.3 Design of the Isotopic Separation System and Tritium Inventory

The fuel recycling requirements for both steady-state and pulsed mode operation of WILDCAT have been analyzed. Because a small amount of tritium is needed for startup, it is of considerable significance whether the reactor is

Table 5-2. WILDCAT Vacuum Pumping Parameters

	WILDCAT (Cat-D)	STARFIRE (D-T)
Gas load, Pa-m ³ /s	44	18.7
Total pressure in limiter slot, Pa	0.04	0.04
Hydrogen pressure in limiter slot, Pa	0.024	0.024
Helium pressure in limiter slot, Pa	0.016	0.016
Total effective pumping speed, m ³ /s	1100	480
For helium, m ³ /s	1100	490
No. of pumps (on-line/total)	24/48	24/48
Rated pump speed, m ³ /s		
D-T	120	120
He	200	200
Limiter duct conductance, m ³ /s	4000	4000
Plenum width, cm	50	70
Plenum conductance, m ³ /s	7000	13,700
No. of vacuum ducts	24	24
Duct length, m	2	10
Duct diameter, m	1.2	1.0
Vacuum duct conductance, m ³ /s	3800	730

in steady-state or pulsed mode. The use of tritium introduces a complex operating step in the pulsed mode. For steady-state operation the primary function of the fuel reprocessing system is to remove the protium waste (after separation of debris and condensable gases) from the spent fuel. Tritium for startup is supplied from a separate source. For pulsed mode operation the reprocessing system must provide the startup tritium in addition to removal of protium. General consideration of fuel processing have previously been discussed.^{1,6} The cryogenic distillation system for WILDCAT is discussed below.

5.3.1 Distillation Cascade

The flow rates required for a typical set of operating conditions for WILDCAT are the following:

Protium	10 g/day
Deuterium	2100 g/day
Tritium	10 g/day
Total	607 g-mol/day

For the steady-state mode the cascade arrangement is shown in Fig. 5-3 excluding column 4. The products from each column (using 30 theoretical plates) are shown in Table 5-3. The final product streams are: (1) protium waste as the top product from column 3 and (2) the recycled fuel as the bottom product from column 1. Since the concentration of tritium in the protium waste is low ($<0.002\%$), this stream may be directly discharged into the environment. The protium content in the recycled fuel is $<0.1\%$. Thus, a three-column cascade appears to be adequate since the basic purity conditions are met.

A second set of calculations has been carried out for the above cascade with each column containing 50 theoretical plates instead of 30. The analytical results, which are summarized in Table 5-4, show that the purity of the products is improved. For steady-state operation it should be noted that after the tritium content of the initial fuel mixture is extracted from the spent fuel, columns 2 and 3 are put under standby conditions. Only one column (column 1) is needed to separate the protium impurity from the recycled fuel.

For reactor operation under pulsed mode a fourth column is needed (column 4 in Fig. 5-4) to redistill the heavy product from column 1 in order to provide a start-up fuel mixture of deuterium and tritium. Fig. 5-4 shows that when a product stream equal to $\sim 0.25\%$ of the feed stream is withdrawn as a heavy fraction from column 4, it essentially meets the start-up fuel requirements. The composition of the top and the bottom product is shown in Table 5-5. An examination of the composition of the bottom products shows that the ratio of D to T ≈ 1 , and the protium impurity fraction is less than 1 PPB. Thus, extra tritium for startup can be obtained by redistilling the heavy product from column 1.

5.3.2 Tritium Inventory

An exact calculation of the tritium inventory has not been done due to lack of sufficient data related to liquid holdup, height equivalent to a theoretical plate (HETP) and the size of the chemical equilibrators. A conservative approach has been taken in the calculations by assuming that the HETP is 2 in. and that the liquid holdup is equal to 20% of the column volume. Further, it assumed that the liquid volume in the transfer lines, pumps, valves, and chemical equilibrators is equal to the liquid holdup in the columns. The dimensions and the other pertinent data for the four columns are summarized in Table 5-6.

PC: Partial Condenser
 RB: Reboiler
 CE: Chemical Equilibrator

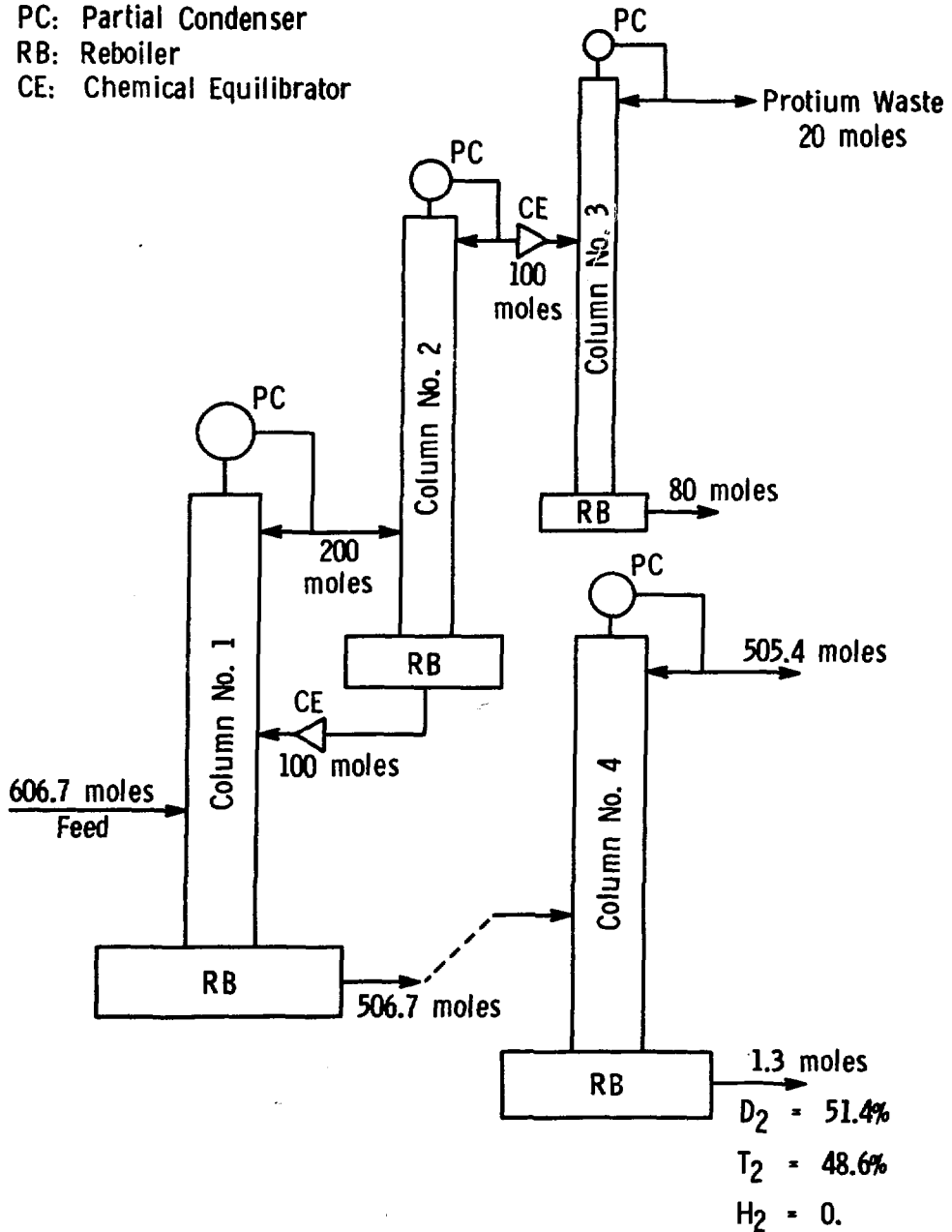


Fig. 5-3. Schematic of the isotopic separation system for a D-D fusion reactor. The fourth column is used to provide tritium for startup in the pulsed case.

Table 5-3. Product Compositions for Three-Column Cascade (30-Plate Column)

SUMMARY OF ANALYTICAL RESULTS FOR COLUMN : 1

PROD.COMP	N-H2	HD	HT	N-D2	DT	N-T2	APH	APD	APT
1	6.007663D-04	4.456141D-02	6.396954D-05	9.539641D-01	8.096402D-04	1.290987D-07	2.291D 00	9.766D 01	4.369D-02
30	7.064233D-03	1.691246D-03	1.652380D-05	9.917875D-01	6.490643D-03	1.404381D-05	8.540D-02	9.959D 01	3.268D-01

SUMMARY OF ANALYTICAL RESULTS FOR COLUMN : 2

PROD.COMP	N-H2	HD	HT	N-D2	DT	N-T2	APH	APD	APT
1	1.201529D-03	8.883767D-02	1.188539D-04	9.097299D-01	1.120356D-04	9.712394D-10	4.568D 00	9.542D 01	1.154D-02
30	3.512565D-09	2.851495D-04	9.085185D-06	9.981983D-01	1.507245D-03	2.572261D-07	1.471D-02	9.991D 01	7.584D-02

SUMMARY OF ANALYTICAL RESULTS FOR COLUMN : 3

PROD.COMP	N-H2	HD	HT	N-D2	DT	N-T2	APH	APD	APT
1	2.670490D-02	2.992370D-01	1.112225D-05	6.740265D-01	2.044405D-05	1.040803D-10	1.763D 01	8.237D 01	1.578D-03
30	1.363541D-05	2.600164D-02	3.803143D-06	9.737040D-01	2.768503D-04	2.674767D-03	1.302D 00	9.868D 01	1.404D-02

Table 5-4. Product Compositions for Three-Column Cascade (50-Plate Column)

SUMMARY OF ANALYTICAL RESULTS FOR COLUMN : 1

PROD.COMP	N-H2	HD	HT	N-D2	DT	N-T2	APH	APD	APT
1	6.009107D-04	4.633960D-02	6.391955D-05	9.525393D-01	4.062693D-04	1.210594D-08	2.380D 00	9.760D 01	2.351D-02
50	8.843299D-10	9.362480D-04	1.653258D-05	9.925272D-01	6.506044D-03	1.396229D-05	4.764D-02	9.962D 01	3.275D-01

SUMMARY OF ANALYTICAL RESULTS FOR COLUMN : 2

PROD.COMP	N-H2	HD	HT	N-D2	DT	N-T2	APH	APD	APT
1	1.201821D-03	9.265852D-02	1.234089D-04	9.059864D-01	2.987930D-05	7.144627D-12	4.759D 00	9.523D 01	7.664D-03
50	3.326357D-12	2.067493D-05	4.430241D-06	9.991922D-01	7.826589D-04	2.420473D-08	1.255D-03	9.996D 01	3.936D-02

SUMMARY OF ANALYTICAL RESULTS FOR COLUMN : 3

PROD.COMP	N-H2	HD	HT	N-D2	DT	N-T2	APH	APD	APT
1	2.887589D-02	3.142545D-01	7.651605D-06	6.568568D-01	5.208052D-06	2.323070D-12	1.860D 01	8.140D 01	6.430D-04
50	6.899938D-07	2.597213D-02	2.636228D-06	9.733383D-01	1.857322D-04	1.184416D-08	1.299D 00	9.859D 01	9.420D-03

Table 5-5. Product Composition for Redistillation of Heavy Fraction from Column 1 (see Table 5-3)

SUMMARY OF ANALYTICAL RESULTS FOR BLANKET PROCESSING: NP= 50

PROD.COMP	N-H2	HD	HT	N-D2	DT	N-T2	APH	APD	APT
1	7.081787D-03	1.695459D-03	1.656492D-05	9.941760D-01	4.111944D-03	1.853194D-09	8.561D-02	9.971D 01	2.054D-01
50	9.223439D-21	9.121418D-11	5.965201D-10	3.395730D-02	9.604193D-01	5.623423D-03	3.439D-03	5.142D 01	4.856D 01

5-8

Table 5-6. Distillation Column Data

	Columns			
	1	2	3	4
I.D., cm	2.54	1.90	1.27	2.54
Height, m	1.52	1.52	1.52	1.52
Liquid holdup, cm ³	309	174	77	309
Weight of liquid, g (essentially pure deuterium)	53	30	13	53
At-% tritium	0.1858	0.0341	0.0084	16.4

Tritium inventory: Column 1 + Column 2 + Column 3 = 0.2 g.
 Column 4 = 13 g.

The tritium inventory for the three-column cascade is 0.2 g. Although the tritium inventory in the fourth column (pulsed mode) is significantly larger than that in the first three columns, the total tritium inventory is low and does not present a safety problem in case of an accident situation.

5.4 Tritium Inventories and Source Terms

The rationale for locations and amounts of tritium in a fusion power reactor are discussed in considerable detail in the STARFIRE report.¹ The tritium inventories in WILDCAT are compared to those of STARFIRE in Table 5-7. It is evident that the amounts of tritium are greatly reduced; however, appropriate safety systems and containment strategies are still required. Further, whereas STARFIRE has large quantities of the oxide form of tritium (T₂O), no significant amount of T₂O has been identified for WILDCAT. Since T₂O is orders of magnitude more toxic than T₂, the above fact translates to a considerable relative safety advantage.

Sources of tritium for WILDCAT have been studied as well. In particular, the migration of tritium in water coolants has been investigated. Tritium in water coolants is a function of wall area, wall temperature, particle energy, and triton flux. The total tritium inventory rate was estimated to be ~10 Ci/day in STARFIRE. The rate for WILDCAT is estimated by scaling from particle fluxes and wall areas with STARFIRE:

Table 5-7. Tritium Inventories (g)

	WILDCAT	STARFIRE
"Vulnerable"		
Vacuum pumps (DT)	13.4	63
Fueling (DT)	2.0	54
Blanket processing (T ₂ O)	----	280
"Non-Vulnerable"		
Breeder Blanket (T ₂ O)	---	~10,000
Storage (T ₂)	20	1070
Fuel processing (DT)	<1.0	154
Distillation system (DT)	0.2(13) ^a	50

^aIncreases to 13 g for pulsed mode of operation.

$$I_1 = \frac{4.6 \times 10^{17} \text{ T/m}^2\text{-s (WILDCAT)} \times 1250 \text{ m}^2 \text{ (WILDCAT)} \times 10 \text{ Ci/day}}{3.15 \times 10^{19} \text{ T/m}^2\text{-s (STARFIRE)} \times 780 \text{ m}^2 \text{ (STARFIRE)}}$$

$$= 0.2 \text{ Ci/day .}$$

Further, ⁷LiOH is used for corrosion control in water coolants. In STARFIRE reactions of ⁷Li with 14 MeV neutrons was estimated to produce ~1 Ci/day of tritium in the first-wall coolant. Scaling with the 14-MeV neutron power, we obtain:

$$I_2 = \frac{620 \text{ MW (WILDCAT)} \times 1.0 \text{ Ci/day}}{3810 \text{ MW (STARFIRE)}} = 0.2 \text{ Ci/day .}$$

The total tritium accumulation rate in the water coolant is then 0.2 + 0.2 = 0.4 Ci/day. This is balanced by losses including decay, leakage, and permeation. Permeation is very small and is assumed to be negligible. Tritium decay is calculated to be approximately equal to tritium loss through leakage. The appropriate steady-state level of tritium is 0.0066 Ci/liter; leakage is 0.20 Ci/day; and decay is also 0.20 Ci/day.

Tritium source terms can be compared to those in STARFIRE. (See Table 5-8.) It is seen that there are substantial reductions in both routine losses (0.3 Ci/day vs. 13 Ci/day) and potential accidents. In addition, losses of tritium in the oxide form are greatly reduced.

Table 5-8. Tritium Source Terms

	WILDCAT	STARFIRE
Source terms, Ci/day		
Coolant (HTO)	0.2	10
Fuel processing	$\sim 10^{-2}$	~ 1
Solid wastes	$\sim 10^{-2}$	~ 1
Building leakage	$\sim 10^{-1}$	~ 1
Total	0.3	13
Maximum conceivable releases, g		
Vacuum pump	0.58	2.6
Blanket processing	-----	10 (T ₂ O)
Isotope separation system	0.2(13) ^a	50

^aIncreases to 13 g for pulsed mode of operation.

REFERENCES

1. C. C. BAKER, ET AL., "STARFIRE - A Commercial Tokamak Fusion Power Plant Study," Argonne National Laboratory, ANL/FPP-80-1 (1980).
2. W. R. Wilkes, "Distillation of He Isotopes," in Proc. ICEC-4 (IPC & Technology Press, 1972), p. 119-121.
3. W. R. Wilkes, ³He-⁴He Distillation Apparatus," Mound Laboratory, MLM-2005 (1973), p. 15.
4. T. B. Rhinehammer and L. J. Wittenberg, "An Evaluation of the Fuel Resources and Requirements for the Magnetic Fusion Energy Program," Mound Laboratory, MLM-2419 (1978), p. 102.
5. W. R. Wilkes, Mound Laboratory, private communication.
6. K. Evans, Jr., et al., "D-D Tokamak Reactor Studies," Argonne National Laboratory, ANL/FPP/TM-138 (1980), Chap. 5.

6. COST ANALYSIS

This section presents the basis, development, and analysis of a cost estimate for the WILDCAT reactor. Since the physical design for WILDCAT is conceptually similar to the previous STARFIRE¹ design, the cost estimate is developed using the STARFIRE estimate as a starting point and as a point of comparison. The cost ground rules and cost accounts are in conformance with the DOE guidelines as specified in Ref. 2. Costs are expressed in constant 1980 dollars and then-current year dollars which represent the facility cost in the first year of operation. The cost basis is the same as used for STARFIRE, so that the costs are directly comparable. Table 6-1 illustrates the summary of the capital costs for both STARFIRE and WILDCAT, broken down by major cost category. Similar to STARFIRE, the largest cost is for the Reactor Plant Equipment.

The steady-state and the pulsed WILDCAT power plants each has a considerably higher cost than STARFIRE. The buildings are not significantly different from STARFIRE (some are lower in cost, some are higher). The blanket is almost exclusively stainless steel, but it is very massive and almost twice the cost of STARFIRE. The shield is constructed in a similar manner to STARFIRE but is almost double the weight and double the cost. The magnets are larger and have almost four times the stored energy of STARFIRE with the cost being more than double. The steel centerpost also raises the cost of the primary structure. The largest cost increases are associated with the pulsed-version power supplies. The power supplies for the OH and EF coils are estimated at \$216 M and \$100 M respectively, which is an order of magnitude larger than for the steady-state version. Most of the other Reactor Plant Equipment subsystems are at or below the corresponding STARFIRE subsystem costs. The above named subsystems, however, have pushed the Reactor Plant Equipment to \$1496 M for the steady-state and \$1889 M for the pulsed reactor versus \$968 M for STARFIRE. The Turbine Plant Equipment is reduced from STARFIRE except for the Thermal Energy Storage subsystem required for the pulsed version which adds approximately \$140 M to this account. The remainder of the plant costs are slightly reduced from the STARFIRE values.

Table 6-1. Summary of Capital Costs

Account No.	Cost Account Title	Cost (M\$)					
		STARFIRE	WILDCAT (Steady-State)	WILDCAT (Pulsed)			
20	Land and Land Rights	3.30	3.30	3.30			
21	Structures and Site Facilities	346.58	346.59	366.77			
22	Reactor Plant Equipment	968.62	1496.63	1888.78			
23	Turbine Plant Equipment	249.68	215.38	357.21			
24	Electric Plant Equipment	117.28	111.08	109.22			
25	Miscellaneous Plant Equipment	40.77	39.66	39.66			
26	Special Materials	<u>0.25</u>	<u>0.25</u>	<u>0.25</u>			
	Total Direct Cost	1726.48	2212.89	2765.19			
91	Construction Facilities Equipment and Services (10%)	172.65	221.29	276.52			
92	Engineering and Construction Management Services (8%)	138.12	177.03	221.21			
93	Other Costs (5%)	<u>86.32</u>	<u>110.64</u>	<u>138.26</u>			
	Subtotal	2123.57	2721.85	3401.18			
		<u>1980 Constant</u>	<u>1986 Then Current</u>	<u>1980 Constant</u>	<u>1986 Then Current</u>		
94	Interest During Construction	276.70	671.69	354.66	860.92	443.17	1075.79
95	Escalation During Construction	<u>0.00</u>	<u>402.63</u>	<u>0.00</u>	<u>516.06</u>	<u>0.00</u>	<u>644.86</u>
	Total Capital	2400.27	3197.89	3076.51	4098.83	3844.35	5121.83
	Cost/Generating Capacity (\$/kWe)	2000	2665	3788	5048	4528	6033

If time would permit, more cost effective approaches could be pursued and the cost of WILDCAT might be lowered somewhat. On the other hand, problems associated with the advanced nature of the high field toroidal coils, the current-drive concept, and the generally larger reactor are difficult to evaluate but would undoubtedly add to the cost. In addition, an in-depth assessment of the cost impact of the reduced tritium inventories and lack of need to breed tritium with regard to licensing, maintainability, and safety is also difficult to evaluate, but could provide a factor which could make WILDCAT more cost-effective.

6.1 Economic Guidelines and Assumptions

All costs are reported in 1980 year dollars and are directly comparable to the STARFIRE economic analysis. The costs are developed based upon a mature fusion industry with the WILDCAT design representing the tenth-of-a-kind design to eliminate the effects of research and development costs and allow comparison with current fission and fossil plants. This tenth-of-a-kind assumption is used to estimate the learning curve effects of quantity purchased equipment.

The reference site is assumed to be a midwestern town of Middletown as defined in Ref. 1. This standard site facilitates the costing analysis and provides a basis for the labor and material costs. A design allowance is not used for the well-understood accounts 21, 23, 24 and 25. The Reactor Plant Equipment uses design allowances depending upon the estimated development of each system. Contingency allowance, which is an allowance to provide for unforeseen cost overruns, is estimated at 15% for all cost accounts as recommended in Ref. 3. An allowance for spare parts is also provided for all cost categories. The adopted spare cost allowances from Ref. 3 are shown below. These allowances are applied only to purchased parts and to material costs and not to labor. The only exception is for Account 22, which is largely purchased equipment, and the allowance is applied directly to the total cost.

<u>Cost Account</u>	<u>Spare Parts Allowance</u>
21, 22, 23	2%
24	4%
25	3%
Others	0%

Any costly component that requires a spares inventory is separately identified. Section 6.2.3.16 details the major items identified as spare parts in the Reactor Plant Equipment. These major items are additive to the standard allowances given previously.

Indirect cost allowances are also provided to cover expenses resulting from the support activities required to design, fabricate, assemble, and check out the entire power plant. Some cost ground rules are recommended in Ref. 1, but these were slightly modified in the development of the STARFIRE cost estimate, based upon the design and construction techniques employed (Ref. 4, p. 22-8). These same indirect cost allowances are applied to WILDCAT.

	<u>Cost Account</u>	<u>Indirect Cost Allowances</u>
91	Construction Facilities, Equipment and Services	10%
92	Engineering and Construction Management Services	8%
93	Other Costs	5%

Time related costs include an allowance for funds used during construction (AFDC) and are the expense of the interest charges of financing the debt, the charges on the equity (common stock) portion of the financing, and any administration charges on the financing. Reference 1 has a complete set of cost guidelines in this area and these are adopted and shown below:

- Utility is investor-owned.
- Capital structure is 53% debt financing and 47% equity financing.
- Nominal cost of debt financing is 8% per year.
- Power plant economic lifetime is 30 years with no salvage value.
- Cost escalation and general inflation is 5% per year.

Although the above values are not in concert with today's economic picture, these guidelines can be used for comparison purposes between various economic studies. In particular, the guidelines are the same as those used for STARFIRE. The capital cost accounts used for WILDCAT are also the same as those presented in Ref. 1 for STARFIRE.

6.2 Capital Costs

This section presents the logic and supporting data for the generation of the WILDCAT capital cost estimate. Factors which determine and influence the cost are examined. If the equipment and material usage is common to STARFIRE, the STARFIRE cost basis is adopted. If different equipment or materials are used, a new basis for the cost estimate is justified. The total capital costs for WILDCAT are shown in Table 6-2. The total direct cost for the steady-state plant is \$2212 M, and the total capital cost is \$3077 M in constant 1980 dollars and \$4099 M in the then-current 1986 dollars. The pulsed reactor costs are \$2765 M for the direct costs and \$3844 M (1980 \$) and \$5122 M (1986 \$) for the total capital costs. The following subsections discuss the individual capital costs and their generation.

6.2.1 Land and Land Rights (Account 20)

The reference plant site, similar to STARFIRE, has been chosen to be 1,000 acres in a midwestern location. The land requirements are less severe than for an LWR in regard to exclusion boundaries and hence the 1,000 acres are deemed adequate. Sufficient space is provided for constructing multiple plants at the common site. The cost associated with the land and privilege acquisition is estimated at 1,000 acres times \$3,000/A,¹ so that $C_{20.01} = \$3.0$ M. The cost of the initial clearing of the land, demolition of existing structures, and relocation of buildings, highways, and railroads is estimated to be 10% of the land cost, i.e. $C_{20.02} = \$0.3$ M. This is a reasonable value because the topography and site characteristics are amenable to the WILDCAT requirements and the site access, i.e., roads, railways, and barge facilities are adequate.¹ The value of the land is really a non-depreciable asset, but following the recommendations in Ref. 1,

Table 6-2. Capital Costs

Account No.	Account Title	Costs (1980 \$)			
		STARFIRE		WILDCAT, Steady State	WILDCAT, Pulsed
20	<u>Land and Land Rights</u>	3.30	3.30	3.30	3.30
20.01	Land and Privilege Acquisition		3.0	3.00	3.00
20.02	Relocation of Buildings, Utilities, Highways, and Other Services		0.3	0.30	0.30
21	<u>Structures and Site Facilities</u>	346.58		346.59	346.77
21.01	Site Improvements and Facilities		11.15	11.15	11.15
21.02	Reactor Building	157.44		160.38	160.38
21.03	Turbine Building		35.92	35.92	35.92
21.04	Cooling System Structures		7.96	6.38	5.65
21.05	Electrical Equipment and Power Supply Building		9.16	9.16	26.44
21.06	Plant Auxiliary Systems Building		3.26	3.26	3.26
21.07	Hot Cell Building		53.69	55.39	55.39
21.08	Reactor Service Building		1.88	1.88	1.88
21.09	Service Water Building		0.66	0.57	0.52
21.10	Fuel Handling and Storage Building		8.63	6.90	6.90
21.11	Control Room Building		3.10	3.10	3.10
21.12	On-Site ac Power-Supply Building		2.05	2.05	2.05
21.13	Administration Building		0.87	0.87	0.87
21.14	Site Service Building		0.87	0.87	0.87
21.15	Cryogenics and Inert Gas Storage Building		0.91	1.49	1.57
21.16	Security Building		0.31	0.31	0.31
21.17	Ventilation Stack		1.81	0.00	0.00
21.98	Spare Parts Allowance		1.96	1.96	2.07
21.99	Contingency Allowance		44.95	44.95	48.44

Table 6-2. Capital Costs (Contd.)

Account No.	Account Title	Costs (1980 \$)		
		STARFIRE	WILDCAT, Steady State	WILDCAT, Pulsed
22	Reactor Plant Equipment	968.62	1496.63	1886.78
22.01	Reactor Equipment	589.26	1046.95	1385.73
22.01.01	Blanket and First Wall	82.36	132.23	132.23
22.01.02	Shield	186.07	352.50	352.50
22.01.03	Magnets	171.57	352.66	389.78
22.01.04	RF Heating Current Drive	33.49	34.88	34.88
22.01.05	Primary Structure and Support	52.74	115.13	113.09
22.01.06	Reactor Vacuum	4.86	8.68	8.68
22.01.07	Power Supply, Switching and Energy Storage	52.90	32.20	335.90
22.01.08	Impurity Control	2.45	3.07	3.07
22.01.09	ECRH Plasma Breakdown	2.82	15.60	15.60
22.02	Main Heat Transfer and Transport Systems	69.84	51.92	46.24
22.02.01	Primary Coolant System	63.10	44.10	38.79
22.02.02	Intermediate Coolant System	-	-	-
22.02.03	Limiter Cooling System	6.19	7.27	6.90
22.02.04	Residual Heat Removal System	0.55	0.55	0.55
22.03	Cryogenic Cooling System	14.90	30.07	32.47
22.03.01	Helium Liquefier Refrigerator	7.70	15.54	16.78
22.03.02	LHe Transfer and Storage	3.60	7.27	7.85
22.03.03	He Gas Storage	2.80	5.65	6.10
22.03.04	LN ₂ System	0.80	1.61	1.74
22.04	Radioactive Waste Treatment and Disposal	4.80	4.80	4.80
22.04.01	Liquid Waste Processing and Equipment	1.70	1.70	1.70
22.04.02	Gaseous Wastes and Off-Gas Processing System	1.80	1.80	1.80
22.04.03	Solid Wastes Processing Equipment	1.30	1.30	1.30

Table 6-2. Capital Costs (Contd.)

Account No.	Account Title	Costs (1980 \$)		
		STARFIRE	WILDCAT, Steady State	WILDCAT, Pulsed
22.05	Fuel Handling and Storage Systems	38.60	31.70	31.70
22.05.01	Fuel Purification Systems	8.80	7.80	7.80
22.05.02	Liquefaction	-	-	-
22.05.03	Fuel Preparation Systems	0.30	0.60	0.60
22.05.04	Fuel Injection	1.40	2.10	2.10
22.05.05	Fuel Storage	2.00	0.50	0.50
22.05.06	Tritium Extraction and Recovery	5.40	0.00	0.00
22.05.07	Atmospheric Tritium Recovery System	20.70	20.70	20.70
22.06	Other Reactor Plant Equipment	43.75	43.13	42.81
22.06.01	Maintenance Equipment	38.30	38.30	38.30
22.06.02	Special Heating Systems	0.00	0.00	0.00
22.06.03	Coolant Receiving, Storage and Make-Up Systems	0.24	0.24	0.24
22.06.04	Gas Systems	0.08	0.08	0.08
22.06.05	Inert Atmosphere System	0.00	0.00	0.00
22.06.06	Fluid Leak Detection	2.00	2.00	2.00
22.06.07	Closed Loop Coolant System	1.97	1.58	1.38
22.06.08	Standby Cooling System	1.16	0.93	0.81
22.07	Instrumentation and Control	23.41	23.41	23.41
22.07.01	Reactor I&C Equipment	7.61	7.61	7.61
22.07.02	Monitoring Systems	1.76	1.76	1.76
22.07.03	Instrumentation and Transducers	14.04	14.04	14.04
22.98	Spare Parts Allowance	66.38	79.85	86.55
22.99	Contingency Allowance	117.68	184.80	235.07

Table 6-2. Capital Costs (Contd.)

Account No.	Account Title	Costs (1980 \$)		
		STARFIRE	WILDCAT, Steady State	WILDCAT, Pulsed
23	<u>Turbine Plant Equipment</u>	249.68	215.38	357.21
23.01	Turbine-Generators	77.33	67.00	70.00
23.02	Main Steam System	4.37	3.77	129.67
23.03	Heat Rejection System	44.34	36.80	33.02
23.04	Condensing Systems	19.18	16.05	14.48
23.05	Feed Heating Systems	9.39	7.64	6.76
23.06	Other Turbine Plant Equipment	50.84	44.77	41.74
23.07	Instrumentation and Control (I&C) Equipment	8.70	8.70	10.70
23.98	Spare Parts Allowance	3.41	2.94	4.88
23.99	Contingency Allowance	32.12	27.71	45.96
24	<u>Electric Plant Equipment</u>	117.28	111.08	109.22
24.01	Switchgear	12.39	12.39	12.39
24.02	Station Service Equipment	17.04	17.04	17.04
24.03	Switchboards	7.80	7.80	7.80
24.04	Protective Equipment	2.11	2.11	2.11
24.05	Electrical Structures and Wiring Containers	17.40	15.66	15.14
24.06	Power and Control Wiring	35.99	32.39	31.31
24.07	Electrical Lighting	8.20	8.20	8.20
24.98	Spare Parts Allowance	1.21	1.15	1.13
24.99	Contingency Allowance	15.14	14.34	14.10
25	<u>Miscellaneous Plant Equipment</u>	40.77	39.66	39.66
25.01	Transportation and Lifting Equipment	15.68	15.68	15.68
25.02	Air and Water Service Systems	12.35	11.39	11.39
25.03	Communications Equipment	6.22	6.22	6.22
25.04	Furnishing and Fixtures	0.75	0.75	0.75

Table 6-2. Capital Costs (Contd.)

Account No.	Account Title	Costs (1980 \$)						
		STARFIRE		WILDCAT, Steady State		WILDCAT, Pulsed		
25.98	Spare Parts Allowance		0.52		0.51		0.51	
25.99	Contingency Allowance		5.25		5.11		5.11	
26	<u>Special Materials</u>		<u>0.25</u>		<u>0.25</u>		<u>0.25</u>	
	<u>Total Direct Cost</u>		1726.48		2212.89		2765.19	
91	<u>Construction Facilities, Equipment and Services (10%)</u>		172.65		221.29		276.52	
92	<u>Engineering and Construction Management Services (8%)</u>		138.12		177.03		221.21	
93	<u>Owner's Costs (5%)</u>		<u>86.32</u>		<u>110.64</u>		<u>138.26</u>	
	<u>Subtotal</u>		2123.57		2721.85		3401.18	
			<u>1980</u>	<u>1986</u>	<u>1980</u>	<u>1986</u>	<u>1980</u>	<u>1986</u>
			<u>Constant</u>	<u>Then-Current</u>	<u>Constant</u>	<u>Then-Current</u>	<u>Constant</u>	<u>Then-Current</u>
94	<u>Interest During Construction</u>		276.70	671.69	354.66	860.92	443.17	1075.79
95	<u>Escalation During Construction</u>		<u>0.00</u>	<u>402.63</u>	<u>0.00</u>	<u>516.06</u>	<u>0.00</u>	<u>644.86</u>
	<u>Total Capital</u>		2400.27	3197.89	3076.51	4098.83	3844.35	5121.83
	<u>\$/kWe</u>		2000	2665	3788	5048	4528	6033

the cost of land is treated as a depreciating asset to simplify the economic analysis. Thus:

$$C_{20} = \$3.30 \text{ M}$$

6.2.2 Structures and Site Facilities (Account 21)

This account covers all direct costs associated with the physical buildings, cooling system structures, site improvements and facilities, and miscellaneous structures and building work. The cost estimates for this account have been prepared by the Ralph M. Parsons Company based upon a comparison with the previous STARFIRE design. Any design and cost differences are noted in the following descriptions. The facility is in most respects virtually identical to STARFIRE in size, location, and types and functions of the buildings. Only the size and the internal arrangements of a few buildings are modified. The labor and material rates are identical to those used for STARFIRE.

The total cost for this account for the steady-state version of WILDCAT is essentially identical to STARFIRE, while the pulsed version is roughly \$20 M more. The Reactor Building is only slightly more expensive in both versions, reflecting the larger reactor size. The largest increase is in the pulsed WILDCAT Electrical Equipment and Power Supply Building, which would house the motor/generator sets for the OH and EF power supplies. Other buildings only reflect minor changes. The total cost for this account including spares and contingency is:

$$\begin{aligned} C_{21} &= \$346.59 \text{ M (Steady State)} \\ &= \$366.77 \text{ M (Pulsed)} \end{aligned}$$

6.2.2.1 Site Improvements and Facilities (Account 21.01)

The site improvements and facilities for WILDCAT are identical to STARFIRE and thus are:

$$C_{21.01} = \$11.15 \text{ M}$$

6.2.2.2 Reactor Building (Account 21.02)

The slightly larger size of the reactor envelope for the WILDCAT design requires the maintenance monorail track to be enlarged one meter in radius. However the basic STARFIRE reactor building floor plan accommodates this minimal increase without enlarging the floor area. The reactor envelope has increased 2 m in height to accommodate the upper vacuum pumps with piping emerging from the top of the pump covers. This increases the building height 3 m resulting in a 3% building cost increase due to superstructure costs. Reductions in the main steam system do not lead to any reduction in building floor areas. Any space gained is utilized as an additional laydown space, which is currently at a premium. Thus the overall building size is rectangular (120 m long by 50 m wide and 45.5 m high above ground level). The cost of the reactor building is:

$$C_{21.02} = \$160.38M$$

6.2.2.3 Turbine Building (Account 21.03)

The thermal power input to the turbine is reduced in both the steady-state and the pulsed version as compared to the STARFIRE design. The actual size of the turbine is reduced only slightly, and all other required equipment is unchanged. Thus the cost for this account remains the same at:

$$C_{21.03} = \$35.92 M$$

6.2.2.4 Cooling System Structures (Account 21.04)

This cost account covers the circulating water system, which discharges all the waste heat of the power plant. The costs associated are directly proportional to the waste heat of the two versions. The costs of this account are:

$$\begin{aligned} C_{21.04} &= \$6.38 M \text{ (Steady State)} \\ &= \$5.65 M \text{ (Pulsed)} \end{aligned}$$

6.2.2.5 Electrical Equipment and Rf Power Supply Building (Account 21.05)

Like STARFIRE, WILDCAT requires a special building to house the power supplies for the TF, EF, OH, and CF coils and the rf heating and current drive system (a compressional Alfvén wave system for WILDCAT). The space requirements for the steady-state version are very similar to STARFIRE, but the pulsed WILDCAT requires almost an order-of-magnitude larger space for the OH and EF coil power supplies. The building for the steady state version is a steel-framed three-story building similar to the STARFIRE building. The building for the pulsed version houses the motor/generator sets for the OH and EF power supplies in an enlarged subgrade portion of the Electrical Equipment and Rf Power Supply Building. The associated silicon controlled rectifier components and switchgear are housed in a building located between the Electrical Equipment and Rf Power Supply Building and the Reactor Building. This increase in requirements significantly influences the building costs.

C_{21.05} = \$9.16 M (Steady State)
= \$26.44 M (Pulsed)

6.2.2.6 Plant Auxiliary Systems Building (Account 21.06)

This two-level building houses the heat exchangers and the pumps for the closed cooling system. It also houses the chillers, pumps, instruments, air equipment, and a maintenance area. All of these functions are identical in size, thus the building is the same size as for STARFIRE:

C_{21.06} = \$3.26 M

6.2.2.7 Hot Cell Building (Account 21.07)

The anticipated longer life of the first wall and blanket for WILDCAT (20 y versus 6 y) reduces the need for frequent utilization of the Hot Cell, but the unscheduled reactor maintenance requires a similar sized facility.

Also the maintenance, repair, decontamination, and inspection equipment areas are also similar to size to STARFIRE. The larger sized blanket modules require a taller Hot Cell Building. The cost for WILDCAT is:

$$C_{21.07} = \$55.39 \text{ M}$$

6.2.2.8 Reactor Service Building (Account 21.08)

The Reactor Service Building is a ground-level high-bay area between the Hot Cell and the Turbine Building and is adjacent to the Plant Auxillary building. The STARFIRE Reactor Service Building is sufficiently tall to accommodate the larger WILDCAT modules, thus the same building would suffice at:

$$C_{21.08} = \$1.88 \text{ M}$$

6.2.2.9 Service Water Building (Pump Houses) (Account 21.09)

The make-up water and the firewater pump house remain the same as for the STARFIRE design. The circulating water pump house building is scaled down in relation to the lower circulating water requirements of the two WILDCAT versions (80% for the steady state and 70% for the pulsed). Thus the costs for this account are:

$$\begin{aligned} C_{21.09} &= \$0.57 \text{ M (Steady State)} \\ &= \$0.52 \text{ M (Pulsed)} \end{aligned}$$

6.2.2.10 Fuel Handling and Storage Building (Account 21.10)

The Fuel Handling and Storage Building handles the fuel reprocessing equipment and the storage of the fuel. Since there is no tritium required as fuel, most of the tritium storage equipment, the transfer pump units, and the tritiated waste recovery units can be eliminated. The elimination of this equipment leads to a reduced building size of 40 m by 30 m

corresponding to a 20% reduction in floor area. Thus the cost of the building is:

$$C_{21.10} = \$6.90 \text{ M}$$

6.2.2.11 Control Room Building (Account 21.11)

This building is identical in size and function with respect to STARFIRE and is costed at:

$$C_{21.11} = \$3.10 \text{ M}$$

6.2.2.12 Onsite ac Power Supply Building (Account 21.12)

This building is identical to the STARFIRE design:

$$C_{21.12} = \$2.05 \text{ M}$$

6.2.2.13 Administration Building (Account 21.13)

This building is also identical in size and function and is costed at:

$$C_{21.13} = \$0.87 \text{ M}$$

6.2.2.14 Site Service Building (Account 21.14)

This building which houses the maintenance shop and warehouse, is unchanged, thus costing:

$$C_{21.14} = \$0.87 \text{ M}$$

6.2.2.15 Cryogenics Building (Account 21.15)

The cryogenics requirements for WILDCAT are roughly twice as much as those for STARFIRE. The outdoor storage facilities vary directly with the requirement, but the generation systems, which are housed indoors, would not scale directly with the requirement. For the purposes of costing it is

assumed the building size (and cost) scale to the 0.7 power of the requirement. Thus the cost of the two versions are:

$$\begin{aligned} C_{21.15} &= \$1.49 \text{ M (Steady State)} \\ &= \$1.57 \text{ M (Pulsed)} \end{aligned}$$

6.2.2.16 Security Building (Account 21.16)

The security requirements are unchanged, thus the cost is:

$$C_{21.16} = \$0.31 \text{ M}$$

6.2.2.17 Ventilation Stack (Account 21.17)

The stack usually provides for disposal of low-level radioactive gases above ground level. In the WILDCAT design the safety analysis (Sec. 7) indicates the stack is not required. Thus the cost for this account is:

$$C_{21.17} = \$0.0 \text{ M}$$

6.2.3 Reactor Plant Equipment (Account 22)

This account summarizes all the fusion reactor plant equipment and accounts for the major changes of WILDCAT with respect to STARFIRE. The systems are either similar to ones designed specifically for fission or are adapted from these for the fusion application. However, the research and development costs for these systems are not included. The costs for this portion of the plant are in excess of 65% of the total plant costs. The total cost of the Reactor Plant Equipment including spares and contingency is:

$$\begin{aligned} C_{22} &= \$1496.63 \text{ M (Steady State)} \\ &= \$1888.78 \text{ M (Pulsed)} \end{aligned}$$

6.2.3.1 Blanket and First Wall (Account 22.01.01)

This cost account includes the first wall and inner and outer blanket elements, such as coolant and structural materials. A tritium breeder, a

neutron multiplier, and a reflector are not required in the WILDCAT design. Instead, the design uses only PCA stainless steel and water. Other components which may be an integral part of the blanket sector are costed under the account which represents their functional usage (e.g., limiters). The costs are estimated using a cost-per-weight basis, which is consistent with the degree of design definition. Table 6-3 lists the structural materials and the cooling tube and coating materials. The majority of the material cost is for the blanket region (\$128.69 M). The total cost of the first wall and blanket is:

$$C_{22.01.01} = \$132.23 \text{ M}$$

Table 6.3. First-Wall/Blanket Costs

Material	Mass (Tonnes)	Installed Cost (\$/kg)	Total Cost (M\$)
First wall			
PCA SS	49.8	35	1.74
Be (coating)	7.2	250	1.80
Blanket			
PCA SS	<u>3676.9</u>	35	<u>128.69</u>
Total	3733.9		132.23

6.2.3.2 Shielding (Account 22.01.02)

Table 6-4 lists the principal materials of the low flux and high flux shielding. The costs have been calculated on a cost per unit weight basis. The bulk FE-1422 steel cost reflects the cost of thick plates with minimal machining costs. The structural cost, which is higher, for FE-1422 represents the coolant tubes, cladding for the B₄C, structural elements, and pressure jackets. Very little fabrication is considered for Pb, B₄C, and W with these being cast or pressed into shape. The total cost for the shielding is:

$$C_{22.01.01} = \$352.50 \text{ M}$$

Table 6-4. Shielding Costs

Material	Mass (Tonnes)	Installed Cost (\$/kg)	Total Cost (M\$)
<u>Inboard Shield</u>			
FE-1422, structural	48.5	20	0.97
FE-1422, bulk	68.7	9	0.62
B ₄ C	12.8	35	0.45
TiH ₂	69.0	2	0.14
W	858.1	50	42.90
	<u>1,057.1</u>		<u>45.08</u>
<u>Outboard Shield</u>			
FE-1422, structural	815.7	20	16.31
FE-1422, bulk	7,927.3	9	71.35
B ₄ C	357.9	35	12.53
TiH ₂	829.5	2	1.66
Ti ₆ Al ₄ V	127.8	65	8.31
	<u>10,058.2</u>		<u>110.16</u>
<u>Vacuum Duct and Pod</u>			
FE 1422, structural	1,413.5	20	28.27
FE 1422, bulk	12,722.0	9	144.50
B ₄ C	537.9	35	18.82
Ti ₆ Al ₄ V	87.3	65	5.67
	<u>14,760.7</u>		<u>197.26</u>
Total			<u>352.50</u>

6.2.3.3 Magnets (Account 22.01.03)

The magnet systems for WILDCAT are significantly different from the STARFIRE design with respect to the size and the amount of stored energy. The toroidal field magnets contain approximately four times as much stored energy as for the STARFIRE design and weigh over twice as much. Based on a cost per weight basis, Table 6-5 illustrates that the steady-state TF coils cost \$293.02 M exclusive of the TF coil dewars and \$336.31 M with the dewars included. The EF coils are approximately 45% more costly than STARFIRE while the CF and OH coils are somewhat lower in cost as a result of the less D-shaped plasma equilibrium. The overall cost for the steady-state magnet coil set is \$352.66 M excluding dewars. Table 6-6 illustrates the cost of the pulsed magnet set. Although the pulsed-version TF coils are less costly, (\$279.3 M versus \$293.02 M for the steady-state version), the higher cost of the pulsed OH system (\$56.73 M) makes the total pulsed magnet system

Table 6-5. Cost of the Magnets (Steady State)

Material	Unit Cost (\$/kg)	TF (12 Coils)		EF (8 Coils)		CF (4 Coils)		OH (6 Coils)	
		Wt (MT)	Cost (M\$)	Wt (MT)	Cost (M\$)	Wt (MT)	Cost (M\$)	Wt (MT)	Cost (M\$)
Nb ₃ Sn	109			-	-	-	-	-	-
NbTi	55	4,498	151.15	39.6	2.18	-	-	4.7	0.26
Copper stabilizer	16			540.3	8.65	-	-	63.0	1.01
Copper conductor	25	-	-	-	-	121.9	3.05	-	-
SS structure	14	4,820	67.48	567.8	7.88	8.7	0.12	65.6	0.92
SS helium tank	26	2,462	64.01	708.2	18.41	-	-	82.6	2.15
SS vacuum dewars	26	(a)	(a)	361.5	9.40	-	-	44.9	1.17
G-10CR insulator	20	134	2.68	104.5	2.09	-	-	12.3	0.25
Fiberglass insulator	13	-	-	108.3	1.41	-	-	12.6	0.16
Alumina insulator	25	-	-	-	-	13	0.33	-	-
Superinsulation	100/m ⁻²	(a)	(a)	1792 m ²	0.18	-	-	225,7 m ²	0.02
<u>Circuit protection</u>	-	-	<u>7.70</u>	-	<u> </u>	-	<u> </u>	-	<u> </u>
Total			293.02		50.20		3.50		5.94

(336.31 W/Vacuum Dewars)

Total Magnet System Cost: C_{22.01.03} = \$352.66 M (Steady State)

^aIncluded in Account 22.01.05.

6-19

Table 6-6. Cost of the Magnets (Pulsed)

Material	Unit Cost (\$/kg)	TF (12 Coils)		EF (8 Coils)		CF (4 Coils)		OH (6 Coils)	
		Wt (MT)	Cost (M\$)	Wt (MT)	Cost (M\$)	Wt (MT)	Cost (M\$)	Wt (MT)	Cost (M\$)
Nb ₃ Sn	109			-	-	-	-	-	-
NbTi	55	4,315	145.01	39.6	2.18	-	-	44.6	2.45
Copper stabilizer	16			540.3	8.65	-	-	603.2	9.65
Copper conductor	25	-	-	-	-	121.9	3.05	-	-
SS structure	14	4,540	63.56	562.8	7.88	8.7	0.12	627.4	8.78
SS helium tank	26	2,347	61.02	708.2	18.41	-	-	790.2	20.55
SS vacuum dewars	26	(a)	(a)	361.5	9.40	-	-	429.5	11.17
G-10CR insulator	20	128	2.56	104.5	2.09	-	-	117.4	2.35
Fiberglass insulator	13	-	-	108.3	1.41	-	-	120.5	1.57
Alumina insulator	25	-	-	-	-	13	0.33	-	-
Superinsulation	100/m ⁻²	(a)	(a)	1792 m ²	0.18	-	-	2121 m ²	0.21
<u>Circuit protection</u>	-	-	7.20	-	-	-	-	-	-
Total			279.35		50.20		3.50		56.73

(320.60 W/Vacuum Dewars)

Total Magnet System Cost: C22.01.03 = \$389.78 M (Pulsed)

^aIncluded in Account 22.01.05.

more expensive (\$389.78 M exclusive of TF dewars). The dewars are not included in the magnet system cost because they are considered as an integral element in the primary structural system, Account 22.01.05. The total magnet system cost is:

C_{22.01.03} = \$352.66 M (Steady State)
= \$389.78 M (Pulsed)

6.2.3.4 Rf Heating and Current Drive (Account 22.01.04)

The capital costs associated with this system are attributed to the compressional Alfvén wave (CAW) heating and current-drive system. The system consists of 120 intermediate and high power amplifiers operating at 3.5 MHz. Table 6-7 lists the costs of the CAW system. The costs of the intermediate power amplifiers (IPA) and high power amplifiers (HPA) have been estimated by Varian as these are commercially available components. The remaining system elements are estimated from a Princeton Plasma Physics Laboratory cost estimate for an ion cyclotron resonance heating system,⁴ which has similar requirements. The antenna and Faraday shield are estimated by analogy to a similar antenna. The total system cost is:

C_{22.01.04} = \$34.88 M

6.2.3.5 Primary Structure and Support System (Account 21.01.05)

The primary structure and support system is comprised of all the structural elements which support and react the loads generated by the magnetic, gravitational, and seismic forces on the reactor components. Table 6-8 lists the major structural components and their costs. The cryogenic center post is comprised of Nonmagne 30 and is a very large structural element at 3,808 metric tonnes. The toroidal field (TF) coil dewars are included in this system because they are an integral structural element in the anti-torque structural system. The pulsed version of the TF dewars is slightly smaller than the steady-state version. A set of materials have been considered as possible candidates for the anti-torque structure and the shield

Table 6-7. Cost of the CAW Heating/Current-Drive System

Component	Unit Cost (\$)	Total Cost (M\$)
Power		
IPA, Eimac 4CW100,000E tetrode (120 Units)	5,500 ^a	0.66
HPA, Eimac X2176 triode, 3.5 MHz, 1 MW (120 units)	28,850 ^a	3.46
IPA screen supply, filament supply and plate blocking cap	5,700 ^b	0.68
Misc rf system hardware (capacitors, tuning networks, filament supplies, filters enclosures, drivers, attenuators, switches, blowers and meters)	--	10.88
Transmission		
Antenna and Faraday shields (120 units)	50,000	6.00
Bushings, neutron shield, windows, safety breaks, coax, couplers and elbows (120 units)	110,000	13.20
Total		34.88

^aVarian discounted book price.

^bRef PPPL 1410 (1977) B. W. Reed et al (see Ref. 4).

Table 6-8. Primary Structure and Support Systems Cost

Material	Mass (MT)	Installed Cost (\$/kg)	Total Cost (M\$)	
Reactor centerpost				
- Nonmagne 30	3,808	16	60.93	
Centerpost support struts				
- G-10CR	19.1	20	0.38	
Common dewar				
- Nonmagne 30	109.8	20	2.20	
- Superinsulation	750 m ²	100 m ⁻²	0.08	
TF coil dewars				
	<u>Steady State</u>	<u>Pulsed</u>	<u>Steady State</u>	<u>Pulsed</u>
- Nonmagne 30	2,134.1	2,033.6	42.68	40.67
- G-10CR	4.16	4.0	0.08	0.08
- Superinsulation	5,255 m ²	5,009 m ²	0.53	0.50
Anti-torque structure				
- Concrete	5,172	0.70	3.60	
- Nonmagne 30	50	20	1.00	
Shield pedestal				
- Concrete	2,585	0.70	1.81	
- Nonmagne 30	25	20	0.50	
Equipment support structure				
- Nonmagne 30	59.3	20	1.19	
- G-10CR	7.73	20	0.15	
			Steady State: 115.13	
			Pulsed: 113.09	
Total				

pedestal, and a cost trade study has been conducted. Table 6-9 illustrates the comparative costs of the various materials. A concrete structure with steel alignment structure is the lowest cost option even with considerable more material wastage and complexity of the forms and reinforcing. The total cost for the primary structure and support system is:

C22.01.05 = \$115.13 M (Steady State)
 = \$113.09 M (Pulsed)

Table 6-9. Primary Structure Cost Trade Studies

Material	Quantity (MT)	Cost Unit (\$/kg)	Total (M\$)
<u>Comparison of Anti-torque Structural Materials</u>			
Concrete/rebar	5,142	0.70	3.60
Steel alignment structure			1.00
			4.60
Aluminum	1,061	10	10.61
Stainless steel	2,313	16	37.00
G-10 fiberglass epoxy	1,054	20	21.08
<u>Comparison of Shield Pedestal</u>			
Concrete	2,585	0.70	1.81
Steel alignment structure	-	-	0.50
			2.31
Aluminum	530.4	10	5.30
Stainless steel	639.2	16	10.22
G-10 fiberglass epoxy	527	20	10.54

6.2.3.6 Reactor Vacuum System (Account 22.01.06)

The reactor vacuum system is similar to the STARFIRE system but is somewhat larger. The size of the cryogenic vacuum pumps is scaled in proportion to the plasma chamber volume (ratio of 2.16). The valves are also increased in size from 1.0 to 1.2 m. The vacuum ducts and pods are considered as a part of the shielding and are costed in Account 22.01.02.

The hardware associated with the reactor vacuum system is shown in Table 6-10. The cost of the reactor vacuum system is:

$$C_{22.01.06} = \$8.68 \text{ M}$$

Table 6-10. Reactor Vacuum System Costs

Component	Equipment Cost (M\$)	Installation Cost (M\$)	Total Cost (M\$)
Plasma chamber cryopumps (48)	5.20	0.52	5.72
Right-angle valves (48)	1.04	0.06	1.10
Gate valves, 1.2m diameter (48)	1.40	0.08	1.48
Regeneration system	0.12	0.12	0.24
TF roughing pump piping	0.06	0.06	0.14
Total			8.68

6.2.3.7 Power Supply, Switching, and Electrical Energy Storage (Account 22.01.07)

The power supply, switching, and energy storage system provides conditioned power to the magnet coil system, the CAW heating and current drive system, and the ECRH plasma breakdown system. The pulsed version exhibits a need for large energy storage. In the WILDCAT pulsed design the storage system is a motor/generator/flywheel (MGF) set coupled with transformers and silicon controlled rectifier/invertor power supplies. The power supply for the TF magnets provides a low voltage, high current system and is estimated at \$80/kW including component costs, installation and system checkout. The EF and the OH systems use the MGF sets as the energy storage system, and these systems are costed at \$100/kVA. The power supplies for the correction field coil system are roughly one half the size of those for the STARFIRE system. The CAW heating and current drive system is a low voltage system which is also costed at \$80/kW. The ECRH plasma breakdown system costs are developed from the STARFIRE cost basis at \$125/kW. The total system costs for both the steady-state and the pulsed systems are shown in Table 6-11 and are:

$$C_{22.01.07} = \$ 32.2 \text{ M (Steady State)}$$

$$= \$335.9 \text{ M (Pulsed)}$$

Table 6-11. Power Supply, Switching, and Electrical Storage

Subsystem	Costs (M\$)			
	Steady-State		Pulsed	
Toroidal Field Coils		0.3		0.3
- Power supply	0.3		0.3	
- Protective circuit (Included in 22.01.03)				
Equilibrium field coils		8.3		100.0
- Power supply (83 MVA SS; 1,000 MVA Pulsed)	8.3		100.0	
Ohmic heating coils		4.0		216.0
- Power supply (40 MW SS; 2,160 MW pulsed)	4.0		216.0	
Correction field coils		5.7		5.7
- Power supply	0.3		0.3	
- Capacitive energy storage (5MJ)	1.0		1.0	
- Coil 1 and 3 choppers	0.7		0.7	
- Coil 2 and 4 choppers	3.7		3.7	
CAW heating and current drive		11.6		11.6
- Power supplies (145 MW to HPA)	11.6		11.6	
ECRH plasma breakdown		2.3		2.3
- Power supplies (10.5 MW output)	2.3		2.3	
Total		<u>32.2</u>		<u>335.9</u>

6.2.3.8 Impurity Control (Account 22.01.08)

In the STARFIRE design several materials were considered for the limiter material with a niobium alloy (FS-85) being chosen. This same material and limiter configuration is chosen for WILDCAT, and the only difference from a cost standpoint is the larger perimeter of the belt limiter (ratio is 1.25). Thus, the cost of the limiter is estimated at:

$$C_{22.01.08} = \$3.07 \text{ M}$$

6.2.3.9 ECRH Plasma Breakdown (Account 22.01.09)

This system is very similar to the STARFIRE system except it is at a higher frequency (230 GHz vs. 160 GHz). The power level to the plasma is roughly one-half the STARFIRE value (approximately 2.6 MW out of the tubes and approximately 2.1 MW delivered to the plasma). Current experience with 28 and 60 GHz gyrotrons in the 250 kW range indicates that quantity purchases could be for about \$1/W. The higher frequency tube would likely be

more expensive and is estimated at \$2/W in a quantity purchase. Thus, the tube cost is \$5.2 M. Other system costs include launcher assemblies, launcher cooling systems, two to three waveguide windows per waveguide, window cooling systems, directional couplers, SF₆ pressurization system, switches, power dumps, arc detectors, and switch gear. These costs add to approximately \$4/W, yielding a total cost for the ECRH system of:

$$C_{22.01.09} = \$15.6 \text{ M}$$

6.2.3.10 Main Heat Transfer and Transport (Account 22.02)

This cost account includes the costs of the primary (light water) coolant system, the limiter cooling system (which provides the feedwater heating), and the residual heat removal system (which circulates coolant through the blanket sectors during the shutdown maintenance periods). The costs are scaled from the STARFIRE estimate based upon the thermal energy transported in each system. Table 6-12 lists the thermal and electrical power levels of STARFIRE and the two WILDCAT versions. Most elements (pipes, steam generator, heat exchangers, etc.) in the primary and limiter cooling systems scale directly with power level. Table 6-13 lists the system costs for both STARFIRE and the two WILDCAT versions. The primary coolant is a high pressure (2200 psi), high-temperature (320°C) water system as compared to the lower temperature and pressure limiter system (600 psi, 150°C). The residual heat removal is retained exactly as in the STARFIRE system. For details on the system cost breakdown, see Ref. 3. The total system cost is:

$$\begin{aligned} C_{22.02} &= \$51.92 \text{ M (Steady State)} \\ &= \$46.24 \text{ M (Pulsed)} \end{aligned}$$

Table 6-12. Comparison of STARFIRE and WILDCAT
Thermal and Electrical Powers

Parameter	STARFIRE	WILDCAT	
		SS	Pulsed
Primary coolant (MWth)	3800	2656	2336
Limiter (MWth)	200	235	223
Turbine input (MWth)	4033	2915	2580
Gross electric (MWe)	1440	1041	921
Net electric (MWe)	1203	812	849
Recirculating (MWe)	237	229	72
Percent recirculating (%)	16.4	22.0	7.8

Table 6-13. Main Heat Transfer and Transport System Costs

Subsystem	System Costs (M\$)		
	STARFIRE	WILDCAT, SS	WILDCAT, Pulsed
Primary cooling	63.10	44.10	38.79
Limiter cooling	6.19	7.27	6.90
Residual heat removal	0.55	0.55	0.55
Total	<u>69.84</u>	<u>51.92</u>	<u>46.24</u>

6.2.3.11 Cryogenic Cooling Systems (Account 22.03)

The cryogenic cooling system is a central facility which supplies all the liquid helium and nitrogen needs for the power plant. The dominant user for the cryogens is the superconducting magnet systems, so all costs have been scaled directly from the STARFIRE estimate on a volume-of-the-coil basis, as shown in Table 6-14. The TF coil volumes are more than twice as large as STARFIRE. The EF coil volumes are slightly larger. The OH coil volume for the steady-state version is similar in size to STARFIRE while the pulsed version is roughly 10 times as large. Table 6-15 illustrates the costs for the cryogenic system. The total system cost is:

$$\begin{aligned}
 C_{22.03} &= \$30.07 \text{ M (Steady State)} \\
 &= \$32.47 \text{ M (Pulsed)}
 \end{aligned}$$

Table 6-14. Comparison of Coil Dewar Volumes

Design Concept	Volume (m ³)			
	TG	EF	OH	Total
STARFIRE	781	164	34	979
WILDCAT, Steady state	1710	238	28	1976
WILDCAT, Pulsed	1638	233	266	2134

Table 6-15. Cryogenic System Costs

Account No.	Subsystem	Total Cost (M\$)	
		Steady-State	Pulsed
22.03.01	He liquefier/refrigerator	15.54	16.78
22.03.02	LHe transfer and storage	7.27	7.85
22.03.03	GHe storage	5.65	6.10
22.03.04	LN ₂ system	1.61	1.74
	Total	30.07	32.47

6.2.3.12 Radioactive Waste Treatment and Disposal (Account 22.04)

This system processes all radioactive waste products (excluding tritium) for disposal by storage or by transportation off-site. The radioactive products can be liquid, solid, or gaseous. The processing takes place in the Hot Cell Building. It is assumed that the requirement for this system is similar to that for the STARFIRE design and is costed at:

$$C_{22.04} = \$4.80 \text{ M}$$

6.2.3.13 Fuel Handling and Storage System (Account 22.05)

The Fuel Handling and Storage System accomplishes the extraction, recovery, purification, preparation, storage, and injection of the fuel elements. The elimination of tritium as a fuel element for WILDCAT simplifies the complete process, but all the functions must still be accomplished. There is no distinction between the steady-state and the pulsed

version for this system. Table 6-16 lists the systems required and their respective costs. The total system cost is:

$$C_{22.05} = \$31.70 \text{ M}$$

Table 6-16. Fuel Handling and Storage System Costs

Account No.	Title	Costs (M\$)	
22.05.01	Fuel Purification	7.8	
	- Isotope Separation Units (4)		4.8
	- Fuel Cleanup Units (2)		1.0
	- Misc pumps, piping, valves and installation		2.0
22.05.02	Liquification (included in 22.05.01)	N/C	
22.05.03	Fuel Preparation	0.6	
22.05.04	Fuel Injection	2.1	
22.05.05	Fuel Storage	0.5	
22.05.06	Tritium Recovery (from blanket and coolant)	0.0	
22.05.07	Atmospheric Tritium Recovery Systems	20.7	
	Total	31.7	

6.2.3.14 Other Reactor Plant Equipment (Account 22.06)

This account considers the reactor maintenance equipment, the special heating equipment, the coolant receiving, storage, and makeup system, gas systems, inert atmospheric systems, leak detection system, closed loop coolant system, and the standby coolant system. The maintenance equipment is different than that proposed for STARFIRE, but most of the functions are similar. The overhead crane (covered in Account 25.01) is larger to handle the heavier blanket modules, but the manipulators and handling equipment are assumed to be no larger than for STARFIRE. The cost for the maintenance equipment, like the cost for most of the remaining systems in this account is assumed to be the same as for STARFIRE and is shown in Table 6-17. The costs for the Closed Loop Cooling System and the Standby Cooling System are scaled as a function of the thermal power. The total Other Reactor Plant Equipment cost is:

$$C_{22.06} = \$43.13 \text{ M (Steady State)}$$

$$= \$42.81 \text{ M (Pulsed)}$$

Table 6-17. Other Reactor Plant Equipment Costs

Account No.	Title	Cost (M\$)	
		Steady State	Pulsed
22.06.01	Maintenance Equipment	38.30	38.30
22.06.02	Special Heating Systems	0.00	0.00
22.06.03	Coolant Receiving, Storage and Make-up System	0.24	0.24
22.06.04	Gas Systems	0.08	0.08
22.06.05	Inert Atmosphere (included in 22.06.04)	N/C	N/C
22.06.06	Fluid Leak Detection	2.00	2.00
22.06.07	Closed Loop Coolant Systems	1.58	1.38
22.06.08	Standby Cooling System	0.93	0.81
	Total	43.13	42.81

6.2.3.15 Instrumentation and Control (Account 22.07)

There are no perceived differences in this system as compared to STARFIRE, thus the costs are considered to be identical at:

$$C_{22.07} = \$23.41 \text{ M}$$

6.2.3.16 Reactor Spare Parts Allowance (Account 22.98)

This account collects the costs of all of the spare parts to allow routine scheduled and unscheduled maintenance in a minimal time. Table 6-18 lists the major components identified as requiring a spares inventory along with a column denoting the regular replacement frequency of known items. In addition to these large cost spare parts, the cost for the items of lesser costs are covered under a 2% allowance for all the Reactor Plant Equipment (Acct. 22). The total cost of the spare parts is:

$$C_{22.98} = \$79.85 \text{ M (Steady State)}$$

$$= \$86.55 \text{ M (Pulsed)}$$

Table 6-18. Cost of the Reactor Plant Equipment Spare Parts

Major Components	Quantity in Service	Quantity of Spare Parts	Cost of Spares (M\$)	Quantity Replaced Annually
Wall/Blanket/Limiter/ rf Duct Sector	24	(a)	0	1/20
TF Coil	12	0	0	0
EF Coil	8	2	12.55	0
	4	4(30° segments)	0.29	0
OH Coil	6	2	1.98	0
Vacuum Cryopumps	48	2+24 MOL Sieves	0.56	Refurb 24 MOL Sieves
Vac Isol Vlv, Rt Ang	48	4	0.06	Refurb 24 Vlv Stems
Vac Isol Vlv, Gate	48	4	0.12	0
Shield Access Door	12	2	5.60	Replace Seal
ECRH Gryotrons	10	2	0.52	0
RF HPA/IPA	120	60	2.06	Refurb 40
RF Windows	120	15	1.65	12
RF Waveguide Elbows	12	1	0.23	0
Vacuum Pods	24	2	16.44	0
Primary Coolant Pump	4	1	0.55	0
Maintenance Equipment	-	1 set	<u>12.60</u>	0
Subtotal			55.21	
Allowance (2% of Accounts 22.01 through 22.07)			24.64 (Steady State)	
			<u>31.34</u> (Pulsed)	
Total			79.85 (Steady State)	
			86.55 (Pulsed)	

^a Included in Annual Scheduled Component Replacement Cost, Account 50.

6.2.4 Turbine Plant Equipment (Account 23)

This account summarizes all of the costs associated with the Turbine Plant Equipment, which takes the thermal energy from the reactor and converts it to electrical energy and rejects the remaining thermal energy to the environment. Most of the equipment is of a conventional design for a central generating station. The total direct cost for this account including spares and contingency is:

$$\begin{aligned} C_{23} &= \$215.38 \text{ M (Steady State)} \\ &= \$357.21 \text{ M (Pulsed)} \end{aligned}$$

6.2.4.1 Turbine Generator (Account 23.01)

The powers to the WILDCAT turbines are significantly less than for STARFIRE (2915 MW for the steady-state case and 2580 MW for the pulsed case versus 4033 MW for STARFIRE). However the costs do not scale directly with the reduction in power level. It is assumed the turbine generator cost for the steady-state case is 85% of the STARFIRE turbine cost or \$67.0 M, and the pulsed version is 80% or \$62.0 M. These costs are estimated from current experience in scaling turbine generator systems from their rated powers. Many subsystem elements do not change appreciably with respect to changes in the thermal power. Consequently the costs are estimated to change in proportion to the ratio of the powers to the 0.5 power. To accommodate the proposed technique of thermal storage for the pulsed reactor, an allowance of \$8.0 M is assumed for turbine modifications to add extra stages which operate at 1250 psi (versus the main turbine at 950 psi). The total cost of the turbine is:

$$\begin{aligned} C_{23.01} &= \$67.00 \text{ M (Steady State)} \\ &= \$70.00 \text{ M (Pulsed)} \end{aligned}$$

6.2.4.2 Main Steam System (Account 22.02)

The same basic cost scaling factors as for the turbine generator apply to the main steam system, yielding \$3.77 M and \$3.47 M for the steady-state and pulsed versions respectively. In addition, the pulsed version of

WILDCAT requires a thermal energy storage system to assure a continuous flow of steam to the turbine and to yield a constant electrical output. A thermal energy storage system has been devised (Appen. A) which supplements the regular steam system during those periods of reduced power production. The system is designed as a separate system valved into the regular steam system and delivers steam at a higher turbine inlet pressure to the turbine. Table 6-19 lists the major elements of the Thermal Storage System which are included in Account 22.02. Other elements include \$8.0 M for turbine modifications and \$2.0 M for an instrumentation and control (I&C) allowance. The costs for the thermal storage elements have been obtained from the sub-system designers. The total Main Steam System costs are:

C22.02 = \$3.77 M (Steady State)
 = \$129.67 M (Pulsed)

Table 6-19. Thermal Storage System Costs

Component	Cost (M\$)
Charging pumps (2)	9.6
Piping allowance	5.0
Valves (8)	8.0
Condensate storage with pumps	4.0
Water storage vessels (6)	99.6
Total	126.2

6.2.4.3 Heat Rejection System (Account 22.03)

The elements in this account are similar to those for the STARFIRE design but are scaled as the rejected thermal heat. The costs are reduced to:

C23.03 = \$36.80 M (Steady State)
 = \$33.02 M (Pulsed)

6.2.4.4 Condensing System (Account 23.04)

This system is also reduced in cost in proportion to the thermal power handled by each WILDCAT option. The costs are:

$$\begin{aligned} C_{23.04} &= \$16.05 \text{ M (Steady State)} \\ &= \$14.48 \text{ M (Pulsed)} \end{aligned}$$

6.2.4.5 Feedwater Heating System (Account 23.05)

This system is also reduced in size and cost in proportion to the system power:

$$\begin{aligned} C_{23.05} &= \$7.64 \text{ M (Steady State)} \\ &= \$6.76 \text{ M (Pulsed)} \end{aligned}$$

6.2.4.6 Other Turbine Plant Equipment (Account 23.06)

This account includes the gas storage, chemical treatment, condensate and steam blowdown systems, turbine plant cooling water system, and the associated process piping. It also is scaled down in proportion to the input power to the turbine, and the system cost is:

$$\begin{aligned} C_{23.06} &= \$44.77 \text{ M (Steady State)} \\ &= \$41.74 \text{ M (Pulsed)} \end{aligned}$$

6.2.4.7 Instrumentation and Control (Account 23.07)

This account includes the BOP instrumentation and control and the BOP computer and accessories. It is assumed that no cost reduction is justified from the system as defined in STARFIRE, thus the same system and cost are included. The pulsed version requires added I&C functions for the thermal energy storage system. This adds a \$2.0 M allowance. The I&C system costs are:

$$\begin{aligned} C_{23.07} &= \$8.70 \text{ M (Steady State)} \\ &= \$10.70 \text{ M (Pulsed)} \end{aligned}$$

6.2.5 Electrical Plant Equipment (Account 24)

The Electrical Plant Equipment includes the switchgear for the generator circuits and station service, station service equipment, switchboards, protective equipment, electrical structures, and wiring containers, power and control wiring, and lighting. Table 6-20 illustrates the cost of the subaccounts under this major account. This first four accounts are estimated to be virtually identical to the STARFIRE systems and to have the same costs. The Electrical Structures and Wiring Containers and the Power and Control Wiring have been scaled down in cost to 90% and 87% for the steady-state and pulsed version due to the reduced station power requirements. These values are estimated based upon consideration of elements which directly scale with the electrical power. The Electrical Lighting remains the same. Thus the total system cost including spares and contingency is:

$$C_{24} = \$111.08 \text{ M (Steady State)}$$

$$= \$109.22 \text{ M (Pulsed)}$$

Table 6-20. Costs of the Electrical Plant Equipment

Account No.	Title	Cost (M\$)	
		Steady-State	Pulsed
24.01	Switchgear	12.39	12.39
24.02	Station Service Equipment	17.04	17.04
24.03	Switchboards	7.80	7.80
24.04	Protective Equipment	2.11	2.11
24.05	Electrical Structures and Wiring Containers	15.66	15.14
24.06	Power and Control Wiring	32.39	31.31
24.07	Electrical Lighting	8.20	8.20
24.98	Spare Parts Allowance	1.15	1.13
24.99	Contingency Allowance	14.34	14.10
	Total	111.08	109.22

6.2.6 Miscellaneous Plant Equipment (Account 25)

This account includes those systems which support the complete facility as shown in Table 6-21. The Transportation and Lifting Equipment is very similar to that for STARFIRE. Although some elements of the WILDCAT components may be heavier than those for STARFIRE, the overhead cranes are still adequate to lift the major system components. The Air and Water Service can

be reduced in the areas of raw water pumps, makeup water system, makeup water treatment system, and raw water piping. The remainder of the systems are similar in cost. The total system cost including spares and contingency is:

$$C_{25} = \$39.66 \text{ M}$$

Table 5-21. Costs of the Miscellaneous Plant Equipment

Account No.	Title	Cost (M\$)
25.01	Transportation and Lifting Equipment	15.68
25.02	Air and Water Service Systems	11.39
25.03	Communications	6.22
25.04	Furnishings and Fixtures	0.75
25.98	Spare Parts Allowance	0.51
25.99	Contingency Allowance	5.11
	Total	<u>39.66</u>

6.2.7 Special Materials (Account 26)

This account includes the cost of the special (nonfuel and nonstructural) materials and special (other than natural water) heat transfer fluids or gases. It is assumed that this account is also similar to the STARFIRE allowance of:

$$C_{26} = \$0.25 \text{ M}$$

6.2.8 Construction Facilities, Equipment, and Services (Account 91)

This account includes the cost of the facilities which are removed or dismantled after completion of construction, the net cost or rental expense of equipment used during construction, labor force education, receiving and storage, testing, site cleanup, and operational and maintenance (O&M) of facilities and equipment. It is estimated that, as for STARFIRE, 10% of the direct cost would be allowed for this account:

$$C_{91} = \$221.29 \text{ M (Steady State)}$$

$$= \$276.52 \text{ M (Pulsed)}$$

6.2.9 Engineering and Construction Management Service (Account 92)

This cost account includes the cost of all engineering services associated with this tenth-of-a-kind plant. It is assumed that, as for STARFIRE, an 8% allowance of the reactor direct cost is adequate. The cost for this account is:

$$\begin{aligned} C_{92} &= \$177.03 \text{ M (Steady State)} \\ &= \$221.21 \text{ M (Pulsed)} \end{aligned}$$

6.2.10 Other Costs (Account 93)

This account includes the property and all-risk (non-nuclear liability) insurance, staff training, plant startup, and owners General and Administrative (G&A) costs. This account is estimated to be 5% of the direct cost as for STARFIRE, yielding:

$$\begin{aligned} C_{93} &= \$110.64 \text{ M (Steady State)} \\ &= \$138.26 \text{ M (Pulsed)} \end{aligned}$$

6.2.11 Interest During Construction (Account 94)

The interest cost during the six year construction time period is estimated by a factor of 0.1303 for constant year dollars (1980) and 0.3163 for the current dollars (1986) as for STARFIRE. See Ref. 1 and Ref. 2 for a complete explanation of the technique and the assumptions:

$$\begin{aligned} C_{94} \text{ (Constant)} &= \$ 354.66 \text{ M (Steady State)} \\ &= \$ 443.17 \text{ M (Pulsed)} \\ C_{94} \text{ (Then Current)} &= \$ 860.92 \text{ M (Steady State)} \\ &= \$1075.79 \text{ M (Pulsed)} \end{aligned}$$

6.2.12 Escalation During Construction (Account 95)

This account estimates all the capital costs attributed to escalation during construction. The escalation factor for a six-year construction period is 0.1896 for the then-current dollar analysis mode, which yields a cost of:

$$\begin{aligned} C_{95} &= \$516.06 \text{ M (Steady State)} \\ &= \$644.86 \text{ M (Pulsed)} \end{aligned}$$

6.3 Busbar Energy Costs

The busbar energy cost is defined as the unit cost of generating a kilowatt-hour of electricity available at the generator busbars. The total energy cost for a fusion-reactor, electricity-producing facility is calculated as a function of the following components:

- Total capital cost
- Financing assumptions
- Fixed charge rate for the annual cost of capital
- Annual operating and maintenance (O&M) cost
- Annual scheduled component replacement cost
- Annual fuel costs
- Plant availability
- Plant net capacity

Several of these parameters have previously discussed or estimated. The remainder will be developed in the next sections.

6.3.1 Annual Levelized Capital Cost

The cost of capital is levelized over the economic life of the facility (30 years) by utilizing a fixed charge rate.⁵ This fixed charge rate, when applied to the total facility capital investment cost, yields the annual capital expense. This annual cost covers payback of capital, depreciation, interim replacement, property insurance, federal income taxes, and state and local taxes. The fixed charge rate used in these analyses is 10% for the constant dollar analysis and 15% for then-current dollar analysis.¹

	<u>Steady-State</u>	<u>Pulsed</u>
Annualized capital cost:		
Constant dollar	\$307.65 M	\$384.44 M
Then-current dollar	\$614.82 M	\$786.27 M

6.3.2 Annual Operations and Maintenance Cost

Operation and maintenance (O&M) costs are the routine day-to-day expenditures to operate and maintain the facility. Table 6-22 lists the subaccounts in this category and their respective costs. The costs are judged to be similar to the STARFIRE design. Reference 1 has a complete explanation of this account and the cost justification for each subaccount. The total of the O&M costs are:

$$C_{40-47} = \$19.407 \text{ M.}$$

Table 6-22. Operations and Maintenance Costs

Account No.	Account Title	Cost (M\$)
40	Annual salaries of facility personnel	8.710
41	Annual miscellaneous supplies and equipment	5.200
42	Annual outside support services	0.792
43	Annual general and administrative	2.205
44	Annual coolant makeup	0.000
45	Annual process materials	1.000
46	Annual fuel handling	0.000
47	Annual miscellaneous	<u>1.500</u>
	Total	19.407

6.3.3 Annual Scheduled Component Replacement Cost

The scheduled component replacement costs are the expected annual cost of routine scheduled maintenance or replacement of major reactor components as shown in Table 6-23. The first wall and blanket are replaced once every 20 y. The cost of the first wall and blanket also includes all the CAW heating antennas and the limiters. An allowance is estimated for replacement of the CAW High Power Amplifier (HPA) and Intermediate Power Amplifier (IPA) because the specific lifetimes are not known. No costs have been included for the pulsed power supply although there may be a requirement for a

replacement cost on some components of this subsystem. The total cost of this account is:

$$C_{50,51} = \$7.665 \text{ M}$$

Table 6-23. Scheduled Component Replacement Costs

Component	Unit Price on Refurbishment Cost (\$)	Replacement Frequency	Annual Cost (M\$)
First Wall and Blanket	141.30 M (Total)	1/20 y	7.065
CAW IPA	5,590	Unknown	0.100
CAW HPA	28,850	Unknown	0.500
Total			<u>7.665</u>

6.3.4 Annual Fuel Cost

The only fuel cost for WILDCAT is for deuterium. The deuterium fuel burnup, scaled from STARFIRE, is 650 g/day (steady state) and 568 g/day (pulsed). Considering a small leakage (5%) and a plant availability of 75%, a prorated daily usage of D₂ would be 511 g (steady state) and 447g (pulsed). At a price of \$2175/g (Ref. 3), this equates to an annual cost of:

$$C_{02} = \$406,000 \text{ (Steady State)}$$

$$= \$355,000 \text{ (Pulsed)}$$

No offsite processing and disposal facilities are required, thus no costs are reported:

$$C_{03} = \$0$$

6.3.5 Plant Availability

Plant availability is the ratio of the expected amount of energy generation and the amount of energy generation that would occur if the plant operated 100% of the time. The WILDCAT reactor may have a slightly better

availability factor because of a much longer wall lifetime which results in reduced scheduled outages and because of faster maintenance owing to the reduced tritium hazard. The unscheduled outages are assumed roughly similar to STARFIRE. In general, the balance-of-plant (BOP) outages tend to dominate the overall availability. Thus, it may be possible to predict an improved availability for WILDCAT, but in lieu of an extensive analysis, the same value of 75% is adopted.

6.3.6 Plant Capacity

The plant capacity is the net electrical energy that would be produced annually if the plant were operating continuously at the design level of power generation and all recirculating power demands were subtracted from the gross generation. For WILDCAT the gross power levels are 1041 MW and 921 MW for the steady state and the pulsed versions respectively. The recirculating power demands are 229 MW and 72 MW, yielding net power levels of 812 MW and 849 MW for the steady state and pulsed versions, respectively.

6.3.7 Busbar Cost of Electricity

The Cost of Electricity (COE) is the most important economic parameter to gauge how competitive the power plant will be. The prior development of the costs pertaining to WILDCAT have been preparatory to evaluating the applicable COE. The general equation for COE is:

$$COE = \frac{C_{AC} + (C_{O\&M} + C_{SCR} + C_F)(1 + E)^P}{PC \times PAF \times 10^{-3}}$$

where:

- COE = Cost of Electricity in Constant or Then-Current Dollars (mills/kWh)
- C_{AC} = Annual Capital Cost Charge
- C_{O&M} = Annual Operations and Maintenance Costs (C₄₀ through C₄₇)
- C_{SCR} = Annual Scheduled Component Replacement Cost (C₅₀ + C₅₁)
- C_F = Annual Fuel Costs (C₀₂ + C₀₃)
- E = Escalation Rate (0 for Constant Dollars and 0.05 for Then-Current Dollars)

- P = Construction Period in Years
- PC = Plant Capacity in kWh
- PAF = Plant Availability Factor

COE: Steady-State, Constant Dollars

$$\text{COE} = \frac{307,650,000 + (19,407,000 + 7,665,000 + 406,000)}{812,000 \times 8,750 \times 0.75 \times 0.001}$$

= 62.8 mills/kWh

COE: Steady-State, Then-Current Dollars

$$\text{COE} = \frac{614,820,000 + (19,407,000 + 7,665,000 + 406,000) (1.05)^6}{812,000 \times 8,760 \times 0.75 \times 0.001}$$

= 122.1 mills/kWh

COE: Pulsed, Constant Dollars

$$\text{COE} = \frac{384,440,000 + (19,407,000 + 7,665,000 + 355,000)}{849,000 \times 8,760 \times 0.75 \times 0.001}$$

= 73.8 mills/kWh

COE: Pulsed, Then-Current Dollars

$$\frac{768,270,000 + (19,407,000 + 7,665,000 + 355,000) (1.05)^6}{849,000 \times 8,760 \times 0.75 \times 0.001}$$

= 144.3 mills/kWh

These values of COE are compared to those for STARFIRE in Table 6-24 along with other parameters which determine the final COE. It should be noted that the cost of the Reactor Plant Equipment is more than 50% higher than STARFIRE for the steady-state version and 100% higher for the pulsed versions. However, the total plant capital cost did not rise in that proportion (only by 28% and 60%). The lower power outputs for both versions, however, drastically increase the cost of capacity (by 87% and 123%). The

Table 6-24. Economic Comparison of STARFIRE and WILDCAT

Parameter	STARFIRE	WILDCAT	
		Steady State	Pulsed
Plant Capacity, MW	1200	812	849
Cost of Reactor Plant Equipment, M\$	969	1497	1889
Total Capital, Constant M\$	2400	3077	3844
Then-Current M\$	3198	4099	5122
Cost of Capacity, Constant \$/kWe	2000	3788	4528
Then-Current \$/kWe	2665	5048	6033
COE, Constant mills/kWh	35.1	62.8	73.8
Then-Current mills/kWh	67.1	122.1	144.3

same factors are also the key reasons for the COE being increased by 79% and 110% over the STARFIRE COE.

REFERENCES

1. C. C. Baker, et al., "STARFIRE - A Commercial Tokamak Fusion Power Plant Study," Argonne National Laboratory, ANL/FPP-80-1 (1980).
2. S. C. Schulte, et al., "Fusion Reactor Design Studies - Standard Accounts for Cost Estimates," Pacific Northwest Laboratories, PNL-2648 (1978).
3. S. C. Schulte, et al., "Fusion Reactor Design Studies - Standard Unit Costs and Cost Scaling Rules," Pacific Northwest Laboratories, PNL-2987 (1978).
4. B. W. Reed, et al., "Preliminary Report on the Development of RF Auxiliary Heating System for TEPR-1," Princeton Plasma Physics Laboratory, PPPL-1410 (1977).
5. "Guide for Economic Evaluation of Nuclear Reactor Plant Design," NUS Corporation NUS-8531 (1980).

Section 7

SAFETY ASSESSMENT



7. SAFETY ASSESSMENT

A preliminary study of the safety and environmental aspects of the WILDCAT design is presented in this chapter. The objective is to identify the safety issues pertaining to WILDCAT, to assist with design tradeoffs, and to ensure that safety considerations are incorporated in the conceptual design. While a detailed safety analysis is beyond the scope of this study, safety considerations have been considered in deciding key material and design choices for WILDCAT. This design follows many of the safety-related precedents which were established in the STARFIRE conceptual design.¹ Wherever it is appropriate, comparisons or distinctions are made between the two designs.

Fusion power will have several significant safety advantages compared to current methods of generating electricity. The nuclear aspects of safety are decidedly improved when compared to fission reactors. The problems of accidental criticality and of prompt criticality are not applicable. Prospects and consequences of a loss-of-coolant accident are considerably less. The biological hazard of radioisotopes in the plant is much lower. Radiation doses to the general public due to routine or accidental releases of radioactivity are also reduced. Generally, the concerns regarding protection against diversion of weapons-grade material, such as plutonium or ^{235}U are eliminated. Radioactive waste storage and/or disposal requirements are less complicated due to the absence of fission products and actinides.

Fusion, like fission, does not involve combustion of hydrocarbons in air; thus the routine chemical releases are much lower than for fossil power plants. The dangers due to fuel mining and other associated activities including transportation are greatly reduced.

The public risk associated with different energy production concepts must take into account the total fuel cycle. In this regard utilizing CAT-D for fuel in fusion reactors should make such reactors preferable from the standpoint of fuel resources and transportation considerations. The deuterium involved is not radioactive. Only the initial, start-up requirements of tritium (approximately 12 g) need to be shipped to the plant.

The incorporation of safety into the design at the conceptual stage is done to ensure that the environmental and safety advantages inherent in fusion are fully realized. The emphasis on safety must include concern for the gen-

eral public, the plant personnel, and the plant itself -- generally in that order.

The primary approach in this safety assessment is based on deterministic methods, rather than on probabilistic methods. It is not possible to do a quantified probabilistic risk assessment at this time, due to lack of sufficient design detail, statistical operating data, and physical models pertaining to hazard rates.

This chapter addresses the specific issues of concern and how they were solved or resolved in Sec. 7.1. The methodology of the safety analyses is briefly described in Sec. 7.2. The accident-related dose rate due to corrosion products in the primary coolant loop is given in Sec. 7.3. Tritium dose rates are shown in Sec. 7.4. The engineered safety features of the WILDCAT design are described in Sec. 7.5. The basic conclusions are reiterated in Sec. 7.6.

7.1 Issues of Concern

Induced Activity -- There will be induced radioactivity in the first wall, blanket, and shield materials. No mechanism which would cause melting of the structural material has been identified as being credible. Since there is a massive bulk shield around the blanket, the likelihood of this activity becoming mobile in the event of a major loss-of-flow accident, even without plasma shutdown, is not considered to be credible. Nevertheless, some of this induced activity in the form of corrosion products imposes constraints on access for maintenance and repair activities on the reactor internals, and therefore it has a strong influence on the design of the reactor and the choice of structural materials. This radioactivity, though not present at the beginning of reactor operation, increases with time and reaches a significant level for access considerations after only a few days of operation.

The amount of decay heat which would need to be dissipated following reactor shutdown has been calculated and is shown for the total system in Table 7-1 for the three primary regions (beryllium-coating, first wall, and blanket) in Table 7-2. The first table indicates that the total system decay heat of 39 MW at the time of shutdown in WILDCAT is less than half the value determined for STARFIRE. This difference becomes even greater at longer times after shutdown. Thus, the cooling of WILDCAT during maintenance or in the

Table 7-1. System Decay Heat in WILDCAT Versus STARFIRE

Time After Shutdown	Decay Heat (MW)		Fraction of Operating Nuclear Power ^b (%)	Fraction of Operating Total Reactor Power ^c (%)
	WILDCAT	STARFIRE	WILDCAT	WILDCAT
0	39	88	2.6	1.3
1 min	36	70	2.4	1.2
10 min	33	65	2.2	1.1
1 hr	27	61	1.8	0.92
6 hr	11	52	0.70	0.36
24 hr	4.7	39	0.32	0.16
1 week	4.2	14	0.28	0.14

^aIntegral neutron wall load before reactor shutdown: 9 MW-y/m².

^bTotal operating nuclear power: 1506 MW.

^cTotal operating reactor power: 2915 MW.

^dThe STARFIRE design with the Zr₅Pb₃ neutron multiplier.

Table 7-2. WILDCAT Zone Average Heating Rate (MW/m³)

Time After Shutdown	Beryllium Coating	First Wall	Blanket
During Operation ^a	6.9(0)	1.1(1)	2.6(0)
0	2.0(-1) ^a	1.7(-1)	7.0(-2)
1 min	2.2(-2)	1.5(-1)	6.5(-2)
10 min	2.0(-2)	1.4(-1)	6.1(-2)
1 hr	1.7(-2)	1.1(-1)	4.9(-2)
6 hr	7.9(-3)	4.6(-2)	1.9(-2)
24 hr	4.7(-3)	2.2(-2)	8.7(-3)
1 wk	4.3(-3)	1.9(-2)	7.6(-3)

^aIntegral neutron wall load before reactor shutdown: 9 MW-y/m².

^bReads as 2.0 × 10⁻¹.

case of an accident should be easier than for STARFIRE. The second table shows the zone-average heating rate during operation due to decay heat after shutdown.

Thus, the associated after heat is small, only about 1.3% of the operating thermal power at the beginning of shutdown, and drops to about 0.14% after

one week. These values of afterheat are much less than those of a pressurized water reactor of comparable generating capacity and are distributed over a much larger volume, thus easing the problem of ensuring adequate cooling in the case of emergency shutdowns.

For WILDCAT special effort was given to the selection of materials in order to minimize both long-term radioactivity in all components outside the blanket and to minimize rad-waste storage. The reactor is also designed to be accessible within 24 h after shutdown, even though completely remote operations are planned for all maintenance.

Pressurized Water Coolant -- Pressurized (~2200 psig) water is used as primary coolant. The minimum subcooling is that which exists at the outlet of the first wall and amounts to ~30°C. In the event of sudden loss of pressure, due either to a pipe break or due to failure of the primary coolant pumps, the coolant would flash into steam. This steam, if allowed to escape into the plenum region, would raise the temperature and pressure in the vacuum boundary. Such an environment in the vacuum vessel could act as a cause for a common-mode failure. (Common-mode failures are those in which some single event prevents multiple and identical components from performing in accordance with design.)

Loss-of-Flow-Accident -- The pressurized water coolant for removal of heat in the first wall and blanket is subcooled to a minimum of 30°C. In the event of a loss-of-flow accident such as a loss of pumping power or a loss of pressurization, if the plasma were not shut down, the coolant would go into nucleate boiling and subsequently to film boiling and would then burn out. Although the first wall and the blanket have a large thermal inertia, if the plasma were not shut down within a short time of occurrence of loss of flow, ablation of the first wall beryllium coating would occur and would extinguish the plasma. The decay heat is not sufficient to cause melting in the WILDCAT design. The two independent primary coolant loops have been incorporated in the WILDCAT design in order to significantly reduce the likelihood of either complete loss-of-flow or loss-of-coolant accidents.

Loss-of-Coolant Accident -- A condition which is even more critical than a loss-of-flow accident is a loss-of-coolant accident. Such an event could result from a pipe break, an inadvertent valve closure, or a coolant tube blockage. If the loss of coolant were due to a break in the first wall

panels, the coolant would interfere with the plasma and extinguish it. If the break were internal to the blanket, adequate detection would be needed to discern from which of the two cooling loops the leak were occurring, and the plasma would have to be extinguished as quickly as possible. The blanket module walls are not designed to withstand primary coolant system pressure, so adequate relief valves must be incorporated into the vacuum plenum boundary. The leakage must be detectable: such a break could possibly cause a small amount of tritium to escape into the reactor building and possibly into the environment in the event of a common-mode failure of the reactor building. The hypothetical break could also occur outside of the reactor in the headers, piping, and valves of the primary coolant system, and even in the tubes in the steam generator. In the event such an accident occurred within the reactor, the reactor would have to be repaired before it could be put back into operation.

Tritium -- On the average the steady-state tritium inventory in WILDCAT would be about 120 Ci/MWth, or 36 g for 2915 MWth. Of this amount 0.40 Ci/day would accumulate in the primary cooling water. Details about the tritium in the coolant are given in Sec. 5. Being an isotope of hydrogen, tritium has a high permeability in most materials, especially at high temperature, and is therefore difficult to contain. If the design is inadequate, tritium would permeate through walls from one region of the system to another and could reach the environment by many different paths. Thus, there exists a potential for continuous release of tritium both as tritium gas (T_2) and tritiated water (HTO and T_2O). Pulsed releases of tritium are also possible as a result of system failure, accidents, and fires.

The WILDCAT design effort to reduce the problems associated with tritium has involved attempting to minimize the tritium inventory in the vacuum pumps and fueling systems and using triple barriers wherever practical. The use of a limiter/vacuum system greatly reduces the tritium throughput, and hence, inventory of the fuel handling system. In addition, the use of parallel, redundant systems has reduced the maximum tritium accidental release in a single event to 0.56 g.

The startup tritium requirements for WILDCAT are much less than those for STARFIRE (12 g vs. 10 kg). Thus, one LP-50 shipping container should be adequate to ship the tritium to the plant.

Cryogenic Liquid Helium -- Liquid helium is used for maintaining cryogenic temperatures of the superconducting TF, OH, and EF coils, and also in the cryopumps. In the event of a helium pipe break, the liquid helium would be spilled into the reactor building, which is maintained at slightly negative differential pressure. Then the liquid helium would flash into a two-phase vapor liquid mixture. The presence of helium extracts the heat from reactor structures and causes thermal strains in the structures and in the pressurized water coolant piping. Although the volume of the reactor building is large, a certain degree of pressurization results from the production of helium vapor, and the design must ensure that this does not exceed the design pressure of the reactor building. Thus, spilling of liquid helium into the reactor building represents a potential cause for a common-mode failure of the reactor. Furthermore, if the superconducting coils are in operation, the loss of helium would drive the conductor(s) normal. Because the coils are wound in series and are in a common dewar, this event should not lead to an accident scenario.

Mechanisms and redundancy to prevent cryogenic failures and magnet accidents have been employed in the WILDCAT design.

Plasma Disruption Onto the First Wall -- When the plasma comes into sudden contact with the first wall, the plasma deposits its kinetic energy (~8.3 GJ), which is about ten times greater than the value for STARFIRE, on a part of the wall. Such a deposition of energy at a very rapid rate could cause ablation of the wall coating material in a very short time (milliseconds) over a thickness on the order of the penetration length of hot ions.

Various plasma shutdown modes have been developed to prevent plasma disruptions (see Appen. B), but disruptions are a potential problem for WILDCAT. The principal safety problem would be cleanup of the water and corrosion products if a first wall were to fail.

Hydrogen Detonations or Explosions -- Deuterium and tritium as isotopes of hydrogen are susceptible to combustion and detonation. The typical range of concentrations for which hydrogen is flammable in air are from 4 vol-% up to 75 vol-%. Hydrogen detonates in air at values from 18 to 50 vol %.¹ Thus, deuterium and tritium gas handling systems have to be designed to prevent air in-leakage or gas out-leakage that would result in hazardous concentrations. In order to reach the explosive limit in a large capacity reactor building, large quantities of hydrogen isotopes would have to be released. However,

small pockets of an explosive mixture could be formed in a confined volume immediately adjacent to a D₂ or T₂ leak. Hydrogen explosions represent potential, but low probability, causes for common-mode failure of WILDCAT.

RF Heating — A preliminary assessment has been made of the biological hazard due to the rf heating system. There should be no rf leakage unless there is a crack in the rf plumbing. The effect of such a crack would be readily detectable from changed system behavior. The permissible exposure to rf waves is 10 MW/cm². In addition, rf generation requires high voltages, which produce X-rays as well as other hazards associated with high voltages.

Stored Energy in the Magnets — The amount of inductive energy stored in the various magnet systems is quite large. The values which have been calculated are shown in Table 7-3. (Refer to Chap. 4 for more details about the magnets.)

Table 7-3. Inductive Energy Stored in WILDCAT and STARFIRE Magnet Systems

System	Energy Stored (GJ)		
	WILDCAT		STARFIRE
	(Steady State)	(Pulsed)	(Steady State)
TF Coils	192.	179.	50.
OH Coils	0.415	20.	1.1
EF Coils	20.9	21.6	10.4

7.2 Methodology of the Safety Assessment

The safety assessment of the WILDCAT design draws upon experiences from other technologies, such as the fission reactor industry, and upon earlier assessments of conceptual fusion reactor designs including STARFIRE.¹⁻⁶ At the present time there are basically two methods of analysis employed in the safety evaluation of fission reactors, the deterministic method and the probabilistic risk assessment method. These are not really two distinct methodologies, but rather they are complementary techniques for conducting a safety analysis. Only the deterministic method has been utilized in the WILDCAT study.

Historically, the deterministic method of safety analysis has been employed first in the licensing of fission power reactors, and it can be thought of as the conventional method. In the deterministic method of safety analysis the reactor plant is first studied to identify what conditions can lead to accidents that can cause harm to the public.

The advantage of the deterministic method of safety analysis is that it provides an evaluation of the worst situations. The disadvantage is that the method has become somewhat formalized in the selection and treatment of potential accidents, and therefore, does not consider the wide range of possible accident cases of relatively low consequence, but of relatively high probability.

7.3 Accident-Related Dose Rates Due to Corrosion Products

The induced radioactivities in the first wall and the structural materials in the blanket and shield are major sources of radioactivities in commercial fusion power plants and could produce an important contribution to the dose rate if they were capable of being released in an accident. However, no mechanisms have been found which could mobilize the radioactive structural materials in the first-wall/blanket other than corrosion and erosion in the coolant passages. Also, no mechanisms for volatilizing corrosion and erosion products has been found.

The accidental release of radioactivity induced in the coolant per se is not considered to be a problem with water coolant because the isotopes formed have such short half-lives, e.g. ^{16}N (7.2 s), ^{17}N (4.2 s), ^{19}O (29.0 s).

The structural material selected for WILDCAT is PCA (primary candidate alloy), which is a titanium-modified Type 316 stainless steel. This portion of the safety study relates to the use of realistic alloy compositions, including typical impurities, and the use of appropriate neutron fluxes and energy spectra for a detailed first-wall/blanket design. The compositions used in the calculations are given in Table 7-4.

The specific activities (Ci/MWth) of these alloys have been calculated for several design conditions both during reactor operation (from 1 s to 2 y) and following reactor shutdown (from time zero to 1000 y). The computation for the radioactivity-related parameters, such as biological hazard potential

(BHP) and decay β/γ spectrum, has been performed by using the RACC⁷ code in conjunction with the associated data libraries. (See Sec. 3.2. for more information on those calculations.)

Table 7-4. Structural Material Composition: PCA Versus Type 316 Stainless Steel

Element	Stainless Steel			
	PCA		Type 316	
	wt-%	atom/b-cm	wt-%	atom/b-cm
B	0.005	2.188(-5)		
C	0.050	1.971(-4)	0.058	2.286(-4)
N	0.010	3.380(-5)	0.007	2.366(-5)
Al	0.030	5.264(-5)		
Si	0.500	8.427(-4)	0.460	7.752(-4)
P	0.010	1.528(-5)	0.026	3.974(-5)
S	0.005	7.382(-6)	0.011	1.624(-5)
Ti	0.300	2.965(-4)	0.040	3.953(-5)
V	0.100	9.292(-5)		
Cr	14.000	1.274(-2)	16.700	1.520(-2)
Mn	2.000	1.723(-3)	1.430	1.232(-3)
Fe	64.880	5.499(-2)	64.440	5.462(-2)
Co	0.030	2.410(-5)	0.030	2.410(-5)
Ni	16.000	1.290(-2)	13.900	1.212(-2)
Cu	0.020	1.490(-5)	0.060	4.470(-5)
As	0.020	1.264(-5)		
Nb	0.030	1.529(-5)		
Mo	2.000	9.868(-4)	2.840	1.401(-3)
Ta	0.010	5.453(-10)		

Since the corrosion products in the primary coolant loop have been identified as the most likely means by which activated structural material in the WILDCAT reactor could be released into the reactor building in the case of a hypothetical accident, the nature of the corrosion products has been studied. An evaluation of the importance of corrosion products in the WILDCAT primary coolant is presented. Included for consideration are the appropriate water chemistry conditions, necessary control equipment, and the associated corrosion product inventory and distribution. Although the data base for water corrosion of reactor materials is generally more extensive than for any other potential fusion reactor coolant, some information is still lacking. Even though WILDCAT has stronger magnetic fields than STARFIRE, the influence of

magnetic fields on the corrosion process has been determined to be minor, provided that proper water chemistry conditions are maintained.

The proper water chemistry operating conditions have been determined to be as follows: pH @ 25°C ~ 9.5; ~5 ppb of O₂; ~5 ppm of H₂; ~0.22 to 2.2 ppm of ⁷Li from LiOH; and 0 to 1500 ppm of boron from boric acid. The WILDCAT optimum conditions are similar to those for pressurized water reactors.

In Appendix G of the STARFIRE final report¹ the methodology was presented for calculating the activity levels in the coolant, the deposits on the tube wall, and the transport of the corrosion products. The total potentially releasable corrosion products from a loss of coolant accident (LOCA) in WILDCAT have been estimated for three different cases. The upper bound release estimate is obtained by assuming that the coolant in one of the two independent primary coolant loops as well as the entire outer surface oxide layer is released into the reactor building during the LOCA. The mass of corrosion products involved would be 36 kg, and the associated activity would be 2700 Ci. This corresponds to <0.001% of the total blanket radioactivity inventory. It is difficult to determine what fraction of the mobilized corrosion product material could reach the environment by leaking from the reactor building; however, deposition and settling should decrease the material by about a factor of 10. Thus, the maximum corrosion product release to the environment is probably 0.0001% of the blanket activity inventory. If the break were to occur within the reactor itself, the bulk of the corrosion products would likely be contained within the shield. Thus, numerous barriers exist.

The dominant difference between the WILDCAT and STARFIRE designs is the decrease in the structural activity for WILDCAT. The structural activity is approximately a factor of 10 lower for WILDCAT.

Using the same assumptions as were made in STARFIRE, the maximum release in Ci (by isotope) would be:

⁶⁰ Co	85
⁵⁵ Fe	2037
⁵⁴ Mn	144
⁵⁸ Co	123
⁵⁹ Fe	5
⁵¹ Cr	170
⁵¹ Mn	158
Total	2722

The atmospheric dispersion of structural material has been examined for an accident based on a short-term uniform release from a point source. This simple type of model has been utilized to determine external doses due to structural material. The materials as corrosion products have been assumed to be partially mobilized by a hypothetical reactor accident, leak from the reactor into the reactor building, leak out of the reactor building, and then be dispersed in a Gaussian plume. Regulatory Guide 1.4⁸ methodology and worst case conditions (such as Pasquill Type F, average wind velocity of 1 m/s, and a ground-level release) have been used. Long-term, ingestion-type effects have not been included.

It has been assumed that because of the nature of the reactor design and the driving forces that would be involved in accident scenarios, the release fraction of structural material into the containment would be only 0.001% of the structural material activity based on the assumption that corrosion product release is the pathway. The leakage rate from the reactor building is assumed to be 0.1 vol-%/day for the post-accident pressurization condition.

The external doses due to structural material dispersion are shown in Fig. 7-1. These doses are based on extremely conservative assumptions and are for ground-level exposures at the centerline of the plume. The NRC guideline is 20 rems whole-body dose in 2 h following an accidental release of radioactive material.⁹ This guideline translates to an average value of 2.78 mrem/s, which is more than three orders of magnitude higher than the highest doses shown in Fig. 7-1. This is one of the values used to establish the tentative exclusion radius at the construction permit stage; 25 rem is used for the final determination of the exculsion boundary at the operating license stage. Even with these conservative assumptions, the releases and calculated doses are far below current limits.

7.4 Tritium Dose Rates

The details regarding the calculation of tritium dose levels for WILDCAT are presented. All tritium processing pipes and components are designed with at least double containment walls. The buildings containing tritium inventory all have leak-resistant steel liners. Thus, there are numerous barriers to tritium leakage.

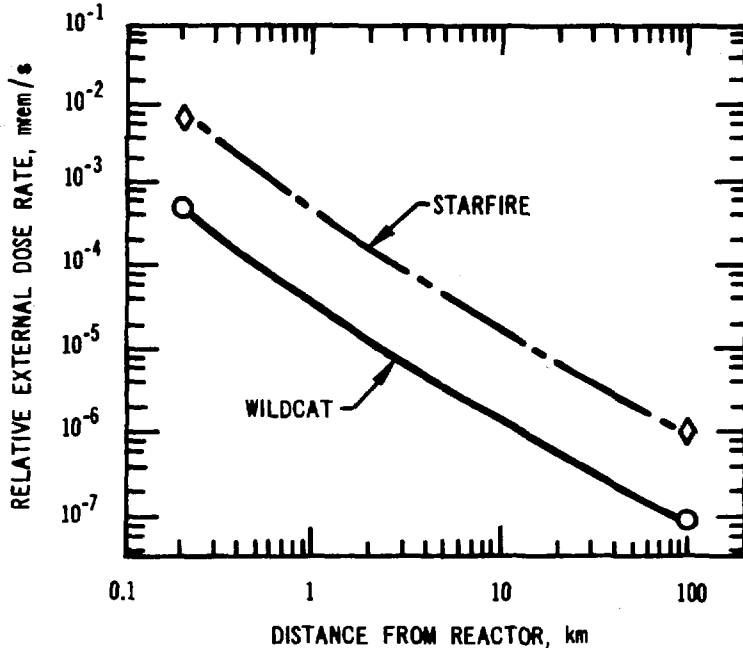


Fig. 7-1. External dose rates due to an accidental release of corrosion products.

The ease of handling tritium for WILDCAT has been generally improved compared to that for STARFIRE¹ because the tritium inventory is approximately two orders of magnitude lower, even though the tritium handling systems are similar for both designs. The tritium startup requirements are much less -- 12 g for WILDCAT vs. 10 kg for STARFIRE. STARFIRE, being a D-T fueled device, requires lithium as a breeder. A solid breeder material LiAlO₂ was selected for several reasons. That material may (significantly) increase the amount of tritium contained in the blanket. Table 7-5, which compares the design goals for tritium handling, illustrates the similarities and differences between the two designs. The concentration of tritium in the primary cooling water is expected to be sufficiently low that there will be no need to process it.

Another consideration is the maximum potential release of tritium due to an accident. In the case of STARFIRE that value was 10 g. For WILDCAT the maximum amount of tritium which would be held at any time on the cryopumps is 0.56 g. It is that portion of the tritium inventory which is considered to be the maximum which would be released in case of an accident. In this case the maximum release of tritium for WILDCAT is approximately one-twentieth of that

Table 7-5. Design Goals for Tritium Handling

Specific Goal	WILDCAT (Ci/d)	STARFIRE (Ci/d)
Permeation through first wall	0.21	10
Generation due to ⁷ Li corrosion inhibitor	0.19	1
Total tritium into coolant	0.40	11
Leakage across the steam generator	0.20 ^a	10 ^b
Fuel reprocessing	0.01	1
Tritiated solid waste	0.01	1
Building leakage	0.10	1
Total tritium into the environment	0.32	13

^aOr 6.6 mCi/l.

^bOr 0.3 Ci/l.

for STARFIRE. The doses to the public would be reduced proportionally. Even the amount of tritium contained on the distillation columns in the tritium handling facility is only 0.2 g for WILDCAT (or 13 g for the pulsed version) compared to 50 g for STARFIRE.

The methodology used in calculating tritium doses was presented in Appen. B of the final STARFIRE report¹ and is not repeated here. The major assumptions are as follows. Chronic exposures to the public are calculated on the assumption the intake is by inhalation and by absorption through the skin. The maximum dose is 1.4 mrem/y for routine releases of 117 Ci/y when the releases are at ground level. However, since much of this routine emission is expected to occur through the cooling towers, the maximum dose is much less. Acute exposures to the public due to an accidental release of up to 5600 Ci (0.56 g) of tritium also have been determined. A maximum acute dose of 4.0 rem occurs at 200 m from the reactor building. No building wake effects have been considered. It must be noted that no credit was taken for containment of the released tritium by the reactor building. Thus, the release of 0.56 g outside the reactor building is a very conservative number.

A comparison of the effects of exposure to tritium gas and to tritium oxide (HTO or T₂O) has been made. In general, the hazards due to the gas are

far less, so all of the tritium is assumed to be oxidized as a conservative estimate. Various mitigating factors have been suggested by which the doses could be reduced.

Tritium exposures to plant personnel have also been calculated. Any persons going to either the reactor building or the tritium facility are anticipated to be in anti-contamination suits. Even in an atmosphere in which there is a maximum permissible concentration of tritium for workers ($5 \mu\text{Ci}/\text{m}^3$), the dose rate to a worker without an anti-contamination suite would only be 1.3 mrem/h. In case of an accidental release of 0.56 g of tritium while an unprotected worker is in the reactor building, the acute dose rate would be 4.5 rem/h. A similar release in the smaller tritium building would be much higher (96 rem/h).

The long-term effects of tritium releases on the public have also been evaluated. Ingestion of contaminated food or drinking water in which tritium is taken up directly or through food chain transfer is considered and found to be minor when compared to inhalation or skin absorption.

An estimate of the world-wide population dose due to tritium releases to the environment for 100 WILDCAT-type reactors each releasing 0.32 Ci of tritium per day has been studied. The world dose is predicted to be from 0.026 to 0.038 mrem/y (one-fortieth of the value for STARFIRE).

The risks from tritium releases in transportation accidents and from tritiated solid waste disposal have been assessed and have not been found to significant.

7.5 Engineered Safety Features

The conceptual design of WILDCAT incorporates a number of features that have been previously adopted for STARFIRE in an attempt to reduce or eliminate various safety problems. Several of the most important safety features are discussed in the following sections.

7.5.1 Inerting the Reactor Building Atmosphere

If air were used as the atmosphere in the reactor building of WILDCAT, it would become activated due to the production of ^{14}C , ^{16}N , and ^{41}Ar . The ^{14}C and ^{16}N are due to (n,p) reactions with ^{14}N and ^{16}O , respectively, and the

^{41}Ar comes from radiative capture, i.e., (n,γ) reaction, with ^{40}Ar . Candidate gases for the reactor building atmosphere are helium, nitrogen, and carbon dioxide. Helium has been eliminated from consideration based on the mass (30 tonnes) that would be needed of this resource limited material, the associated expense (which is expected to increase with time), and the leakage problems.

Calculations have been made to determine the activity levels in CO_2 and N_2 compared to air. With regards to the activation of the atmosphere within the reactor building, the results for WILDCAT are more or less comparable to the STARFIRE case. Table 7-6 shows the activation for several candidate gases. It is seen that air achieves a saturated activity within several hundred seconds after reactor startup, and after shutdown the air activation remains almost constant at 1.14×10^{-13} MCi/m^3 even beyond 1000 y. This long-term activation is due to the $^{14}\text{N}(n,p)^{14}\text{C}$ reaction and the long half life (5730 y) of ^{14}C . Thus, air should not be used for the WILDCAT reactor building atmosphere unless the atmosphere exchange for ventilation is much higher than has been assumed for these calculations.

Both CO_2 and N_2 could be considered for inerting the reactor building. The CO_2 activity dies away relatively quickly after reactor shutdown. The activity is less than the maximum permissible concentration (MPC) within a minute after shutdown. The rapid decay is due to ^{16}N which has a 7.1 s half life. The activity for N_2 gas is approximately 50% greater than the MPC for the general public. However, if the building atmosphere is partially ventilated periodically, the activity could be held below the MPC. The MPC's shown on the figure are those for the general public; the MPC's for workers are somewhat higher.

For post-accident considerations where a breach of the reactor building might be involved, a CO_2 atmosphere would seem to be preferable because it would not add to the inventory of potentially released radioactive material.

Inerting the reactor building with CO_2 offers several advantages. The possibility of a hydrogen fire or explosion is reduced, as is the possibility of a fire due to other combustible sources. Production of ^{14}C and ^{41}Ar is reduced. In addition, some components would last longer, building in-leakage should be easier to detect, and tritium removal from the CO_2 should not be a problem. The main disadvantages are that some components might have to be modified to operate properly, and there would be the added cost of the required CO_2 gas itself.

Table 7-6. WILDCAT Reactor Building Atmospheric Activation (MCI/m³)

	CO ₂	Air ^a	⁴¹ Ar	N ₂
<u>Operating time:</u>				
0	0.0 0.0	0.0	0.0	
10 ³ s	5.37(-13) ^b	1.21(-13)	1.0(-2)	3.24(-19)
10 ⁵ s	5.37(-13)	1.21(-13)	1.0(-12)	3.24(-17)
1 mo	5.37(-13)	1.22(-13)	1.0(-12)	8.52(-16)
6 mo	5.37(-13)	1.25(-13)	1.0(-12)	5.11(-15)
1 y	5.37(-13)	1.29(-13)	1.0(-12)	1.02(-14)
5 y	5.37(-13)	1.64(-13)	1.0(-12)	5.10(-14)
15 y	5.37(-13)	2.49(-13)	1.0(-12)	1.53(-13)
<u>Time After Shutdown</u>				
0	5.37(-13)	2.49(-13)	1.0 (-12)	1.53(-13)
1 min	1.67(-15)	1.29(-13)	1.0 (-12)	1.53(-13)
10 min	1.48(-19)	1.28(-13)	1.0 (-12)	1.53(-13)
1 h	1.48(-19)	1.28(-13)	1.0 (-12)	1.53(-13)
6 h	1.48(-19)	1.28(-13)	1.0 (-12)	1.53(-13)
24 h	1.48(-19)	1.28(-13)	negligible	1.53(-13)
1 wk	1.48(-19)	1.28(-13)		1.53(-13)
1 mo	1.48(-19)	1.28(-13)		1.53(-13)
1 y	1.48(-19)	1.28(-13)		1.53(-13)
10 y	1.48(-19)	1.28(-13)		1.53(-13)
100 y	1.47(-19)	1.27(-13)		1.51(-13)
1000 y	1.32(-19)	1.14(-13)		1.36(-13)

MPC: ¹⁶N: 3.0(-14), ¹⁶N: 3.0(-14), ⁴¹Ar: 4.0(-14), ¹⁴C: 1.0(-13)
(for the public).

^aDoes not include ⁴¹Ar activation.

^bReads as 5.37×10^{-13} .

7.5.2 Reactor Building Overpressurization Following a LOCA

Due to the fact that high-pressure water has been chosen as the primary coolant for WILDCAT and there is a substantial amount of radioactive material present in the reactor, as well as some vulnerable tritium (~0.56 g); a containment-type reactor building is still envisioned as necessary. It has a leak-resistant steel liner similar to the reactor building for STARFIRE.

The over-pressurization of the reactor building resulting from a primary coolant LOCA has been estimated on the basis of the similarities of WILDCAT coolant pressures and temperatures to those of present-day pressurized water reactors. For WILDCAT the reactor building volume is $\sim 2.9 \times 10^5 \text{ m}^3$, and the

coolant volume in each of two primary loops is 250 m³. The decision to locate the steam generators in the reactor building is based on safety considerations, e.g., fewer penetrations and larger building volume. Based on the scaling of a number of LWR accident scenarios, the differential pressure on the WILDCAT reactor building walls is 70 to 90 kPa (10 to 13 psig) depending on the location and nature of the coolant system break. Generally it is conceded that if a break occurs, especially in one of the coolant legs between the reactor and the steam generator, the entire inventory of one of the two loops would escape into the reactor building within 20 to 200 seconds. The two primary coolant loops in WILDCAT are designed to be independent.

The principal difference between the over-pressurization of a LWR (typically ~415 kPa or 60 psi) and WILDCAT relates to the larger volume of the building selected for the fusion device. The WILDCAT reactor building also has post-accident building isolation and internal heat removal systems, similar to LWR's. One engineered safety feature which should not be needed for fusion is a building spray system which is incorporated in LWR's to remove iodine from the building atmosphere and to limit pressures following a LOCA.

7.5.3 Ventilation Stack

The merits of incorporating a 100-m stack into the WILDCAT design are debatable. The value of having such a system in the STARFIRE design¹ was shown to be of some merit in handling larger quantities of accidental releases of activated corrosion products or tritium in order to reduce the radiation dose to the general public. In the case of WILDCAT, where the tritium accidental release has been calculated to be twenty times lower and the activated structural material somewhat lower, the need for a stack is reduced. For the purpose of a conceptual design -- considering the uncertainty in being able to direct all of the radioactive material which might be released in any variety of potential accidents into and up the stack (and in some instances not wanting to) -- it has been decided not to incorporate a stack.

7.6 Conclusions

To summarize the results of this safety assessment, no runaway-type accidents which would affect the public or the plant personnel have been identified. Although no method of generating electricity is capable of completely

eliminating environmental impact and risk to society, the application of fusion reduces the adverse effects and potential impacts to very low levels when compared to other methods.

The following sources of hazards have been identified in Sec. 7.1 for the WILDCAT design:

- Induced activity in the first wall, blanket, shield and magnet structural materials.
- Pressurized water primary coolant.
- Corrosion products in the primary coolant.
- Tritium inventory.
- Stored energy in the superconducting magnet system.
- Cryogenic liquid helium.
- Plasma disruptions.
- Rf heating.

The following potential accidents has been indentified for WILDCAT:

- Release of activated structural material in the form of corrosion products.
- Loss of flow to the first wall and/or blanket.
- Loss of coolant to the first wall and/or blanket.
- Tritium release, both in a continuous and a pulsed (e.g., startup and shutdown) mode.
- Loss of cryogenic liquid helium.
- Failure of the first wall due to a plasma disruption.
- Hydrogen detonations or explosions.
- Rf heating system failure.
- Stored energy in the magnets.

Materials have been selected in order to minimize long-term radioactivity in all components outside the blanket; those components represent over 90% of the total reactor mass. Efforts to reduce tritium-related problems have in-

volved attempting to minimize the tritium inventory and using triple barriers wherever practical. Two independent primary coolant loops have been incorporated to significantly reduce the likelihood of either complete loss-of-flow or loss-of-coolant accidents. Mechanisms and redundancy to prevent cryogenic failures and magnet accidents have been employed. Various plasma shutdown modes have been developed to prevent plasma disruptions from damaging the first wall. The rf heating system is designed such that it will not pose any problems due to rf leakage, high voltages, or X-rays.

The approach applied in this safety assessment has been based upon deterministic methods.

Although radioactivity is induced in the structural materials of the WILDCAT reactor, only radioactive corrosion products in the coolant are considered to be vulnerable to release into the reactor building in the case of certain, highly unlikely, accidents.

The nature of the corrosion products in the WILDCAT primary coolant loop has been assessed. The optimum operating conditions for the primary loop are similar to those for pressurized water reactors. The radioactivity of corrosion products which would be released according to the upper bound estimate corresponds to ~0.001% of the total blanket radioactivity inventory. The accident-related dose rates due to activation products are based on this information.

Tritium dose rates have been calculated for both routine and accidental tritium releases for both the public and plant personnel. The maximum dose to an individual is 1.4 mrem/y for routine releases of 117 Ci/y when the releases are at ground level. However, much of this routine release is expected to go through the cooling towers, resulting in a smaller dose for the individual. This can be compared with a typical dose of ~100 mrem/y due to natural background radiation. The maximum acute inhalation and skin absorption dose to the public, 4.0 rem from an accidental release of 0.56 g of tritium, occurs at 200 m from the reactor building. Workers unprotected by an anti-contamination suit could work in the reactor building or tritium facility, and their tritium dose would be 1.3 mrem/h with all shields in place. The reactor building maintenance, however, is designed to be fully remote. The long-term effects of potential tritium releases have been studied and found to be minor. The risks from tritium releases on a global scale, in transportation accidents,

and from solid waste disposal have each been evaluated and found to be insignificant.

A number of engineered safety features have resulted from safety-related decisions. These include inerting the reactor building, developing multiple emergency plasma shut-down methods, and providing for containment of the anticipated reactor building overpressure following a loss-of-coolant accident. A vent stack has been considered, but has been determined not to be necessary for the design.

Since fusion power is still in such an early stage of development, the licensing and regulatory requirements are difficult to predict. A fusion reactor has inherent features, including a lack of fission products and actinides and an absence of potential for runaway nuclear reactions, which strongly suggest that the commercial application of fusion power may avoid a lengthy and complicated licensing process. WILDCAT, although it utilizes some tritium as fuel, is characterized by much lower inventories of tritium.

Although this study does not involve a detailed environmental impact assessment, environmental issues have been considered in the design choices for WILDCAT. The materials requirements (for only the reactor portion) of 100 reactors based on the WILDCAT design have briefly been considered and compared to United States and world reserves and resources of elements. Tantalum and tungsten in particular are predicted to be potential resource problems; however, these are optional materials for the limiter and inner shield, respectively, and can be replaced by other materials.

No method of producing power in a central station on a commercial scale is without some environmental impact. However, it is felt that fusion will reduce the adverse effects and potential impacts to very low levels. The WILDCAT design should be representative of Cat-D fueled tokamak power plants in terms of environmental impacts. The environmental impacts should be similar in nature and magnitude to those of the STARFIRE design, except for the lithium resource requirement.

REFERENCES

1. C. C. Baker, et al., "STARFIRE - A Commercial Tokamak Fusion Power Plant Study," Argonne National Laboratory, ANL/FPP-80-1 (1980).

2. H. J. Willenberg, ed., "Workshop Proceedings: Safety and Environmental Aspects of Deuterium-Tritium Fusion Power Plants," Electric Power Research Institute, ER-821-WS (1978).
3. W. Häfele, et al., Fusion and Fast Breeder Reactors (IAEA, Vienna, 1977), Rev.
4. W. E. Kastenberg and D. Okrent, "Some Safety Considerations for Conceptual Tokamak Fusion Power Reactors," Electric Power Research Institute, EPRI-ER-546 (1978).
5. T. C. Chawla, "Preliminary Considerations of Safety and Reliability of Tokamak Experimental Power Reactor," Argonne National Laboratory, ANL/CTR/TM-73 (1976).
6. "Hybrid Reactor Safety Study: Annual Report," General Atomic Company, GA-A15578 (1979).
7. J. Jung, "Theory and Use of Radioactivity Code RACC," Argonne National Laboratory, ANL/FPP/TM-122 (1979).
8. "Assumptions Used for Evaluating the Potential Radiological Consequences of a Loss-of-Coolant Accident for Pressurized Water Reactors," U. S. Nuclear Regulatory Commission, Regulatory Guide 1.4 (June 1974), Rev. 2.

Appendix A

THERMAL STORAGE SYSTEM (PULSED VERSION)



Appendix A

THERMAL STORAGE SYSTEM (PULSED VERSION)

A preliminary design of a thermal storage system for the pulsed version of WILDCAT has been made in order to focus on the design problems, engineering implications, and costs for a system which sustains the thermal power to the turbine of WILDCAT during the shutdown, dwell, and start-up portion of its cycle. Toward this goal a number of thermal storage systems have been investigated including metals, ceramics, and heat transfer fluids, all of which appear less promising than the pressurized water/steam system described herein. It should be noted that this is a conceptual design which appears to satisfy all the apparent needs of the WILDCAT thermal storage in a safe and reliable manner using existing technology. However, additional detailed analyses are necessary to assure its viability, adequacy, and desirability from both the cost and operational viewpoints.

A.1 Thermal Storage System

The thermal storage system selected is shown schematically in Fig. A-1. This figure shows the components and methodology required for a stored energy steam supply to supplement and sustain the reactor steam supply to the turbine generator at the rated 2580 MWth gross during a zero power production period whose reference interval is 30 s. There exists some thermal storage within the reactor system which can be optimized and utilized to offset the losses during the reactor low-power period. This stored energy is estimated to be adequate to cover the shut-down and start-up periods (sectors A and C) in Fig. A-2, which shows a simplified diagram of the reactor power profile. The thermal storage supplies an amount of energy equal to sector B, although the energy is supplied over the entire low-power period. In the thermal storage system, pressurized water is stored just under saturation pressure (1600 psi) in large vessels, heated to high temperature by a side stream from the main reactor coolant system, and reintroduced into the steam generator inlet via a heat exchanger arrangement which separates the two systems.

When called upon, the storage vessels discharge steam flashed from the thermal storage into a high temperature turbine stage unit through a throttle valve. Steam leaving the high pressure turbine flows through the remaining

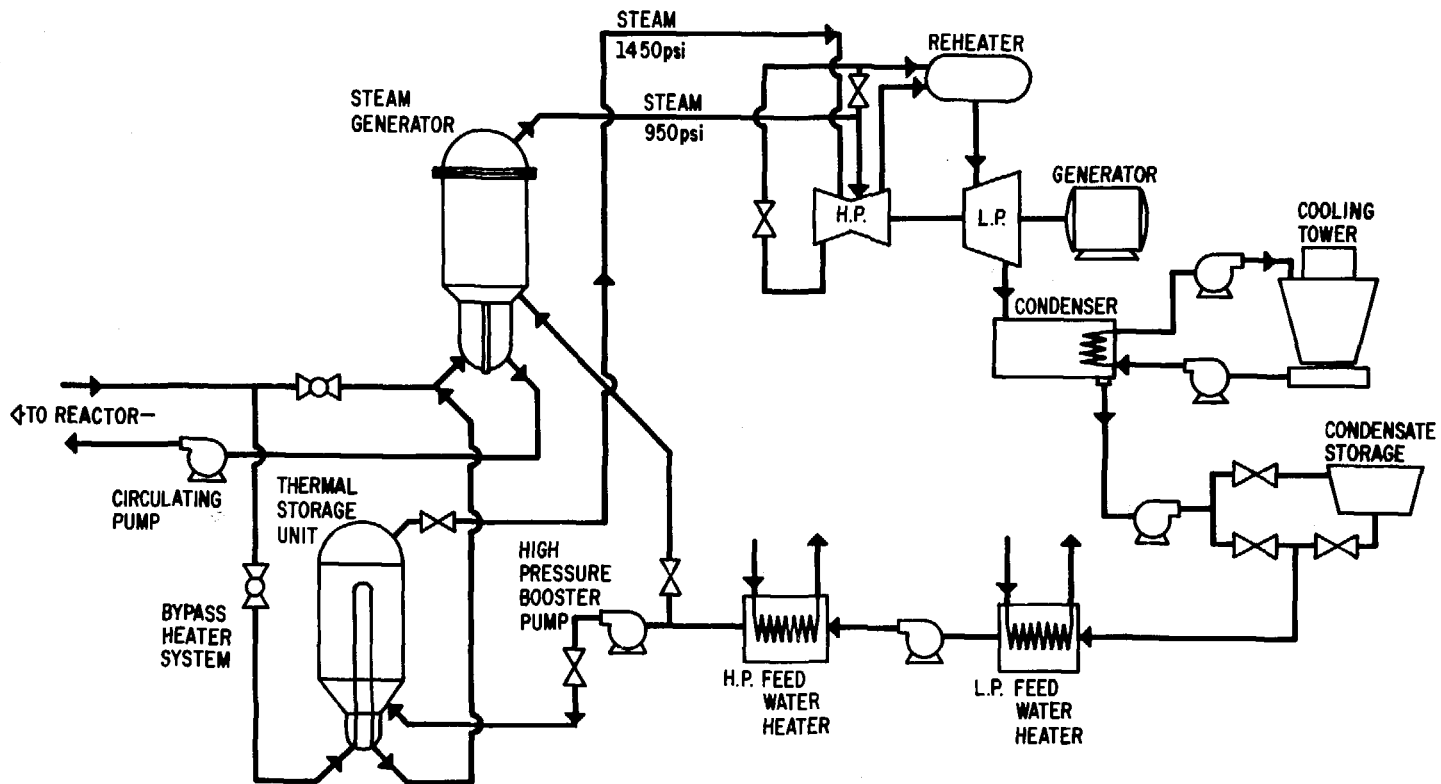


Fig. A-1. Conceptual design of the thermal storage system necessary for the pulsed version of WILDCAT.

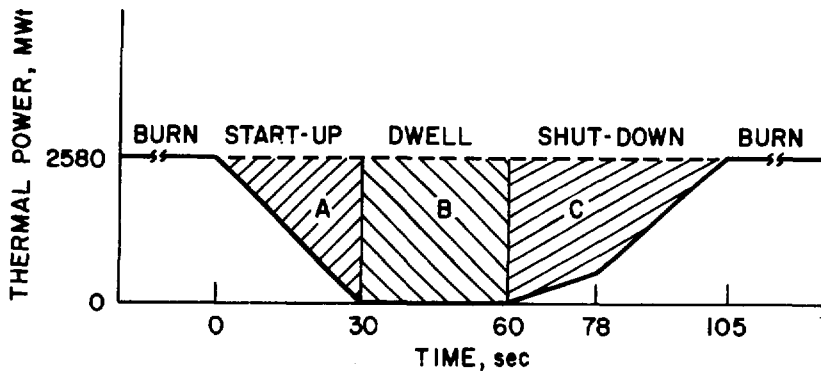


Fig. A-2. Reactor thermal power between pulses.

portions of the turbine until it reaches the condenser, where it is stored as liquid in low pressure tanks awaiting termination of the thermal storage operation. After the operation is over, a booster pump in series with the reactor steam generator feed water system recharges the thermal storage units with water and makes them ready for the next cycle. The thermal storage and the reactor steam systems are intermixed and feature the ability to operate concurrently. The reactor cooling system is continuous during all operations with only modest flow adjustments.

The system consists of six large thermal storage vessels with integral heat exchange coils (comparable to LWR steam generators), two booster pumps, a turbine stage capable of utilizing 1450-psi steam, low-pressure condensate storage tanks, valves, piping, and instrumentation and controls. The cost of the system is roughly estimated to be \$150 million dollars. Additional thermal storage capacity could be supplied at an estimated \$4.0 M/s of reactor downtime. This relatively expensive and complex system is needed only for pulsed operation. The fact that it is not needed for steady-state operation is one of the major benefits of steady-state operation.

A.2 Design Features

The major components along with some of the pertinent design features are:

Storage Vessels: These vessels operate at a pressure of 1600 psi and 310°C stored water temperature. They are approximately 13 m high and 3.3 m in diameter and contain an integral heating coil to carry the reactor primary coolant. The storage capacity is ~13 GJ (~12 × 10⁶ BTU).

Turbine: High pressure add-on stages to the present light water reactor type turbine are required. These stages are capable of taking steam during the thermal storage discharge at 1450 psi (vs. 950 psi for the reactor loop) and at a slightly higher temperature.

Condensate Storage: These are low pressure (~10 psi storage tanks fed from the thermal storage condenser through valving and level controls.

Booster Pump: A multi-stage booster pump of 950-1600 psi capacity is required to boost the side stream of preheated water from the boiler feed pumps into the storage vessels.

The above major components are well within the realm of existing technology and production. The system also has the following advantages:

- Low, if not lowest, degradation of overall power performance is obtained during all periods of the cyclic operation.
- The thermal storage system can be operated concurrently with the reactor system for matching reactor power ramps.
- Less stored energy is required than if the water were stored in the reactor primary coolant system.
- Relatively high deliverable specific thermal storage capacity is provided; i.e., there is no degradation caused by a heat transfer circuit.
- The thermal storage secondary loop is tritium free (as is the reactor secondary loop).
- Existing fabrication techniques are used for all components.
- The system can be used as a topping cycle.
- The system provides relatively low cost and safety in terms of other methods considered.

The major disadvantages of this system are apparent in the overall mass of material and number of components involved. This, however, is generic to all thermal storage systems contemplated for this purpose.

A.3 System Operation

A digest of the system operation is given as follows (refer to Fig. A-1):

Reactor Coolant System: The reactor coolant exits through a throttling valve allowing a side stream to flow into the thermal storage vessel heater controlled by a side stream throttling valve. After surrendering its heat to thermal storage (maximum temperature 310°C), the side stream returns to the steam generator inlet at a slightly degraded temperature, where it mixes with the main flow stream. The main coolant system continues to circulate at its normal flow rate at all times whether the reactor is operating or not. This is a safety advantage, as no major switching of the reactor primary coolant circuit is required. When the thermal capacity of the storage system is reached, the bypass flow is throttled to a low level, and the system is ready for operation.

Thermal Storage Operation: Assuming the system is filled at maximum temperature and ready to operate, the following events occur: A throttle valve at the outlet of the pressurized water thermal storage vessel (~1600 psi, 310°C) causes steam to be flashed and introduced to the high pressure head of the turbine (~1450 psi). The reactor system (950 psi) is throttled back as needed. Both systems deliver steam to the turbine, and both may be controlled using water level/pressure regulation as required for stability and safety. Steam discharge from the high pressure turbine then flows through successive turbine stages in a normal fashion with adjustment to reheat as necessary. Upon reaching the condensate receiver, the volume of water begins to mount and is then transferred to storage tanks until the thermal storage delivery cycle is completed. The above process continues until the end of the dwell cycle is complete, when the reactor loop again provides sufficient heat to control the steam supply. During the thermal storage delivery process most of the stored pressurized water is used, leaving only a required minimum accumulation for safe operation of the system components.

Thermal Storage Refill: At the termination of the thermal storage delivery cycle the vessels are refilled one at a time using the booster feed water pumping system, which adds water as needed from the condensate storage tanks. Once the thermal storage vessels are filled with preheated water, the reactor bypass heating valves are opened and the water is brought up to stored energy conditions ready for the next cycle.

Appendix B

PLASMA DISRUPTION EFFECTS



Appendix B

PLASMA DISRUPTION EFFECTS

Plasma disruptions are a potential problem for all tokamak reactors. Unfortunately they are not sufficiently well understood that accurate predictions of the plasma behavior can be made. For this reason it is difficult to assess the severity of the damage they might cause to the first wall or to determine how many disruptions a particular device could take. Since WILDCAT has substantially more stored energy (79 GJ, pulsed; 8.3 GJ, steady state) in the plasma than other devices such as STARFIRE¹ (1.0 GJ) or INTOR² (240 MJ), the effects are in any event substantially worse than for smaller devices. This appendix presents an assessment of the potential disruption problem for WILDCAT.

B.1 Disruption Characteristics

For the spatial energy deposition it is common to take the energy, U_p , stored in the plasma and to assume it is deposited on only a fraction, f_w , of the wall. In addition, the deposition over this fraction is not expected to be uniform, and the nonuniformity is represented by a peaking factor, p , in the one-dimensional calculations used to assess the response of the wall. The maximum energy deposited per unit area is then $J = pU_p / (f_w A_w)$, where A_w is the wall area. For WILDCAT the wall area is 1250 m². The energy deposition would be 630-660 J/cm² if spread uniformly over the whole wall and 6300-6000 J/cm² for a more realistic case with a peaking factor of 3 over 30% of the wall.

The temporal energy deposition is also not well known. More sophisticated models include a thermal quench and a current quench period, and various temporal profiles can be used. For this analysis the deposition is assumed uniform over the disruption time, Δt . A theory and a formula for the disruption time is given in Ref. 3 as:

$$\Delta t = 900 \mu s [R_0(m)^2 A_1(\text{amu}) n_1(10^{19} \text{ m}^{-3}) B_{t0}(T) a(m)^6 V(V)^{-3}]^{1/5},$$

where R_0 is the major radius, A_1 is the average ion mass, n_1 is the average ion density, B_{t0} is the toroidal field in the plasma, a is the minor radius,

and V is the plasma voltage. Independently of the validity of the theory, this formula gives a good empirical fit to existing devices for disruption times from $\sim 1 \mu\text{s}$ to $\sim 1 \text{ms}$.³ The predictions of this formula for the various periods in the WILDCAT burn cycle are shown in Table B-1 along with the energy deposition. The inductive voltage corresponding to the current change was taken for V except for the steady-state periods, where the resistive voltage was used.

There is little or no empirical information on disruptions in steady-state, rf-driven tokamaks. There may, in addition, be little reason to expect the theory of Ref. 3 to apply for steady-state devices. The same considerations may well apply to the flat-top portion of the burn cycle for the pulsed case. The prediction of the long disruption times ($< 100 \text{ms}$), then, may well be inaccurate, since they are extrapolations of both the current data and the current theory.

B.2 First-Wall Response Models

The energy deposited on the first wall during a plasma disruption can lead to vaporization of the surface regions, melting of the surface regions, and conduction of heat into the bulk material. The analyses for the materials responses are based on analytical models developed by Merrill^{2,4} and Hassanien.⁵ Both models determine the extent of wall melting by solving equations which define the net energy content in the wall resulting from the plasma disruption. Merrill's model solves the following energy equation for the first-wall material:

$$\rho \frac{\partial E}{\partial t} = q + \nabla \times k \nabla T ,$$

where:

- E = material energy in J/kg
- q = bulk heat rate density in W/m^3
- k = thermal conductivity in $(\text{W/m})/\text{K}$
- T = material temperature in K
- ρ = material density in kg/m^3 .

Table B-1. WILDCAT Disruption Times

	U_p (GJ)	A_i (amu)	n_i (10^{19} m^{-3})	V (V)	J^a (J/cm ²)	Δt (ms)
Pulsed version						
Ohmic heating period	0.2	2.0	5	21.4	150	3
Main heating period	7.9	2.2	20	4.2	6300	9
Steady-state period	7.9	2.2	20	0.02	6300	210
Steady-state version						
Ohmic heating period	0.1	2.0	2	2.6	50	8
Current inducement period	0.2	2.0	2	0.2	210	32
Fusion power ramp period	8.3	2.2	21	0.1	6600	74
Steady-state period	8.3	2.2	21	0.03	6600	200

^aAssuming a peaking factor of 3 with deposition on 30% of the wall.

This equation defines the time and space-dependent energy content of the wall material. Those wall regions predicted to have energies in excess of the amount required to melt the material represent the melt layer. A convective mass term is added to this equation to account for the moving boundary at the melt/vapor interface. Subsequent to each solution time interval, the mode structure at the back of the wall is restructured. This procedure conserves both mass and energy during the evaporation process.

The Hassanein model solves separate conduction equations for the solid and liquid phases:

Solid Equation

$$\rho_s C_s \frac{\partial T_s}{\partial t} - \nabla \times k_s \nabla T_s = 0$$

Liquid Equation

$$\rho_l C_l \frac{\partial T_l}{\partial t} - \nabla \times k_l \nabla T_l = 0,$$

where:

C = material specific heat in (J/kg)/K

T = material temperature in K

k = material conductivity in (W/m)/K

ρ = material density in kg/m³.

The subscripts s and l correspond to the solid and liquid phases. Two interfaces exist for this model: the solid/melt and melt/vapor interfaces. The equations needed to specify the propagation across these interfaces are the following energy balances:

Solid/Melt

$$-k_l \frac{\partial T_l}{\partial x} = -k_s \frac{\partial T_s}{\partial x} + \rho_s L_f (V_s/m)$$

Melt/Vapor

$$q_s(t) = -k_l \frac{\partial T_l}{\partial x} + \rho_l(T_v)L_v v_{m/v} + \sigma(T_v^4 - T_0^4),$$

where:

q_s = surface heat flux from plasma disruption in J/m²

L_f = material heat of fusion in J/kg

v = interface velocity in m/s

L_v = material latent heat of evaporation in J/kg

σ = Stefan-Boltzmann constant in J/K

The subscripts s/m, m/v, and v correspond to the solid/melt, melt/vapor, and vapor interfaces.

The solid/melt energy balance implies that the difference in the rate of energy conducted to the interface by the liquid phase and that conducted away from the interface by the solid phase produces melting. The rate of melting is proportional to the material density and heat of fusion. The melt/vapor energy balance provides the boundary condition for the liquid conduction equation through the conductive term. The rate that energy from the plasma disruption arrives at this interface is equal to the rate that energy leaves the interface due to vaporization, conduction, and radiation. The last term on the right-hand side of the equation represents the energy radiated away from the surface. The material emissivity has not been considered.

The Merrill and Hassanein models both consider the kinetics of surface evaporation. The Merrill model adopts the Schrage⁶ modified phase change relationship:

$$j = \left(\frac{M}{2\pi R} \right)^{1/2} \left(\Gamma \sigma_c \frac{P_v}{T_v^{1/2}} - \sigma_s \frac{P_s}{T_s^{1/2}} \right),$$

where

j = vaporization mass flux in (kg/m²)/s

M = vapor molecular weight in kg/mole

$P_{v,s}$ = vapor pressure, first-wall surface in N/m^2

$T_{v,s}$ = vapor temperature, first-wall surface in K

R = universal gas constant in $(J/kg)/mole\ K$

$\Gamma, \sigma_c, \sigma_e$ = condensation or evaporation multipliers.

The terms of this equation predict the rate of condensation and evaporation respectively. The melt surface temperature and pressure for the evaporation term are determined from saturation relationships and the predicted surface energy. These same properties for the condensation term are obtained from a solution of the vaporized-material transport equations. The boundary condition is that the surface heat flux for the first-wall energy equation is the difference of the incident plasma flux and the convective vapor energy flux (the product of vaporization rate and latent heat of evaporation).

The Hassanein model solves a similar equation for the evaporation process:

$$j_e(T_v) = (2\pi mkT_v)^{-1/2} \sigma_e P_s(T_v) .$$

The condensation term is based on transport calculations,⁷ which indicate that the condensation rate asymptotically approaches 20% of the evaporation rate after 20 collision times. The resulting net vaporization rate is determined to be:

$$j(t) = j_e [0.8 + 0.2 \exp(-t/\tau_R)] .$$

Vaporized material transport is addressed differently in these models. The transport of the vaporized material away from the first-wall surface for the Merrill model has been determined by a solution of the continuum theory conservation equations:

Conservation of Mass

$$\frac{\partial \rho}{\partial t} + \frac{\partial \rho u}{\partial x} = 0$$

Conservation of Momentum

$$\rho \left(\frac{\partial u}{\partial t} + u \frac{\partial u}{\partial x} \right) = \frac{\partial P}{\partial x} - \rho g_c \cos \theta$$

Conservation of Energy

$$\frac{\partial \rho E}{\partial t} + \frac{\partial \rho E u}{\partial x} = -P \left(\frac{\partial u}{\partial x} \right) + q ,$$

where:

u = vapor velocity in m/s

P = vapor pressure in N/m²

E = vapor energy in J/kg

q = vapor heat rate density in W/m³

ρ = vapor density in kg/m³.

The solution of these equations provides the required vapor temperature and pressure for the condensation term of the vaporization equation.

For the Hassanein model the influence of the vapor transport in the condensation term of the vaporization equation appears through the relaxation time constant, τ_R . With this time constant the asymptotic condensation flux reaches 98% of its asymptotic value after 20 collision times, and is given as:

$$\frac{1}{\tau_R} = 1.6 \times 2\pi^{1/3} \left(\frac{3}{4} \Omega \right)^{2/3} j_e ,$$

where Ω is the elastic scattering cross section.

The Hassanein model considers the effects of plasma attenuation by the vaporized material stream. The adopted approach for this attenuation is based on the premise that the vaporization of the quantity of material equivalent to the penetration depth of 10 keV ions in the solid phase provides vapor shield with an atom density sufficient to attenuate the incident plasma. As a result, the mechanism of wall heating changes from one of deposition of ions to radiation, and since this radiation is isotropic, only one-half is directed toward the wall so that the intensity of wall heating is one-half the

unattenuated value. The transition in intensity of heating is assumed to be linear with vaporized depth until the depth exceeds that of the original penetration depth of the ions.

B.3 First-Wall Response Analysis

Figures B-1 and B-2 compare the predicted melt layer thicknesses and vaporization depths for several materials as calculated with the Hassanein and Merrill models as functions of plasma energy density for disruption times of 5 and 20 ms. As can be noted, good agreement results for the case of no vapor shielding even though the modeling approaches differ. The predictions of melt layer thickness at 5 ms are in closer agreement than at 20 ms. The opposite is noted for vaporization depth. This would seem to imply that the different modeling approaches for vaporized material transport are a major contributor to this difference. Figures B-2 and B-3 illustrate the impact of the vapor shield. For stainless steel the vaporized depth decreases by approximately an order of magnitude, whereas the melt layer thicknesses are affected only slightly.

Figures B-4 through B-10 contain predictions of melt layer thickness and vaporized depth for beryllium, molybdenum, tungsten, and carbon. The results for beryllium and tungsten are from the Merrill model and as a consequence do not include the effects of vapor shielding. The results for melt layer thickness, Figs. B-4 through B-6, suggest that a maximum value exists for a given disruption time. This characteristic is a consequence of vaporization's becoming more predominant as energy density is increased. The vaporized depths in Figs. B-2 and B-7 through B-10 indicate that increased vaporization occurs as a result of decreased disruption times at a given energy density. A transition to a linear dependence of vaporized depth with energy density is noted.

Table B-2 summarizes the required energy densities to produce melting, one micron of vaporization, and the maximum melt layer thickness for the case of no vapor shielding. These points have been interpolated or extrapolated from Figs. B-1 through B-10. The results for stainless steel and beryllium are fairly similar with the differences becoming more pronounced at longer disruption times. This similarity is attributed to the fact that the total energy change (per unit mass) from the initial value of 573 K to vaporization

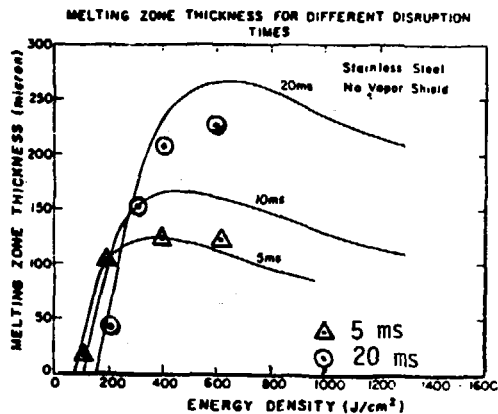


Fig. B-1. Stainless steel melting zone thickness with no vapor shield as a function of energy density. The curves are for the Hassanein model. The points are for the Merrill model.

MATERIAL EVAPORATED FOR DIFFERENT DISRUPTION TIMES

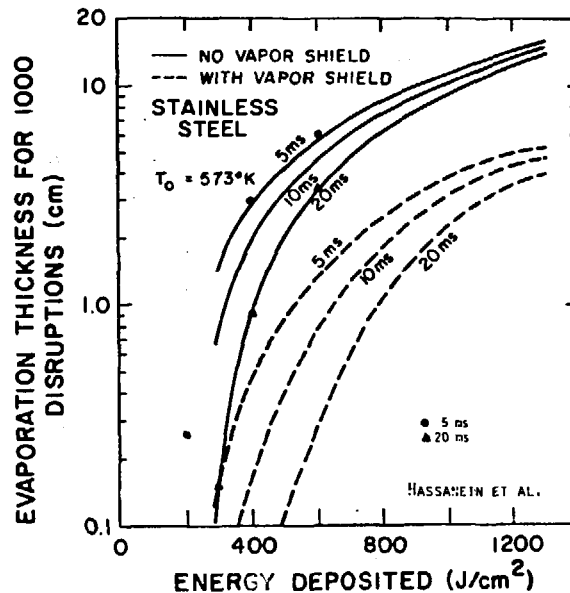


Fig. B-2. Evaporation thickness of stainless steel for 1000 disruptions for different energy deposited. The curves are for the Hassanein model. The points are for the Merrill model.

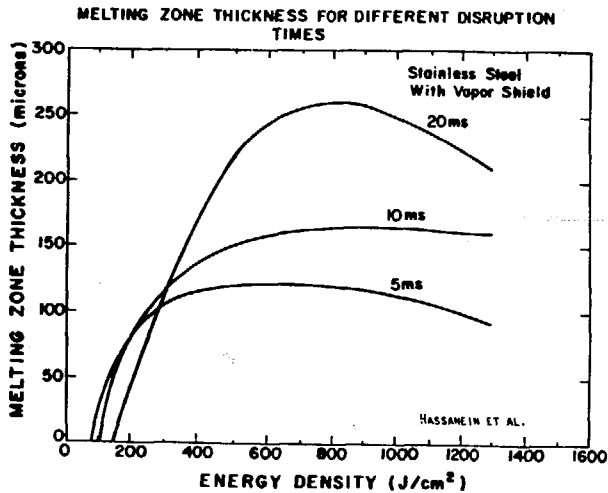


Fig. B-3. Stainless steel melting zone thickness with vapor shield as a function of energy density (Hassanein model).

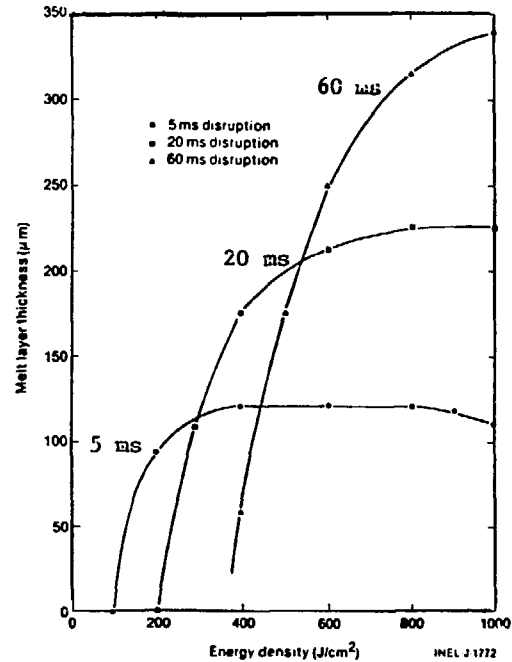


Fig. B-4. Beryllium maximum melt layer thickness for plasma disruptions of 5, 20, and 60 ms duration (Merrill model).

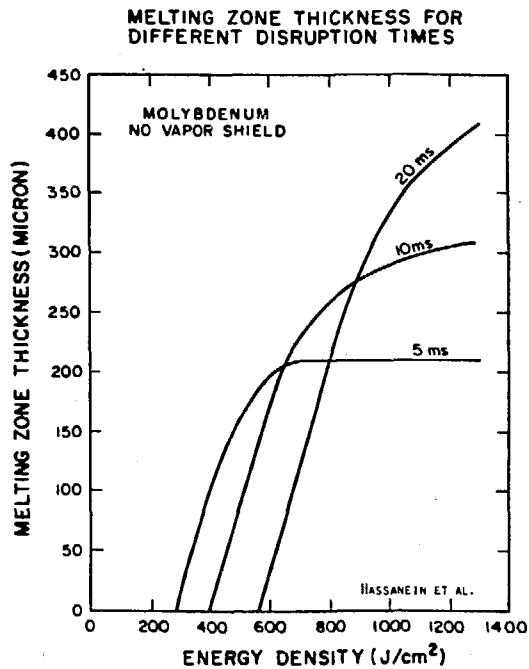


Fig. B-5. Molybdenum melting zone thickness with no vapor shield as a function of energy density (Hassanein model).

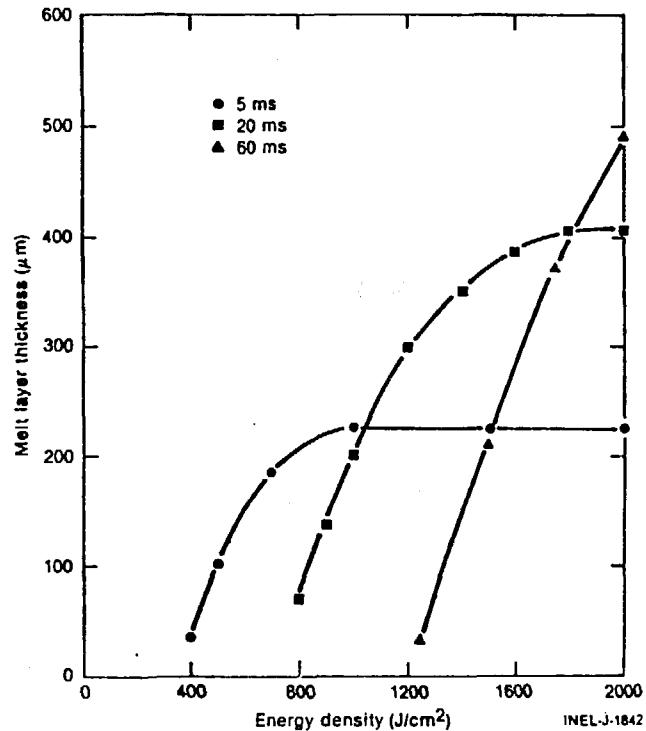


Fig. B-6. Tungsten melt layer thickness for plasma disruptions of 5, 20, and 60 ms duration (Merrill model).

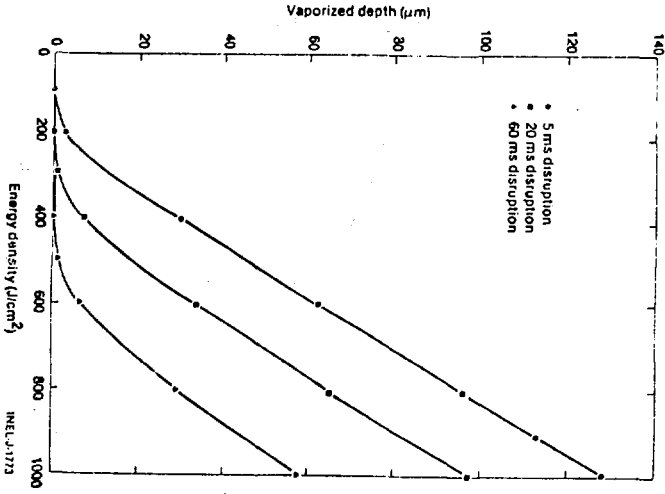


Fig. B-7. Beryllium vaporization depth for plasma disruptions of 5, 20, and 60 ms duration (Merrill model).

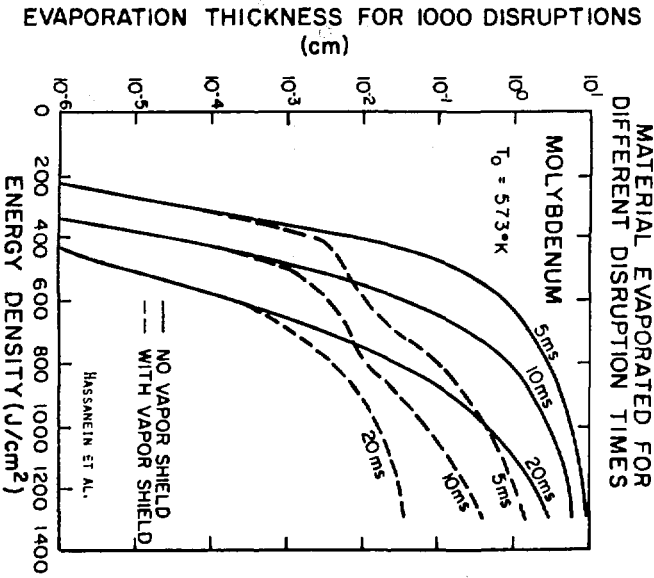


Fig. B-8. Evaporation thickness of molybdenum for 1000 disruptions as a function of energy density (Hassanein model).

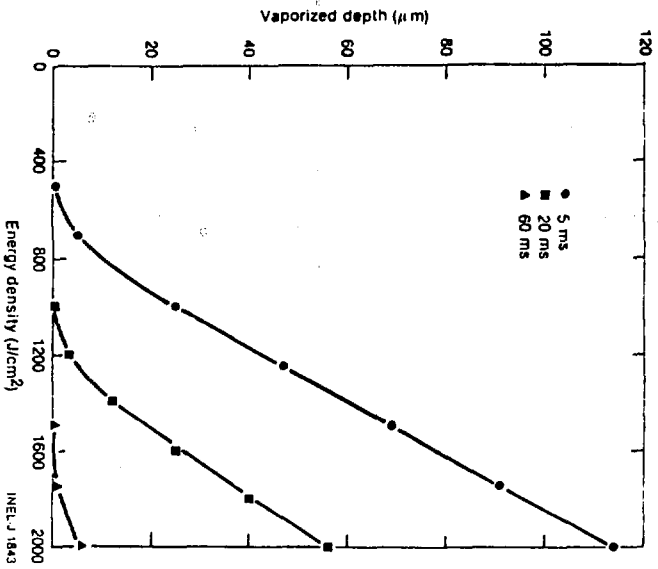


Fig. B-9. Tungsten vaporization depth for plasma disruptions of 5, 20, and 60 ms duration (Merrill model).

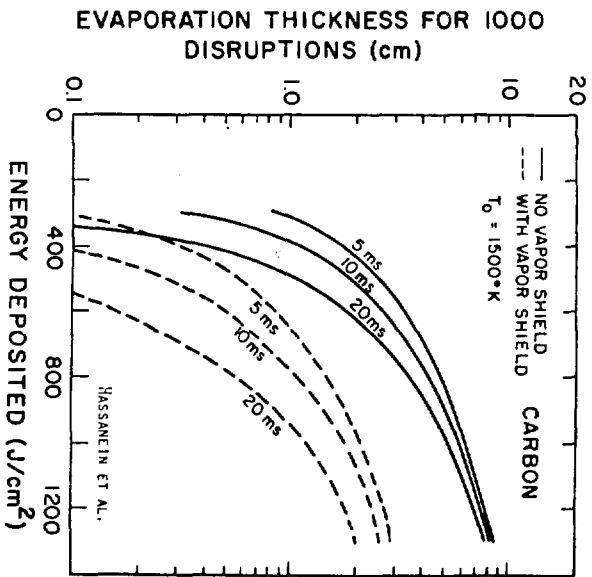


Fig. B-10. Evaporation thickness of carbon for 1000 disruptions as a function of energy density (Hassanein model).

Table B-2. Required Energy Densities for Several Phenomena^a

Material	Disruption Time (ms)	Energy Density (J/cm ²) Required to Cause			Maximum Melt Layer Thickness (μm)
		Melting	1 μm of Vaporization	Maximum Melt Layer Thickness	
Stainless steel	5	90	150	290	120
	20	170	290	600	260
	60	300	480	b	b
Beryllium	5	100	150	350	120
	20	200	300	800	220
	60	360	500	b	350
Molybdenum	5	280	400	700	210
	20	560	750	---	b
	60	b	b	---	b
Tungsten	5	360	560	1000	220
	20	700	1080	1800	400
	60	1220	1750	---	b

^aResults presented are for calculations without consideration of the effects of the vapor shield.

^bNot predicted.

is practically identical for these materials. The energy thresholds for molybdenum and tungsten are significantly higher than for either stainless steel or beryllium. The maximum melt layer thicknesses during a 5-ms disruption for molybdenum and tungsten are both $\sim 220 \mu\text{m}$, while those for stainless steel and beryllium are $\sim 120 \mu\text{m}$. The latter materials are more volatile. On the basis of these results tungsten would be the more resistant metal to erosion by disruption due to the high total energy requirement for melting and vaporization, the high thermal conductivity, and the moderate vapor pressure. Should the melt layer not be stable during this event, a metal with the same characteristics but higher vapor pressure would be more desirable. It is important to point out that the melt layer would exist for only a short time (of the order of the disruption time) and that much of the layer would be molten only a fraction of this time.

Table B-3 summarizes the estimated vaporization erosion thicknesses for the cases of 600 J/cm^2 and 1200 J/cm^2 with the vapor shielding.

Table B-3. Vaporization Thickness for a 60-ms Disruption with Vapor Shielding

Wall Material	Vaporization Thickness (μm)	
	600 J/cm^2	1200 J/cm^2
Beryllium	0.3 ^a	8 ^a
Stainless steel	0.3	18
Tungsten	0.	0

^aAssuming shielding effect similar to graphite.

B.4 Conclusions

The calculations made to date have been for nearer-term devices and unfortunately do not include the higher energy depositions and longer times that are relevant to WILDCAT. It can be seen, however, that the melt-layer thickness saturates with energy deposition and possibly even decreases. These calculations are then adequate to predict the maximum melt-layer thicknesses expected for WILDCAT provided the disruption times are less than $\sim 60 \text{ ms}$. The maximum melt-layer thicknesses for the beryllium cladding are shown in Table B-2 for disruption times of less than 60 ms . Extrapolation of these data in-

dicating the most severe melt-layer thickness to be expected for WILDCAT is 400-600 μm , which would occur if the disruption time is ~ 200 ms, the maximum indicated in Table B-1. Provided the melt layer does not move while it is molten, these thicknesses should prove no serious problem and would not extend past the beryllium cladding except perhaps near the end of the wall lifetime, when the cladding is thin as a result of sputtering.

Movement of the melt layer, however, could significantly increase first-wall erosion. The behavior of the melt layer is affected by such phenomena as the induced magnetic forces, the plasma kinetic pressure and/or surface sputtering, and the acceleration force of the vapor during evaporation. Plasma/vapor interactions should result in a change in the type and intensity of the energy deposition experienced by the first-wall surface through energy absorption and reradiation by the vapor, ionization of the vapor, and increased plasma radiative losses. The Hassanein model addresses this area, but both a theory of plasma vapor interaction and experimental verification of models are required.

Vaporization is more readily seen to be a deleterious effect of disruptions. It can be seen from Fig. B-7 that the vaporization depth becomes linear above 100 J/cm^2 . The vaporization depth can be seen to decrease for higher disruption times. These data should hence be adequate to predict vaporization depths for WILDCAT, at least for disruption times below 60 ms.

The largest amount of vaporization occurs for very short (< 1 ms) disruption times, for which nearly all the energy from the plasma is dissipated by vaporization. The calculations indicate that an energy density of $\sim 6000 \text{ J/cm}^2$ is required to vaporize 1 mm of beryllium, assuming no vapor shield. The vapor shielding should be even more effective at the higher vaporization rates and could be expected to provide an order-of-magnitude reduction in this erosion. In addition, the tendency of the vaporization to saturate at very high densities with the vapor shield indicates the vapor shield may be even more protective for very severe or concentrated disruptions.

Since energy depositions in WILDCAT could easily be as much as 6000 J/cm^2 , these vaporization rates imply WILDCAT could not withstand a large number of disruptions. The normal plasma operation would have to be disruption-free with any disruptions occurring as low probability accidents. The device should be able to withstand a few severe disruptions without catastrophic

damage, however, even in the worst case. These results, for example, indicate it is unlikely that the integrity of a beryllium-clad wall would be lost under a very serious disruption.

There are several factors which would indicate an ability to survive a larger number of disruptions: (1) the probability is low that a concentrated disruption would repeatedly occur on the same small area; (2) the vapor barrier effects substantially reduce the maximum indicated vaporization; and (3) the longer-time scale disruptions expected for WILDCAT correspond to reduced vaporization.

REFERENCES

1. C. C. Baker, et al., "STARFIRE - A Commercial Tokamak Fusion Power Plant Study," Argonne National Laboratory, ANL/FPP-80-1 (1980).
2. W. M. Stacey, Jr., et al., "U. S. INTOR," United States INTOR Group, USA INTOR/81-1 (1981).
3. B. Carreras, B. V. Waddell, and H. R. Hicks, "Analytic Model for the Non-linear Interaction of Tearing Modes of Different Pitch in Cylindrical Geometry," Oak Ridge National Laboratory, ORNL/TM-6175 (1978).
4. B. J. Merrill, "INTOR First-Wall Erosion During Plasma Disruption," Proc. 9th Symp. on Engineering Problems of Fusion Research, IEEE Pub. No. 81CH1715-2 NPS (1981), p.1621.
5. A. M. Hassanein, G. L. Kulcinski, and W. G. Wolfer, "Vaporization and Melting of Materials in Fusion Devices," University of Wisconsin, UWFD-422 (1981).
6. R. W. Schrage, A Theoretical Study of Interphase Mass Transfer (Columbia University Press, 1953).
7. S. I. Anisimov and A. Kh. Rakumatulina, Sov. Phys. JETP 37, 422 (1973).